WA School of Mines: Minerals, Energy and Chemical Engineering

Rapid Pyrolysis of Raw and Pretreated Biomass under Conditions Pertinent to Pulverized Fuel Applications

Qiqing Shen
0000-0002-1687-9326

This thesis is presented for the Degree of
Doctor of Philosophy
of
Curtin University

June 2021

DECLARATION

To the best of my knowledge and belief, this thesis contains no material previously published by any other person except where due acknowledgement has been made.

This thesis contains no material which has been accepted for the award of any other degree or diploma in any university.

Signature:.....

Date: June 2021

To my beloved family

ABSTRACT

The rapidly growing global energy demand leads to the increased utilization of fossil fuels, which results in significant greenhouse gas (GHG) emissions. These emissions aggravate climate change and global warming. The decarbonisation of the energy sector is therefore crucial and has received a lot of attention recently. Biomass as a fuel is renewable and carbon-neutral, and some pretreated biomass (e.g., torrefied/leached biomass) has quite satisfying properties for energy generation.

Various thermochemical technologies have been studied for biomass utilization, such as combustion, pyrolysis, gasification, and hydrogenation. Among these technologies, the direct combustion of raw or pretreated biomass in pulverized-fuel (PF) power plants is very attractive because only slight retrofit of the existing facilities is required to replace fossil fuels with biomass, which is very economic. Rapid pyrolysis, being the first stage of biomass conversion process, happens at the same combustion temperature inside pulverized-fuel boilers and generates char and volatile. As the capacity of a boiler is limited by char conversion, the investigation of char properties after rapid pyrolysis is of great importance.

Despite many studies for the rapid pyrolysis of biomass at high temperatures, a few questions remained unaddressed for decades. Firstly, the true/experimental char yield during biomass rapid pyrolysis under conditions pertinent to pulverized-fuel applications was unavailable. Therefore, the ash-tracer method has been widely used for decades as an indirect way to determine the char yield based on a key assumption (no ash loss during conversion) and a simple equation: char yield = $A_f/A_c \times 100$, where A_f and A_c are the ash content in the fuel and char, (both on a dry basis). But it is well-known that this method is prone to error due to the evaporation of ash elements during rapid pyrolysis. Secondly, previous studies always assumed a spherical particle shape for biomass and char when modeling and calculating various conversions. However, the transformation of particle shape and size for biomass particles during rapid pyrolysis is drastic, which cannot be neglected for an accurate estimation of conversion. So far, little information is available about the change of biomass particle shape and size during rapid pyrolysis by quantitative analysis.

This Ph.D. thesis provides a better understanding of the rapid pyrolysis of raw and pretreated biomass under conditions pertinent to pulverized-fuel applications, focusing on the physical and chemical properties of resultant char. The specific objectives of this research are to investigate: (1) the effects of biomass particle size; (2) the evolution of biomass pyrolysis; (3) the effects of torrefaction on biomass powder; (4) the effects of torrefaction and pulverization on wood chips; (5) the effects of water and acid leaching, on the char yield, the release of inorganic species, and the transformation of particle shape and size, during the rapid pyrolysis of biomass at high temperature. The rapid pyrolysis was conducted in the novel drop-tube furnace, which enables the direct determination of char yield. These objectives are successfully achieved and the main research outcomes are summarized below.

Firstly, the analysis of the char samples after rapid pyrolysis of mallee and pine wood samples with different particle sizes at 1300 °C indicates the dependence of resultant char properties on the particle size. Char yields of large mallee and pine particles (250-355 μm) are several times higher than the char yields for small particles (90-106 μm), which is mainly ascribed to the much higher heating rate for small particles. The estimation of the heating rate for a spherical particle shows that the heating rate experienced by small particles is 5.4 times faster than large particles. The extensive release of inorganic species from biomass/char during the thermochemical conversions leads to the significant overestimation of char yield, especially for small biomass particles. Further investigation of major inorganic elements in mallee and pine wood, which are alkali and alkaline earth metallic species (AAEM species: Na, K, Mg, and Ca), shows that retentions of AAEM species relate to the chemical properties of the elements and the biomass particle size. As the particle size reduces from 250-355 μm to 90-106 μm, the retentions of AAEM species decrease by more than half, which can be partly attributed to the difference in heating rate. The changes in particle dimensions and aspect ratio show that rapid pyrolysis leads to severe shrinkage for both biomass species. But for mallee wood, only small biomass particles form near-spherical char particles, while large particles tend to retain their elongated shape as only partial melting is experienced by them. Contrary to mallee wood, all pine wood samples with different sizes have a substantial reduction in the particle aspect ratio and a cenosphere structure, suggesting a high degree of particle deformation during pyrolysis.

Secondly, the evolution in char yield (determined by direct experimental method as the first time in the field), in transformation of alkali and alkaline earth metallic (AAEM) species in chars, and in char particle shape/morphology during rapid pyrolysis of mallee and pine wood powders (250–355 μm) is investigated. The char yield decreases with particle residence time but remains unchanged at 3.8% and 2.8% after 0.51 s and 0.41 s for mallee and pine chars, respectively, indicating the pyrolysis reaction is mostly completed. But O/C and H/C molar ratios continue to decline as char continue to undergo thermal cracking and annealing at high temperatures. Similarly, the retention of AAEM species decreases with particle residence time. But the retentions of AAEM species in pine char continue to decrease after 0.41 s, which indicates AAEM species in nascent char can continue to vaporize due to the scission of oxygen-containing groups where AAEM species are bounded during thermal cracking or annealing. Chemical fractionation of partially and completely pyrolyzed mallee char samples shows the transformation of decomposed water-soluble Na and K species to ion-exchangeable Na and K. But with the continuous deoxygenation of char matrix, the Na and K bound to oxygen-containing groups are released. Furthermore, the percentages of water-soluble and ion-exchangeable Mg and Ca in mallee wood drop because they become increasingly incorporated into char matrix due to rapid deoxygenation during pyrolysis. Results of char morphology show char particle length and diameter continue to shrink, and the char particles become increasingly spherical as pyrolysis progress. Mallee wood shows stronger resistance to deformation as its original elongated shape is maintained. On the contrary, pine char particles rapidly melt and deform during the early stage of pyrolysis.

Thirdly, the rapid pyrolysis of torrefied mallee wood powder samples with the size fraction of 150-250 μm is studied. The results of char yields for raw and torrefied mallee wood after pyrolysis show that although torrefaction at 220 °C, 250 °C, and 300 °C cause increasing mass loss, rising torrefaction temperature leads to significantly higher char yield. The reasons for this include the much higher content of acid-insoluble lignin and inorganic species in torrefied biomass, indicating extensive cross-linking and charring reactions happen during torrefaction, especially at high torrefaction temperature 300 °C. The results also show that torrefaction alters the occurrence of AAEM species in biomass, making them more stable during conversions. Therefore, significantly higher retentions of AAEM species are observed

after rapid pyrolysis. Another reason for the higher retentions of AAEM species for torrefied mallee is the less extensive devolatilization process, which favors the gradual release and re-combining to char matrix for AAEM species. Despite some dehydration and degradation of biomass constituents, the torrefaction process has negligible effects on particle size and shape. But after rapid pyrolysis, high-temperature torrefaction at 300 °C can noticeably alleviate the shrinkage of biomass particles, producing larger char particles.

Fourthly, a set of experiments were carried out to evaluate the effects of torrefaction temperature on the pulverization of mallee and pine wood chips and then the behaviour during rapid pyrolysis. Different torrefaction temperature (220 °C, 250 °C, and 300 °C) and two size fractions (90-106 μm and 250-355 μm) of biomass particles sieved from torrefied biomass powder were used. The comparison of particle shape and size for pulverized particles shows that higher torrefaction temperature can significantly reduce the particle length, equivalent diameter, and aspect ratio for large particles under the same pulverization conditions, while these parameters for small particles is not affected by torrefaction. Further rapid pyrolysis for torrefied samples in two size ranges shows that higher torrefaction temperature facilitates the formation of char, but large particles still have higher char yields. The investigation of AAEM species suggests that higher torrefaction temperature can mitigate the variation in the retentions of AAEM species caused by different particle sizes. Reasons could be the closer actual particle size (equivalent diameter) for torrefied biomass particles in two size fractions, the higher stability of AAEM species, and the lower volatile content in torrefied biomass. Besides, analysis for cross-sectional images presents the compact internal structure for char particles produced from torrefied biomass, especially those having high torrefaction temperature, which hinders the escape of volatilized AAEM species and facilitates the re-bonding of AAEM species with reactive char matrix.

Lastly, the impacts of water and acid leaching on the contents of inorganic species in mallee wood are investigated and the char products after rapid pyrolysis of leached mallee wood are characterized. The quantification of the AAEM species in samples and leachates shows that water-leaching can remove most Na and K but only a small amount of Mg and Ca, whereas the removal efficiency by acid-leaching can reach up to 97~98% for all AAEM species. Except for the significant reduction in the content

of inorganic species, no considerable variation is induced to other properties of biomass. Char yields of water-leached and acid-leached mallee are significantly lower than raw mallee wood. Meanwhile, increasingly aggressive leaching agents can lead to higher retentions of AAEM species during pyrolysis, which can be ascribed to the higher proportions of less reactive (acid-insoluble) AAEM species after the removal of water-soluble (such as chlorides and sulphates) or acid-soluble elements with relatively lower thermal stability. The morphology of char shows that raw and leached mallee wood particles have similar particle size and shape, whereas their char particles exhibit distinct shape and surface morphology. Char particles pyrolyzed from raw mallee wood have elongated shape and complex internal char structure, while acid-leached mallee wood produces char particles that resemble cenospheres with rough surface. Besides, the summary of particle porosity shows that leached char particles have higher cross-sectional porosity. These results indicate the pivotal role of inorganic species during the deformation process of biomass particles.

ACKNOWLEDGEMENTS

I gratefully acknowledge Curtin University for providing Curtin International Postgraduate Research Scholarship (CIPRS) to sponsor my Ph.D. study and the partial support received from the Australian Research Council via the Discovery Projects scheme.

I would like to express my sincere gratitude to my supervisor, Professor Hongwei Wu, who came up with the primary idea and devoted a lot to patiently guide and persistently support me. Throughout my entire Ph.D. period, I have learned so much from his invaluable advice and inspiration, which I would treasure for a lifetime. Without his encouragement, I would not be able to finish my Ph.D. research.

I am very grateful to my associate supervisor Dr. Sui Boon Liaw, and Dr. Yun Yu for their numerous assistance throughout my research. Dr. Sui Boon Liaw gave me unreserved advice. I benefit a lot from his help regarding experimental work and instruments. My special thanks go to deceased Professor Mario Costa, who offered me valuable ideas and advice at the beginning of this Ph.D. study. I also want to express my gratitude to my thesis committee chairperson, Professor Ranjeet Utikar, for his kind assistance.

I would like to thank other current and former members of our research group, Dr. Mingming Zhang, Dr. Wenran Gao, Dr. Xujun Chen, Dr. Mingyang Li, Dr. Yee Wen Chua, Mr. Rashedul Khondakar, Dr. Changya Deng, Ms. Jinxiu Cao, and Mr. Zhiliang Wu, Mr. Md Rahmad for their support in various ways. Great thanks go to Mr. Victor Olet for proofreading the literature review in my thesis. I also acknowledge all the lab technicians for their help.

I am especially indebted to my parents, for their endless love, understanding, encouragement, and support. Their company means everything to me.

LIST OF PUBLICATIONS

Papers Published or Submitted in Refereed Journals:

(1). **Shen, Q.**; Liaw, S. B.; Costa, M.; Wu, H., Rapid pyrolysis of pulverized biomass at high temperature: Effect of particle size on char yield, retentions of alkali and alkaline earth metallic species and char particle shape. Energy & Fuels 2020, 34, 6, 7140–7148.

(2). **Shen, Q.**; Liaw, S. B.; Wu, H., Evolution of Char Properties during Rapid Pyrolysis of Woody Biomass Particles under Pulverized Fuel Conditions. Energy & Fuels 2021, 35, (19), 15778-15789.

Papers to Be Submitted to Refereed Journals:

(3). **Shen, Q.**; Wu, H., Rapid pyrolysis of pulverized biomass at high temperature: Effects of torrefaction temperature on char yield, retention of alkali and alkaline earth metallic species and char particle shape (to be submitted to Energy & Fuels)

(4). **Shen, Q.**; Wu, H., A study of particle size, shape, and elements retentions during rapid pyrolysis based on industrial utilization of torrefied wood chips (to be submitted to Fuels)

(5). **Shen, Q.**; Wu, H., Effect of biomass leaching on the properties of char after rapid pyrolysis (to be submitted to 39th International Symposium on Combustion)

TABLE OF CONTENTS

LIST OF FIGURES

LIST OF TABLES

CHAPTER 1 INTRODUCTION

1.1 Background and motives

There are rapidly growing demands for energy worldwide but fossil fuels remain as the primary source of power. Reports showed that coal accounted for 64% of electricity generated in Australia. The extensive burning of fossil fuels brings about severe problems about the emission of carbon and other greenhouse gases, which is known for their contribution to climate change and global warming. Studies showed that the emission of CO_2 has increased by 63% since the 1990s.[1] Therefore, it is of urgent need to reduce the reliance on fossil fuels by developing clean and renewable energy sources. Many countries have announced their plans to gradually switch to renewable energy. Globally, half of the renewable energy consumed in 2017 was bioenergy. In European countries, more than 30% of transportation fuels will be required to be derived from biofuels in 2040;[2] In the US, most renewable fuels need to be produced and derived from Cellulosic Biomass after 2016.[3] It can be found that biomass is considered an important source of renewable energy.

In western Australia, native mallee wood as short-cycle coppice crops, were initially planted to combat the dryland salinity in wheatbelt region of Western Australia, thanks to its diverse and vigorous characteristics.[4] Thus there is no competition between the production of mallee and the production of agricultural crops. Over decades, the scale of mallee production is quite considerable. The feasibility for mallee as an energy crop has been comprehensively studied and proved to be promising.[4-6]

There are various technologies designed for biomass utilization, including direct combustion,[7] gasification[8], and pyrolysis[9], converting biomass into other useful bio-fuels like bio-oil and biochar products by thermal treatment. [10-11] Among these methods, the direct combustion of biomass in existing power generation plants is very attractive because it can take advantage of the existing power generation infrastructure and reduce the reliance on fossil fuels by partially or completely substituting coal by biomass. Studies for biomass combustion have been carried out to investigate the behaviour of biomass,[12] gaseous products,[13] particulate matter emission,[14-15] and etc. Attentions were also placed on the first stage of biomass combustion which is the rapid

pyrolysis of biomass at the same temperature. The reactions of this stage determine the properties of char residue, which will govern the subsequent oxidation process by affecting the heat and mass transfer and etc. The effect of temperature,[16-19] heating rate,[17] atmosphere,[20] types of biomass[21], and the distribution of pyrolysis products[18] on rapid pyrolysis have been widely studied.

However, the basic problem of rapid pyrolysis is the determination of char yield, which has not been answered due to the poor char collection efficiency after reactions. The value of char yield is critical when modelling the conversion and designing the reactors (combustor or gasifier).[22] Therefore, a novel drop-tube furnace was designed by Liaw and Wu to tackle this problem.[23] The new configuration was proved to achieve a near-complete collection of char products and thus the direct determination of char yield is realized. A systematic investigation of char yield for biomass rapid pyrolysis is then possible.

Regarding the application of biomass in pulverized fuel plants, there are a few more concerns. Firstly, the poor grindability of biomass can cause a high energy demand when pulverizing the biomass wood chips to the required particle size range suitable for pulverized fuel furnaces.[24] Moreover, the intrinsic inorganic species in biomass can be released during thermochemical conversions and are harmful to equipment and the environment. Torrefaction is an efficient method to improve biomass grindability but few studies investigated the rapid pyrolysis of torrefied biomass so far.[25-26] The inorganic species in biomass can be removed by leaching but little is known about the release extent of those inorganic species that are remained in leached biomass. Besides, the particle shape of biomass fine particles has been found to be elongated, whereas most models established for biomass conversions assume a spherical shape for biomass and their char particles.[27] Consequently, the effects of particle shape on the conversion rate and products were not considered. This is partially because the transformation of particle shape after rapid pyrolysis is still unknown.

1.2 Scope and objectives

The present study aims to provide a better understanding of raw and pretreated biomass rapid pyrolysis at high temperatures which is carried out in a novel DTF. The detailed objectives of this study are as follows:

- To investigate the effects of particle size on the chemical and physical properties of char derived from the rapid pyrolysis of biomass powder samples.
- To study the evolution of char properties during rapid pyrolysis at a high temperature.
- To evaluate the pretreatment of biomass powder by torrefaction and the effects on the subsequent rapid pyrolysis.
- To simulate the industrial usage of biomass wood chips and torrefaction technology and study the particle shape of their resultant char.
- To examine the impacts of leaching on the properties of biomass and the rapid pyrolysis of leached biomass.

1.3 Thesis outline

This thesis comprises 9 chapters in total (including this chapter). The structure of this thesis can be found in the thesis map (Figure 1.1) and a brief introduction for each chapter is outlined below:

- Chapter 1 introduces the background and objectives of the current research
- Chapter 2 provides a review of up-to-date studies of the biomass/char physical and chemical properties and thermal conversion technologies of biomass. This chapter identifies the current research gaps and the objectives of the current Ph.D. study.
- Chapter 3 summarizes the research methodology for this study. The details of samples preparation steps, experiments procedures, instruments, and sample characterization methods are introduced.
- Chapter 4 studies the effects of different particle sizes on the experimental char yields, retentions of AAEM species, and the shape of char particles for mallee and pine wood after rapid pyrolysis at a high temperature.
- Chapter 5 reveals the evolution of mallee and pine wood particles by characterizing the char yields, the gradual release of AAEM species, and the particle shape during the process of rapid pyrolysis at a high temperature.
- Chapter 6 reports the fundamental research about the results of different torrefaction temperatures and their impacts on the subsequent rapid pyrolysis for torrefied biomass.

- Chapter 7 investigates the results of particle shape, char yield, and the release of AAEM species for biomass treated by torrefaction and rapid pyrolysis.
- Chapter 8 demonstrates the influence of biomass leaching by water and acid and compares the physical and chemical properties of char samples derived from the rapid pyrolysis of raw and leached biomass.
- Chapter 9 summarises the conclusions drawn in this Ph.D. study and also lists some recommendations for future work.

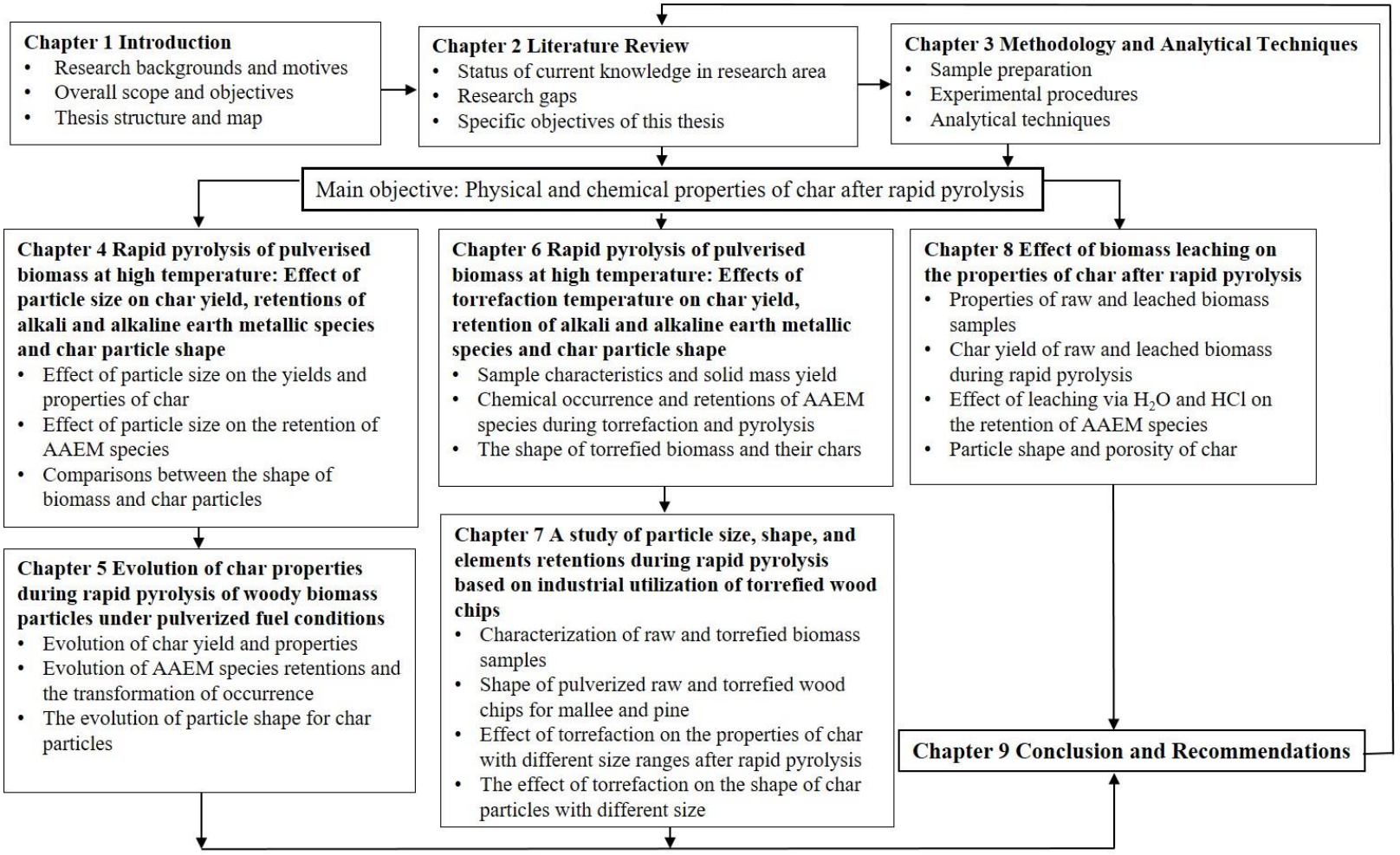

Figure 1.1 Thesis map

CHAPTER 2 LITERATURE REVIEW

2.1 Introduction

Extensive efforts have been dedicated to the study of developing clean and renewable energy to meet the rapidly growing demands for power, thereby reducing the dependence on fossil fuels, which has cast severe environmental problems over decades. Biomass as a sustainable energy source has attracted worldwide interest. Numerous research studies have been carried out to study biomass conversion technologies, such as combustion, gasification, pyrolysis, and beneficial biofuels derived from biomass. The combustion of biomass in sophisticated power plants for coal is economically competitive as it can minimize the extra investment for biomass combustion facilities. However, this technology still faces several challenges, partially due to the discrepancies in fuel properties between coal & biomass and the diversity in biomass samples. Therefore, investigations have been carried out on the multiple aspects of biomass properties and its thermal behaviour, particularly during the pyrolysis process when some key reactions happen.

This chapter aims to have a comprehensive review of the current literature relating to biomass properties and its pyrolysis conversions under pulverized-fuel (PF) combustion conditions. This literature review will first discuss the significance of biomass (especially mallee biomass in Western Australia) utilization with a brief introduction of the biomass properties and a list of the popular thermochemical conversion technologies for biomass. Then, a more detailed review on the rapid pyrolysis of biomass will be presented, with further discussion on the limitations on the current lab equipment to carry out rapid pyrolysis. Next, a brief summary will be given about studies on the behaviour of inorganic species and the evolution of particle size and shape during rapid pyrolysis. Besides, two common pretreatment methods for upgrading biomass before rapid pyrolysis will be introduced. Lastly, this chapter will identify the research gaps based on the literature review and propose the scope and objectives of this Ph.D. study.

2.2 Biomass utilization

2.2.1 The advantages of biomass and its thermochemical conversions

There have been many concerns about greenhouse gases (GHGs) pollution and the dreadful consequences as the annual emission of GHGs has been continuously increasing for decades.[28] Inventory of U.S. Greenhouse Gas Emissions and Sinks reports a total of 6,577 million metric tons of carbon dioxide equivalents mission in 2019.[29] The data reported by British Petroleum in 2018 show that there are 33,431 million tonnes of CO_2 surrounding earth.[30] Over decades, carbon dioxide (CO_2) is the main contributor to GHG. Data shows that CO_2 emission consists the dominant part (81%) of the total GHGs emitted in the U.S. in 2018.[29] Other GHGs include methane (CH_4), nitrous oxide (N_2O), and fluorinated gases, which are relatively fewer in quantity but have much higher Global Warming Potential (GWP). Fossil fuels are the primary source for CO_2 production for their mining process, transportation, and combustion generate a significant amount of CO_2 and other gases such as CH_4 and N_2O.[29] They are widely used as the fuels for machines, vehicles, power generating plants and etc., to provide heat and electricity. The economic and population growth mean that more fuels are needed to meet the massive demands nowadays. Therefore, it is critical to develop a clean energy and reduce the reliance on fossil fuels. In Western Australia, the government set the goal to achieve net zero emissions of GHGs by 2050,[31] which further highlights the great importance of renewable energy.

The near carbon neutrality of biomass is a very attractive characteristic in reducing carbon emission. The abundance of biomass means that a large-scale biomass utilization to control the GHGs emission is feasible. Other advantages of biomass include cheap resources, low contents of harmful elements, high reactivity, etc.[32] However, the utilization of biomass also faces several major problems, such as low energy density, poor uniformity of property, seasonal availability, and ash problems. The advantages and disadvantages of biomass are summarized in Table 2.1.

Table 2.1 The advantages and disadvantages of biomass[32]

Advantages:
• Being environmentally friendly, renewable from nature, and carbon neutral • Low in contents of ash and other harmful inorganic species. • High reactivity • Low emission of hazardous gases, including GHGs • Some hazardous emission can be captured by ash after combustion • Cheap resources, and high fuel diversity and abundance • Contribution to the local economy
Disadvantages:
• Dependence on the location • No standards due to biomass variety • High contents of alkali metals • Low energy density • May compete with food plantation • Potential soil damage • Emission control problems • High logistical expense • No mature waste materials treatment technology

The thermo-chemical process of biomass is an efficient way to convert biomass into useful biofuels considering its higher reaction rate in comparison to bio-chemical process.[33-34] Typical thermo-chemical conversions include 1. Combustion; 2. Pyrolysis; 3. Gasification; 4. Liquefaction; 5. Hydrogenation.[9, 34] Briefly, combustion of biomass directly releases the energy stored inside biomass and leaves ash in the end, whereas the rest of thermo-chemical conversion methods can transform biomass into other useful biofuels, such as charcoal, bio-oil, synthetic gas, which can be utilized in different ways. The conditions for these conversions vary widely, including the conversion temperature, atmosphere, equipment, pressure, reaction time, etc. The

utilization of biomass by thermo-chemical conversions needs huge investment, and it depends on many other aspects. Therefore, it is important to do a feasibility investigation and choose the suitable biomass and conversion method according to the local circumstances.

In Western Australia, Mallee Eucalyptus was intentionally planted to combat the dryland salinity in the wheatbelt region of Western Australia in the early 1990s.[4] Until now, there are more than 15000 hectares of mallee trees which can produce 10-20 gt (green tonne) of biomass annually, with optimal environmental conditions (rainfall and soil fertility).[35] Research about the feasibility/environmental performance/carbon balance/energy balance has systematically demonstrated the massive potential of a sustainable bioenergy system with mallee wood as the feedstock.[4-6, 36-38] The combustion of mallee has already been commercialized in a local company called Macco Feeds. About 3500~4000 tonnes of mallee woodchips are burnt in one year in their gasification boiler to generate up to 1.7MW of thermal power.[39]

2.2.2 Biomass co-combustion in pulverized-fuel boilers and its challenges

Biomass combustion is regarded as the most straightforward energy release process. The generated heat can be further transformed into other forms, such as mechanical power, electricity, etc. Considering the economic efficiency, biomass combustion in existing power generation plants that were initially built for coal combustion is very cost-effective. The prediction given by Spliethoff and Hein shows that a total cost of 800~1500 DM/(kW of installed thermal capacity) would be needed to build a new plant dedicated to biomass combustion, while the investment for the update or modification (retrofit) of a coal-firing plant to a co-combustion plant of coal and biomass only needs 300 DM/(kW of installed thermal capacity).[40] The combustion of biomass can also reduce the reliance on fossil fuels to mitigate the problems brought by fossil fuel combustion.[41] Moreover, less emission of NO_x and SO_x can be achieved if using biomass for combustion.[42]

However, there are still some limitations on biomass combustion. For example, direct combustion is not achievable if the moisture content in biomass is larger than 50%.[9] Besides, detrimental products of biomass combustion, such as fuel gas, particulate matter, ash, will cause serious problems to the environment and human health. Two of

the main challenges faced by the combustion of biomass in pulverized-fuel (PF) boilers are summarized below.

Pulverization of biomass

Particle size plays a dominant role in determining the pathways and kinetics of reactions. The regular particle size of coal burnt in a furnace is <100 μm to ensure the high heating rate and conversion rate for coal.[42-43] Therefore, the particle size of biomass needs to meet the requirements of feeding system in power plants. Besides, particle size can restrict the burnout degree of biomass particles. Spliethoff and Hein found that the particle size for straw and Miscanthus must be less than 6 mm and 4 mm to ensure a complete burnout, and co-combustion with coal requires smaller biomass particles.[40] The normal particle size for fluidized bed reactors is reported to be 0.5-20 mm, whereas the typical particle size for pulverized coal-fired boilers is only 0.1-1 mm.[44] In lab research furnaces such as drop tube reactors (DTR) and entrained flow reactors (EFR), the particle size of biomass is usually required to be <1 mm to achieve a high heating rate.[45] Therefore, size reduction of biomass prior to combustion in PF boilers is necessary. However, the pulverization process of biomass is known to be energy-intensive because of its fibrous nature. Phanphanich and Mani reported that the regular grinding energy for coal is 7~36 kW h/t, while the raw pine wood chips they investigated need about 250 kW h/t of specific energy for grinding.[46] Therefore, the pulverization of biomass would be the major energy-demanding process that requires more investigation. Using large biomass particles could reduce the cost, but the increase in particle size is related to the ignition delay and partial burnout.[47-48] Mock et al. investigated the combustion behaviour of large biomass particles and found that particles >425 μm would drop to the bottom of the furnace and cannot achieve complete burnout.[49] Therefore, it requires more research on the optimal particle size of biomass for combustion.

Discrepancies in fuel properties

Problems of biomass combustion in coal boilers are usually because of the discrepancies in fuel properties between biomass and coal.[42] The energy density of biomass (<5GJ/m^3) is much lower than coal (~35GJ/m^3),[50] which is partly due to the chemical properties of biomass, such as higher moisture content, but lower fixed

carbon content. The higher moisture content in biomass than coal can cause problems in ignition and combustion. On the other hand, the fibrous nature of biomass particles after pulverization makes the bulk density for biomass very low and thus increases the logistics cost for biomass powder.[51] Due to the low bulk density and carbon content but high ash, oxygen, moisture contents, the energy density and heating value for biomass are much lower than coal. It will cause a lower burning rate and lower flame temperature, which will eventually lead to problems on biomass co-combustion, such as flame instability.[42] For example, the lower burning rate and lower temperature can result in the delay of char oxidation, which in the end, would cause the existence of unburnt carbon materials. It will not only decrease the fuel conversion efficiency but also lead to more detrimental gas pollution.[52] Therefore, biomass is seldom used in blast furnaces because of its high requirement of energy density.[53]

The composition of inorganic species in biomass is distinct from coal. Usually, biomass has higher contents of alkali and chlorine elements,[54] but less aluminum and iron.[42] There have been many works focusing on the ash behaviour after biomass combustion. Biomass ash exhibits lower ash and deposit fusion temperature due to the abundance of alkali content.[55] A more complicated issue is related to the combined effects of different ash elements on the ash behaviour in boilers, considering the various species of biomass and their different inorganic species composition. Heinzel et al. found that mixing biomass with coal can introduce differences in the fusion and slagging during combustion, suggesting the interaction between biomass and coal.[55] Many researchers have observed the release of inorganic species during the thermochemical conversions.[56-64] These evaporated elements would also influence the combustion reactions and may damage the boiler as they lead to serious corrosion and slagging problems. Demirbas mentioned that the vaporized biomass AAEM species and chlorine would interact and mix with gases generated by coal during cofiring and produce different gaseous products and particulate matter.[42]

2.3 Rapid pyrolysis of biomass at temperatures pertinent to combustion

2.3.1 Rapid pyrolysis of biomass

Pyrolysis

Pyrolysis receives increasing attention as it is the first and vital step for many thermal conversion processes, including combustion, gasification, and liquefaction.[16-17, 41, 65] It is also considered to be an efficient method to convert biomass with low energy density to more useful fuels with higher energy density. Demirbas and Arin proposed the primary pyrolysis reaction as the degradation of biomass into charcoal and volatile matter.[66] There are various operation conditions for pyrolysis, but the critical point is to keep an inert atmosphere during biomass heating. Different pyrolysis processes and conditions are designed to meet the requirements of target products and other economic or environmental concerns. Research about pyrolysis divides the pyrolysis procedure into three types based on biomass heating rate: slow pyrolysis, fast pyrolysis, and rapid (flash) pyrolysis,[9] which have char, bio-oil, and gas as the main pyrolysis product, respectively.

Rapid pyrolysis

PF boilers are usually maintained at high temperatures (> 1000 °C). The conversion of biomass during combustion was divided into three steps: drying (moisture evaporation); pyrolysis (devolatilization), and combustion (oxidation) of char, volatile, and gas.[34, 67] It is believed that under conditions of PF combustion, fuel particles will undergo complete pyrolysis before being ignited.[68] Therefore, rapid pyrolysis would be the first thermal conversion process experienced by biomass after being injected into the boiler. It is believed that this rapid pyrolysis happens at the same temperature of combustion.[16] Studies for coal have demonstrated that rapid pyrolysis governs the behaviour of coal combustion, including the ignition temperature and flame stability, as well as other behaviours of coal particles, such as the degree of swelling and agglomeration.[69] This can be partly ascribed to the relation between the oxidation rate and the reactivity of char, the latter being directly linked to the pyrolysis reactions.[22] The oxidation of char is also significantly influenced by the diffusion of oxidative gases, which is mainly dependent on the char matrix formed during pyrolysis.

Due to the discrepancy in the fuel properties of coal and biomass, the rapid pyrolysis of biomass under conditions of PF combustion needs further investigation. For instance, biomass has a much higher volatile content compared to coal.[41] A large amount of volatile matters being released during the pyrolysis stage generates higher reactive char samples, resulting in better burnout during the following oxidation

stage.[70-71] For some char samples, the oxidation of char is even the rate-limiting step during combustion. Thus the rapid pyrolysis of biomass under conditions of PF combustion urgently needs better understanding.[22-23]

In recent years, many works have been carried out aiming at the rapid pyrolysis of various biomass species and multiple aspects of pyrolytic products. Below are some of the studies that clearly stated that their rapid pyrolysis experiments were conducted at temperature >1000 °C and heating rate >10^3 °C/s.

Pyrolysis conditions are numerously studied, such as different temperatures, pressure, gases, heating rate. Hu et al. pointed out that the pyrolytic conditions have strong influences on the char reactivity by affecting the evolution of pore structure and morphology of rice husk char. They observed the formation of a more carbonaceous and thermally stable structure after rapid pyrolysis.[72] Zhang et al. found a peculiarity in the carbon conversion extent for sawdust pyrolyzed in DTF at a wide range of temperatures (600 °C-1400 °C) and they ascribed the decrease of char yield at >1000 °C to the gasification of char and reactive pyrolysis gases H_2O and CO_2.[16] The effects of pyrolysis temperature were also studied by Johansen et al. who conducted the rapid pyrolysis for pine and miscanthus at 1405-1667 K with particle heating rate reaching 10^5 K/s.[73] They investigated the devolatilization rates via a unique methodology and found that the actual devolatilization kinetics for pyrolysis with heating rates on the order of 10^3-10^5 K/s were higher than what was reported previously that underestimated the heating rate (< 10^3 K/s) for biomass.[73-74] This again emphasizes the importance of studies concerning rapid pyrolysis at high temperatures. Biagini and et al. studied the effects of heating rate on the structure, shape, and other superficial parameters for wood pellets and olive residue. They compared the evolution of size and shape during pyrolysis for two biomass species.[68] Most importantly, they proposed a method to evaluate the shape of char by analyzing the SEM images.[75] Dall'Ora et al. investigated the effects of heating rate and temperature on the char yield, char morphology, and the oxidation rate of resultant char.[76] Their results show that a high heating rate (10^5 K/s) can considerably lower char yield than using a low heating rate (10 K/s) pyrolysis at the same temperature (1273 and 1573 K), and it also has a critical role in the transformation of char particle shape.

Studies listed above also suggested that different biomass species play a dominant role in rapid pyrolysis. Trubetskaya et al. conducted a series of experiments of rapid pyrolysis at high heating rate and high temperature for different biomass and provided important data for the char reactivity, char structure, char yield, particle shape, and composition of inorganic species in char samples.[43, 77-78] Different biomass species also mean variation in particle size and shape. The effects of particle size and pyrolysis temperature on the solid mass yield and surface morphology of Norway spruce were investigated.[45] A systematic study of the influence of biomass particle size and shape on the properties of char and reaction rates was carried out. The results indicated that the geometric parameters (size and shape) can determine the actual heating rate inside the particle, the pyrolysis kinetics, and products distribution.[79] This finding of the evolution of particle shape for biomass is a new area for researchers to explore because it is crucial to understand the deformation of biomass particles as it will have a noticeable influence on the later conversion stage: oxidation. These studies indicated that apart from the rapid pyrolysis process, there are variances in the char particle shape and size among different biomass species, even after being pyrolyzed in the same conditions.

The effects of residence time and char thermal annealing for biomass rapid pyrolysis were relatively rarely investigated, probably due to the limitations in the experimental equipment. Septien et al. observed changes in the char matrix and the crystallinity of mineral matters for char prepared in a DTF at > 1000 °C and ascribed it to the char thermal annealing.[80] The reactivity of char was found to be drastically decreased during a very short thermal annealing time (< 2s) and showed high dependence on the peak temperature.[81] Apart from the organic changes, a loss of inorganic species, especially for K, happened during the thermal annealing process. Hu et al. obtained rice husk char with various reaction ratios after rapid pyrolysis in a DTF at 1200 °C and observed the smoother surface, changes of pore size, decreased H/C and O/C ratio, and the loss of C-O, C-H function groups, as the evolution of char structure during rapid pyrolysis.[72]

The kinetic analysis for biomass conversion is usually done by TGA which can monitor the sample weight, temperature, and gaseous products if coupled with *in situ* gas chromatography, FTIR, and other analysis equipment, as the conversion evolves.

However, the kinetics of biomass undergoing rapid pyrolysis at PF combustion temperature is difficult to obtain due to the fixed reaction time, the difficulties in solid mass yield determination, or other limitations. Only several papers have been found concerning biomass rapid pyrolysis kinetics and have experimental data as evidence. Umeki et al. determined the char yield of a Norway spruce in an EFR to verify their model, which considered the pyrolysis temperature, particle size, and conversion rate.[45] It is important to note that while the model had good agreement with the experimental data for small particles, the model significantly underestimated the char yield for large particles. This suggests that particle size has a vital part in the thermal conversion of biomass.

The above-mentioned research covered many aspects of biomass rapid pyrolysis. However, there are still things unclear, such as the release of inorganic species, the evolution of particle shape, the true char yield for biomass when subjected to rapid pyrolysis at high temperature.

2.3.2 Typical equipment for conducting rapid pyrolysis of biomass

Table 2.2 A list of studies using Drop-tube furnaces (DTF), Entrained flow reactors (EFR), and, Wire mesh reactor (WMR) to carry out rapid pyrolysis of biomass at high temperatures (>1100 °C).

Typical equipment deployed for rapid pyrolysis at high temperatures (>1100 °C)			
		Temperature	Heating rate
Drop-tube furnaces (DTF)	Zhang et al.[16]	600 to 1400 °C	not provided
	Trubetskaya et al.[43]	≤ 1500 °C	10^4 – 10^5 °C/s
	Panahi et al.[7]	≤ 1127 °C	10^4 °C/s
	Cetin et al.[82]	≤ 1500 °C	~10^5 °C/s
	McNamee et al.[83]	1100 °C	not provided
Entrained flow reactors (EFR)	Trubetskaya et al.[77]	≤ 1600 °C	not provided
	Lu et al.[79]	≤ 1377 °C (wall)	~10^4 °C/s
	Dall'Ora et al.[76]	1000 °C and 1300 °C	2×10^4 to 4×10^5 °C/s

	Gil et al.[84]	≤ 1500 °C	not provided
	Johansen et al.[73]	1132-1394 °C	~10^5 °C/s
Wire mesh reactor (WMR)	Trubetskaya et al.[43]	≤ 1700 °C	≤5000 °C/s
Flat flame burner	Schiemann et al.[27]	≤ 1597 °C	not provided

After pulverized fuel is injected into the boilers maintained at high temperatures (>1000 °C), it is reported that these fuel particles will be rapidly heated at a rate of ~10^5 °C/s.[63] To simulate the conditions for biomass inside industrial PF boilers, two basic requirements have to be satisfied: high temperature and high heating rate. A high heating rate at about 10^4-10^5 °C/s is necessary to simulate the conditions for industrial power plant furnaces.[65]

Drop-tube furnaces (DTF) or sometimes being called as drop-tube reactors are commonly used for conducting the combustion and gasification for coal and biomass in the presence of air or oxy-fuel gases.[27] Most DTF can reach high temperature >1100 °C, as many papers reported. The heating rate for DTF is in the order of 10^4-10^5 °C/s, which corresponds to the situation in PF boilers. Another advantage of DTF is that it is easier to estimate the residence time of fuel particles in DTR because their movement inside is considered linear and with constant velocity. There are slight differences in the furnace configuration of DTF used by researchers to carry out rapid pyrolysis. The DTFs used by Zhang et al.,[16] Trubetskaya et al.,[43] Panahi et al.,[7] Cetin et al.,[82] McNamee et al.,[83] are externally heated by electrical furnaces. There are other DTFs that are heated by CH_4/H_2 understoichiometric pilot flame used by Johansen et al.[73] Panahi et al. developed a DTF with a transparent quartz tube that allows direct observation of the conversion process for biomass particles.[7]

Entrained flow reactors (EFR) are also widely used to perform rapid pyrolysis at high temperatures. The EFR used by Trubetskaya et al. can be heated to 1000-1500 °C and provide heating rates up to 10^4 °C/s.[77] Lu et al. used a smaller EFR, with a syringe feeder on the top and two cyclone separators coupled after the exist of the furnace.[79] The EFR used by Dall'Ora et al. can achieve a high heating rate of $2 \times 10^4 \sim 5 \times 10^5$

and a high temperature up to 1600 °C, providing an average residence time of 1.5~2 s for biomass particles with various particle size.[76] Char particles are collected at the bottom of EFR through a sampling probe, such as the schematic diagram provided by Gil et al.[84]

There are other less common reactors for conducting rapid pyrolysis. One is the fluidized bed reactors (FBR) which cover a wide range of heating rates (10^3-10^5 °C/s) and are suitable for high heating rate pyrolysis, but the operating temperatures for FBRs are lower than PF combustion temperature, being 400-600 °C.[68] Wire mesh reactor (WMR) or sometimes called heated wire grid (HWG) usually can provide a heating rate in the order of 10^3 °C/s. It is a bit lower compared to the temperatures in PF boilers.[63] Trubetskaya et al. used a WMR that can perform at a heating rate of 5000 °C/s and a maximum temperature of 1700 °C.[43] Biagini et al. described a Platinum Filament Pyrolyzer with three parts: a pyrolysis probe, a heated interface, and a control system.[85] It can reach a temperature up to 16070 K and a maximum heating rate of 20,000 K/s. However, the actual temperature and heating rate may not be as high as the maximum value. The above-mentioned studies are summarized in Table 2.2.

2.3.3 Current studies involving char yield

Char yield and reactivity are two critical data in designing the capacity of PF boilers or gasifiers.[17, 22] As the rate of combustion or gasification is limited by the oxidation of char, low char yield but high char reactivity generated after pyrolysis is preferred to maximize the conversion capacity. Char burning rate is an essential parameter in designing PF boilers.[27] Numerous studies investigated the effects of pyrolysis temperature, heating rate, particle size, biomass species, pyrolysis atmosphere, and particle size on the properties of char samples and pyrolytic gases produced under conditions pertinent to PF combustion as stated in Section 2.3.1. However, few of them achieved an accurate quantification of char yield for biomass. This is an inevitable consequence of conducting rapid pyrolysis in DTF or EFR at high temperatures. The char collection in most DTF or EFR faces two problems: 1. Incomplete collection; 2. Mixed char particles with other products. For instance, DTF used by Zhang et al. collects the char in the bottom hopper but is not able to avoid possible coke deposition on char or the wall of the hopper.[16] The drop-tube laminar flow reactor used by

Johansen et al. not only fails to achieve acceptable char collection efficiency but also cannot collect char under desired conditions either.[74] The EFR and DTF used by Trubetskaya et al. employ a char bin at the bottom of the reactor to collect the solid particle dropped, which bring about the same problem that char collected inside the bottom is mixed with other condensable materials, such as soot/coke.[43, 77] The EFR used by Lu et al. is coupled with a staged cyclone separation, but two problems remain that 1. There is a gap between the collection probe and the outer tube, where the trapped char particles cannot be collected; 2. It is not verified that solid samples (< 25 μm) collected in the second cyclone are all char samples.[79] Dall'Ora et al. used an EFR with a cyclone and a sampling probe that was heated to 723-823 °C to avoid tar from depositing on the tube wall and the surface of char particles, but the collection may still be incomplete as the char yields they reported were based on ash-tracer method.[76]

Therefore, many studies listed in 2.2.1 conducted rapid pyrolysis in DTF, but most of them quantified char yield indirectly due to the above-mentioned difficulties in char determination. The ash-tracer method has been widely used by many researchers to calculate the char yield of biomass pyrolyzed at high temperatures.[76, 83-84] Sometimes, researchers would choose a particular element as the tracer instead of the total ash amount. Johansen et al. used Ca as the tracer to calculate the char yield of several biomass species at pyrolysis temperature of 1405-1667 K.[73] Hu et al. assumed stable contents of carbon and ash in rice husk and calculated the reaction (conversion) ratio based on the data obtained in thermogravimetric analysis (TGA).[72] Ballantyne et al. used the synthetic ash as the tracer when calculating the conversion of low-ash coal.[86] This reflects the disadvantages of using ash-tracer method for biomass char yield determination, including: 1. The more or less evaporation of ash elements during conversions has been verified by many researchers;[19, 23, 56] 2. Ash evaporation during biomass rapid pyrolysis at high temperature is noticeable, which would make the impacts of ash evaporation on the calculated char yield significant;[87] 3. The low ash contents of biomass than coal can bring higher errors due to instrument analysis.

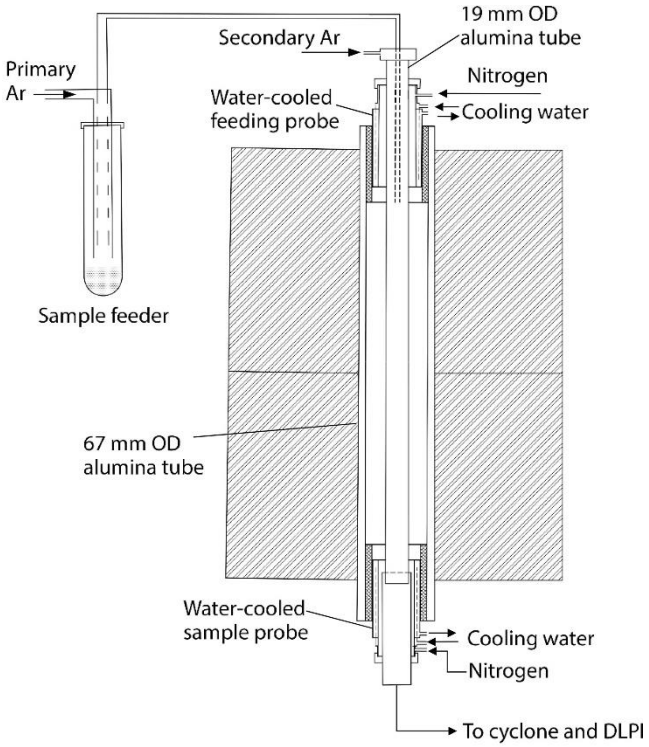

Figure 2.1 Schematic diagram of the innovative drop-tube furnace with double-tube configuration.[23]

The first study that successfully quantified the char yield after rapid pyrolysis in a DTF by experiments is conducted by Liaw and Wu, who developed a novel drop-tube furnace that deployed a unique feature of double-tube configuration (see Figure 2.1).[23] The detailed operation of this furnace can be found elsewhere.[23, 87] In brief, such configuration enables the direct determination of char yield by achieving a near-complete collection of char particles during rapid pyrolysis of pulverized biomass particles at 1300 °C. Their study also shows the significant overestimation of char yield for low-rank fuels (e.g., biomass) during rapid pyrolysis at high temperature using ash tracer method.[23]

Some studies developed other methods to determine the char yield. Leth-Espensen summarized the reported char yields obtained under conditions representative for suspension firing, then proposed a model based on chemometrics to predict the char yields. But they also admitted that more devolatilization experiments are required to replenish the database, and this model is limited by many uncertainties.[88]

2.4 Fate and behaviour of inorganic species inherited from biomass during thermal conversions

2.4.1 Inorganic species in biomass

Biomass initiatively takes the inorganic species from the soil. As the nutrients and counter ions, these inorganic species have an essential role in the growth of biomass.[89] Woody biomass contains relatively lower concentrations of inorganic species compared to herbaceous plants and other energy crops that are fertilized and irrigated regularly.[90] It is reported that inorganic species have < 1% of weight percentage in woody biomass, while they can take up to 15% of the weight percentage in herbaceous biomass.[91] However, the species of elements are various for biomass, including more than 19 metals.[92] Usually, a high amount of K and Ca is found in woody biomass. However, the detailed composition of inorganic species depends on biomass species.[32, 56] Different biomass parts (i.e., leaf, trunk, bark) show the different compositions of inorganic species.[93] For mallee wood, previous studies have shown that the ash content of mallee is 4.1%, 7.1%, and 0.6% for leaf, bark, and wood components.[93]

The review paper by Bryers firstly made a comprehensive summary of the inorganic species in biomass and their occurrence.[94] Later, a few papers are dedicated to the existing forms of inorganic species in biomass.[95] However, due to the variety of biomass, the contents of inorganic species in different biomass species and their occurrence are diverse. Therefore, it is still necessary to investigate the detailed composition and occurrence of inorganic species in the specific biomass species to better understand the reactions and conversions these inorganic species could experience.

For anion elements, Bryers stated that sulfur (S) existed as sulfates or combined with other organic species as reduced S. S is required for metabolic synthesis and can be converted to organic sulfur.[96] Chlorine (Cl) were often found as water-soluble salts, while phosphorus (P) could be phosphate salts or act as organic phosphorus. Unlike anion elements, the occurrence of metal elements is less complicated. Alkali metal elements are accumulated inside the biomass, especially for halophyte biomass such as Mallee in Western Australia, to combat the salinity. The main inorganic species are

K and Ca, being ~ 0.07% and ~ 0.131% of weight percentages for mallee wood.[23] K can bond with functional groups to form organic-associated K, which can be either stably left in char or released with other gaseous products or ejected materials.[97-98] Ca is an essential element for biomass because it bonds to carboxyl groups to contribute to the strength of cell wall. Other forms of Ca include nitrate, chloride, oxalate, and carbonates, which can be contained in biomass fluids or organic structures. Other species (such as Na, Mg) occur as positive cations. Silica (Si) is often found in grass biomass.[90] The occurrence of Si is less understood as it could be in oxidized forms or combined with other metal elements.[95] Other elements with lower contents are found in biomass, including aluminum (Al), iron (Fe), manganese (Mn), titanium (Ti).[32, 96]

Generally speaking, AAEM species are the major metal elements in woody biomass. AAEM species in woody biomass exist in two forms: organically connected to oxygen-containing groups or inorganic salts.[60] The carboxylic groups are commonly considered as the primary bonding sites for ion-exchangeable elements.[99] According to the solubility of inorganic species in different solutions, a method was proposed to clarify those species in several groups. This method was initially established for coal,[100-101] then it was also used to investigate the occurrence of inorganic species in biomass. Many studies have used and described this step-washing method. Briefly, this method involves a series of leaching in different chemical solutions, including water, ammonium acetate, acid. Elements that can be washed out by water are considered in a water-soluble state, represented by alkali chlorides, sulfates, and carbonates. Ammonium acetate can leach out those elements that are organically bound to the biomass structure, which are referred to as ion-exchangeable elements. Acid-washing can dissolve those carbonates and sulfates of alkaline earth elements, oxalates, which are classified as acid-soluble elements. After all step-leaching, those elements retained in biomass are considered as acid-insoluble elements, which normally are silicates, stable-bound elements. Shoulaifer et al. investigated the chemical forms of inorganic species in raw and torrefied birch wood, deploying this method.[96]

Apart from the inherent inorganic species inside biomass, the harvest activities, transportation, pulverization, and other processes can add more ash elements to

biomass, which will eventually cause ash-related problems. These inorganic species accumulated in biomass as inherited or contaminated can be removed by washing.

2.4.2 The impacts of inorganic species on biomass utilization

Positive effects

The intrinsic inorganic species in biomass could have positive effects on the thermal conversions of biomass.[59] Various inorganic species could be catalysts to influence the degradation rate of biomass during thermal conversions.[92]

Pyrolysis

Generally, it is believed that the catalytic effects of ash content in biomass pyrolysis are ascribed to several main elements, including Na, K, Mg, and Si.[10, 102] There are many works trying to figure out the exact effects of inorganic species on the pyrolysis, by removing inorganic species using different solutions and compare the degradation behaviour of washed and unwashed biomass.[91] Nowakowski et al. used raw and acid-washed biomass to conduct pyrolysis in TGA and studied their differences in pyrolysis rate and products.[103] TGA analysis was also conducted by Hsisheng et al. for water-washed rice hull, which had lower inorganic species contents.[104] It was found that inorganic species were responsible for lower decomposition temperature and more solid products. A similar observation of the relation between char yield and volatile yield was also reported by Shafizadeh et al.[105] Their experimental results showed a positive relationship between inorganic species contents and secondary reactions. Fahmi et al. also observed that the pyrolysis and combustion of biomass greatly depended on the inorganic species, particularly alkali metals, as they can influence the temperature and rate of biomass components degradation, as well as the degradation products. More inorganic species can facilitate the breakup of large molecules.[106] Aho et al. studied the organically bound metals by removing inorganic species then impregnated cations of K, Na, and Ca back on the pine wood. Those elements were organically combined with the biomass structure. They realized that those elements could lead to higher bio-oil yield during pyrolysis but lower char and gas yields.[106] The hydrothermal pretreatment done by Stephanidis et al. removed a part of inorganic

elements and the subsequent pyrolysis showed that reactions that happened during pyrolysis had changed due to a lack of catalytic elements, leading to more dehydration reactions, cracking reactions, aromatization, and polymerization reactions. Therefore, the pyrolysis products show higher percentages of sugars in bio-oil.[107] Considering the dependence of pyrolysis reactions on the contents of inorganic species, Liden et al. developed a model to predict the pyrolysis pathways and evaluate the effects of inorganic species.[108] Their model indicated the two main ways of inorganic species affecting pyrolysis. When contents of inorganic species are high, the main effects were considered as the scission of large or aromatic compounds and producing small molecules. In contrast, when there are few inorganic species in biomass, the depolymerization dominates the reactions, which will cause more large molecules produced. A few studies revealed that alkali metal elements can catalyze the formation of char structure.[102, 109-111]

Experiments were carried out to study the effects of inorganic species on the pyrolysis of biomass. However, most of these studies adopted mild pyrolysis conditions, which have lower temperatures and heating rates. Only several papers were found concerning the impacts of inorganic species in rapid pyrolysis at temperature > 1000 °C. Experiments done by Trubetskaya et al. illustrated the positive effect of K on char yield when pyrolysis took place at 1000-1400 °C with a heating rate of 10^3 °C/s.[78] Research on the effects of inorganic species at higher heating rates (> 10^3 °C/s) is even rarer.[43, 73, 76] Johansen et al. investigated the effects of K on the char yield under high heating rate (10^5 °C/s) and high temperature (1378–1566 K) and their data confirmed that a higher content of K facilitates the production of char even at conditions of PF combustion.[73] Trubetskaya et al. believed that the different plasticization behaviour of herbaceous biomass and woody biomass is because of the different contents of K and Ca, which could enhance the char stability and prevent melting after rapid pyrolysis.[43] Apart from the influence on pyrolysis products yield, the presence of inorganic species is reported to have influence on the shape of char particles.[43]

Other biomass thermochemical conversions

Other biomass thermal conversions, such as gasification, were found to be catalyzed by inorganic species like K,[112] and Na.[113] Those inorganic species in other forms, for example, oxide and carbonates of calcium, aluminum, and silicon, can also act as the

catalysts of gasification.[114-116] A study carried out by Zolin et al. indicated that those vaporized inorganic species could be the catalysts to promote the conversion of gaseous products.[117]

The catalytic effects of AAEM species on the gasification of char produced by the rapid pyrolysis of biomass have been well investigated by Kaijita et al.[118] They compared the gasification rate of raw char and acid-washed char and found that the gasification rate for raw char was noticeably higher than acid-washed char. They deduced that it was due to the removal of K from raw char, which was the most abundant inorganic element in their samples and had the highest removal efficiency by acid. Other researchers also recognized the important catalytic effect of K.[119] It was discovered by Kramb et al. that Ca is the main contributor to catalyzing the gasification of birch wood.[120] An interaction between different inorganic species is suspected considering the unique behaviour of raw birch wood during pyrolysis and gasification.[120]

The catalytic effects of inorganic species have been found during biomass torrefaction, which is a mild pyrolysis process at low temperatures (< 300 °C). Shoulaifar et al. investigated the mass loss of several biomass species during torrefaction at 240 °C and 280 °C.[121] By acid-washing and doping with K, Na, Ca, or Mn, they discovered that K and Na could significantly increase the mass loss of biomass, indicating the more severe decomposition during torrefaction. However, the catalytic effect of Ca on mass loss and reaction rate was reported to be negligible. Similar results were obtained by Saddawi et al.[122] They compared K played a vital role in torrefaction and the removal of it leaded to a rise in the volatile matter content and back-impregnation of K into the biomass could increase the mass loss again.

It can be found from the above studies that the individual effects of Na, K, Mg, and Ca are various and they also have different impacts during different conversions, which suggests the necessity to carry out systematic studies concerning the behaviour of AAEM species during thermal conversions, especially rapid pyrolysis which is a critical stage of biomass PF combustion.

Negative effects

Inorganic species are responsible for many unwanted problems in different equipment, including furnaces, reactors, tubes, heat exchangers, turbines, emission control devices, and many other equipment.[90]

Inorganic species can cause serious fouling, slagging deposits on the devices. For heat exchangers, fouling is a major problem caused by inorganic species. Alkali salts generated by the combustion of biomass inside a boiler will deposit on the surface of the heat-exchanging tube as some molten salt mixture[89] and this process will be exacerbated after long-time effects of inertial impaction, chemical reactions between the deposit and the gases, and thermophoresis. An aerodynamic wedge inside the tube will form if the deposit continues to grow.[90] The combustion of biomass that has abundant K, Cl, Si, and S often faces serious fouling problems, which will lead to inefficient heat transfer and deterioration from corrosion. KCl is the main contamination during the combustion of rice straw, while Ca and Mg chemicals are the main concern for wood combustion.[89] For fluidized bed reactors, inorganic species also contribute to the agglomeration of bed materials and de-fluidization in the end.[90] For example, silica sand as the common bed material of fluidized bed reactors could react with the vaporized alkali elements and form low-melting materials to damage the fluidity.[123]

Corrosion is another typical adverse result of the deposition of inorganic species on the surface of the equipment. Cl and S are considered the major elements contributing to corrosion, metal wastage, and atmospheric pollution because they can promote the release of other inorganic species, especially alkali metal elements.[90] In the meantime, Cl can form acidic solutions when in contact with moisture released by fuel inside reactors, which will cause serious corrosion for the equipment. Besides, the presence of K is also highly responsible for reducing the capacity and efficiency in the power generation plants burning biomass.[89]

Therefore, a thorough understanding of the destiny of inorganic species during thermal conversions is vital. The behaviour of inorganic species during rapid pyrolysis at high temperatures is particularly important due to the huge potential of biomass combustion in PF boilers.

2.4.3 Pathways of inorganic species during biomass thermal conversions

The presence of inorganic species would bring about problems including slugging, erosion, and corrosion for the combustion in PF boilers and de-fluidization in fluidized bed reactors during the thermal conversion of biomass.[60, 117, 124] The behaviour/release of inorganic species during pyrolysis will influence the later thermal conversion of biomass, which means it is extremely important to understand the release of inorganic species at this stage.

The release of inorganic species is mentioned by many researchers.[45] The SEM images provided by Umeki et al. showed the absorbance of released inorganic species on the char surface, which is believed to be the result of variation in the velocity of solid and gas.[45] Temperature is an important parameter for the release of inorganic species. Previous studies with coal showed that elevating combustion temperature from 500-550 °C to 1000-1300 °C results in a reduction of 20-70% in the yield of low-temperature ash or high-temperature ash.[32, 56] Okuno et al. pyrolyzed pine sawdust and sugarcane bagasse powder in a WMR and TGA at temperatures of 300-900 °C.[60] Their analysis for the contents of inorganic species in biomass and char showed that more inorganic species were released as the pyrolysis temperature increased. K is a key element in biomass. Therefore, many studies so far focus on the release of K. Some researchers believed that K has the most important role during biomass conversions, which is being the major catalyst.[103] The literature shows that K starts to react with the organic structure at around 200-400 °C. The main activity of K at this temperature is the breakage of K-C bonds and the formation of KCl and the dispersion of it throughout the structure. The true release of K begins at ~700 °C, when KCl starts to evaporate.[103] The release of K is not significant until the temperature is raised to > 700 °C.[125] High temperature can cause the transformation of organic K to K_2CO_3, which may be the reactions that are responsible for the release of K at high temperature.[64, 126] At high temperatures, Si could react with metal elements to form thermally stable constituents, such as K silicates, [97, 127] Cl which is abundant in biomass is a very volatile element which can be released in low-temperature conversion. Literature shows that at least 20-60% of Cl is vaporized at <700 °C.[62, 64, 128] Cl-containing salts such as KCl or NaCl can react with the oxygen-containing groups. These functional groups will bond to the

metal elements and form HCl, CHCl, and tar-Cl, which can be easily released at low temperature.[127, 129]

In WMR, 30% of Mg, Ca, and K were lost at 800 °C with a heating rate of 10^3 °C/s, while 20-10% of Mg and Ca, and ~60% of K were released with the heating rate being 1 °C/s. The same slow heating rate (1 °C/s) in TGA caused no release of Mg, Ca, and K, which was believed to be the consequence of the reaction between volatile and nascent char, causing desorption and re-adsorption of inorganic species in the gas phase.[62] This indicated that the heating rate contributes more to the release of Mg, Ca, and K than the temperature, and extending the reaction time facilitates the release of K more than Mg and Ca, suggesting the more stable bond of Mg and Ca with char matrix.[60] Keown et al. found that when the heating rate is > 1000 K/s, more than 80% of Na and K are released, but when the heating rate is 10 K/s, less than 20% of AAEM species would be released after pyrolysis at 900 °C.[130] The release of Cl, K, and S during combustion at temperature up to 1150 °C was determined by Knudsen et al.[62] Although the heating rate was relatively low, the release of K and Cl was rapidly increased from < 50% at 500 °C to > 80% at 1150 °C for most biomass species, while the release of S was relatively less. The release of these inorganic species was found to be related to their intrinsic properties and the biomass species. It is widely believed that Cl will facilitate the release of K by forming volatile KCl, which has been verified by Keown et al. and Bjorkman et al.[128, 130] S is also reported to contribute to the release of alkali metal elements,[90] which will worsen the ash-related problems of corrosion and pollution. Jiang et al. presented the release ratio of AAEM species at different stages of pyrolysis at 900 °C.[59] It was found that the release ratios of AAEM species continuously increase at the beginning of pyrolysis, but the release rates of Mg and Ca slow down when pyrolysis conversion reaches > 70%. Under the conditions they used, 53-76% of Na and K, and 27-40% of Mg and Ca vaporized during pyrolysis. The impacts of free radicals on the release of inorganic species were discussed. It is believed that free radicals like H could substitute the inorganic species that are bond with char matrix, thus promoting the release of inorganic species.[59, 130] Besides, the difference in the release ability of alkali elements and alkaline earth elements is clearly demonstrated in this study, that alkali elements have higher tendency of being released.[59] This is ascribed to the chemical valence of alkaline earth elements which are divalent elements with higher stability.[130-131]

Usually, the release of inorganic species is quantified by analyzing the contents of each inorganic element in biomass and char, and determining the mass yield after the conversion. However, due to the difficulty in obtaining the actual char yield of rapid pyrolysis at high temperatures, no data is available for the release of inorganic species under conditions pertinent to PF combustion. Other methods have been employed to investigate the release of inorganic species. Davidsson et al. placed a surface ionization detector inside a single-particle pyrolysis reactor which can simultaneously but indirectly detect the release of inorganic species as the pyrolysis of biomass.[89, 132] Particle size and biomass species were found to influence the release of alkali metals significantly.[89, 132] Fuel washing by water and acid was proven to be useful in reducing the alkali evaporation during pyrolysis.[89] Dayton et al. used a molecular beam mass spectrometer (MBMS) system inside the furnace to measure the relative amounts of released inorganic molecules during the thermal conversion of biomass at 1100 °C.[90]

Studies about the release of inorganic species in different occurrences indicate a few things. Firstly, water-soluble and ion-exchangeable elements are less stable and are prone to be released when heated.[133] The pyrolysis experiments done by Davidsson et al. used raw and washed biomass as feedstock. The detected signal of released alkali elements suggested that water or acid-leaching can reduce the amount of alkali elements vaporized during pyrolysis.[89] They concluded that the reason for reduced alkali elements release after washing was that the retained alkali elements in washed biomass were stably combined with the biomass structure so that the bonds between them were difficult to break up.

Parts of inorganic species are retained in pyrolytic products, such as char and bio-oil. It was mentioned that some of the retained inorganic species could stay on the surface of char when pyrolyzed at moderate temperature, and they can have catalytic effects on the formation of char structures and other conversions.[91] Therefore, a sound understanding of the evaporation of AAEM species during rapid pyrolysis of biomass at high temperatures is necessary for preventing and controlling the adverse effects of ash-related problems.

2.5 Shape and size of biomass particles and derived char particles

2.5.1 The importance of particle shape and size characterization

The importance of particle shape and size has been recognized as it concerns the transportation, fluidity, conversion rate, etc., of biomass particles. Podczeck and Mia investigated the flow behaviour of biomass particles and found that needle-like biomass particles can have a large angle of internal friction.[134] The stability of a slope of a poured biomass granular pile was studied by Robinson and Friedman.[135] The effects of particle shape were considerable as more angular particles could reduce the slope angle. The higher particle length/width ratio can significantly increase the difficulty in the shear flow of particles due to higher strength.[136] During biomass utilization, the size, shape, and density of the raw biomass particles are known to affect the feeding system, flow properties,[137] as a low aspect ratio is preferable for powder flow ability,[138-139] Tests done by Reaction Engineering International showed that wood particles only meet the requirements of flowability by mixing with coal particles, which are relatively rounder and can improve the total flowability of the fuel through the bunker.[54, 140] Particle size can also affect other physical behaviours, such as the bridge tendency of powder particles. Therefore, research has been carried out to study the various parameters of ground biomass.[141] Usually, focuses are placed on particle size, particle size distribution, particle shape, and irregularity. Several parameters are used to indicate the particle shape, such as sphericity, aspect ratio, angularity, whose definitions are summarized in Section 2.5.2. Guo et al. studied the particle shape for several biomass species and found that they all have large aspect ratios, and particles from different biomass species differed a lot for their particle size and distribution, even after the same procedure of milling.[141]

Over decades, many models of biomass/coal conversions developed by researchers assume biomass/coal particles to be spherical to simplify the question. Coal particles are generally spherical particles, whereas biomass particles after pulverization are highly irregular. Usually, for woody biomass particles, they have a needle-like shape, as stated above. However, it was found that particle size, shape, and surface area had significant impacts on pyrolysis and combustion characteristics of biomass and coal[79, 142] For biomass, Leth-Espensen et al. investigated the devolatilization process

(moderate pyrolysis conditions) and its dependence on size and morphology.[143] The experimental data and model results showed that 1. The devolatilization rates for smaller particles were much higher than large particles; 2. Elongated particles showed a higher devolatilization rate compared to spherical particles. Rezaei et al. pointed out that ignition temperature and kinetics of drying and thermal decomposition were related to the particle size and shape.[137] After the initial pyrolysis process, char particle size is also crucial as it affects the ignition temperature and emissions during the combustion stage.[144] Shiemann et al. systematically studied the effects of particle size on the char burning kinetics.[27] The initial particle shape of biomass particles and the change of shape during the combustion process were recorded by pyrometric measurements. A model was proposed to evaluate the impacts of particle shape. The experimental results showed that different particle shape has noticeable effects on the burning of char. Spherical particles showed a higher burning rate compared to long particles, which was ascribed to the ratio of mass and surface area for each particle. A similar study has been conducted by Pattanotai et al.[145] However, they used large particles (2-8 mm) with different aspect ratio to carry out slow pyrolysis at 1423 K. The effects of particle shape were clear that it could affect the pyrolysis products yield (less tar when aspect ratio higher), the reactivity of resultant char (higher reactivity for particles with low aspect ratio), the internal structure.

2.5.2 Shape and size of biomass particles after pulverization

After pulverization, biomass powders usually exhibit a wide size distribution. Different indexes were used in literature to represent the particle size distribution.

1. Cumulative mass fraction: $\mathrm{D} = \frac{d}{d_a}$, $d_i = \sum_i \frac{m_i d_i}{m}$

where D is a dimensionless index to represent particle size, d_a is the average particle size, m_i is the mass of particles in the size range of i, d_i is the average value of the upper and lower limits of the size range i, and m is the total mass of particles.

1. Rosin–Rammler distribution: $Y_d = exp\left[-\left(\frac{d}{\bar{d}}\right)^n\right]$

where n, d, and $\bar{d}$ refer to the distribution spread, the diameter of a particle, and Rosin–Rammler mean diameter, respectively.[73]

2. Frequency distribution over Martin minimal diameter: $q_3(x_{Ma,min}) = \frac{dQ_3(x_{Ma,min})}{x(x_{Ma,min})}$

where $x_{Ma,min}$ and Q_3 refer to the Martin minimal diameter and the cumulative particle size distribution normalized to the volume.[43]

Biomass particles exhibit extremely various particle shapes after pulverization. Researchers classified those biomass particles using different methods. For example, based on the aerodynamic behaviour, ground biomass particles of sawdust and poplar smaller than 300 µm are separated into categories: flake-like, cylinder-like, and equant by Lu et al.[79] Needle-shaped biomass parties has been reported for many species, including pine and miscanthus,[73]

The shape of a particle can be evaluated by several parameters:

$$\text{Sphericity} = \frac{4\pi A}{p^2}$$

$$\text{Aspect ratio: AR} = \frac{l}{d}$$

where A, p, l, and d are the projected area of a particle, the perimeter of the projection, the particle length, and the particle width.

Operational sphericity, $\varphi = \sqrt[3]{\frac{Volume\ of\ the\ particle}{Volume\ of\ Circumscribing\ Sphere}}$,[146]

2.5.3 Transformation of shape and size during thermal conversions

The transformation of particle shape and size for biomass particles after pyrolysis has been observed previously. Zhang et al. compared the SEM pictures of Hinoki cypress sawdust (<500 µm) pyrolyzed in a DTF at 600-1400 °C. They noticed that the original shape and size of biomass particles were maintained for char obtained at 600 °C, but higher pyrolysis temperature caused melting and fusion of char particles.[16] It is reported that biomass with higher silicon content tends to hold its original particle shape after pyrolysis.[73, 77] Trubetskaya et al. examined the particle shape and surface morphology for char particles after rapid pyrolysis at three temperatures between 1000 °C, 1250 °C, and 1400 °C.[43] A difference in particle shape was observed for pine char and beechwood char, with pine char particles being more spherical and smooth

on the surface, as the SEM images showed.[43] Besides, the authors also suspected that the char particle shape involves the pyrolysis temperature but stops at a certain point. The effects of pyrolysis temperature on the char particle shape were also investigated by Panahi et al.[7] They used raw and torrefied Miscanthus and Beechwood to conducted rapid pyrolysis at 975K and 1400K. Their findings are in line with the others that higher pyrolysis temperature can accentuate the deformation of biomass particles. They observed the big blowholes on the exterior of molten biomass particles that resemble cenospheres. This is due to the rapid escape of volatile matters.[83] The high heating rate causes the massive amount of volatiles generated in a short time, leading to the overpressure inside the particle. Therefore, the release of volatiles creates openings, and these new openings are left after pyrolysis is completed. Other shape transformation of biomass particles during rapid pyrolysis includes melting, swelling, plastic deformation, and fusion, which have been observed and summarized by many other researchers. The melting start temperature or fusion temperature was investigated and reported to be 739 K for wood,[147] and 722-725 K for cellulose.[148] The melting of biomass particles usually results in the decreased aspect ratio and the increased roundness, which is specifically termed as "spherodization".[7] Such phenomenon is the consequence of the softening and melting of char matrix/structure. In summary, the temperature has a key role in the transformation of biomass pyrolysis. However, among those studies, only a few have been found to quantitatively analyse the changes in particle size and shape of biomass after rapid pyrolysis.

The heating rate has been confirmed by Dall'Ora et al.,[76] Cetin et al.,[8, 82] as the other key parameter that can influence the shape of char particles. It was found that char particles pyrolyzed at 1373 K and low heating rate (10 K/min) maintain the needle-like shape as their parent biomass particles, whereas char particles pyrolyzed at the same temperature but at a much higher heating rate (10^5 K/s) lost all of the original structure and became spheres with internal cavities.[76] The melting phenomena of biomass particles are believed to be related to the depolymerization and repolymerization steps during pyrolysis.[149] The high heating rate makes these two steps take place consecutively, thus promoting biomass melting. In contrast, these two steps happen simultaneously at low heating rates, and therefore, no noticeable molten structure is observed. Another explanation for the more significant melting behaviour of biomass particles at high heating rates is proposed by Cetin et al.[82] They pyrolyzed

pine wood at 950 °C in a tubular reactor with a low heating rate and a WMR with a high heating rate. It was believed that the intrinsic pores in biomass structure allow the gradual and gentle release of volatiles during pyrolysis, which cause no apparent change to the fibrous structure. On the contrary, the high heating rate leads to the rapid generation of volatiles that are forced to be released through the molten cell structure, further damaging the structure. Besides, Solomon et al. pointed out that the slightly different rate of cross-linking can lead to significant difference in the fluidity of char.[69] For biomass pyrolysis, there are many aspects that could influence the cross-linking. For example, the higher oxygen content can facilitate the cross-linking.

Apart from the many biomass species mentioned above, Gil et al. deployed four kinds of biomass to conduct rapid pyrolysis at 1300 °C in an EFR. All of them exhibited noticeable shape changes.[84] McNamee et al. also noticed melting for Willow and Eucalyptus.[83] Such phenomenon of melting biomass particles as summarized above seems to be a general characteristic of different biomass types. Besides, it was found that the melting of particles occurs very quickly after particles being exposed at a high temperature of 1000 °C.[82]

Different biomass species always introduce variation in the contents of inorganic species. Some inorganic species such as Ca and K are known to catalyze the cross-linking reactions, leading to higher char yield. It seems that they are also responsible for the less plasticization of biomass during pyrolysis.

The effects of other pyrolysis conditions on the shape of char particles were investigated by researchers. Cetin et al. investigated the influence of pyrolysis pressure on the char morphology.[8, 82] Their analyses show that increasing pyrolysis pressure can cause the increase in char particle size and internal cavities but the decrease in the thickness of the char wall.[8] Umeki et al. qualitatively investigated the evolution of Norway spruce particles by changing the residence time of particles and found that particles <500 μm would lose their original morphology after pyrolysis conversion completed whereas particles >500 μm could reserve some structure, which can be ascribed to the lower heating rate of large particles.[45] Pretreatment for biomass, such as torrefaction, has been found to affect the final morphology of char after pyrolysis. McNamee et al. compared the char morphology pyrolyzed from raw and torrefied biomass.[83] Their SEM images show that the char particles produced from raw biomass

have smooth edges but are still elongated as entire particles. However, the deformation of torrefied biomass derived char particles appears to be more severe, which can be ascribed to the degradation of biomass structure during torrefaction. Panahi et al. compared the AR of original biomass particles and torrefied biomass particles and found that torrefaction at 275 °C for 30 min could decrease the AR, which suggested that particles became more round after torrefaction.[7] The direct observation of the initial combustion stages of a biomass particle shows that the biomass particle is surrounded by enveloping flames due to the ignition of evaporated volatile matters, and in the meantime, the biomass particles rapidly rotate and shrink, forming a spherical particle before being burnt.[7] The effects of pyrolysis atmosphere gas on the shape changes of biomass particles was studied as well.[84]

2.5.4 Summary of size and shape characterization methods for biomass and char particles

The most common method to characterize particle size is mechanical sieving.[138] There are other ways like laser diffraction,[150] Image analysis, principal component analysis (PCA) for particle shape and size evaluation.[138]

Image analysis has been widely used because images for particles provide the most direct and detailed information of the observable surface morphology. Optical microscopy was deployed by Zygourakis to study the macroporosity of char particles. Digital image analysis quantified the pore volume and surface area (>1-2 μm) for particles in images.[151] The scanning electron microscope (SEM) is the most popular tool to study the morphology details at the micro-level. For instance, Guerrero et al. qualitatively compared the morphology of char particles produced at different heating rates by their SEM images and found that the high heating rate created large internal cavities and surface openings due to the rapid release of volatile matters.[152] Panahi et al. took SEM pictures for char particles and observed the blowholes on the surface of char particles.[7] SEM analysis has also been used by Cetin et al.,[82] Gil et al.,[84] McNamee et al.,[83] However, there are disadvantages to use SEM analysis. For instance, such SEM analyses are basically visual comparison and qualitative description. Besides, SEM analysis can be biased if the observed particle represents the unusual situation. Using image analysis to conduct quantitative analysis is challenging due to

several facts. Table 2.3 revealed the difference in the number of qualitative and quantitative studies about the transformation of biomass particle shape and size. Firstly, works related to SEM images analysis usually require a massive amount of time. Secondly, a comprehensive description may need a large number of images to be taken due to the heterogeneous characteristics for each particle.[68] Lu et al. developed an algorithm to rebuild the three-dimensional structure of a biomass particle based on the images taken on three orientations, then derive the particle surface area, volume, and other parameters based on the model.[79]

Table 2.3 Qualitative and quantitative studies of the particle shape and size during the biomass thermal conversions

Studies of the particle shape and size during the biomass thermal conversions	
Qualitative studies	Quantitative studies
Zhang et al.[16] Trubetskaya et al.[43] Panahi et al.[7] McNamee et al.[83] Dall'Ora et al.[76] Cetin et al.[8, 82] Solomon et al.[69] Gil et al.[84] Umeki et al.[45]	Johansen et al.[73] Zhang et al.[16] Lu et al.[79] Biagini et al.[68]

Nowadays, there are several specialized instruments designed for quick and massive analysis of particle shape. A Netzsch CAMSIZER XT was used by Johansen et al. to collect the characteristic length for pine and miscanthus powder that were initially mechanically sieved to 63–90 and 106–125 μm using sieving screens.[73] A similar instrument but with a different brand CAMSIZER XT (Retsch) was used by Trubetskaya et al. to generate the projected area, Martin minimal and Feret maximal diameters, sphericity, and aspect ratio for biomass and char particles. The advantage of this instrument is that its air pressure dispersion can avoid the agglomeration of particles and provide the true dimensional parameters for individual particle.[43] Another laser diffraction instrument SEISHIN, LMS-30 with water and methanol as the dispersion medium was used to analyse the particle size of char particles, the minimum diameter being 1 μm.[16]

The cross-sectional structure of char particles is rarely reported. Research done by Cetin et al. shows the cross-sectional images of char particles pyrolyzed at different pressure. They found that higher pyrolysis pressure can produce char particles with thinner particle wall and larger size.[82]

2.6 Biomass upgrading via torrefaction

2.6.1 Torrefaction and its impacts on the properties of biomass

Biomass accounts for the largest proportion among renewable energies (including biomass, solar, wind energies) so far.

The utilization of biomass is hindered because of its disadvantages, including high moisture content and low energy-density. The high moisture content due to the hydrophilic nature of biomass feedstock not only increases the cost of thermochemical conversion,[153] but also makes biomass not suitable for long-term storage.[154] Fibrous properties lead to high energy consumption for grinding; poor spherical shape causes poor fluidization behaviour and low flowability.[155] heterogeneity of biomass makes process design and control more complicated. A pretreatment technology (Torrefaction) for biomass was proposed aiming to mitigate those disadvantages of biomass.

Torrefaction can be defined as the heat treatment of biomass in an inert environment and under a temperature of 200 °C-300 °C. This has become a promising pretreatment method that can convert biomass to energy-intensive solid fuels with higher grindability and lower moisture content. During the torrefaction process, biomass will partially decompose and release various types of volatile substances. These volatile substances can be divided into condensable volatile substances (including water and acid) and non-condensable volatile substances (including CO and CO2). The impacts of torrefaction on the properties of biomass are listed below:

Grindability

In lignocellulosic biomass, cellulose microfibers are embedded in a hemicellulose matrix, where hemicellulose and cellulose are densely packed by the lignin layer. After torrefaction, biomass cell walls are destroyed and a part of the hemicellulose is

removed. This microstructure change can significantly improve the torrefied biomass grindability. Under the same grinding conditions, the improved grindability of biomass leads to an increase in the weight percentage of fine particles, which is the desired feedstock for the utilization in PF boilers[155] In other words, torrefaction can also reduce energy consumption for grinding torrified wood chips by ~90%, compared to raw wood chips.[46]

Moisture content

As a high moisture content will cause high energy loss during thermal conversion processes (e.g., combustion, pyrolysis), it is important to reduce the moisture content of biomass. For example, the water content of biomass feedstock is required to be less than 30 wt % (preferably, < 15 wt%) in the syngas production process and less than 10% by weight in the pyrolysis process.[156] Reducing water content of biomass can directly increase the energy density, improving the quality of product and reducing emissions during the combustion process.[157] In general, the water content of biomass ranges from 30 to 60 wt%, depending on biomass feedstocks, storage method, time of harvest.[156] Wu's et al. work has shown that the torrefaction process can significantly reduce moisture content in biomass, as the biomass has been converted to be hydrophobic.[158] For example, Felfri et al. reported that the moisture content in wood briquettes was approximately reduced by 73% after torrefaction.[159] When the biomass is torrefied, the hydroxyl groups will be partially destroyed and water will be released from biomass.[160] This can make biomass become hydrophobic by preventing the formation of hydrogen bonds.[161]

H/C and O/C ratio

Torrefaction changes the chemical composition of biomass, which upgrades the fuel properties of biomass. The carbon content of the torrefied biomass increases as the torrefaction temperature increases, while the hydrogen and oxygen content decrease due to the release of hydrogen- and oxygen-rich volatiles (e.g. water and carbon dioxide),[3] resulting in the decrease of H/C and O/C ratios.[162] Torrefied woody biomass has a similar chemical composition to sub-bituminous coal under high temperature and long residence time and can be directly used for gasification and co-firing as well.[163]

2.6.2 Rapid pyrolysis of torrefied biomass and the products

During the pyrolysis process, non-torrefied biomass undergoes a three-stage reaction with increasing temperature:[164] evaporation of free water in biomass feedstock; main decomposition; a slow period of degradation; formation of bio-char; secondary/tertiary reactions between pyrolysis products. Because of the char-like thermal properties of torrefied biomass, the starting temperature of pyrolysis of such biomass samples increases,[165] and pyrolysis peak temperature increases with increasing torrefaction temperature.[166]

The torrefaction process will significantly affect the pyrolysis products in terms of product yields and chemical composition.[167] For example, as the torrefaction temperature increases, pyrolysis of torrefied biomass produces less bio-oil,[168] more char,[165] and a similar amount of non-condensable gas.[169] Wannapeera and co-workers reported that the higher char yield is due to the cross-linking reaction during torrefaction.[170] The biochar produced from pyrolysis of torrefied biomass shows lower activity, relatively poor mechanical strength, and lower specific surface area.[171] The adsorption performance of the biochar produced from pyrolysis of torrefied biomass is improved.[172]

The moisture content of the bio-oil produced from the pyrolysis of torrefied biomass significantly drops, indicating that fuel properties of bio-oil have been improved compared to non-torrefied biomass.[173] The heating value of the bio-oil produced from pyrolysis of torrefied biomass becomes higher because the oxygen content reduces, but the bio-oil yield significantly decreases.[174] Moreover, the acidity of the produced bio-oil decreases with an increasing degree of torrefaction,[175] which reduces corrosion in bio-oil.[176]

With recent improvements in the conversion process, pyrolysis of torrefied biomass has become promising.[164] Researchers have been focused on a low to medium temperature (< 900 °C), and there are little studies on the pyrolysis of torrefied biomass at a high temperature (≥ 1100 °C).[177] The effects of torrefaction temperature on the properties of bio-char produced from pyrolysis of torrefied rice straw at 800 °C, 1000 °C, and 1200 °C were investigated.[171] It was found that char yields increase with increasing torrefaction temperature. Li et al. studied the size distribution of char

samples produced from torrefied and non-torrefied forest residue at 1200 °C, and ash-tracer method was used to determine the carbon and other organic element conversions of these char samples.[178] However, due to the evaporation of ash-forming elements, the ash-tracer method might not be accurate. Thus, it is vital to find a method to directly determine the char yield of rapid pyrolysis of torrefied biomass.

2.7 Biomass upgrading via leaching process

2.7.1 The significance of biomass leaching and its impacts

The deposit of inorganic species on the equipment surface can be mitigated if the concentrations of inorganic species in fuel gases can be reduced.[90] Biomass washing is the critical step to tackle ash-related issues during pyrolysis, gasification, and combustion by decreasing the reaction rate between deposits and gaseous inorganic species.

Table 2.4 summarizes some examples of biomass leaching. Generally, water washing is used as a common pretreatment method to remove AAEM and other inorganic elements (such as Cl, S, and P). Water washing is also used as the first step in sequential leaching of biomass to quantify water-soluble compounds in biomass.[95] Moreover, some researchers used water washing method to remove AAEM species from biomass to study their effects on pyrolysis of biomass,[110] the product yields, and compositions of bio-oil.[179]

Table 2.4 Previous studies of biomass leaching

Reference	Purpose of leaching	Methods
Wu et al.[180]	To quantify the nutrients from biomass components and the derived biochars	Batch
Arvelakis et al.[181]	Pre-treatment method. To remove water-soluble Na, K, and Cl from biomass to prevent agglomeration problems in a gasifier	Batch

Jenkins et al.[182]	Pre-treatment method. To remove Na, K Cl in biomass to reduce slagging and fouling in a furnace.	Batch, water spray, and flushing
Turn et al.[183]	Pre-treatment method. To remove inorganic elements in biomass to prevent ash-related issues in thermochemical conversions.	Mechanical dewatering and leaching
Davidsson et al.[89]	Removing AAEM from biomass to study its effect on AAEM release during pyrolysis	Semi-batch
Arvelakis et al.[184]	To remove water-soluble and ion-exchangeable inorganic elements in biomass	Batch
Skoulou et al.[185]	Pre-treatment method. To study the effect of leaching of hydrogen production during biomass gasification	Batch
Werkelin et al.[95]	Water leaching is the first step of chemical fractionation.	Batch
Jensen et al.[110]	Pre-treatment method. To study the effect of KCl on biomass pyrolysis	Batch
Mourant et al.[179]	Pre-treatment method. To study the effect of AAEM on the yield/composition of bio-oil	Batch

Biomass water leaching as a pretreatment strategy

The leaching method is mainly used to remove or reduce AAEM species and other elements in the biomass, as most of them are soluble in water (see Table 2.4). For example, Turn and co-workers reported that the combination of leaching method and mechanical dewatering of biomass could remove 98% of Cl, 90% of K, 68% of Na, and 72% of P, in addition to the reduction of 45% of ash.[183] Dayton et al. found that

leaching of various biomass samples can remove 55% of Na2O, 83% of K2O, 91% of Cl, and 51% of MgO on average.[90] The removal of these elements greatly reduces the ash-related issues during biomass gasification and pyrolysis. Arvelakis and co-workers reported there were no deposition or caking problems during the combustion of water-washed olive residues.[186]

Leaching of Organic Matter from Biomass

In addition to inorganic species, organic matters can also be removed when biomass samples are washed with water. Turn et al. found that sugar monomers accounted for ~ 4wt % of biomass (dry basis) that can be leached.[183] Recently, Wu and co-workers found that 30 % of organic matters were leached from mallee leaves, possibly because mallee leaves have high extractive contents.[180] In addition, various studies have been conducted on biomass as an adsorbent for metal pollutants. For example, organic matter is leached from the absorbent prepared from seaweed.[187-188] Other researchers have also reported that organic matter is leached from algal biomass to remove metal contaminants,[189] and organic matter can be leached from wood and bark materials.[190] The leaching of organic matters from biomass after a water-washing method may result in acidic leachate. For instance, Arvelakis and coworkers found that the pH of the water leachate decreases during wheat straw leaching.[191]

2.7.2 Thermochemical processes of leached biomass

Combustion and Gasification of Leached Biomass

Biomass can be directly burned to produce heat and power. However, the use of raw biomass in conversion systems such as fluidized bed reactors is associated with serious ash-related problems, which can lead to severe operating problems (e.g., agglomeration, deposition, and corrosion). Arvelakis et al. reported that leaching had been proven to significantly reduce the ash-related operating problems during the combustion of wheat straw samples.[186] However, the authors still found that the agglomeration occurred during combustion tests with leached wheat straw samples. This is because the discharge of AAEM species and chlorine from the wheat straw during the leaching process is limited, which can still cause ash-related problems afterward. But the problems were much lesser compared to those from the combustion

tests with raw wheat straw samples. Some researchers had reported similar results,[182] and more studies are required to understand the mechanism of leaching.

Ash-related problems have also been found during gasification processes. Researchers found that K and Cl in ash are the most important factors causing operating problems during gasification.[192-193] Therefore, ash-related problems can be addressed by removing those elements. For example, Arvelakis and coworkers reported that using leached biomass samples could significantly reduce the agglomeration problems than using untreated biomass samples during gasification.[184] Because most AAEM species and Cl in ash have been washed out via leaching methods, thereby reducing agglomeration and deposition problems during gasification.

Pyrolysis of Leached Biomass

Tan et al. reported that the contents of metallic elements in biomass decreased after being washed with hydrochloric acid (HCl), which leads to an increase in the release rate of volatiles during pyrolysis.[194] The increase in the release rate of volatiles leads to an increase in bio-oil yield but a decrease in secondary reactions of volatiles. Cellulose pyrolysis produces a higher yield of bio-oil compared to lignin and hemicellulose, whereas they produce more char and gas.[195] Strong acid washing reduces the amount of hemicellulose and cellulose in the biomass due to hydrolysis, thus increasing the proportion of lignin. This finally leads to a decrease in bio-oil yield but an increase in the yield of char and gas.[196] Fahmi and co-workers studied the contents of lignin and inorganic species on pyrolysis of biomass. They found that the yields of bio-oil samples produced from washed biomass samples were much higher compared to those produced from raw biomass samples.[197] According to results in this paper, a lower level of water is produced if ash/metals are washed, resulting in a higher heating value of the bio-oil and lowering the possibility of phase separation. This means that more stable bio-oil samples can be produced after biomass washing as a pretreatment method. Besides, this idea was also confirmed by Bank et al.,[198] who found that the yield of bio-oil produced from Triton X-100 (surfactant) washed biomass was 76.21 wt.%, in comparison to untreated biomass (64.05 wt.%) and water washed (64.13 wt.%). The Triton X-100 washed bio-oil had the lowest water content than other bio-oil samples produced from pretreated and raw biomass. They believed

more bio-oil was the result of less inorganic species in biomass, which significantly reduces secondary reactions during pyrolysis.

samples produced from torrefied and non-torrefied forest residue at 1200 °C, and ash-tracer method was used to determine the carbon and other organic element conversions of these char samples.[178] However, due to the evaporation of ash-forming elements, the ash-tracer method might not be accurate. Thus, it is vital to find a method to directly determine the char yield of rapid pyrolysis of torrefied biomass.

2.8 Conclusions and research gaps

From the literature review above, there are a few conclusions that can be made:

- Mallee biomass is an important energy resource with a high potential for local renewable energy improvement.
- Biomass combustion in existing pulverized coal boilers is an attractive technology as it is economically efficient. However, it still faces many problems due to the different properties between biomass and coal.
- The rapid pyrolysis of biomass under conditions pertinent to PF combustion receives increasing attention because the reactions that happened during rapid pyrolysis will influence the subsequent combustion stage. The properties of char produced after pyrolysis significantly affect combustion behaviour.
- A major problem regarding the studies of rapid pyrolysis at high temperatures for biomass is the determination of char yield due to the limitation of experimental instruments. The ash tracer method has been widely used. It is based on the assumption of no loss of ash elements during rapid pyrolysis. However, several papers have observed the evaporation of inorganic species for biomass rapid pyrolysis at high temperatures, which suggests the unreliability of the ash-tracer method. Although DTF is ideal to simulate the conversion of biomass under PF conditions, yet so far, most of the works done in DTF still use the ash tracer method to determine char yield.
- A few works have been done on the fate and behaviour of inorganic species during the conversion of biomass at temperatures <1000 °C. A common finding is that those major or minor inorganic species in biomass are subject to different extents of evaporation during the conversion, which can be

determined quantitatively. However, there is very little work in literature that revealed the behaviour of inorganic species during rapid pyrolysis of biomass at high temperatures (>1000 °C). This could be the result of inaccurate char yield that prevents the quantification of element retention. No direct data had been found concerning the release of inorganic species under PF combustion conditions and thus it is unknown the extent of evaporation for biomass when going through rapid pyrolysis at high temperature.

- TGA is the most common method to investigate the evolution of biomass particles during pyrolysis. However, the heating conditions for biomass experienced in TGA are not comparable to the conditions of rapid pyrolysis, which means those data obtained by TGA cannot be comparable to the actual reactions happened under PF conditions and is not reliable to guide the future industrial biomass application.
- Biomass particles show diverse and irregular shapes after pulverization, which is an essential step for biomass PF combustion. Studies on the shape and size distribution of biomass particles showed their complexity. Besides, previous researches revealed that most biomass particles went through deformation (plasticization/ melting/ swelling) during rapid pyrolysis, especially at high temperatures and high heating rates. But a quantitative study has not been found regarding the change and transformation process of particle shape during biomass rapid pyrolysis.
- Torrefaction and leaching are two useful pretreatment methods to improve the properties of raw biomass. Studies have been carried out focusing on the effects of torrefaction/leaching on the properties of torrefied/leached biomass and their thermal conversion behaviour under mild/moderate pyrolysis conditions (heating rate $<10^3$ °C/s, temperature <1000 °C). Nevertheless, it is extremely important to understand the pyrolysis performance of the pulverized biomass fuels treated by torrefaction/leaching.

Therefore, further research and development are required to address the above-mentioned research gaps, including:

- Investigating the impacts of pulverized biomass powder with wide particle size distribution on the properties of char particles after rapid pyrolysis at high

temperature. The previous studies did not reveal the true char yield for biomass pyrolysis carried out at high temperatures and high heating rates (~10^4-10^5 K/min). But the modified drop-tube furnace can realize experimental determination of char yield at 1300 °C. The dependence of particle shape and release of inorganic species on particle size during pyrolysis needs to be studied.

- A study for the evolution of biomass during rapid pyrolysis at high temperatures is necessary as precious studies about the pyrolysis evolution were usually done in a thermogravimetric analyzer. The actual progress of solid mass loss should be reported. The data about the gradual release of inorganic species as the evolving pyrolysis are important to help understand the transformation of inorganic species. Characterization of the evolution of particle size and shape is vital when modeling the reaction rate.
- Torrefaction as a promising pretreatment method for biomass has been used to improve biomass fuel properties. The true char yields of torrefied biomass during rapid pyrolysis at high temperatures need to be reported. Analysis on the retention of inorganic species for torrefied biomass should be carried out to evaluate the effects of torrefaction temperature on ash-related problems. The changes in particle size and shape for biomass with different torrefaction temperatures require detailed investigations as particle size and shape are important factors to the oxidation of char. The actual situation of industrial utilization of biomass wood chips has to be considered. A comparison of particle size and shape for biomass powder particles pulverized from raw and torrefied wood chips is required.
- Biomass leaching would cause variation in the occurrence of retained inorganic species. Therefore, it is of great importance to understand the evaporation ability of retained inorganic species during rapid pyrolysis under conditions pertinent to PF combustion. The lack of inorganic species for biomass can cause changes in particle size and shape for char particles after rapid pyrolysis, which should be carefully studied.

2.9 Research objectives of the current study

The above literature review has identified a few research gaps for biomass combustion in PF boilers/furnaces. Limited by the timeframe of this Ph.D. study, this thesis aims

to fill up some of the research gaps mentioned above. Focuses will be placed on the experimental/true char yield of biomass, the release of inorganic species from biomass, and the evolution of particle size and shape, during the rapid pyrolysis under conditions relevant to PF combustion. The detailed objectives of this Ph.D. study are listed below:

(1). To investigate the effects of biomass particle size on the properties of char derived from biomass rapid pyrolysis at high temperatures.

(2). To understand the evolution of biomass rapid pyrolysis by characterizing the evolving physical and chemical properties of char samples.

(3). To study the effects of torrefaction temperature on the subsequent rapid pyrolysis of torrefied biomass powders and the properties of their char.

(4). To examine the particle size and shape of torrefied biomass by simulating the industrial biomass utilization steps by conducting the torrefaction of wood chips first, before pulverizing and sieving.

(5). To study the impacts of leaching as a pretreatment method for biomass by analyzing the physical and chemical properties of leached biomass and their char samples after rapid pyrolysis at a high temperature

CHAPTER 3 RESEARCH METHODOLOGY AND ANALYTICAL TECHNIQUES

3.1 Introduction

This chapter will introduce the research methodology employed in this Ph.D. study to achieve the objectives outlined in CHAPTER 2. The experiments and analysis methods will be described in detail in Sections 3.3 and 3.4.

3.2 Methodology

This Ph.D. study focuses on the rapid pyrolysis of biomass at high temperatures, which is relevant to the conditions of PF combustion. Two biomass species (mallee wood and pine wood) were studied. Several experiments were carried out to achieve the objectives listed in Section 2.9, which include:

- Rapid pyrolysis in the modified DTF for raw biomass particles with different size fractions.
- Mallee wood was subjected to rapid pyrolysis with various residence times and the properties of pyrolysis products were analysed.
- Torrefaction of biomass powder and wood chips in a drop-tube/fixed bed quartz reactor at different temperatures.
- Leaching of mallee wood powder in semi-continuous and batch mode with water and acid, respectively.
- Rapid pyrolysis of pretreated (torrefied or leached) biomass in the modified DTF.
- Image analysis of biomass and char particles using an optical microscope or scanning-electronic microscope, and image processing software (ImageJ).

Experiments and sample characterization were repeated at least twice to ensure reproducibility. Image analysis was applied to hundreds of particles. An overview of the research methodology is depicted in Figure 3.1.

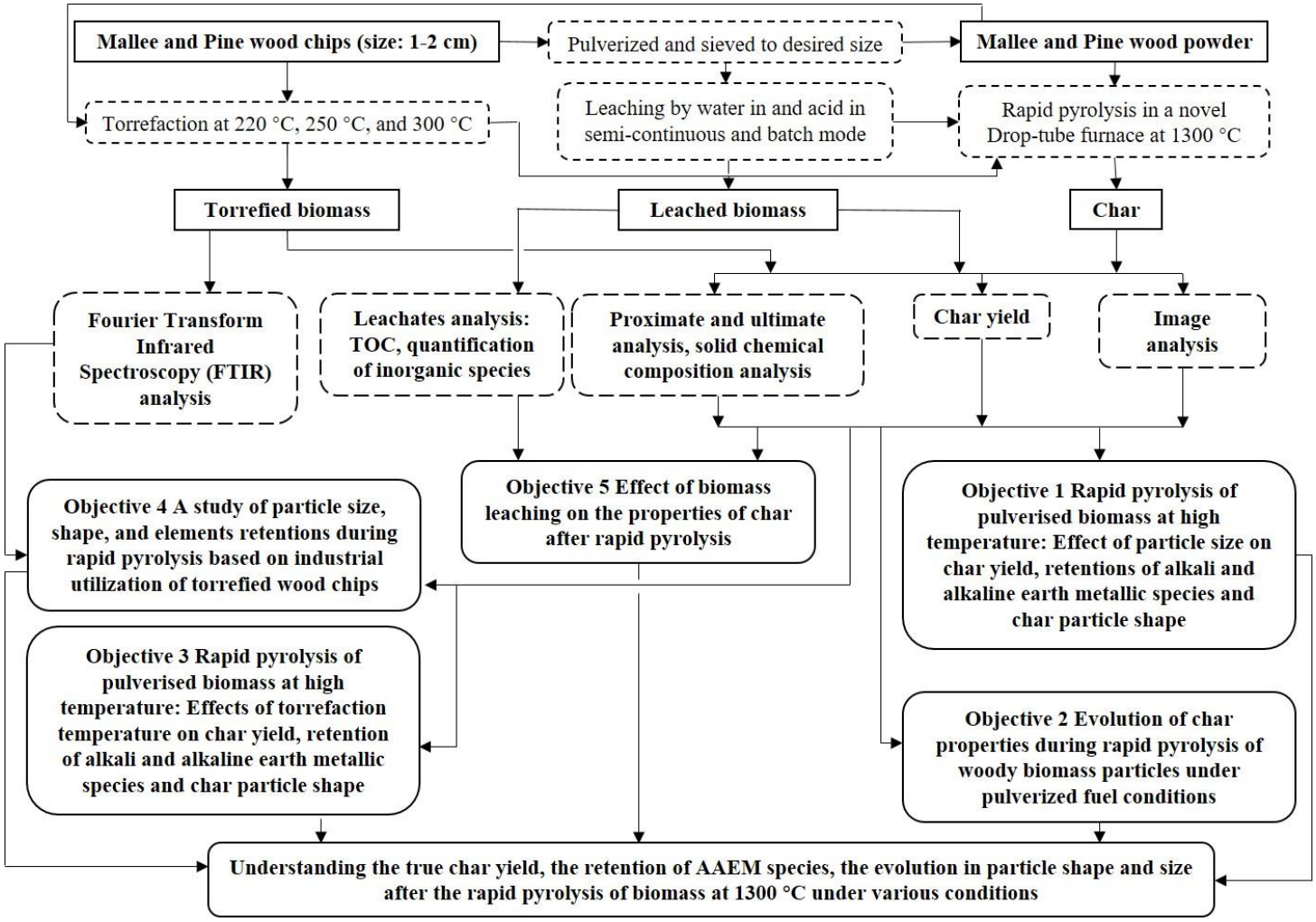

Figure 3.1 Overall research methodology and linkage to research objectives

3.2.1 Effect of particle size on char yield, retentions of AAEM species, and char particle shape

Biomass powders (mallee wood and pine wood) were mechanically sieved to 3 size fractions to study the effects of particle size on the char properties after rapid pyrolysis of biomass (see Section 3.3.1 and Section 3.3.2) at conditions pertinent to PF combustion. The proximate and ultimate analysis, as well as the inorganic composition of char samples with different sizes were conducted (see Section 3.4.2, Section 3.4.3, and Section 3.4.4). Focuses were placed on the experimental char yield obtained in a novel double-tube drop-tube furnace (see Section 3.4.1). The chemical properties of char samples revealed the discrepancy in composition and retentions of AAEM species of biomass with different particle sizes. A model was established to evaluate the heating rates for biomass particles. The impacts of particle size on the morphology of char particles were studied based on image analysis via optical microscope and scanning electron microscope (SEM) (see Section 3.4.7). The results and discussion can be found in CHAPTER 4.

3.2.2 Evolution of char properties during rapid pyrolysis of biomass at high temperature

The evolution of biomass rapid pyrolysis was investigated by adjusting the residence time of biomass particles (mallee wood in size fraction of 250-355 μm) in the novel drop-tube furnace, which was achieved by varying the flow speed of carrying gases for biomass particles. Char samples with different residence times were collected and subjected to proximate and ultimate analyses, chemical composition analysis, and image analysis. Based on the collected data, the change of char yield with time, the gradual release of AAEM species from biomass, and the evolution of char particle shape with time were derived. The contents of structural carbohydrates were quantified via a National Renewable Energy Laboratory (NREL) method (see Section 3.4.6). The occurrence of AAEM species in partially pyrolyzed char and completely pyrolyzed char was examined by the chemical fractionation analysis (see Section 3.4.5). The results and discussion for this part are stated in CHAPTER 5.

3.2.3 Rapid pyrolysis of pulverized biomass at high temperature: Effects of torrefaction temperature on char yield, retention of alkali and alkaline earth metallic species and char particle shape

Biomass powder (mallee wood) was sieved to the size fraction of 150-250 μm firstly. Torrefaction experiments were carried out in a drop-tube/fixed bed quartz reactor at three selected temperatures: 220 °C, 250 °C, and 300 °C (see Section 3.3.3). Torrefied biomass samples and the raw biomass sample were all subjected to rapid pyrolysis in the novel drop-tube furnace. Char yields for these samples were determined. Proximate and ultimate analyses were conducted to study the pyrolysis extend of different samples. The retentions of AAEM species were calculated based on the inorganic composition of char samples. The chemical fractionation analysis was applied to raw biomass and torrefied biomass samples, and their char samples after rapid pyrolysis to investigate the effects of torrefaction on the occurrence of AAEM species in biomass and the derived char samples. Image analysis to study the change of shape was carried out for biomass particles before and after torrefaction, as well as char particles. The detailed results are presented and discussed in CHAPTER 6.

3.2.4 Wood chips torrefaction, pulverization, and rapid pyrolysis

Wood chips of mallee and pine proximately in the size of 1-2 cm were torrefied in a drop-tube/fixed bed quartz reactor using the same method as described before. They were kept at the desired torrefaction temperature (220 °C, 250 °C, and 300 °C) for 30 min. The torrefied wood chips, as well as the raw wood chips, were pulverized with the same conditions before being sieved to get two size fractions: 90-106 and 250-355. The effects of torrefaction on the shape of pulverized biomass particles were investigated via image analysis. The main functional groups in torrefied biomass were determined by Fourier Transform Infrared Spectroscopy (FTIR) analysis (see Section 3.4.8). Sieved biomass samples were then pyrolyzed in the novel drop-tube furnace at 1300 °C. Char yields for samples were determined, and proximate & ultimate analyses were conducted for char samples. The retentions of AAEM species were obtained by the data of inorganic species in samples to investigate the influence of torrefaction and particle size. Image analysis was also applied to char particles. CHAPTER 7 includes the results and discussion for this study.

3.2.5 Effect of biomass leaching on the properties of char after rapid pyrolysis

Mallee wood particles in the size fraction of 250-355 μm were subjected to water-leaching and acid-leaching, which were realized through a batch reactor and a semi-continuous reactor (see Section 3.3.4). The leached carbon in leachates was quantified. The quantification of inorganic species composition in raw mallee wood and leached samples was used to determine the leaching efficiency of water and acid (0.1 M hydrochloric acid) regarding AAEM species. Raw and leached biomass particles were used for rapid pyrolysis in the novel-drop-tube furnace to determine the char yields for them. Proximate and ultimate analyses, as well as the quantification of inorganic species in raw & leached biomass and their char samples, were conducted. Image analysis was applied to study the change of shape after leaching and the impacts of leaching on the morphology of char particles. The results and discussion are covered in CHAPTER 8.

3.3 Experimental

3.3.1 Sample preparation

Mallee (Eucalyptus) is locally grown in Western Australia and has huge potential as an energy crop to substitute fossil fuels. Therefore, This Ph.D. study chose mallee wood as one of the research focuses. Pine wood has been widely investigated due to its international abundance. Researches were also carried out using pine wood as a comparison and reference to the behaviour of mallee wood during thermal conversions. Mallee wood and pine wood are categorized as hardwood and softwood, respectively.

Locally harvested mallee wood and pine wood were chipped in a factory and delivered to the lab. Wood chips were sun-dried for days and stored in a fridge at a temperature <4 °C. Before experiments, wood chips were pulverized using a rotor mill (model: Retch ZM 200) with a screen sieve being 0.5 cm. After pulverization, biomass powders were mechanically sieved to three size fractions: 90-106 μm, 150-250 μm, 250-355 μm. Those size-fractionated biomass samples were stored in sealed plastic bags. Before usage, biomass powders were oven-dried at 60 °C overnight and placed at room temperature for several days to reach moisture equilibrium.

3.3.2 Rapid pyrolysis of biomass in the novel Drop-tube furnace

Rapid pyrolysis of biomass was carried out in the novel drop-tube furnace developed by Liaw and Wu.[23] The new design was based on a drop-tube furnace which consisted of the external electrical furnace and the internal alumina tube where reactions took place. The maximum operating temperature for the furnace was 1600 °C, with approximately 600 mm of the isothermal zone.[199] Usually, biomass particles were directed to the alumina tube with 67 mm outer diameter (OD). Char particles free-fell through a water-cooling probe and were collected in a DEKATI cyclone which could segregate particles with aerodynamic particles >10 μm. However, previous studies have demonstrated that a good mass closure using this collection method was not achievable,[19, 23, 56] due to some particles being trapped inside the furnace, including possible places as the inclined surface of the water-cooling probe. The novelty of this design was to achieve a near-complete collection of char particles via a double-tube configuration. A smaller alumina tube (OD: 19 mm) was placed inside the 67 mm OD tube as the area where reactions happened. The bottom of the small alumina tube was inserted into a stainless-steel tube which was directly connected to the DEKATI cyclone. During experiments, biomass powders were entrained into the small alumina tube by a stream of argon (1.0 L/min). On the top of the furnace, a water-cooling probe prevented the early heating of biomass, and another stream of argon (0.2 L/min) was added to avoid the possible back-flow of biomass due to the released volatiles. The pyrolysis products including char, soot, and volatiles, were directed to the DEKATI cyclone through the stainless-steel tube, where a flow of nitrogen (2.4 L/min) was added into the space between the bottom water-cooling probe and the stainless-steel tube, which would go through the stainless-steel tube and cyclone. Between the annulus space of the small and large alumina tubes, a 5.2 L/min flow of nitrogen was introduced. These nitrogen flows could help prevent deposition on the tube wall and forced particles exiting the small alumina tube to enter into the stainless-steel tube and cyclone. Char particles with an aerodynamic diameter >10 μm were collected in a cyclone. A 13-stages DEKATI low-pressure impactor (DLPI) with a backup filter was attached to the outlet of the cyclone to determine the mass distribution of fine carbonaceous materials (CM) based on their aerodynamic diameter. This DLPI can fractionate CM into <0.1 μm, 0.1-1 μm, <1 μm, 1-10 μm, and <10 μm, which are denoted as $CM_{0.1}$, $CM_{0.1\text{-}1}$, CM_{1}, $CM_{1\text{-}10}$, and CM_{10}. It was demonstrated in a previous

study[200] that the CM with aerodynamic diameter <1 μm (CM_1) is soot, while CM with an aerodynamic diameter of 1-10 μm (CM_{1-10}) consists of dominantly char fragments.

3.3.3 Torrefaction

A drop-tube/fixed bed quartz reactor was used to conduct torrefaction of biomass for studies in CHAPTER 6 and CHAPTER 7. The clean quartz reactor was pre-loaded with biomass (powder or wood chips) and weight before being inserted into the electric furnace. The furnace and quartz reactor can operate at temperatures ≤1000 °C. The thickness of biomass samples inside the quartz reactor was <3 cm due to the isothermal zone being ~10 cm. A K-type thermocouple was inserted into the reactor and placed about 1 cm above the biomass samples to monitor the actual temperature of biomass. A stream of argon gas (2.0 L/min) was introduced from the top of the reactor to swap out the initial air and volatiles generated during heating. The furnace was turned on after 5 min of argon flowing to ensure the inert atmosphere inside the reactor. The heating rate was set to be 10 °C/min. Once the thermocouple reached the desired temperature (220 °C, 250 °C, and 300 °C), the reactor was maintained at the temperature for 15 min (for biomass powder samples in CHAPTER 6) or 30 min (for biomass wood chips samples in CHAPTER 7) and then immediately lifted out of the furnace to allow natural cooling. The argon gas was continuously swapping out the volatiles and helped cooling. After biomass samples reached the room temperature, the condensed volatile attached to the surface of reactor (bio-oil) was cleaned before weighing again to determine the yield of solid products.

3.3.4 Biomass leaching

Water-leaching and acid-leaching were carried out for mallee wood powders (250-355 μm). Water-leaching adopted the semi-continuous leaching method as described elsewhere,[201] to maximally avoid the loss of organic matters and acidifying the leachate. Briefly, a ~0.5g mallee wood powder was placed inside the special leaching tube, which is a cylinder enclosed by two stainless steel filters at each end. The leaching tube was then connected to an HPLC pump (Model: Alltech 627) by one end, and the other end was connected to the leachate bottle that was thoroughly cleaned by ultrapure water and dried prior to the leaching process. The HPLC pump delivered a stream of ultrapure water to flow through the leaching tube with a constant flow rate

of 100 mL/min. The contents of inorganic species and total organic carbon (TOC) in the leachate were analysed every one hour as an indicator for the extent of leaching process and the leaching process was considered as completed once the contents of inorganic species and TOC in the leachate cannot be detected. 0.1M of HCl solution was prepared to perform acid leaching in a batch leaching reactor for 6 h with continuous stirring. The weight ratio of biomass/0.1M HCl was kept at 1:100 to minimize the effect of organic acid leached out. The leached mallee wood samples were dried in an oven at 105 °C overnight and the leachates were subjected to further analysis of inorganic species and TOC. Three batches of water and acid leaching experiment for mallee wood were carried out at room temperature and all the leached biomass samples from different batches of leaching were well-mixed and stored for later experiments, while the water and acid leachates were also collected to analyse the total contents of leached inorganic species and TOC.

3.3.5 Determination of the temperature distribution inside drop-tube furnace

The exact length of the isothermal zone was required for the estimation of residence time of particles inside the isothermal zone for the research in CHAPTER 5. Therefore, the temperature profile inside the drop-tube furnace which was maintained at 1300 °C with different gas flow rates was manually detected. The drop-tube furnace was firstly heated to 1300 °C then the gas of a particular flow rate was introduced for a while to make the system stabilized. Due to the limitation of type-K thermocouple, these thermocouples could not resist 1300 °C for a long time. Therefore, the length of isothermal zone was determined by the total length of the furnace minus the total length where temperature < 1300 °C ± 25 °C. The temperature limit was not exactly 1300 °C was because of the temperature fluctuation inside the furnace, which was discontinuously heated once the temperature reached the target temperature. A type-K thermocouple was inserted from the top and bottom of the furnace with marks on it to measure the length. Once the thermocouple detected temperature within 1300 °C ± 25 °C, the length of how long it had been inserted was recorded and it would be pulled out immediately. The tip of thermocouple was avoid from contacting the wall of the small alumina tube because the wall temperature can be higher than the ambient temperature. The lengths of isothermal zone under five gas flow rates used in CHAPTER 5 were measured.

3.3.6 Estimation of particle average heating rate and average residence time

The average heating rate experience by biomass particle of three different particle size fractions was estimated using the heat transfer equation below, similar to the method used by Hayashi et al.[202]:

$$mC_p \frac{dT_p}{dt} = hA\left(T_{gas} - T_p\right) + \varepsilon\sigma A\left(T_{wall}^4 - T_p^4\right)$$

where T_p is particle temperature, C_p is heat capacity, h is convective heat transfer coefficient, T_{gas} is gas temperature, ε is emissivity, σ is Stefan-Boltzmann constant and T_{wall} is furnace wall temperature. The density, heat capacity, emissivity of biomass particle is 360 kg/m^3,[203] 1664 J/kg·K and 0.759, respectively.[204] The DTF is operated under laminar conditions, with the Reynolds numbers experienced by the falling biomass particles being ≤ 0.6. Therefore, the average Nusselt Number, $\overline{Nu}$ of 2 can be used[205] and h can be calculated from the equation, $\overline{Nu} = hk/D$. k is the thermal conductivity of argon gas at 1300 °C which is 0.0586 W/m,[206] with D is average particle size. On the basis of the assumptions given above, the average particle residence times are estimated.

3.4 Instruments and analytical techniques

3.4.1 Char yield and torrefaction yield

Char yields and torrefaction yields were all determined experimentally. Original feedstocks and their products were weighted, and the yields were defined as the mass of product on a dry basis/mass of feedstock on a dry basis.

3.4.2 Proximate and Ultimate analysis

A thermogravimetric analyzer (model: Perkin Elmer TGA 8000) and an elemental analyzer (model PerkinElmer CHNS/O analyzer II) were used to conduct proximate analysis according to ASTM E870-82 and ultimate analysis for raw biomass and their derived char samples after rapid pyrolysis.

3.4.3 Quantification of AAEM species and other cation elements

Samples were firstly placed in platinum crucibles which were previously cleaned by ultra-pure water (resistivity > 18.2 MΩ) and ashed in the muffle furnace using a pre-defined time-temperature program.[207] Usually, the residue in the platinum crucible was controlled to be < 1 mg. Ash content was determined by this step. The platinum crucibles containing ash were placed into Teflon vials and numbered. Then 4 ml of the mixture of concentrated hydrofluoric acid (HF) and nitric acid (HNO_3) with the volume ratio being 1:1 was added into the Teflon vials to dissolve the ash. Those vials were sealed and heated overnight at a temperature of ~ 105 °C, which was described as the acid-digestion step. The vials were heated but opened the next day to let the excessive acid evaporated. After the vials were dry, they were carefully collected for the next re-dissolving step.

AAEM species

0.02 M methanesulfonic acid (MSA) solution was used for re-dissolving the residue after acid-digestion. After being heated overnight, solutions were transferred to IC (ion chromatography) sample vials for later quantification of AAEM species using ion chromatography (IC, Dionex ICS-3000).

Other elements

Another batch of samples was re-dissolved in 5% of nitric acid (HNO_3) using the same procedure. Ion coupled plasma – optical emission spectroscopy (ICP-OES, model: PerkinElmer Optima 8300) was used to quantify elements including Al, Fe, Si, P, Ti. The pretreatment for the determination of Al, Fe, Si followed a procedure which was borate fusion of ash as described in AS 1038.14.1-2003. Briefly, the ash of samples was mixed with borate fusion and heated to 950 °C. Then the bean was dissolved in 5% HNO_3 solution to quantify Al, Fe, Si via ICP-OES.

3.4.4 Quantification of anion elements

Analysis of Cl and S deployed an improved Eschka method described elsewhere.[208] Basically, samples were ashed with Eschka flux (sodium carbonate and magnesium oxide mixture). Ashing temperatures for Cl and S quantification are 600 °C and 850 °C,

respectively. Then the residue was dissolved in ultra-pure water before being analysed by anion IC (Dionex ICS-1100 equipped with IonPac AS22 fast analytical column). A mixture of 3.5 mM NaCO3/1.0 mM NaHCO3 solution was used as the eluent.

3.4.5 Chemical occurrence of AAEM species in biomass and char

Chemical fractionation analysis (CFA) was applied for the determination of the AAEM species occurrences in samples. Samples were step-wisely washed by three increasing-aggressive solutions, ultrapure water with resistivity >18.2 MΩ, 1 mol/L ammonium acetate (NH_4Ac), and 1 mol/L hydrochloric acid (HCl). Leachates were analysed by ICP-OES. AAEM species leached by water, NH_4Ac, and HCl were regarded as water-soluble, ion-exchangeable, acid-soluble AAEM species. Acid-insoluble AAME species in solid residues were determined by difference.

3.4.6 Characterization of structural carbohydrate in biomass

The structural carbohydrates in biomass were characterized based on the National Renewable Energy Laboratory (NREL) method as described elsewhere.[209-210] Extractives in biomass samples were firstly eliminated by washing with a mixture of ethanol and water (vol:vol 1:1) in a Soxhlet tube. The extractive-free samples were dried in the oven at 105 °C overnight. They were then subjected to a two-step acid hydrolysis by 98% and 4% of sulfuric acid (H_2SO_4) at room temperature and 121 °C (in an autoclave) for an hour. A Dionex ICS-3000 IC system coupled with high-performance anion-exchange chromatography with a pulsed amperometric detector (HPAEC-PAD) was used to quantify the sugar monomers in hydrolysis liquors. The details can be found elsewhere[211]). The filtered acid-insoluble residues (A.I.R.) were washed, dried, and weighed, expressed as the weight percent in the original sample. The A.I.R. samples were then ashed to obtain ash-free A.I.R. contents.

3.4.7 Shape analysis of biomass and char particles

Image analysis was conducted for various biomass particles and char particles. An optical microscope (model: OLYMPUS SZ61) was used to take images for raw/torrefied/leached biomass particles, whereas the scanning electron microscope (SEM) (model: NEON Dual-Beam FESEM and Tescan Clara FESEM) for biomass

and char particles. Before imaging, a sufficient number of particles were spread on a glass plate (for optical microscope imaging) or on a double-sided adhesive carbon tape (for SEM imaging). Particles are highly scattered to prevent overlapping. An image analyzing software was used in this study to process all the pictures. The software could pick up the outline of a particle and automatically calculate the projection area (PA), the length, and the width of a particle. It could also generate the Feret length and minimum diameter of the particle. The Feret length (particle length) was defined as the longest distance between any two points on the PA. The minimum diameter (particle diameter) is the minimum caliper diameter. The aspect ratio was derived based on Feret length and minimum diameter and was defined as Feret length/minimum diameter, basing on the definition in Section 2.5.3. The equivalent diameter was calculated by the equation $De = (4 \times PA/\pi)^{0.5}$. SEM was also used to observe the surface morphology of particles.

3.4.8 Fourier Transform Infrared Spectroscopy (FTIR) Analysis

Torrefied wood chips were pulverized and subjected to FTIR analysis directly without sieving. PerkinElmer Spectrum100 FTIR spectrometer was used and the detect wavelength range was set to be 2000-4000 cm^{-1} (spectral resolution being 1 cm^{-1}). The results were taken from the average of three measurements after ATR correction, with 3 scans for each measurement.

3.5 Summary

Raw mallee wood and pine wood were pulverized and sieved to three size fractions: 90-106 μm, 150-250 μm, and 250-355 μm. Rapid pyrolysis of these samples was carried out in a novel DTF to determine the experimental char yields for them. Mallee wood in the size fraction of 250-355 μm was pyrolyzed with different residence times to investigate the evolution of char properties. Torrefaction for original wood chips and pulverized biomass powder were conducted in a drop-tube/fixed bed quartz reactor at various temperatures. Torrefied biomass powder samples were subjected to rapid pyrolysis, whereas torrefied wood chips were pulverized and sieved first, before being pyrolyzed. Leaching of biomass considered two leaching agents (water and acid) and the rapid pyrolysis behaviour of leached biomass was studied. The chemical composition of all biomass samples and their derived char samples were characterized

to determine the release of inorganic species and other organic changes. Image analysis was used to quantitatively investigate the evolution in the particle size and shape for raw or pretreated biomass before and after rapid pyrolysis at high temperatures. The results of these experiments could provide valuable data of char yields, which is essential for quantifying the retention of inorganic species and a better understanding of the transformation in particle size and shape after rapid pyrolysis.

CHAPTER 4 RAPID PYROLYSIS OF PULVERIZED BIOMASS AT HIGH TEMPERATURE: EFFECT OF PARTICLE SIZE ON CHAR YIELD, RETENTIONS OF ALKALI AND ALKALINE EARTH METALLIC SPECIES AND CHAR PARTICLE SHAPE

4.1 Introduction

Pulverized biomass in stationary pulverized fuel applications is one of key technological options for biomass utilization.[212] As reviewed above, a few studies investigated the influence of the particle size on products distribution, char structure and reactivity, and reaction kinetics during biomass pyrolysis.[17-19, 74, 213-219] However, most of those studies were carried out at temperatures <1100 °C. Studies conducted at temperatures ≥1100 °C, particularly those[18-19, 74, 217-218] pertinent to pulverized fuel combustion and/or gasification, are rather rare. One key reason for this is related to the difficulty in determining char yields under such conditions, and the ash tracer method was extensively deployed for indirectly determining char yield, sample mass loss, and/or char burnout rate in flow reactors during thermochemical processing of solid fuels at temperatures ≥1100 °C.[18-19, 65, 74, 217-218, 220-222] However, a recent study[23] has demonstrated that ash tracer method is unreliable in determining char yields under such conditions, especially for low-rank fuels such as biomass, due to extensive vaporization of ash species including refractory elements (i.e., Ca and Mg).

The retentions of AAEM species in char is important as it has a significant effect on char reactivity. Results on the retention of inorganic species, directly determined by experiments, are not available in the literature for rapid pyrolysis of biomass particles at such high temperatures. The effect of the biomass particle size on the retentions of AAEM species in char at such high temperatures has never been reported. Furthermore, biomass powders may experience melting and deformation during rapid pyrolysis under such conditions. While there are several studies revealed the effect of pyrolysis temperature on the shape of char particles,[43, 223] and described char particle shape,[224] no work has been done to clarify the effect of biomass particle size on char particle shape at 1300 °C.

Therefore, this chapter aims at fulfilling the aforementioned gaps by a systematic set of experimental investigations. Mallee wood (MW) and pine wood (PW) were dried, ground, and sieved to 3 size fractions, 90-106 µm, 150-250 µm, and 250-355 µm, using a standard mechanical sieving method. It must be noted that the sieve sizes are not the true sizes of the biomass particles because of the elongated shape of most particles. Only the average particle width is within the sieve size range, while the particle length may be larger than the sieve sizes. Hereafter, PW and MW samples with the size fractions of 90-106 µm, 150-250 µm, and 250-355 µm are denoted as PW100, PW200, PW300, MW100, MW200, and MW300, respectively. Rapid pyrolysis experiments were conducted at 1300 °C using a DTF with a novel doubled-tube configuration (detailed in Section 3.3.2). The char obtained from the pyrolysis of PW100, PW200, PW300, MW100, MW200, and MW300 are denoted as PC100, PC200, PC300, MC100, MC200, and MC300, respectively. The properties of the biomass and its respective chars are presented in Table 4.1 and Table 4.2. The focus is to evaluate the effect of particle size on char yield, retentions of AAEM species, and changes in particle shape and morphology during rapid pyrolysis of biomass particles in a DTF with a novel double-tube configuration at 1300 °C.

Table 4.1 Proximate and ultimate analysis of biomass and chars

Samples	Moisture (wt%, ad[a])	Proximate analysis (wt%, db[b])			Ultimate analysis (wt%, daf[e])				Molar ratio	
		ash	VM[c]	FC[d]	C	H	N	O[f]	O/C	H/C
Biomass										
MW300	4.23	0.6	86.9	12.5	45.57	6.23	0.10	48.10	1.06	0.14
MW200	5.66	0.6	86.1	13.3	45.62	6.23	0.10	48.05	1.05	0.14
MW100	5.66	0.7	87.6	11.8	46.37	6.31	0.13	47.19	1.02	0.14
PW300	3.91	0.3	87.6	12.1	46.82	6.53	0.07	46.58	1.00	0.14
PW200	4.87	0.3	88.3	11.4	47.35	6.40	0.07	46.18	0.98	0.14
PW100	5.16	0.3	89.3	10.4	47.16	6.61	0.06	46.17	0.98	0.14
Chars										
MC300	3.69	11.3	35.5	53.2	83.13	1.93	0.41	14.53	0.17	0.02
MC200	4.43	11.7	28.7	59.6	84.70	1.75	0.23	13.32	0.16	0.02
MC100	3.87	18.3	26.9	54.8	87.10	1.42	0.21	11.27	0.13	0.02
PC300	2.23	5.2	19.8	75.0	86.79	1.27	0.14	11.80	0.14	0.01
PC200	2.46	5.5	18.7	75.8	87.01	1.16	0.13	11.70	0.13	0.01
PC100	1.47	7.0	17.8	75.2	87.78	1.08	0.13	10.97	0.12	0.01

[a] air-dried; [b] dry-basis; [c] volatile matter; [d] fixed carbon; [e] dry and ash-free basis; [f] By difference.

Table 4.2 Concentrations of inorganic species in biomass and chars

	Concentrations of Inorganic Species in Biomass Samples, mg/kg, dry basis					
	MW300	MW200	MW100	PW300	PW200	PW100
Na	99.3 ± 1.2	90.5 ± 0.1	112.2 ± 0.3	21.7 ± 0.2	19.9 ± 0.1	18.9 ± 0.4
K	710.1 ± 50.0	667.0 ± 17.5	690.5 ± 1.7	545.5 ± 29.7	519.2 ± 2.0	526.7 ± 3.2
Mg	290.2 ± 7.5	284.6 ± 13.5	258.2 ± 15.9	225.8 ± 0.9	222.0 ± 2.8	209.1 ± 1.4
Ca	1662.1 ± 52.2	1581.1 ± 28.7	1572.5 ± 84.0	595.1 ± 12.3	593.7 ± 6.6	556.0 ± 6.6
Al	2.9 ± 0.0	1.7 ± 0.4	5.4 ± 3.2	24.0 ± 2.0	26.1 ± 3.6	22.5 ± 5.4
Fe	50.2 ± 0.6	96.6 ± 45.1	50.7 ± 37.7	24.9 ± 4.5	19.7 ± 0.8	17.3 ± 1.5
Ti	0.3 ± 0.0	0.3 ± 0.2	0.3 ± 0.0	1.6 ± 0.1	2.0 ± 0.8	1.4 ± 0.2
	Concentrations of Inorganic Species in Char Samples[a], mg/kg, dry basis					
	MC300	MC200	MC100	PC300	PC200	PC100
Na	573.1 ± 6.3	186.9 ± 18.0	268.7 ± 21.5	57.0 ± 6.5	44.0 ± 5.7	40.1 ± 0.7
K	10572.9 ± 280.1	8606.9 ± 192.3	5511.0 ± 77.6	7305.6 ± 213.2	6747.3 ± 21.7	5412.8 ± 147.1
Mg	5881.7 ± 67.4	6678.6 ± 120.7	10343.1 ± 24.1	4167.1 ± 19.0	4660.6 ± 9.4	5949.2 ± 308.4
Ca	33671.8 ± 598.9	36896.5±1375.1	52874.8±186.3	10999.0 ± 29.4	12666.0 ± 69.6	15668.0 ± 291.9
Al	401.7 ± 19.8	546.0 ± 27.8	935.4 ± 43.8	850.9 ± 45.1	618.4 ± 66.3	1157.3 ± 155.7
Fe	395.5 ± 122.6	692.2 ± 48.5	1925.3 ± 148.4	613.8 ± 74.6	1038.1 ± 171.9	1107.5 ± 161.3
Ti	25.4 ± 16.8	31.1 ± 24.2	33.2 ± 8.9	35.5 ± 2.1	41.8 ± 4.2	30.0 ± 0.6

[a] batches of char samples were mixed before analysis.

4.2 Effect of particle size on char yield

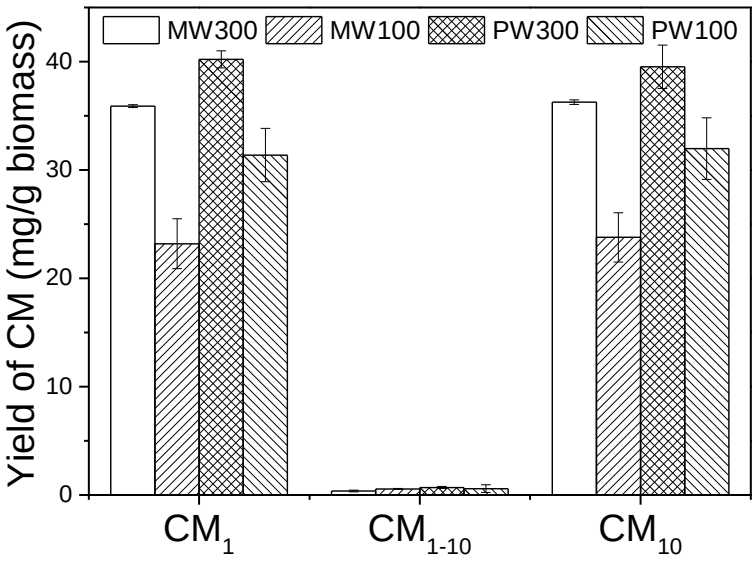

Figure 4.1 Yield of carbonaceous materials (CM) from pyrolysis of MW300, MW100, PW300, and PW100 at 1300 °C

Preliminary experiments were carried out to study the char fragments (CM_{1-10}) passing through the cyclone. Figure 4.1 clearly shows that the yields of CM_{1-10} are negligible for all samples. Therefore, fine char fragments passing through the cyclone are minimal even for the biomass with the smallest size fractions.

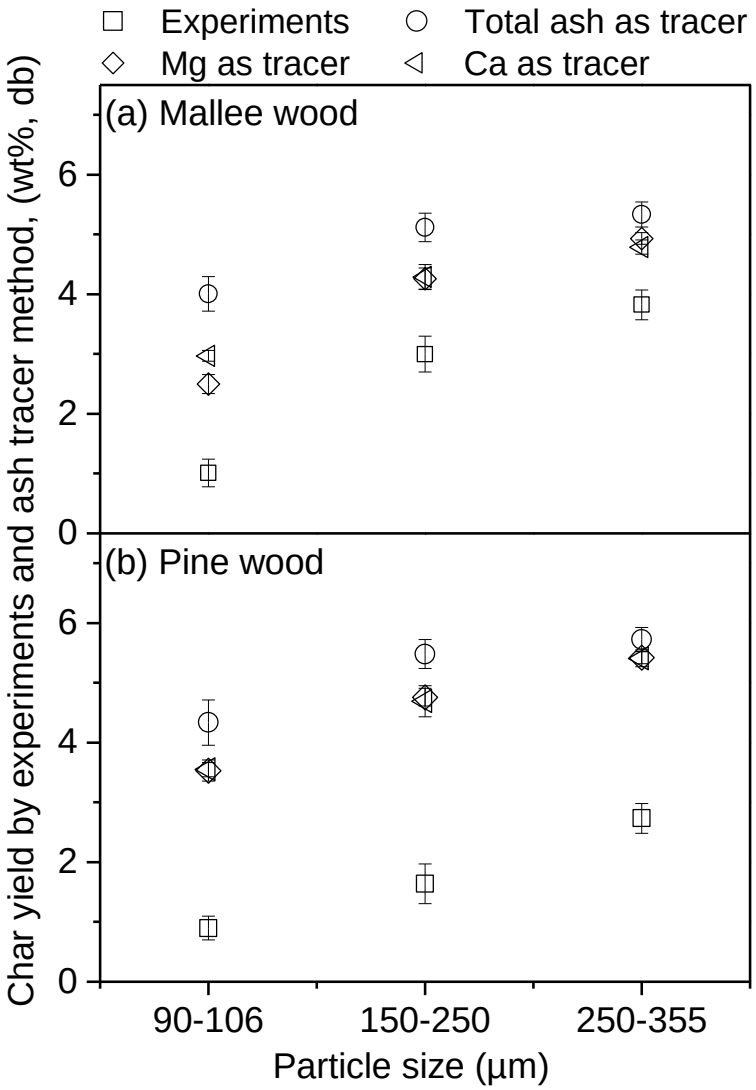

Figure 4.2 Char yields from pyrolysis of (a) mallee wood, (b) pine wood at 1300 °C determined experimentally and using the ash tracer method, expressed as wt% of the biomass fed into the reactor on a dry basis (db)

The char yields determined experimentally from MW and PW pyrolysis at 1300 °C are presented in Figure 4.2. The data indicates that the char yields are very low (less than 5%) for both biomass materials. This is not surprising because pyrolysis of low-rank fuels, such as MW and PW, at high temperature can lead to significant devolatilization and hence low char yields.[76] The char yields for mallee char MC100, MC200 and MC300 are 1.0%, 3.0%, and 3.8%, respectively, while for PC100, PC200 and PC300 are 0.9%, 1.6%, and 2.7%, respectively. The slightly lower PC yields compared to MC yields is mainly due to the variations in fuel properties, particularly inorganic species content (that are known to favor char formation).[17, 43, 109] The results also show that the char yield decreases with decreasing particle size, being particularly

pronounced between the two smaller particle size samples. This can be mainly ascribed to the difference in heating rate experienced by rapid pyrolysis of biomass particles with various particle sizes.

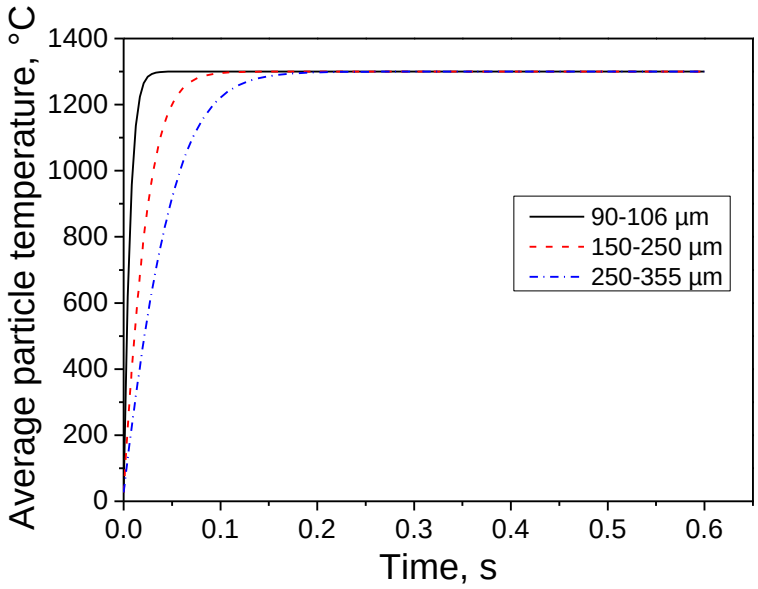

Figure 4.3 Estimated time-temperature history of wood particle with the size fraction of 90-106 µm, 150-250 µm, and 250-355 µm assuming an average particle size of 100, 200 and 300 µm respectively

As shown in Figure 4.3, the estimated average heating rates experienced by biomass particle with the size fraction of 90–106 µm, 150–250 µm and 250–355 µm are ~30,000 °C/s, ~10,000 °C/s and ~5,600 °C/s, respectively. This indicates that average heating rates experienced by smaller biomass particles (i.e. MW100 or PW100) are considerably faster, about 1.8 and ~5.4 times of those experienced by large MW200 or PW200 and MW300 or PW300 particles, respectively. Such differences in the heating rates can significantly influence biomass pyrolysis reactions for several reasons. First, at such a high temperature (i.e., 1300 °C), the biomass particles undergo intense decomposition reactions to form meta-intermediate, which evaporates as volatiles or aerosols or polymerize as char.[225] For small particles such as MW100 and PW100, the pyrolyzing particles are heated to 1300 °C in <0.05s. Smaller biomass particles undergo intense decomposition prior to crosslinking[78] thus favors more towards the formation of volatiles. On the contrary, the slower heating rate experienced by larger biomass particles may lead to less intense decomposition prior to crosslinking which favors the formation of char. Second, during rapid pyrolysis at such high

temperatures, gasification of nascent char by CO_2 and H_2O in pyrolytic gas becomes significant, leading to decreases in char yield.[226] Such gasification reactions are more intensive for small biomass particles (i.e. MW100 and PW100) due to more surface area for reaction and less diffusion resistance. Last, rapid heating of small biomass particles to 1300 °C also means that the resultant nascent char undergoes more extensive thermal cracking/annealing due to extended exposure at high temperature, resulting in reduced char yield. This is further supported by the lower O and H contents in MC100 and PC100 (see Table 4.1) compared to those in char from larger particles.

In addition to the difference in heating rate, two additional factors may also contribute to the reduction in the yield of MC100 and PC100. One is that during rapid pyrolysis of larger particles, the produced volatiles are trapped inside the particle due to increased mass transfer resistance and longer diffusion path length to reach particle surface, leading to increasing char yield. The other is the possible ejection of large molecules from pyrolysing biomass/char particles.[227-228] Such ejected molecules generated from the internal surfaces of a particle are likely to recombine and retain inside the particle, while those molecules ejected from its external surfaces will be released as aerosols.[227] Owing to the higher surface-mass ratio of small particles, more thermal ejections happened at their outer surfaces leading to increased char weight losses.

Ash tracer method is commonly applied to estimate the char yields from pyrolysis at high temperature. Among the common choice of tracers are the total ash and refractory elements such as Mg and Ca. Therefore, the char yields estimated using these tracers are also presented in Figure 4.3. It is clear that the ash tracer method overestimates the char yields. Using the total ash as tracer overestimates more significantly the char yields than using Mg and Ca due to massive evaporation of Na and K (see Section 4.4). The gap between the actual char yields and those estimated using the ash tracer method widen as particle size decreases. The overestimation grows from 1.5-3.0% to 3.0-3.4% in absolute term as the particle size decreases from 250-355 μm to 90-106 μm for mallee and pine. This highlights the inaccuracy of the ash tracer method and indeed one could draw the inappropriate conclusion that particle size has little effect on char yield if the ash trace method is used. The results in Figure 4.2 also suggest that the loss or vaporization of ash species is influenced by the particle size.

4.3 Effect of particle size on chemical properties of char

The proximate and ultimate analysis data in Table 4.1 shows that the variation of biomass properties between different sizes is negligible, while there is some distinction among the chars. For instance, as the biomass size fraction reducing from 250–355 µm to 90–106 µm, the ash content in the PC and MC increase from 5.2% to 7.0% and from 11.3% to 18.3%, respectively. This is due to the enrichment of the ash species in the chars as the extent of devolatilization increases with decreasing particle size. The carbon content also increases with decreasing particle size, indicating a more aromatic and carbonaceous structure. Table 4.2 shows the content of inorganic species in the biomass and char samples. Clearly, the AAEM species are the dominant inorganic species in biomass. Therefore, the discussion on inorganic species is focused on AAEM species. After pyrolysis, it is observed that the contents of Na and K in char decrease, while the contents of Mg and Ca in char increase with decreasing particle size for both MW and PW. It is important to note that the changes in the AAEM species content in chars result from the combined effect of the vaporization of AAEM species and the loss of organic materials, which happened simultaneously during pyrolysis. The results suggest that as the particle size decreases, the vaporization of Na and K outweighed the loss of the organic materials during pyrolysis, causing a reduction in the Na and K contents in the chars. However, the significant enrichment of Mg and Ca in the chars with decreasing particle size suggests that additional release of Mg and Ca is less significant compared to the increase in devolatilisation. A significant variation in the content of the AAEM species in the chars obtained from the pyrolysis of biomass of different particle sizes indicates that particle size has an important impact on the retentions of AAEM species during pyrolysis.

4.4 Effect of particle size on the retentions of AAEM species

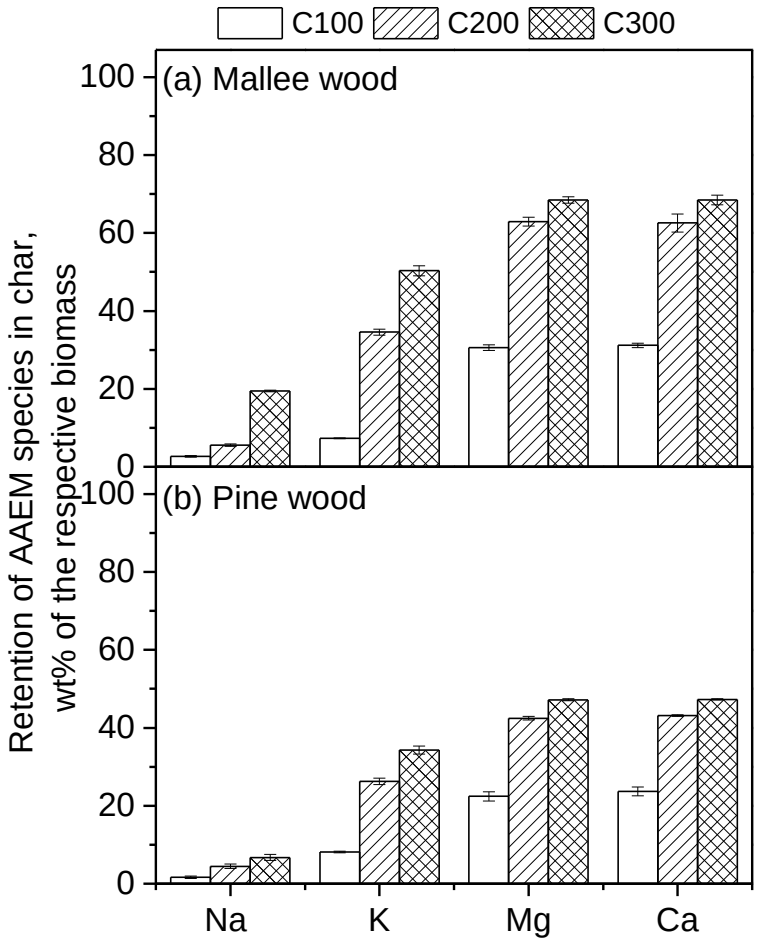

Figure 4.4 Retentions of AAEM species in chars derived from (a) MW and (b) PW, after pyrolysis at 1300 °C. C100, C200, and C300 represent the chars (MC or PC) obtained from pyrolysis of biomass with size fractions of 90-106 µm, 150-250 µm, and 250-355 µm, respectively

Based on the char yield data presented in Figure 4.2 and on the contents of the AAEM species in chars shown in Table 4.2, the retentions of AAEM species in char particles after pyrolysis at 1300 °C were calculated and are shown in Figure 4.4. The effect of particle size on the retentions of AAEM species is clear. The release of AAEM species during pyrolysis intensified with decreasing biomass particle size. For MC300, the retentions of Na and K are ~20% and ~50%, respectively, while the retentions of Mg and Ca are ~70%. However, reducing the particle size to a size fraction of 150-250 µm (MC200) brings a further ~15% reduction in Na retention, ~16% reduction in K retention and ~6% reduction in Mg and Ca retentions. The retentions of AAEM species

in MC100 decreases drastically compared to those in MC200 – only ~3% of Na, ~7% of K and ~30% of Mg and Ca are retained in MC100. Similar trends are observed for PC. The much lower retentions of Na and K can be explained by chemical valence as there is only one bond between monovalent species (Na and K) and char matrix, which requires less energy to break than bonds between divalent species (Mg and Ca) and char matrix.[229]

The low retentions of AAEM species in small char particles can be attributed to several reasons. First, as discussed in Section 4.2, thermal ejection leads to significant loss of organic matter, particularly for small biomass particles due to their higher surface-mass ratio. Part of the non-volatile AAEM species can be transported by aerosols causing a low retention.[228] Second, previous studies suggest that the volatilization of AAEM species can be caused by the substitution of the AAEM species on char matrix by free radicals and high heating rate can accelerate its formation inside the particle.[60] This can explain the lower retentions of AAEM species in MC100 and PC100 considering the considerably faster heating rate experienced by small particles, being ~5.4 times of that experienced by large particles. In addition, the nascent char matrix are highly reactive for AAEM species to recombine with and thus retained in char.[230] Large particles provide more possibilities for AAEM species (volatilized or transported by aerosols) to react with the char matrix during the intra particle diffusion/convection due to a longer diffusion path length and lower inner particle pressure as aforementioned in section 3.1, explaining the higher retentions of these species in MC300 and PC300. Third, a previous study showed that char pyrolyzed at high temperature is highly aromatic with increasing condensation of aromatic-ring structures.[231] As aforementioned in Section 4.2, the higher average heating rate experience by small particles can lead to more extensive thermal cracking/annealing of nascent char matrix, leading to more condensed aromatic ring structure.[232] As shown in Table 4.1, the O/C molar ratio decreases with decreasing particle size. The loss of oxygen-containing groups (e.g., carbonyl and carboxyl groups) and condensation of char structure lead to a reduction in sites on char matrix for AAEM species to bond to. Therefore, lower retentions of AAEM species is observed for MC100 and PC100. The retentions of AAEM species may also be limited by the evaporation rates of these species. Rapid heating of small particles to and remaining at 1300 °C mean the inherent AAEM species are likely to evaporate at higher rates thus lower retentions in chars are

observed. In addition, the average particle residence time in the furnace isothermal zone decreases as the particle size of biomass samples increases, i.e., those for PW300 and MW300 particles being the shortest. Consequently, the evaporation of AAEM species for the larger particles would be likely less, resulting in the observed higher retention of these species in char samples. In terms of the fate of the AAEM species released into the gaseous, it is also noted that those AAEM species might end up as retained in CM_1 and/or reacted with then retained in the reactor tube of the DTF, in various chemical forms as reported previously.[233-235]

4.5 Comparisons between the shape of biomass and char particles

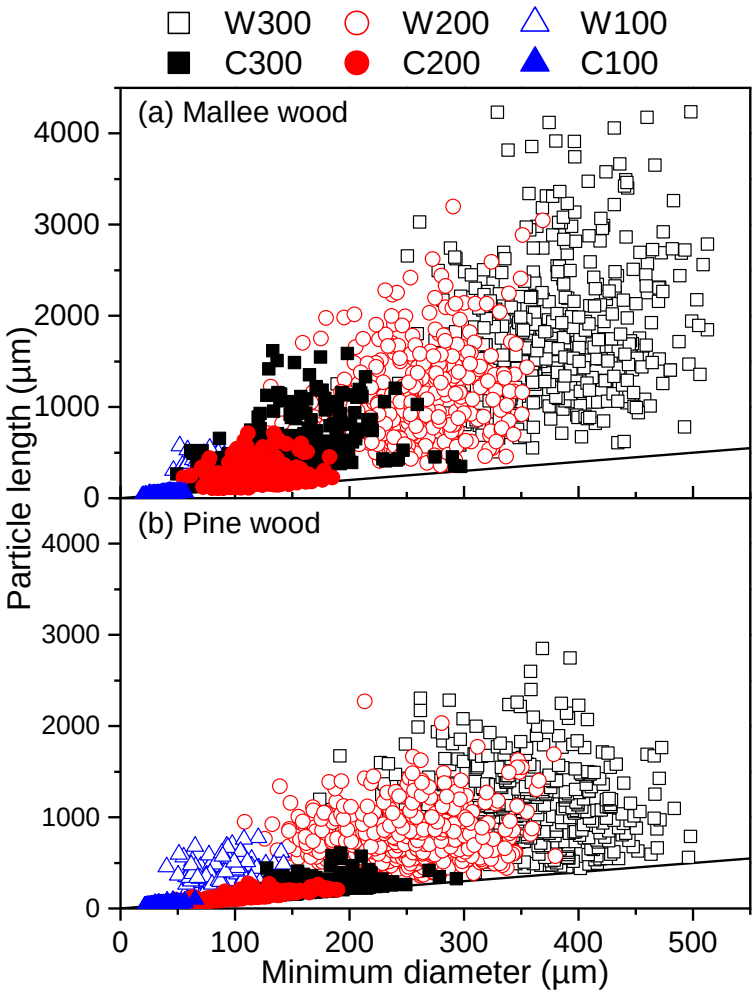

Figure 4.5 Correlation between the particle length and particle minimum diameter of (a) MW and MC, and (b) PW and PC. W in the legend refers to MW and PW, while C refers to MC and PC. 100, 200 and 300 in the legend refer to the size fractions of 90-106 μm, 150-250 μm, and 250-355 μm, respectively. The inclined solid lines represent a particle length to particle minimum diameter ratio of 1

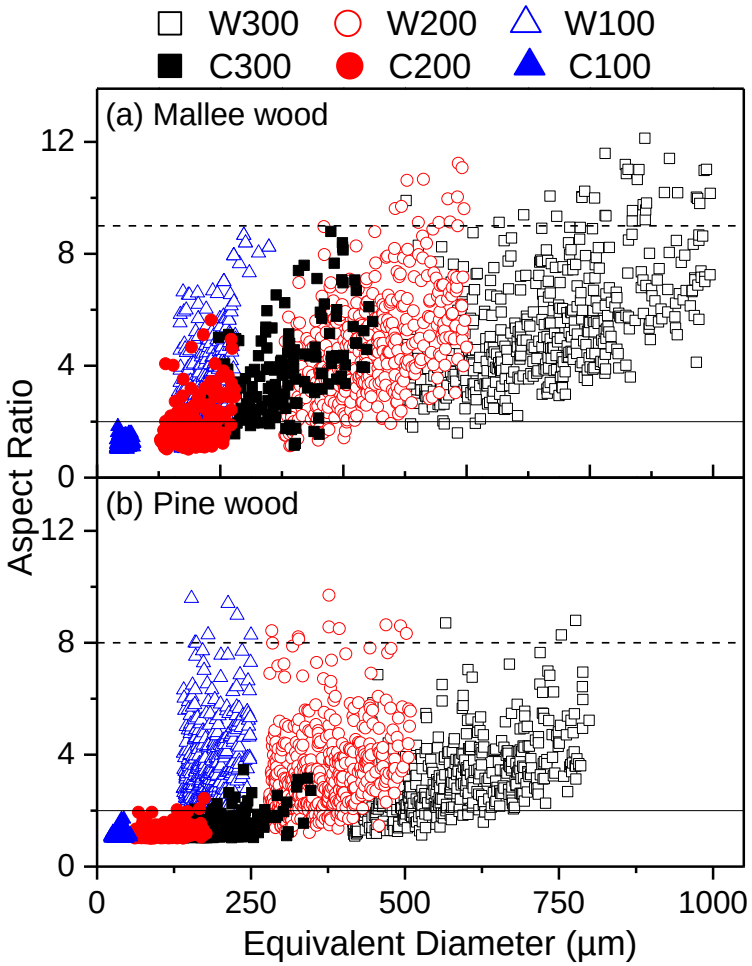

Figure 4.6 Correlation between the aspect ratio and equivalent diameter of (a) MW and MC, and (b) PW and PC. W in the legend refers to MW and PW, while C refers to MC and PC. 100, 200 and 300 in the legend refer to the size fractions of 90-106 μm, 150-250 μm, and 250-355 μm, respectively

Figure 4.5 presents the correlation between particle length and particle minimum diameter while Figure 4.6 illustrates that aspect ratio as a function of particle size, for biomass and the derived chars after rapid pyrolysis under the experimental conditions. It is noted that the solid lines in Figure 4.5 represent a particle length to minimum diameter ratio of 1, being close to the shape of cubes or spheres. Figure 4.5 clearly shows that after rapid pyrolysis, there is a drastic decrease in particle size for all the samples. The minimum diameter for each size range is nearly halved and the particle length shrinks significantly. It is obvious that the distributions for PW/MW particles are widely scattered above the solid lines that indicate elongated shapes of these particles. However, those of PC/MC particles are scattered closely above the solid lines, indicating those particles with shapes resembling closer to cubes or spheres. The

results in Figure 4.6 demonstrate that for the three biomass size fractions, the aspect ratios of biomass particles range from 2 to 9 for MW and from 1.5 to 8 for PW, with the larger biomass particles having slightly greater aspect ratios compared to smaller sized particles. For MW with a size fraction of 250-355 μm, the equivalent diameter De of the resultant char particles (MC300) decreases by half, corresponding to the decrease in particle dimensions (particle length and minimum diameter), but the aspect ratio remains similar in the range of 2-8. Pyrolysis of MW200 also leads to a decrease in De by about half, but there is a small reduction of the aspect ratio to the range of 1-5. Most importantly, after pyrolysis, the De for MW100 shrinks significantly and the aspect ratio reduces to less than 2. An aspect ratio of less than 2 means that the resultant char particles (MC100) have shapes close to spheres. This is consistent with the observation in Figure 4.5 that nearly all the datum points for MC100 particles are located closely above the solid line. A significant reduction in the aspect ratio implies the deformation of particles as results of melting during pyrolysis. Clearly, small particles underwent much severer deformation during pyrolysis. As for PW, pyrolysis originates the shrinkage of the char particle as well. However, there is a substantial reduction in the particle aspect ratio for all PW samples with different sizes. The resultant PC particles normally have aspect ratios <2, except for a few large particles, which present aspect ratios in the range of 2-3.5. A huge reduction in the particle aspect ratio during pyrolysis, even for the largest size fraction, suggests that PW experienced a high degree of particle deformation during pyrolysis.

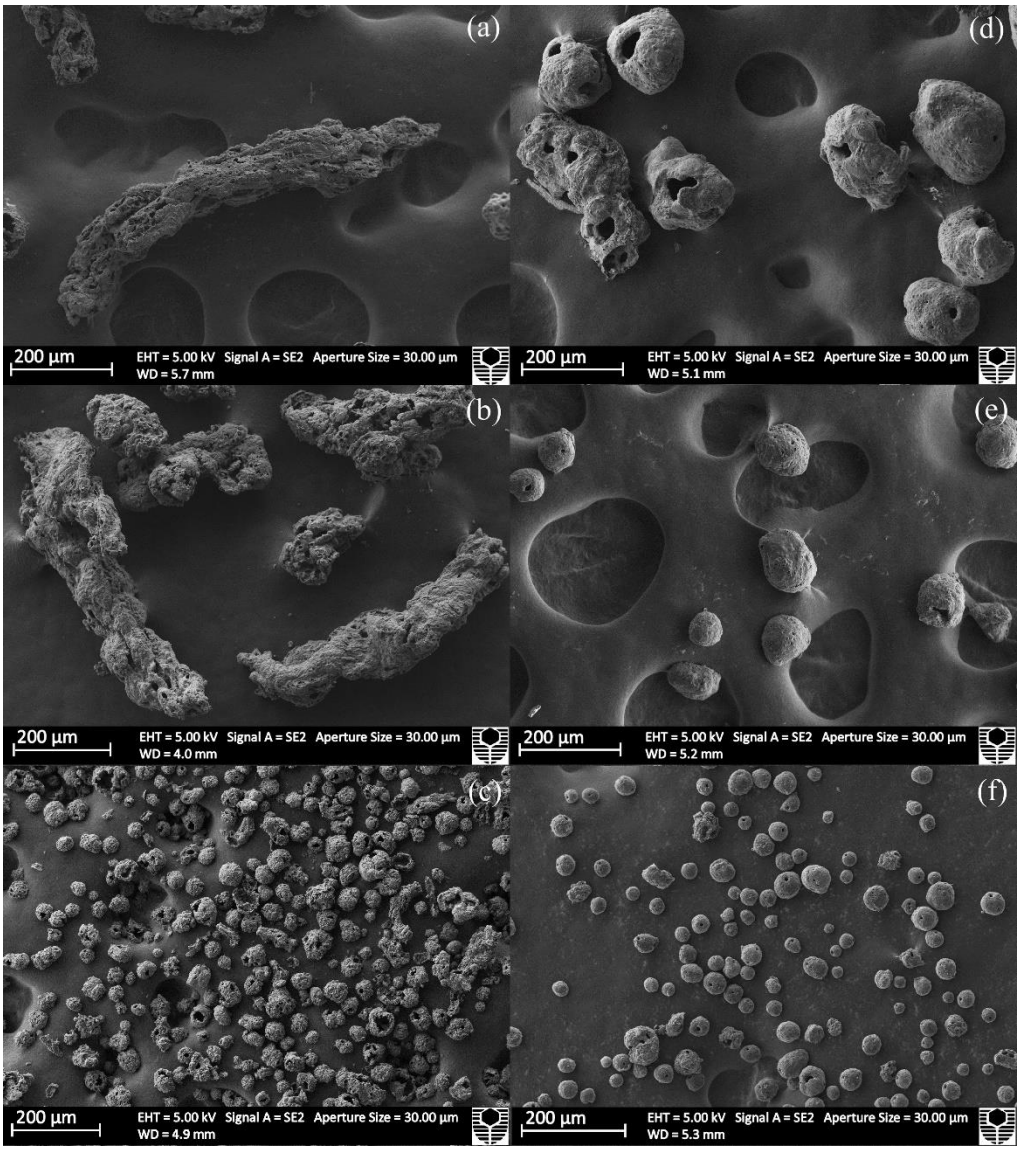

Figure 4.7 SEM images of (a) MC300, (b) MC200, (c) MC100, (d) PC300, (e) PC200, and (f) PC100

Figure 4.7 presents representative SEM images for the char samples collected during rapid pyrolysis of biomass samples under the experimental conditions in this study. Figure 4.7a and Figure 4.7b show that MC300 and MC200 char particles are elongated with partially melted surface and traces of fibrous structure are still visible on these char. Figure 4.7c shows that MC100 char particles are mainly cenospheres with large inner cavities and contain many bubbles and pores on the surface. Figure 4.7d-f show that the morphology for the PC samples is very similar to that observed for MC100 char particles, except for the smoother surface of the PC particles. Residues of bursting

bubbles can be observed on the surface of MC100 particles and PC particles, suggesting the presence of thermal ejection during pyrolysis. The stronger melting of the PC could be due to their higher content of volatile matter. Biomass with higher volatile matter content (cf. Table 4.1) is known to undergo more pronounced melting and swelling.[236] The high particle aspect ratio observed for MC300 and MC200 can be ascribed to differences in heating rate experienced by pyrolyzing particles. The heating rate experienced by large particles (250-355 µm) is considerably lower than that experienced by small particles (90-106 µm). The poor heat conductivity of biomass[237] can lead to high thermal gradient in the large particles. The high heating rate experienced at the surface of the large particles led to the liquefaction of biomass. However, as the heating rate at the center of the particle was significantly lower, the interior was partially melted and part of the parental biomass structure was retained.[237] The retained structure acts as the skeleton for the particle to retain its elongated shape. The deformation of the liquefied part accounted for the cavities inside large particles. For thermally thin particles (i.e., MC100), the temperature gradient was negligible and the high heating rate caused fully melting of the particles. Volatiles produced inside the molten particle expanded and were released through bursting bubbles and large openings due to increased internal pressure, resulting in the formation of cenosphere char particles.

4.6 Conclusions

The effect of particle size (90-106 µm, 150-250 µm, 250-355 µm) of biomass (mallee wood and pine wood) on char yield, retention of alkali and alkaline earth metallic (AAEM) species and char particle shape during fast pyrolysis at high temperature were investigated using a double-tube DTF. Char yield increases from ~1% to 2.5-4% as particle size increased from 90-106 µm to 250-355 µm. An increase in particle size favors the formation of char likely due to the substantially lower heating rate experienced by large particles thus less extensive gasification of char matrix by CO_2 and H_2O and less profound thermal annealing of char. The recombination of the volatile matter with char matrix in large particles and enhanced mass loss in small particles that have higher surface-to-mass ratio through thermal ejection also contributed to lower char yield. The results confirm that the ash tracer method can overestimate the char yield from biomass pyrolysis at high temperature by 50-400%,

especially for small particles, since only <20% of Na, <50% of K and 40-70% of Mg and Ca are retained in char. A decrease in particle size enhances the release of AAEM species. This is because for large particles, the substitution of AAEM species from char matrix by free radicals, thermal annealing which resulted in the loss of oxygen-containing groups for AAEM species to combine with and the evaporation of AAEM species are less extensive under lower heating rate conditions. The particle size can also affect the shape of the resultant char. The high heating rate experienced by the small biomass particles promotes the melting and swelling of the cell structure so that small char particles are more spherical and smooth. However, large particles experienced relatively lower overall heating rate, which resulted in partial melting of the particles and, consequently, much of the fibrous structure of the biomass is retained after pyrolysis.

CHAPTER 5 EVOLUTION OF CHAR PROPERTIES DURING RAPID PYROLYSIS OF WOODY BIOMASS PARTICLES UNDER PULVERIZED CONDITIONS

5.1 Introduction

As rapid pyrolysis is the first step of combustion process, understanding the char properties during biomass rapid pyrolysis is crucial because char conversion is known to be the rate-limiting step during solid fuel conversion in boiler.[22] Besides, a sound understanding of the release and transformation of inorganic species in biomass during rapid pyrolysis are essential to addressing ash deposition/fouling/corrosion issues associated with biomass combustion.[89, 238-239] Surprisingly, little work has been done on the release and transformation of inorganic species during the pyrolysis of biomass powder at temperature >1100 °C in a laboratory drop-tube furnace (DTF) for achieving high heating rates. In addition, the shape and morphology of char particles are known to affect char burnout during subsequent combustion.[27, 48] However, little work has been done thus far to study how the particle shape changes during rapid pyrolysis. Therefore, the new method,[23] recently developed for direct determination of char yield by experiments, has paved the way for insightful investigation into the evolution of char properties during biomass rapid pyrolysis at high temperature (>1100 °C).

Therefore, this chapter aims at a systematic investigation into the evolution of char properties during biomass rapid pyrolysis under pulverized fuel conditions at 1300 °C. The experimental program is focused on the evolution in char yield, char chemistry, retention and transformation of AAEM species in char, and char particle shape during the pyrolysis of two woody biomasses at five particle residence times during rapid pyrolysis.

Mallee wood and pine wood were pulverized then sieved to a size range of 250–355 μm. The pyrolysis experiments for these samples were conducted in the novel DTF at 1300 °C with five different particle residence times for each biomass sample. Due to the limitation from the experimental setup, particle residence time in the furnace was adjusted by varying the gas flow rate in the inner furnace tube from 1.06 L/min to 2.5

L/min. Five gas flow rates were used to obtain five particle residence times for each biomass sample. The length of the isothermal zone for each gas flow rate was determined with a thermocouple. Due to the distributed nature of biomass particle size, the nominal particle residence time is calculated based on the average particle size. The assumptions made to compute the particle residence time include a) the amount of volatiles produced during pyrolysis is negligible; b) particle deformation during pyrolysis is not considered; c) particles are assumed to be spherical with the particle diameter equal to the average sieve size. The calculation indicates the Reynolds number of the falling particle is <0.7, which indicates a creep flow. Therefore, the terminal velocity of the falling particle was estimated from Stokes's law. The corresponding particle residence times are 0.32 s, 0.37 s, 0.43 s, 0.51 s and 0.55 s for MW sample and 0.31 s, 0.41 s, 0.51 s, 0.62 s and 0.68 s for PW sample. Char samples produced from the pyrolysis of MW and PW with different residence times are denoted as MC-0.xxs or PC-0.xxs. The 0.xxs represents the residence time for each sample. For example, mallee char pyrolyzed with a residence time of 0.43s is written as MC-0.43s. All experiments were carried out at least in duplicate. Table 5.1 shows the properties of biomass used and their char samples

Table 5.1 Proximate and ultimate analysis for biomass and char samples

Samples	Moisture (wt%, ad[a])	Proximate analysis (wt%, db[b])			Ultimate analysis (wt%, daf[e])				Molar ratio	
		ash	VM[c]	FC[d]	C	H	N	O[f]	O/C	H/C
Mallee wood	4.23	0.6	86.9	12.5	45.97	6.23	0.10	47.70	0.78	1.63
MC-0.32s	3.51	8.0	56.8	35.3	64.68	4.17	0.22	30.93	0.36	0.77
MC-0.37s	3.12	8.3	49.4	42.3	65.40	4.05	0.43	30.12	0.35	0.74
MC-0.43s	2.94	10.0	39.2	50.8	80.92	2.16	0.38	16.53	0.15	0.32
MC-0.51s	3.69	11.3	35.5	53.2	82.13	1.93	0.41	15.53	0.14	0.28
MC-0.55s	3.22	11.2	21.4	67.4	83.30	1.28	0.42	13.90	0.14	0.19
Pine wood	3.91	0.3	87.6	12.1	46.82	6.53	0.07	46.58	0.75	1.67
PC-0.31s	2.85	3.8	37.6	58.6	75.49	2.67	0.22	21.61	0.21	0.42
PC-0.41s	2.94	5.0	26.4	68.6	82.52	1.72	0.24	15.43	0.14	0.25
PC-0.51s	2.91	5.1	21.3	73.6	84.28	1.44	0.30	13.98	0.12	0.20
PC-0.62s	2.23	5.2	19.8	75.0	86.79	1.27	0.14	11.80	0.10	0.18
PC-0.68s	3.05	5.4	12.1	82.5	87.19	0.97	0.37	11.47	0.10	0.13

[a] air-dried; [b] dry-basis; [c] volatile Matter; [d] fixed carbon; [e] dry and ash-free basis; [f] by difference.

5.2 Evolution of char yield and properties

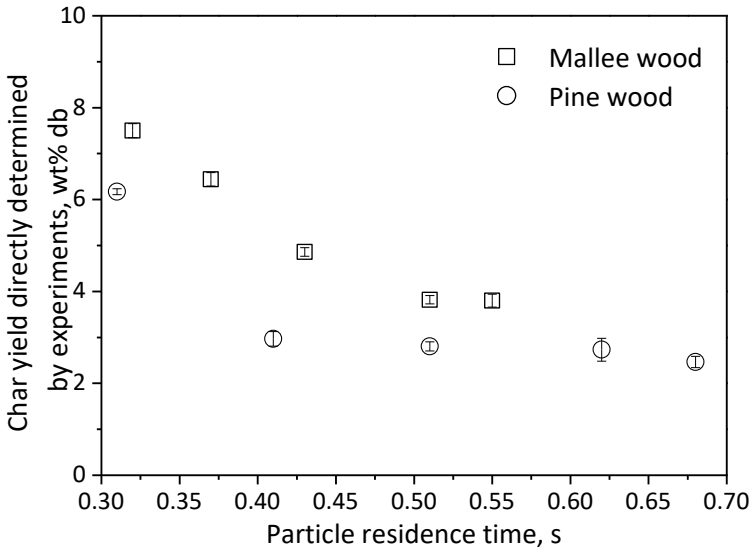

Figure 5.1 Char yield during rapid pyrolysis of mallee wood and pine wood samples at 1300 °C, as a function of particle residence times, determined experimentally (using a recent method reported elsewhere[23]).

The advantage of this study is the ability to directly determine the char yield of biomass rapid pyrolysis using the novel experimental setup. Figure 1 presents the experimental char yields (on a dry basis) during rapid pyrolysis of mallee and pine wood particles at 1300 °C and different particle residence times. As expected, char yield decreases with increasing particle residence time but remained unchanged at a particle residence time of ~0.51s or longer for mallee wood sample and ~0.41 s or longer for pine wood sample, respectively. The results show that rapid pyrolysis of each biomass sample is mostly completed at the respective particle residence time. The results show the char yield of mallee char is higher than pine char, even on a dry and ash free basis (i.e., 3.4% and 2.6% for mallee and pine char, respectively, at the particle residence time of 0.51 s). The differences in char yield are attributed to the differences in the contents of the inorganic species and composition of structural carbohydrates (cellulose and hemicellulose) and lignin in original wood samples (see Table 5.2 and Table 5.3).

Table 5.2 Concentration of inorganic species in biomass and chars, wt% (dry basis)

	Mallee wood	MC-0.32s	MC-0.37s	MC-0.43s	MC-0.51s	MC-0.55s
Na	0.010 ± 0.001	0.098 ± 0.001	0.089 ± 0.001	0.086 ± 0.001	0.062 ± 0.003	0.057 ± 0.003
K	0.076 ± 0.004	0.849 ± 0.014	0.843 ± 0.028	0.988 ± 0.030	0.989 ± 0.022	0.996 ± 0.033
Mg	0.030 ± 0.001	0.389 ± 0.005	0.400 ± 0.007	0.528 ± 0.020	0.533 ± 0.025	0.563 ± 0.015
Ca	0.179 ± 0.005	2.428 ± 0.025	2.480 ± 0.030	3.258 ± 0.029	3.367 ± 0.032	3.428 ± 0.066
Al	0.001 ± 0.001	0.011 ± 0.007	0.013 ± 0.001	0.033 ± 0.008	0.035 ± 0.009	0.033 ± 0.004
Fe	0.005 ± 0.001	0.007 ± 0.001	0.018 ± 0.006	0.024 ± 0.001	0.033 ± 0.001	0.030 ± 0.011
P	0.019 ± 0.001	0.005 ± 0.001	0.004 ± 0.001	0.007 ± 0.001	0.006 ± 0.002	0.005 ± 0.002
Si	0.005 ± 0.002	0.050 ± 0.020	0.056 ± 0.015	0.067 ± 0.001	0.113 ± 0.010	0.108 ± 0.050
	Pine wood	PC-0.31s	PC-0.41s	PC-0.51s	PC-0.62s	PC-0.68s
Na	0.002 ± 0.001	0.018 ± 0.001	0.020 ± 0.001	0.016 ± 0.001	0.006 ± 0.001	0.005 ± 0.001
K	0.055 ± 0.003	0.715 ± 0.003	0.971 ± 0.003	0.989 ± 0.009	0.729 ± 0.005	0.699 ± 0.007
Mg	0.023 ± 0.001	0.294 ± 0.001	0.411 ± 0.002	0.415 ± 0.002	0.420 ± 0.002	0.429 ± 0.005
Ca	0.056 ± 0.001	0.927 ± 0.003	1.130 ± 0.017	1.148 ± 0.007	1.191 ± 0.022	1.201 ± 0.003
Al	0.002 ± 0.001	0.012 ± 0.001	0.019 ± 0.007	0.016 ± 0.020	0.055 ± 0.025	0.039 ± 0.030
Fe	0.002 ± 0.001	0.015 ± 0.022	0.019 ± 0.010	0.027 ± 0.005	0.030 ± 0.021	0.026 ± 0.010
P	0.005 ± 0.001	0.001 ± 0.001	0.022 ± 0.015	0.027 ± 0.020	0.026 ± 0.012	0.018 ± 0.013
Si	0.003 ± 0.001	0.030 ± 0.021	0.047 ± 0.022	0.035 ± 0.014	0.051 ± 0.036	0.054 ± 0.030

Table 5.3 Contents of structure carbohydrates, extractive, and lignin in mallee and pine wood

Constituent	Mallee wood	Pine wood
Extractives	7.79	4.03
Hemicellulose	23.26	23.40
Arabinan	1.20	1.81
Galactan	2.42	3.09
Glucan	2.01	3.14
Xylan	17.18	6.04
Manan	0.46	9.32
Cellulose	40.68	41.83
Lignin		
Acid soluble lignin[a]	8.29	3.50
Acid insoluble lignin	19.97	27.24

[a:] by difference

High contents of inorganics (such as K and Ca) in biomass are also known to enhance char formation during pyrolysis,[76, 240] due to catalysis of these species in repolymerization/cross-linking reactions.[76, 109] Figure 1 also shows that the reduction in the char yield of pine wood with increasing particle residence time is more rapid than that of mallee wood. This indicates that pine wood experiences more rapid pyrolysis than mallee wood, as also supported by similar trends in the reductions in char O/C and H/C molar ratios. Such observations can be attributed to two reasons. One is that mallee wood has a higher density (950 kg/m^3, on dry basis) than pine wood (360 kg/m^3, on dry basis), leading to higher thermal mass, longer time required for the particle to be heated to the pyrolysis temperature (1300 °C) and larger thermal gradient within the particle hence slower pyrolysis/devolatilization process. The other is that mallee wood particles resemble more closely to a cylindrical shape while pine wood particles resemble thin long flasks, as shown in Figure 2. The flaky nature of the pine wood particles means that these particles are more thermally thin and therefore, will experience more rapid heating, hence more rapid pyrolysis, compared to mallee wood particles.

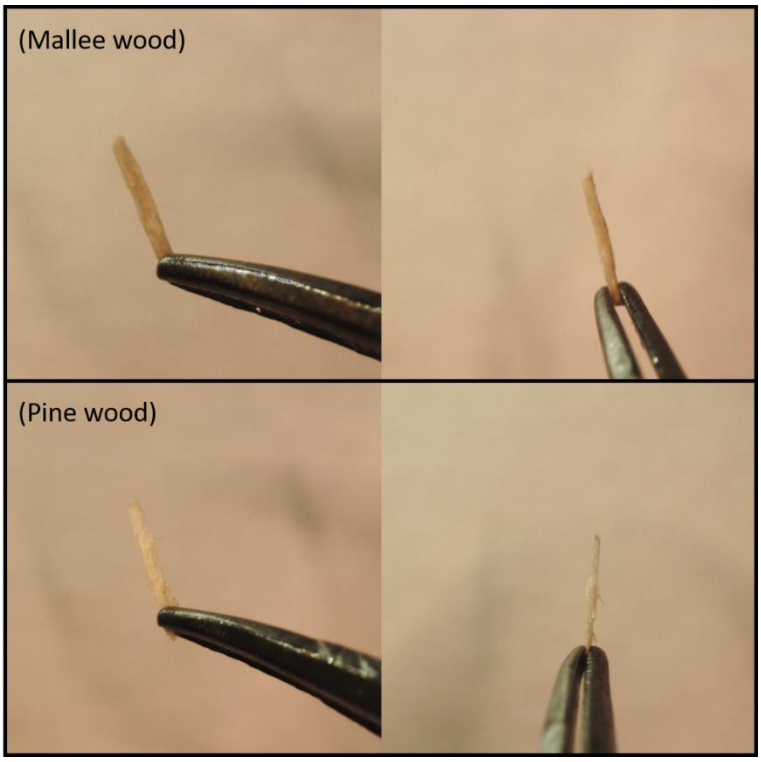

Figure 5.2 Images for typical mallee wood particle and pine wood particle from two orientations

The results in Table 5.1 and Figure 5.1 also show that the char yield experiences little changes after a particle residence time of ~0.51 s and ~0.41 s for mallee wood and pine wood, respectively, suggesting that pyrolysis reactions of these biomass samples has mostly completed. However, the carbon content in both chars continues to increase and the char O/C and H/C molar ratios continue to decrease at longer particle residence times. These clearly indicate that with continuous exposure to a high temperature (i.e., 1300°C), the nascent chars continue to experience thermal cracking or annealing, leading to higher C content and lower O/C and H/C ratios, although such reactions result in insignificant weight losses. As the pyrolysis reactions for mallee and pine wood are mostly completed at a particle residence time of ~0.51 s and ~0.41 s, respectively, mallee and pine chars with particle residence times equal to or greater than these particle residence times are henceforth termed as completely pyrolyzed chars.

5.3 Evolution of AAEM species retentions

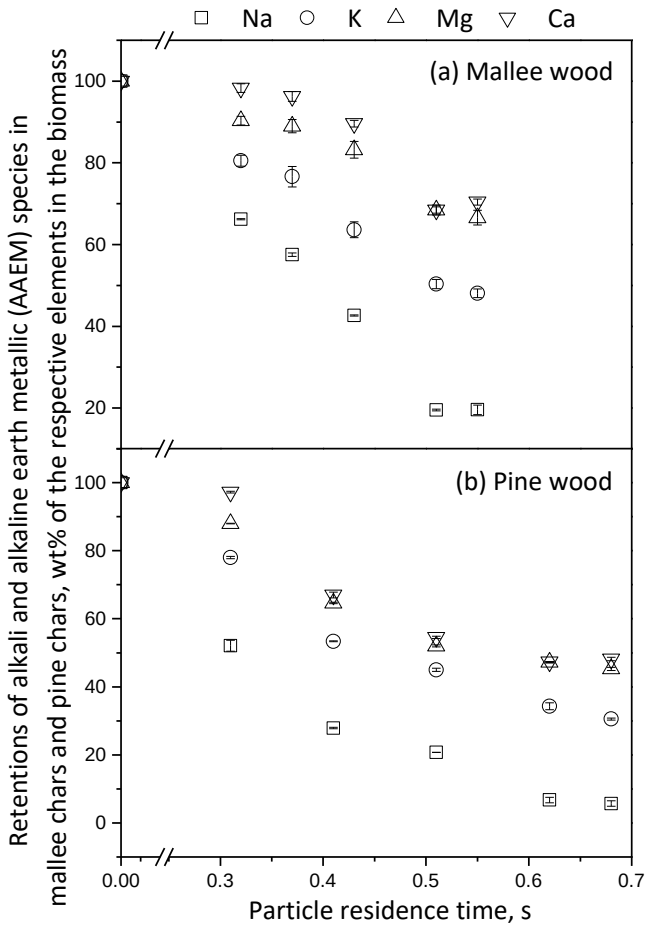

Figure 5.3 Retentions of alkali and alkaline earth metallic (AAEM) species in the chars collected from rapid pyrolysis of (a) mallee wood and (b) pine wood samples, respectively, at 1300 °C and various particle residence times

From the experimentally determined char yield (Figure 5.1) and contents of AAEM species in parent biomass and resultant char (Table 5.2), the retentions of AAEM species in char at different particle residence times were determined and shown in Figure 5.3. The data points for biomass samples are plotted at a particle residence time of 0 s where the retentions of AAEM species are regarded as 100%. The data show that the retentions for AAEM species reduce with the progression of pyrolysis, but the extent of reduction differs for each AAEM species. For mallee chars, the retentions of Mg and Ca reduce to ~70% at a particle residence time of ~0.51 s and remain unchanged at extended particle residence times. Comparatively, the retention of K in mallee chars is lower and reaches a plateau at ~50%. The retention of Na is

the lowest, at ~20%. For pine chars, the retentions of Mg and Ca reduce to ~50% at particle residence times ≥0.62 s. For K and Na in pine chars, their retentions reduce to ~30% and ~5%, respectively. The result clearly shows the higher retentions of Mg and Ca compared to K and Na. This is likely due to two factors. Firstly, the chemical fractionation of mallee wood and pine wood (see

Figure 5.4) shows >80% of the Na and K in these samples are water-soluble, likely to be in the form of chlorides, sulphates, or carbonates. As the melting points of alkali chlorides and sulphates are <900 °C, the species can be released through vaporization and/or thermal ejection during pyrolysis. On the contrary, <30% of the Mg and Ca in mallee and pine wood are water-soluble, which means >70% of Mg and Ca are ion-exchangeable and are organically bound. Secondly, due to the divalent nature of Mg and Ca, more energy is required to break two bonds between Mg or Ca and char matrix, compared to the single valent Na and K,[131, 229, 241] thus less Mg and Ca are released during pyrolysis.

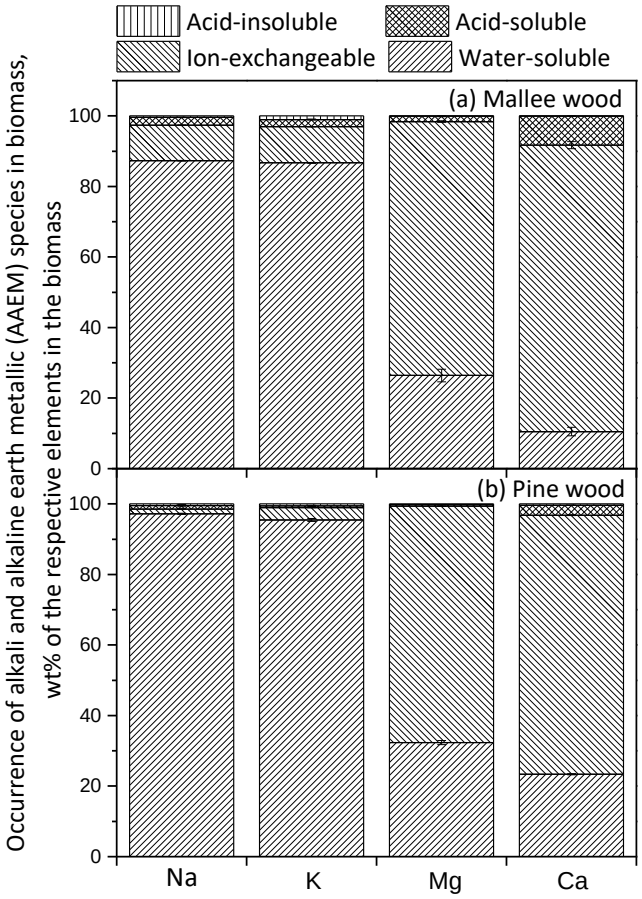

Figure 5.4 Contents (wt % db) of alkali and alkaline earth metallic (AAEM) species of various occurrence forms present in (a) mallee wood and (b) pine wood samples, respectively.

Comparing the AAEM species retentions in mallee and pine chars, it can be seen that the retention of AAEM species is higher in mallee chars than those in pine chars. Such observation is partially due to higher water-soluble Na and K in pine wood (>95%) than in mallee wood (~85%). As aforementioned, these species can be released through vaporization and/or thermal ejection during pyrolysis. A higher fraction of water-soluble Na and K in pine wood translates to a higher fraction of Na and K released during rapid pyrolysis. Furthermore, during pyrolysis, the AAEM species released would firstly diffuse or convect through the char particle before reaching the outer surface of the particle. Oxygen-containing groups, such as carbonyl or carboxyl groups, can act as a reactive site for the AAEM species to bond to and retain in the char through ion-exchange.[125, 242] Slightly higher oxygen contents in mallee chars compared to pine char mean there are more possibilities for AAEM species to recombine with oxygen-containing groups, therefore resulting in higher retention of AAEM species in mallee chars. In addition, as mentioned in Section 5.2, due to the flake-like shape of pine wood particles, they experience a higher heating rate during pyrolysis. This can cause higher inner particle pressure due to extensive decomposition, so the vaporized AAEM species are rapidly ejected from the char particle. Moreover, the flake-like shape also means a shorter intraparticle diffusion path for vaporized AAEM species. Therefore, the vaporized AAEM species are less likely to recombine with char matrix.

Although no significant change in the yields of pine char is observed as particle residence time increase from ~0.41 s to ~0.68 s, the results in Figure 5.3 show the retention of Na, K, Mg, and Ca in these pine chars reduced from ~30%, ~55%, ~65%, and ~65%, respectively, to ~5%, ~30%, ~50%, and ~50%, respectively. This indicates that while pyrolysis reactions are mostly completed, AAEM species may continue to vaporize when exposed to high temperatures. Moreover, as the nascent char undergoes thermal decomposition or annealing, the oxygen-containing groups on the char surface are released as volatiles. The O/C molar ratio for pine chars decreases from 0.14 to 0.10 as particle residence time extending from 0.41 s to 0.68 s. The loss of oxygen-

containing groups can have double impacts on the retention of AAEM species. Firstly, the loss of oxygen-containing groups leads to the release of AAEM species bonded to those oxygen-containing groups. Secondly, a reduction in active sites makes it difficult for AAEM species to bond to as they diffuse to the particle surface. In the contrary, the O/C molar ratio in mallee chars is almost unchanged as particle residence time increasing from 0.51 s to 0.55 s, when pyrolysis is mostly completed. This could explain the similar retentions of AAEM species for MC-0.51s and MC-0.55s. Another aspect attributed to the unchanged retentions for mallee chars after 0.51 s could be the more compact structure of mallee char particles (see Section 5.5), which hinders the release of ejected aerosols containing AAEM species.

5.4 Transformation of AAEM Species during pyrolysis at high temperature

To gain a better insight into the transformation of AAEM species during pyrolysis of woody biomass at high temperature, chemical fractionation analysis was carried out for two mallee char samples, MC-0.32s and MC-0.51s, representing a partially pyrolyzed char and a completely pyrolyzed char, respectively. The distribution of water-soluble, ion-exchangeable, acid-soluble, and acid-insoluble AAEM species in these chars are presented in Figure 5.5. As part of the AAEM species is released during pyrolysis, these are also normalized to the amount of AAEM species retained in MC-0.32s and MC-0.51s, then plotted in Figure 5.6. This will provide a better visualization of how each fraction of the AAEM species transforms during pyrolysis. However, due to low char yields from pine chars and their low ash contents, the AAEM species content in leaching solutions cannot be accurately quantified. Therefore, the occurrence of AAEM species in pine chars was not analysed.

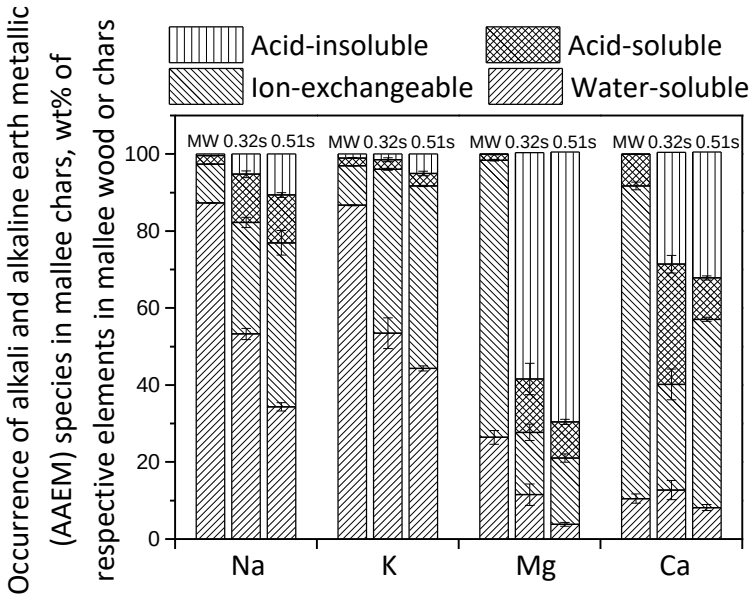

Figure 5.5 Distributions of alkali and alkaline earth metallic (AAEM) species with various occurrence forms in mallee wood and two char samples prepared from rapid pyrolysis of mallee wood sample at particle residence times of 0.32 s and 0.51 s, expressed as wt% of the total content of each element in samples. For the labels in the figure, MW refers to mallee wood sample

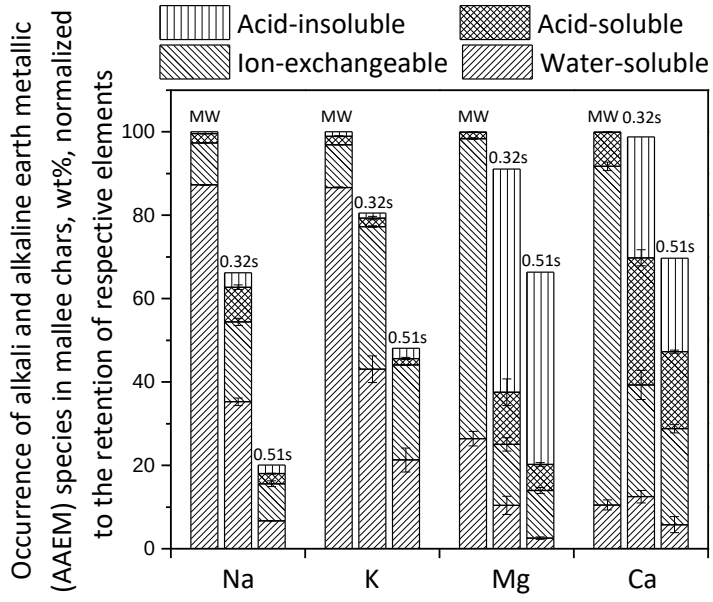

Figure 5.6 Occurrence of alkali and alkaline earth metallic (AAEM) species in mallee wood or retained in mallee chars with particle residence times of 0.32 s and 0.51 s, expressed as the wt% of the total content of each element in samples and normalized to its retetnion

The results show a significant shift in the occurrence of AAEM species during pyrolysis. More than 80% of Na and K in the mallee wood is water-soluble, but it drops to ~55% in MC-0.32s. Only ~35% of Na and ~45% of K in MC-0.51s are water-soluble. This is partly attributed to the vaporization of volatile alkali chlorides, sulphates, and phosphates (as evident from the reduction in water-soluble fraction in Figure 5.6) because most water-soluble Na and K carbonates, chlorides, sulphates, and phosphates have a low decomposition temperature. For instance, sodium carbonate and alkali phosphates have a decomposition temperature of <500°C.[243] Meanwhile, an increase in ion-exchangeable Na and K in MC-0.32s suggests there could be some water-soluble Na and K transformed into the ion-exchangeable form. The Na and K from the decomposed water-soluble Na and K can retain in char matrix and become organically bonded to char organic structures after a series of reactions.[230] For example, previous studies[64, 125, 242] show alkali chloride may react with oxygen-containing groups in biomass, releasing Cl but associating the alkali elements to the oxygen-containing groups. Thus, the Na and K that are newly bonded to oxygen-containing groups contribute to the rise in ion-exchangeable fraction. Further pyrolysis leads to the deoxygenation of nascent char, thus a reduction in oxygen-containing groups and ion-exchangeable Na and K in MC-0.51s observed in Figure 5.6. A slight increase in acid-soluble and acid-insoluble Na and K is likely due to the incorporation of Na and K into char matrix[244] or react with the small amount of silicate or aluminosilicate in mallee wood.[125] Figure 5.5 shows that ~ 95% of Mg and ~92% of Ca in mallee wood are either water-soluble or ion-exchangeable. A reduction (from ~25% to ~3%) of water-soluble Mg retained in char with increasing pyrolysis time observed in Figure 5.6 is likely due to the decomposition and release of $MgCl_2$ or $MgSO_4$ at 1300 °C. On the contrary, much of the water-soluble Ca is retained in the char during pyrolysis because of the high melting point of Ca compounds (such as CaO) or the release of low melting point $CaCl_2$ being compensated by decomposition of $CaCO_3$ and calcium oxalate (a compound known to present in biomass and only soluble in acids[95]) into CaO.[245] During pyrolysis, a significant amount of ion-exchangeable Mg or Ca transformed into acid-soluble or acid-insoluble form. >50% of Mg and >40% of Ca retained in MC-0.32s are in acid-soluble and acid-insoluble fractions. This is likely due to Mg or Ca bonded to the oxygen-containing groups in biomass become incorporated into char matrix (CM), such as CM-Mg-CM or CM-Ca-CM, due to rapid deoxygenation during pyrolysis.[230] The acid-insoluble fraction may also be contributed by the formation of

magnesium or calcium aluminosilicate compounds which are thermally stable.[246] Therefore, no significant decrease in acid-insoluble Mg and Ca as particle residence time increases from 0.32 s to 0.51 s.

5.5 The evolution of particle shape for char particles

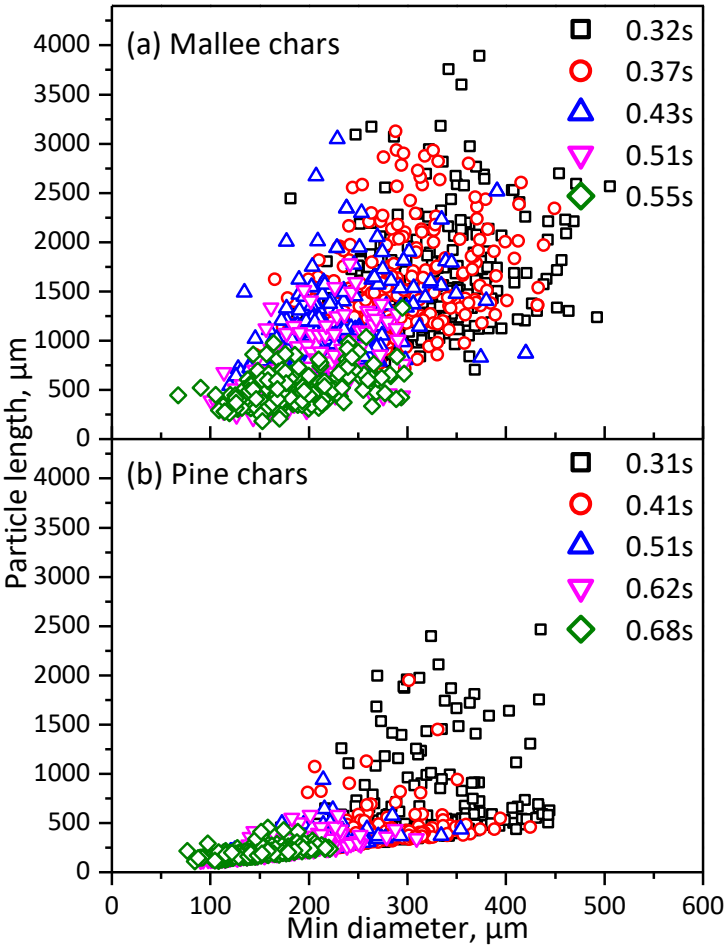

Figure 5.7 Evolution of particle length and minimum (min) diameter for (a) mallee chars and (b) pine char particles during rapid pyrolysis at 1300 °C

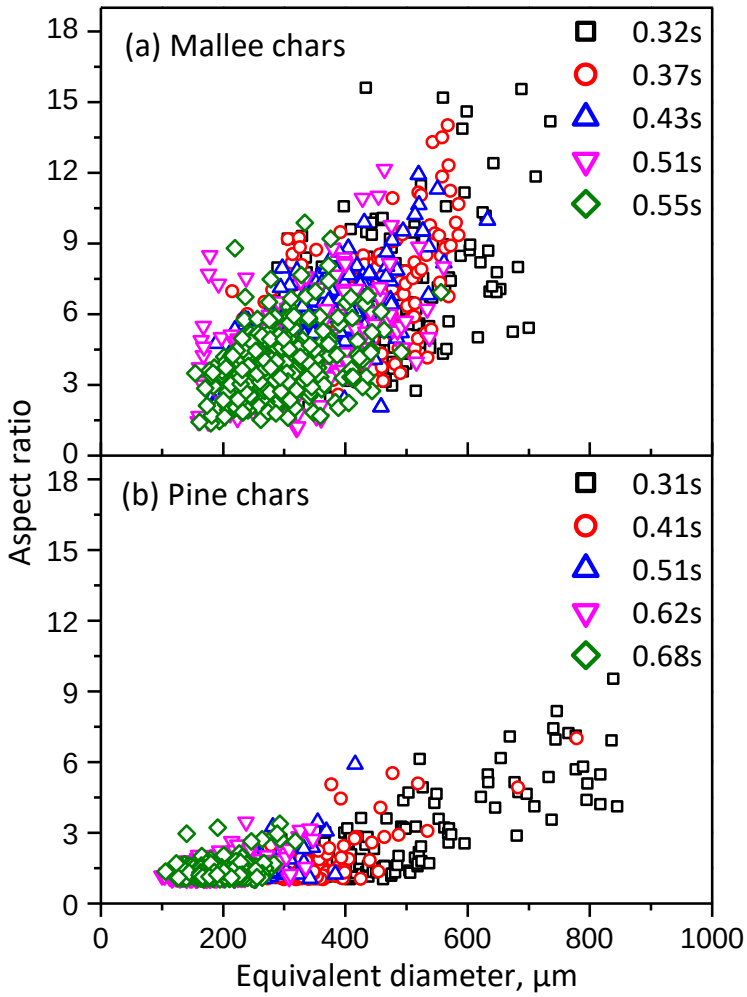

Figure 5.8 Evolution of aspect ratio and equivalent diameter for (a) mallee chars and (b) pine char particles during rapid pyrolysis at 1300 °C

Biomass particles are known to undergo significant deformation during pyrolysis. Figure 5.7 shows the correlation of char particle length and minimum (min) diameter for the particle residence time studied, while Figure 5.8 shows the correlation between char aspect ratio and equivalent diameter for the particle residence time studied. Such correlations for parent biomass particles are also presented in Figure 5.9 and Figure 5.10 for comparison. The average equivalent diameter, aspect ratio, minimum diameter, and particle length for each sample are defined as the median value of the frequency distribution of each parameter and are tabulated in Table 5.4.

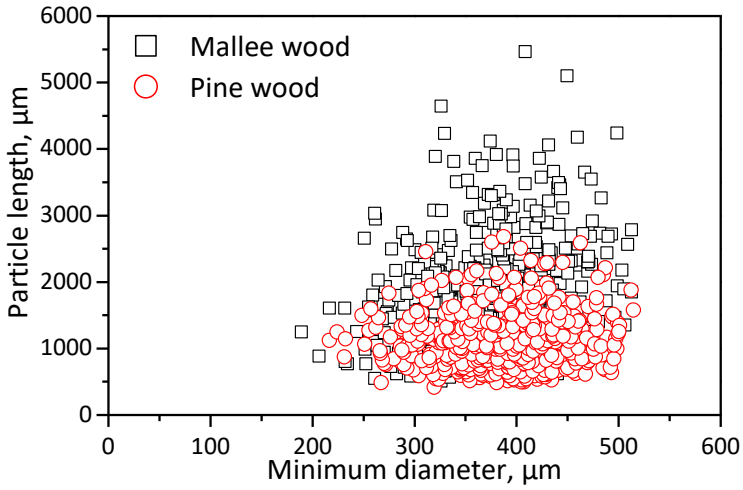

Figure 5.9 Correlation of particle length and minimum diameter for mallee wood and pine wood particles

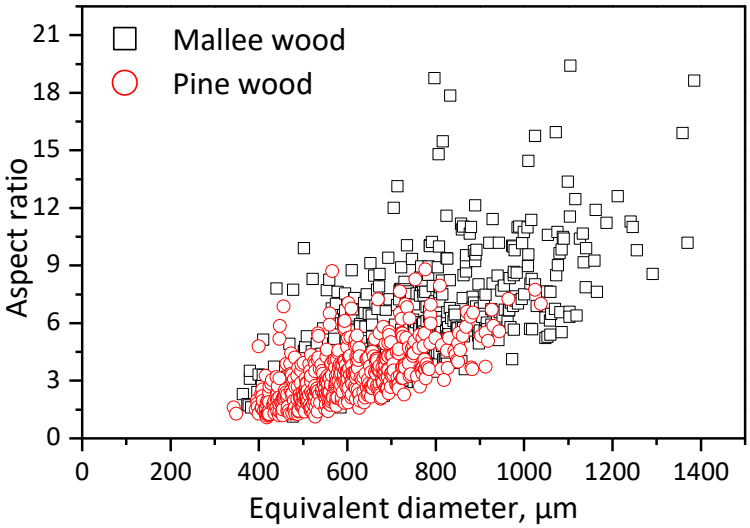

Figure 5.10 Correlation of aspect ratio and equivalent diameter for mallee wood and pine wood particles

Table 5.4 Average equivalent diameter (De), aspect ratio (AR), minimum (min) diameter, and particle length for biomass and char particles. De and AR refer to equivalent diameter and aspect ratio, respectively

	Mallee wood	Mallee chars				
		0.32s	0.37s	0.43s	0.51s	0.55s
Average De/μm	655.5	395.6	365	308.8	302.5	276.4
Average AR	4.9	4.7	4.6	4.4	3.6	3.5
Average min diameter/μm	380.7	305.8	270.6	200.2	185.7	174.2
Average particle length/μm	1837.5	1393.9	1267.2	777.5	496.9	460.7
	Pine wood	Pine chars				
		0.31s	0.41s	0.51s	0.62s	0.68s
Average De/μm	533.2	322.2	266	179.4	174	189.4
Average AR	2.81	1.33	1.24	1.23	1.23	1.19
Average min diameter/μm	393.6	302.7	219.7	164.0	161.7	148.8
Average particle length/μm	1241.6	484.4	281.2	206.6	200.5	191.4

The overall trend observed for both mallee and pine chars is particle dimensions including length and diameter shrink as particle residence time increases. However, the evolution of particle shape for mallee chars is distinctly different from pine chars. Mallee char particles exhibit a progressive and steady decrease in dimensions. Table 5.4 shows ~25% and ~20% reductions in average particle length and minimum diameter for MC-0.32s compared to the parent biomass particles. Some of the particle length for MC-0.32s is in the range of 3000-4000 μm which is close to the upper range of mallee wood particle length (see Figure 5.9). MC-0.37s only sees a further ~5% and ~9% reductions in the average particle length and diameter but a more significant reduction is observed for MC-0.43 s. The average particle length and diameter reduce by ~27% and ~18%, which could be the consequence of massive destruction of fibrous structure in mallee wood during pyrolysis. The average minimum particle diameter remains relatively unchanged at the particle residence time of >0.43 s, but the continuous decline in particle length is evident. This is also understandable because thermal conduction for an elongated particle is always dominant in the radial direction than the axial direction.[247] The small reduction in the average particle aspect ratio for mallee char particles at the early stage of pyrolysis (particle residence time up to 0.43 s) clearly suggests that those particles retain their elongated shape.

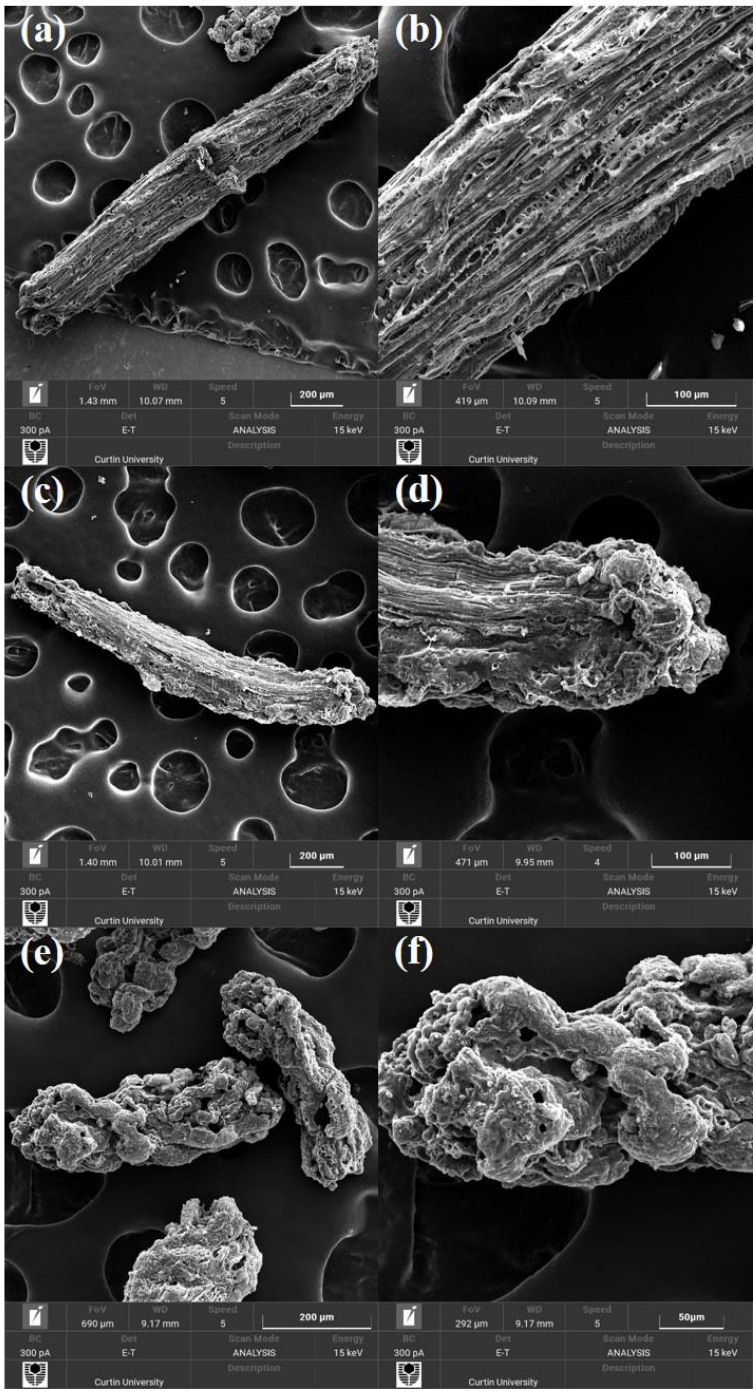

Figure 5.11 SEM images for mallee char particle with different pyrolysis extent.

More significant deformation of char particles is only observed at later stages of pyrolysis with evidence from the SEM images in Figure 5.11. For MC-0.32s, Figure 5.11a and b show that fibrous structure is prominent for the entire particle, and open pores with longitudinal arrangement are observed throughout the char surface. For MC-0.43s, traces of melted structure are discerned, especially at both ends of the particle, where substantial melting of biomass fibrous structure can be seen. The

number of regular pores also decreases remarkably, probably as a result of pore expansion and melting. At a particle residence time of 0.55 s when complete pyrolysis is achieved, the char particles are severely deformed. Particles are shorter and large cavities are noticeable. Although traces of fibrous structure can be found, the surface for char particles predominantly resembles the residue of a molten structure formed during pyrolysis.

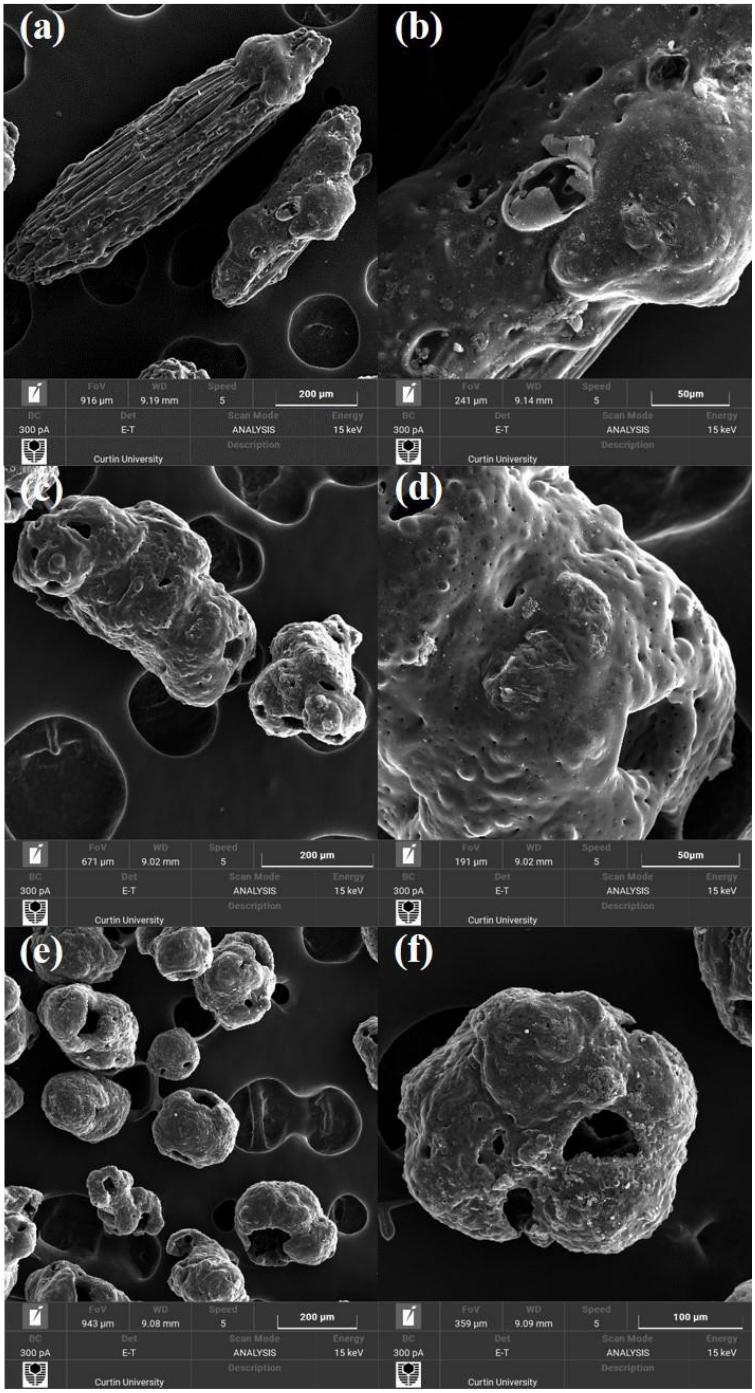

Figure 5.12 SEM images for pine char particle with different pyrolysis extent. Panel a and b: PC-0.31s, panel c and d: PC-0.41s, and panel e and f: PC-0.68s

Unlike mallee char particles, pine char particles seem to have less resistance to particle deformation during pyrolysis. Only a few partially pyrolyzed PC-0.31s particles can retain their particle length above 1000µm despite that the original pine wood particle length can reach more than 2000 µm. Compared to pine wood particles, the average particle length and diameter drop by ~61% and ~23% for PC-0.31s, then a further ~42%

and ~27% reduction for PC-0.41s. After another ~27% and ~25% reduction in average particle length and diameter for PC-0.51s, the dimensions remained unchanged for PC-0.62s and PC-0.68s. The correlation of aspect ratio and equivalent diameter for pine char particles shown in Figure 5.8b is scattered for PC-0.31s but mostly constrained to an aspect ratio of <3 for pine char particles with longer particle residence times. Table 5.4 shows that the average aspect ratio decreases sharply from 2.81 for pine wood to 1.33 for PC-0.31s, then kept at around 1.2 for pine chars with particle residence times ≥0.41 s. This signifies that pine char particles deform to form a spherical shape even at a short particle residence time. The SEM pictures in Figure 5.12 show that PC-0.31s particles are mostly molten at both ends but the fibrous structure can still be seen for some PC-0.31s particles. The surface of other pine char particles is completely melted, with some bursting bubbles left. The feature of PC-0.41s and PC-0.68s particles are similar. These particles appear to be completely plasticized and large cavities resulted from intensive swelling/foaming due to the increased internal pressure and violent release of volatile matter are clearly visible. However, PC-0.68s particles are rounder compared to PC-0.41s. The above observations suggest that deformation happens soon after pine wood being exposed to the high temperature which can be ascribed to the following factors. Firstly, the long flake-like shape of pine wood particles leads to a higher average heating rate experienced by the particles, which results in more extensive plasticization of cell structure during pyrolysis.[8, 152, 248] Besides, the much higher content of K and Ca in mallee wood also contribute to the less severe melting for mallee chars by enhancing those reactions towards char formation, i.e., polymerization/cross-linking, which are considered as important factors to prevent plasticization.[43, 78]

5.6 Conclusions

This study deployed a new DTF system for accurate-determining char yields, which enable a systematical investigation into the evolution in char yield, shape and morphology, and transformation of AAEM species during rapid pyrolysis (at 5 particle residence times) of mallee wood and pine wood particles (250-355 μm) at 1300 °C. The results show that the char yield decreases with increasing particle residence time but remained unchanged after 0.51 s for mallee wood and 0.41 s for pine wood, at which point the pyrolysis process is mostly completed. Pine wood underwent a more

significant mass loss (2.8 wt% char yield) compared to mallee wood (3.8 wt% char yield). Likewise, the retention of AAEM species also decreases with particle residence time. About 70% of Mg and Ca, ~50% of K, and ~20-30% of Na are retained in mallee char and pine at the particle residence time of ~0.51 s and ~0.41 s, respectively. However, the retention of AAEM species in pine char continues to reduce by 15-20% as particle residence time increase from 0.41 s to 0.68 s which can be attributed to the loss of oxygen-containing group on nascent char resulted from thermal annealing/cracking for nascent char. Chemical fractionation of a partially pyrolyzed mallee char (MC-0.32s) and a completely pyrolyzed mallee char (MC-0.51s) shows a portion of water-soluble Na and K transformed to ion-exchangeable Na and K during the early stage of pyrolysis. Further pyrolysis leads to loss of oxygen-containing groups thus a reduction in ion-exchangeable Na and K. However, Mg and Ca transform from water-soluble and ion exchangeable form to acid-soluble and acid-insoluble forms after pyrolysis as they become incorporated into the char matrix. The investigation of particle shape shows that mallee and pine wood particles experience severe deformation during pyrolysis, leading to significantly reduced particle length, diameter, and aspect ratio. However, unlike the extensive melting behavior of pine wood particles, the fibrous structure of the mallee wood is retained during the early stage of pyrolysis.

CHAPTER 6 RAPID PYROLYSIS OF PULVERIZED BIOMASS AT HIGH TEMPERATURE: EFFECTS OF TORREFACTION TEMPERATURE ON CHAR YIELD, RETENTION OF ALKALI AND ALKALINE EARTH METALLIC SPECIES AND CHAR PARTICLE SHAPE

6.1 Introduction

Many investigations about the thermal behaviour of torrefied biomass were carried out by thermogravimetric analysis at a temperature <900 °C using slow heating rates (10-25°C/min).[249-253] One of the key effects of torrefaction on biomass pyrolysis is the increased char yield as reported in many previous studies. However, because the investigation of torrefied biomass under conditions pertinent to pulverized fuel combustion is limited,[177, 254] there is little data available in regards to the effect of torrefaction on char yield at the high heating rate and high temperature (≥1100 °C). Besides, the ash-tracer method has been proved to be inaccurate due to the evaporation of some ash-forming elements.[23] Therefore, the direct determination of char yield for torrefied biomass under rapid heating and high-temperature conditions is needed.

Another interesting aspect is the particle shape of char pyrolyzed at high temperatures. The pulverized biomass particles usually have an irregular and elongated shape because of their fibrous structure. This variation in shape can cause differences in particle physical properties such as surface area-volume ratio, bulk density, and chemical properties, including char burnout and heat/mass transfer efficiency, etc., which consequently affects the biomass thermochemical conversions.[79, 137] Considering the degradation of three major compounds (cellulose, hemicellulose, and lignin) of biomass during torrefaction, it is reasonable to suspect torrefaction could have some impacts on the biomass particle deformation.[255] However, particle size distribution using laser analysis cannot provide detailed shape parameters.[178] The effect of torrefaction intensity on the aspect ratio of char at different burnout levels was also investigated.[256] However, the study about the effect of torrefaction on the particle shape of char produced by rapid pyrolysis has not been found.

Therefore, the objective of this chapter is to evaluate the effect of torrefaction temperature on biomass rapid pyrolysis conducted in a novel double-tube drop-tube furnace (DTF) at 1300 °C. Mallee wood (MW) was cut and sieved to a size fraction of 150-250 um before torrefaction to ensure the uniformity of the original particle size. Three torrefaction temperatures 220 °C, 250 °C, and 300 °C were used and the torrefied biomass produced at these three temperatures are denoted as MW-T220, MW-T250, and MW-T300. After rapid pyrolysis, resultant mallee char samples in the cyclone are referred to as MC, MC-T220, MC-T250, and MC-T300 as the pyrolytic products of MW, MW-T220, MW-T250, and MW-T300, respectively. The properties of these samples are listed in Table 6.1 and Table 6.2. Attentions were paid to the char yield, the retentions of AAEM species in char, and char morphology, including particle size and shape.

Table 6.1 Proximate and ultimate analysis for raw and torrefied biomass and their chars

Samples	Moisture (wt%, ad[a])	Proximate analysis (wt%, db[b])			Ultimate analysis (wt%, daf[e])				Molar ratio	
		ash	VM[c]	FC[d]	C	H	N	O[f]	O/C	H/C
MW	5.11	0.59	87.71	11.70	45.32	6.11	0.20	48.37	0.80	1.62
MW-T220	4.83	0.63	82.50	16.87	47.12	5.82	0.22	46.84	0.74	1.48
MW-T250	3.60	0.82	81.60	17.58	49.26	5.72	0.26	44.76	0.68	1.39
MW-T300	1.95	1.11	75.58	76.69	52.63	4.89	0.28	42.20	0.60	1.11
MC	3.66	11.77	34.28	53.95	85.61	1.77	0.52	11.10	0.10	0.24
MC-T220	3.75	11.64	48.86	39.50	85.52	1.55	0.48	12.45	0.11	0.22
MC-T250	2.07	10.92	53.99	35.09	86.07	1.48	0.49	11.96	0.10	0.21
MC-T300	2.02	6.64	35.09	58.27	87.20	1.05	0.39	11.36	0.10	0.14

[a] air-dried; [b] dry-basis; [c] volatile matter; [d] fixed carbon; [e] dry and ash-free basis; [f] By difference.

Table 6.2 Concentrations of inorganic species in raw and torrefied biomass and their chars, mg/kg (dry basis)

	MW	MW-T220	MW-T250	MW-T300
Na	110.6 ± 0.8	111.3 ± 1.5	112.8 ± 0.3	171.9 ± 0.8
K	724.0 ± 1.2	735.5 ± 5.3	741.4 ± 0.4	1125. ± 11.2
Mg	270.4 ± 10.1	274.8 ± 5.4	278.6 ± 4.8	422.5 ± 2.5
Ca	1594.4 ± 19.4	1639.2 ± 21.4	1658.9 ± 31.1	2503.3 ± 10.8
Mn	157.5 ± 1.2	170.3 ± 2.2	199.0 ± 7.3	261.4 ± 37.1
P	179.2 ± 1.1	170.8 ± 1.7	196.0 ± 2.7	273.2 ± 22.1
Al	13.3 ± 1.5	8.5 ± 0.7	11.0 ± 0.7	11.8 ± 0.5
Zn	8.1 ± 0.1	8.0 ± 0.2	10.3 ± 0.3	12.9 ± 1.1
Cu	1.7 ± 0.7	1.9 ± 0.1	2.8 ± 0.1	3.8 ± 0.3
Si	6.3 ± 1.8	6.0 ± 4.1	14.5 ± 1.5	14.8 ± 3.6
Ti	0.3 ± 0.1	1.1 ± 0.1	1.2 ± 0.6	1.2 ± 0.1
Cl	214.1 ± 10.6	128.1 ± 0.5	75.9 ± 0.3	34.0 ± 5.9
S	99.8 ± 3.1	102.6 ± 2.2	98.4 ± 1.2	129.8 ± 2.9

	MC	MC-T220	MC-T250	MC-T300
Na	205.4 ± 10.2	234.1 ± 4.1	219.9 ± 3.3	150.8 ± 7.0
K	10059.5 ± 253.4	10604.0 ± 316.7	10019.7 ± 305.4	6968.3 ± 47.2
Mg	6129.4 ± 42.6	6096.7 ± 19.2	5489.1 ± 34.1	3074.8 ± 23.2
Ca	36271.5 ± 358.5	36856.0 ± 207.5	33509.8 ± 716.6	18472.3 ± 551.3
Mn	3431.5 ± 90.6	2372.9 ± 46.3	1945.6 ± 32.1	1320.9 ± 5.1
P	3851.8 ± 46.4	2748.0 ± 282.9	2421.8 ± 192.4	2004.6 ± 12.4
Al	226.2 ± 58.4	156.6 ± 19.1	121.2 ± 47.8	132.1 ± 13.6
Zn	34.8 ± 1.2	28.7 ± 1.6	28.8 ± 4.8	23.9 ± 0.7
Cu	252.2 ± 59.8	254.6 ± 90.7	114.4 ± 4.2	91.3 ± 1.3
Si	487 ± 15.8	493.3 ± 23.5	409.8 ± 70.6	238.7 ± 13.5
Ti	55.4 ± 9.6	34.6 ± 10.8	23.88 ± 12.6	23.7 ± 1.9

Table 6.3 Contents of structural carbohydrates in raw and torrefied biomass, wt% (dry basis)

Constituent	MW	MW-T220	MW-T250	MW-T300
Hemicellulose	26.06	24.52	21.28	9.78
Arabinan	1.46	1.01	0.73	0.05
Galactan	2.74	2.36	1.84	0.10
Glucan	2.33	2.84	3.13	7.78
Xylan	18.97	17.75	15.13	1.81
Manan	0.56	0.55	0.45	0.03
Cellulose	41.74	39.74	35.61	22.33
Acid soluble lignin	8.29	6.38	5.34	0.47
Ash-free acid insoluble residue (A.I.R.)	20.17	22.18	25.92	46.65
Others	3.74	7.18	11.85	20.77

6.2 Sample characteristics and solid mass yield

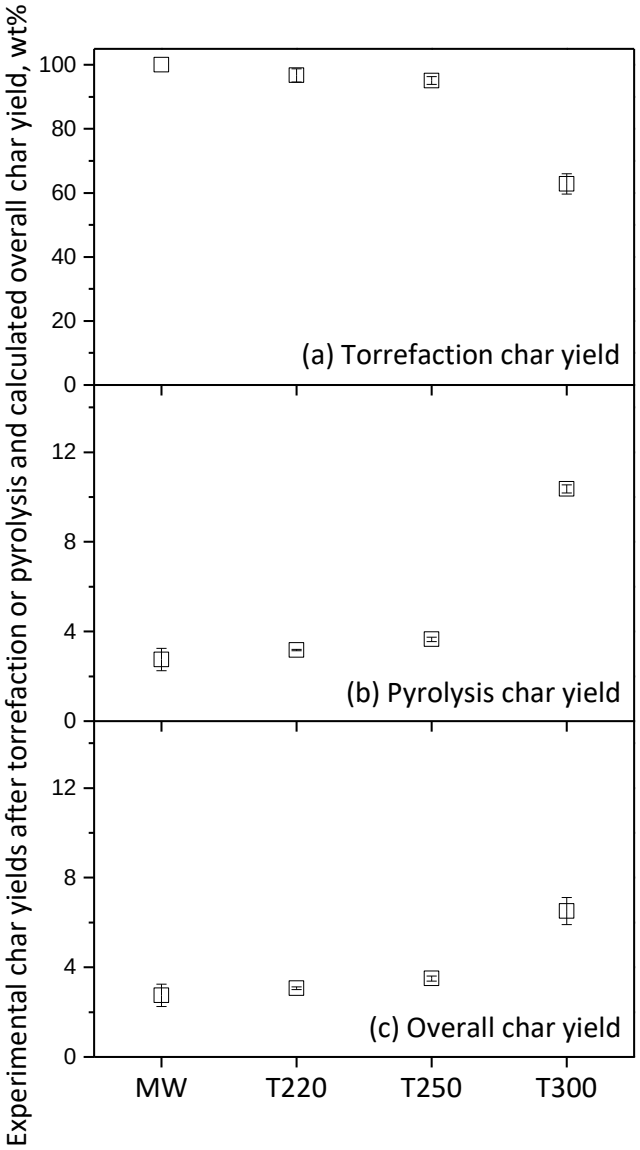

Figure 6.1 . (a) Torrefaction char yield at temperatures of 220 °C, 250 °C, and 300 °C; (b) Pyrolysis char yield at 1300 °C using MW and torrefied biomass; and (c) Overall char yield. Torrefaction char yield for MW is considered as 100%. T220, T250, and T300 indicate that the samples were torrefied at 220 °C, 250 °C, and 300 °C for panel (a) and then pyrolyzed at 1300 °C for penal (b) and (c)

The properties of raw and torrefied biomass (MW, MW-T220, MW-T250, and MW-T300) are listed in Table 6.1-6.3. With the increasing torrefaction temperature, volatile matter contents, O/C and H/C ratio, and two biomass main constituents (hemicellulose and cellulose), all decrease to different extents while contents of ash, fixed carbon, and lignin increase. The results are consistent with previous works on biomass

torrefaction.[257] It can be seen that MW-T300 has distinct properties from other samples. For instance, the significant decrease in the contents of hemicellulose from ~25% for MW and MW-T220 to 9.78% for MW-T300 indicates the severe decomposition of it at 300°C. 90% of xylan which is the dominant fraction of hemicellulose in MW is decomposed after being treated at 300°C. The content of ash-free A.I.R. in Table 6.3 is more than doubled for MW-T300 compared to MW, which could be the result of the extensive cross-linking and charring reactions during torrefaction at 300°C.[174, 258-260] Table 6.2 demonstrates that the concentrations of many inorganic species increased with the higher torrefaction temperature. This is because the degradation of organic structure leads to the release of volatile matter while most inorganic species tend to remain in the solid phase, which causes the accumulation of inorganic species in torrefied biomass. Torrefaction seems to be an effective way to reduce Cl content in MW because ~50% of Cl was released at a low torrefaction temperature of 220°C, as shown in Table 6.2.

Torrefied char yield and pyrolysis char yield were determined experimentally by calculating the weight loss of samples after torrefaction or pyrolysis. Results in Figure 6.1 show that MW-T300 has a much lower torrefied char yield at ~70%, compared to MW-T220 and MW-T250 (both above 95%). Pyrolysis char yields for MC, MC-T220, MC-T250, and MC-T300 are 2.8%, 3.2%, 3.7%, and 10.4%, respectively. It can be seen that the pyrolysis char yield of MW-T300 is about triple that of other samples, suggesting that severe torrefaction can induce considerably higher pyrolysis char yield at 1300 °C. Previous analyses about the properties of torrefied biomass (Table 6.3) indicate that structural carbohydrates in MW-T300 have a higher degree of carbonization and cross-linking, which is known to favor the formation of char during rapid pyrolysis. A simplified mechanism proposed by Zheng et al. shows that during torrefaction, depolymerized cellulose species could bond together by crosslinking which is increasingly significant as torrefaction temperature gets higher, and further to form char by polycondensation.[174] Besides, the higher contents of inorganic species in MW-T300 are considered important catalysts to enhance char formation. Overall char yield presented in Figure 6.1, (c) combines the effect of torrefaction and rapid pyrolysis, and is defined as overall yield=torrefied char yield × pyrolysis char yield. The negligible difference in overall yield for MC, MC-T220, and MC-T250 reveals that mild and moderate torrefaction at 220°C and 250°C have little impact on the final

solid mass while severe torrefaction temperature can noticeably improve the overall char yield, from ~3% for MC, MC-T220, and MC-T250 to ~7% for MC-T300.

6.3 AAEM retention during torrefaction and pyrolysis

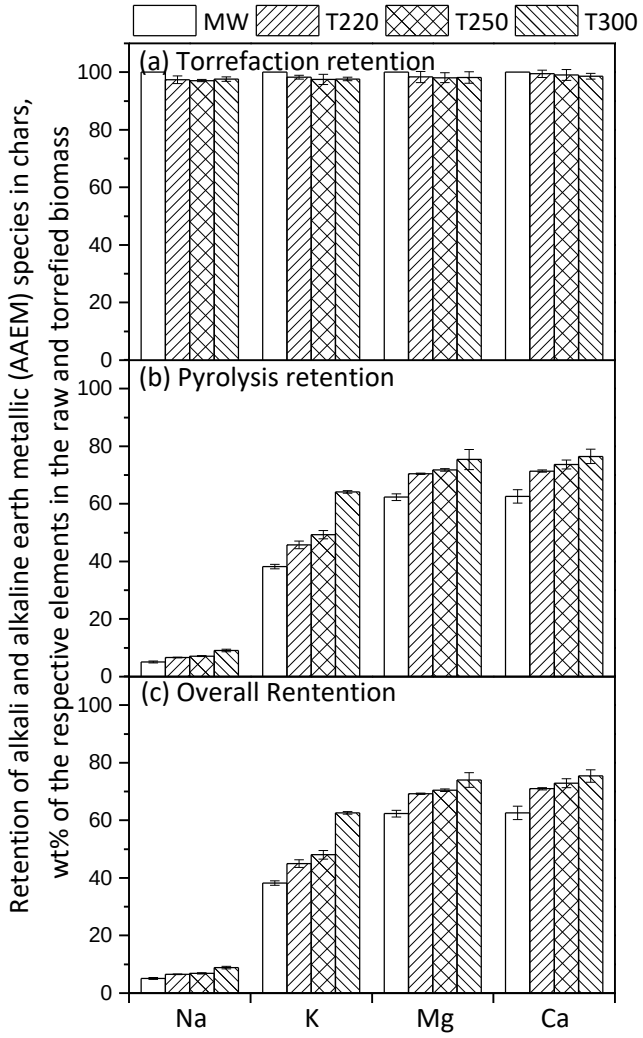

Figure 6.2 Retentions for AAEM species after (a) torrefaction, (b) pyrolysis, and (c) overall retention. Torrefaction retention for MW is considered as 100%. T220, T250, and T300 indicate that the samples were torrefied at 220 °C, 250 °C, and 300 °C for panel (a) and then pyrolyzed at 1300 °C for penal (b) and (c)

Retention of AAEM species after torrefaction, rapid pyrolysis, and the overall retention were calculated and presented in Figure 6.2, referring to as the torrefaction retention, pyrolysis retention, and overall retention. It can be seen that torrefaction retention is close to 100%, suggesting that little AAEM species were released during torrefaction. Therefore, the overall retention of torrefied biomass is similar to their

pyrolysis retention. It is known that rapid pyrolysis leads to extensive evaporation of AAEM species.[261] For MC, MC-T220, and MC-T250, only ~5% of Na is retained but for MC-T300 ~10% of Na is retained. Retention of K is ~40% for MC, then increases to ~45% for MC-T220 and MC-T250, further rising to ~60%. The low retention of Na than K during thermal conversions has been observed in other works.[59, 262-263] The higher retention of K than Na can be explained by the more electropositive nature of K, which can form intercalation compounds with carbon and prevent its vaporization.[262] On the contrary, some Na compounds such as Na_2O and NaCl evaporate easily.[59] Retention of Mg and Ca for MC are ~60%, and have a gradual rise from ~70% to ~75% as the torrefaction temperature increases from 220°C to 300°C. The higher overall retention of Mg and Ca than Na and K indicate that Mg and Ca are relatively more stable, likely because of their divalent chemical character. Besides, the CFA analysis of raw and torrefied biomass presented in Figure 6.3 shows that the majority of Mg and Ca (70-60%) are ion-exchangeable, bonding to the organic matrix, while ~80% of Na and K are in the water-soluble form, which consists of sulfates, chlorides, or carbonates with low melting temperature.[95-96, 264] This difference in the chemical occurrence for AAEM species contributes to the variance of retention after pyrolysis.[263] There is a clear trend that with higher torrefaction temperature, more AAEM species are retained in chars after rapid pyrolysis. A comparison of MC and MC-T300 shows that the pyrolysis retentions of Na, K, and Mg/Ca increase by ~100%, ~50%, and ~25%, respectively. The considerably higher retention of AAEM species in MC-T300 can be ascribed to several reasons. Firstly, torrefaction alters the chemical occurrence of AAEM species, generating higher contents of AAEM species in relatively stable forms (acid-soluble and acid-insoluble form),[95] and this effect becomes more noticeable with increasing torrefaction temperature. For MW, MW-T220, and MW-T250, <2% of Na or K, <5% of Mg, and <10% of Ca are in the forms of acid-soluble and acid-insoluble. However, for MW-T300, the contents increase to 7%, 15%, and 20% for Na or K, Mg, and Ca, respectively. Researches have shown that acid-soluble and acid-insoluble elements are unlikely to be evaporated during thermal conversions,[265] therefore, MC-T300 has the highest retention of AAEM species. Secondly, Figure 6.1 shows that the pyrolysis char yield for MC-T300 is significantly higher, which means the decomposition of solid structures into volatiles is suppressed compared to MC-T220 and MC-T250. Because the organic structures could be released with AAEM species bound on them, the ordered and stable structures in MC-

T300 formed by extensive cross-linking reactions lead to not only the lower mass loss but also a higher tendency for AAEM species to be retained in char.[171, 252] Moreover, a part of small molecules in biomass is already released as volatiles during torrefaction, thus the production of pyrolysis gas by MC-T300 is relatively less intensive during rapid pyrolysis.[178] Prior studies have demonstrated that thermal cracking of volatiles generates free radicals (e.g. H radical), which could contribute to the release of AAEM species by displacing them to bond to char matrix.[229] The less intensive volatilization of MC-T300 leads to a lower concentration of free radicals, therefore, reducing the possibility of AAEM species being replaced and released. The displaced AAEM species could be truly released into the gas phase or re-bond to the reactive sites in the char matrix. It is suspected that this bond-reforming process is favored in MC-T300 due to the following facts. Firstly, the less intensive volatilization of MC-T300 could cause lower inner particle pressure, allowing more time and possibilities for AAEM species to be re-bound. Then, the larger average particle size of MC-T300 than other char samples (see Figure 6.8 and Figure 6.9) makes it more difficult for free AAEM species to be truly released after a longer diffusion/convection path inside the char particle. It is worth noting that mild and moderate torrefaction at 220°C and 250°C has only slight effect on increasing the retention of Na. However torrefaction at 300°C almost doubled the retention of Na, probably due to the significantly reduced volatile content under high torrefaction temperature because the release of Na is reported to be closely related to volatiles emission.[59]

6.4 Chemical occurrence of AAEM species

6.4.1 Chemical occurrence of AAEM species in torrefied biomass

The occurrence of AAEM species in raw and torrefied biomass is classified into four groups, water-soluble (chlorides, sulphates, and carbonates), ion-exchangeable (organically bonded), acid-soluble (oxides, sulphates, and carbonates), and acid-insoluble (silicates and aluminates).

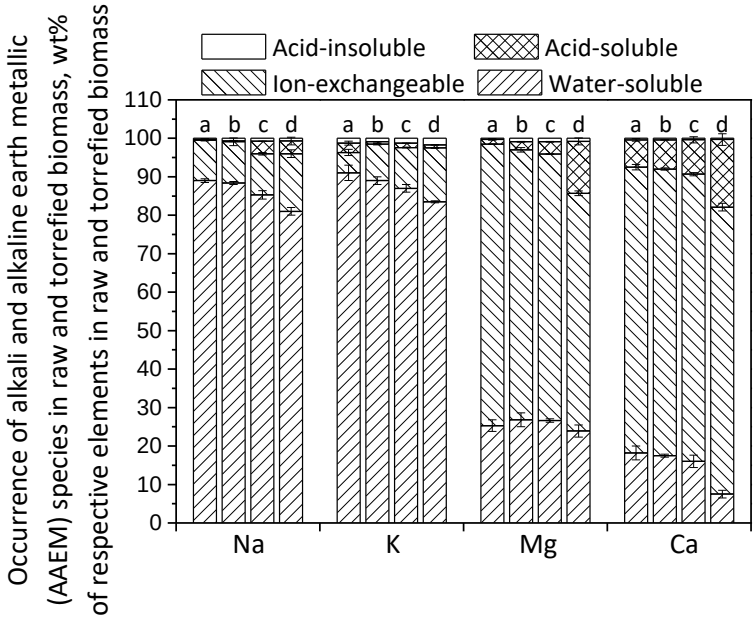

Figure 6.3 Occurrence of AAEM species in raw and torrefied biomass, expressed as the wt% of each element in the sample; a, b, c, and d stand for MW, MW-T220, MW-T250, and MW-T300, respectively

Figure 6.3 demonstrates the occurrence of AAEM species in raw and torrefied biomass with different torrefaction temperatures. It can be found that the dominant existing form for Na and K is the water-soluble form, however, the percentage of it gradually drops from ~90% to ~80% with the increasing torrefaction temperature. On the contrary, the percentages of ion-exchangeable Na and K increase by ~5-10%. This is possible because, during torrefaction, the water-soluble alkali chlorides react with oxygen-containing groups, resulting in the release of Cl and the association of alkali metals to organic matrix by ion-exchange.[128, 242] This could also be the reason for the reduction in the content of water-soluble Ca. The primary change for the occurrence of Mg is the shift from ion-exchangeable fraction to acid-soluble fraction after torrefaction. It is aware that alkaline earth metals in biomass (Mg and Ca) are mainly organically bound to the structure by oxygen-containing groups, e.g. carboxylic groups.[95] Previous studies show that the decomposition of carboxylic groups during torrefaction starts at <200°C, and becomes quite significant at 250°C.[96, 266] Therefore, the decreasing contents of ion-exchangeable Mg and Ca are likely due to the decomposition of carboxylic groups, forming acid-soluble $MgCO_3$ and $CaCO_3$. The formation of other Mg/Ca salts like phosphates and sulfates also could be responsible

for the higher percentages of acid-soluble Mg/Ca because the previous study observed higher contents of phosphates and sulfates in the HCl leachates after torrefaction.[96]

6.4.2 Chemical occurrence of AAEM species in chars

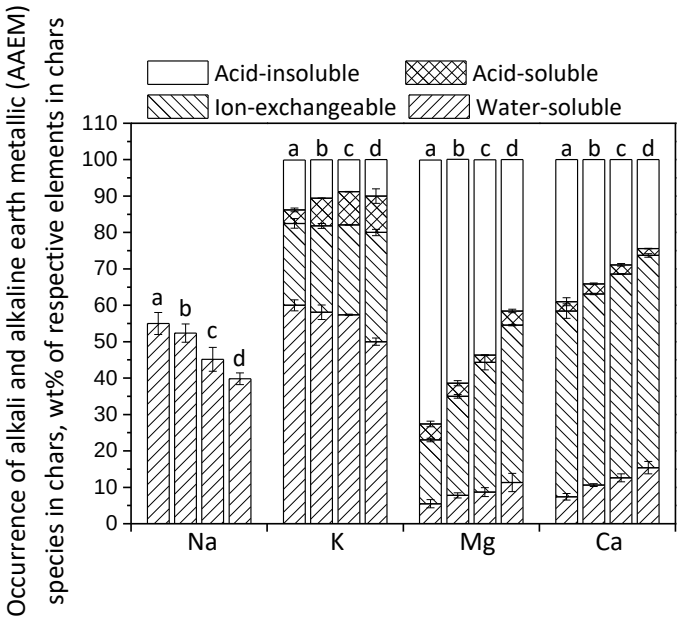

Figure 6.4 Occurrence of AAEM species in chars, expressed as the wt% of each occurrence in the sample; a, b, c, and d stand for MC, MC-T220, MC-T250, and MC-T300, respectively

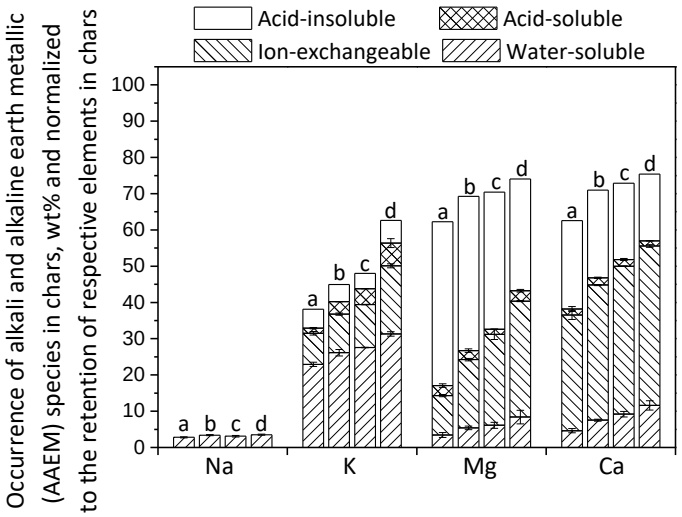

Figure 6.5 Occurrence of AAEM species in chars, normalized to the amount of AAEM species retained in char after rapid pyrolysis; a, b, c, and d stand for MC, MC-T220, MC-T250, and MC-T300, respectively

To investigate the occurrence of AAEM species in char samples, the same chemical fractionation analysis was applied and the results are presented in Figure 6.4. Considering the different evaporation extents of AAEM species, the percentages of difference chemical occurrence for each element are normalized to the actual amount of it retained in chars after rapid pyrolysis and plotted in Figure 6.5. Only the proportions of water-soluble form for Na in chars are presented in Figure 6.4 and Figure 6.5 due to the low concentration of Na meeting the threshold of ICP quantification. As the torrefaction temperature rises, the proportions of water-soluble Na and K in chars decrease from ~55% and ~60% to ~40% and ~50%, respectively. In the meantime, the ion-exchangeable and acid-soluble K increase from ~25% to ~40% in total. This change is consistent with the transition of Na and K from water-soluble form to ion-exchange form in torrefied biomass as mentioned above. Besides, the higher retentions of Na and K indicate that an increasing amount of Na and K are likely to incorporate into the char matrix and form stable bonds such as C-Na and C-K, reducing the relative proportions of water-soluble Na and K in chars. However, the absolute amounts of water-soluble Na and K in Figure 6.5 still increase with higher torrefaction temperature, which suggests that the evaporation ability for water-soluble Na and K in torrefied biomass with higher torrefaction temperature is increasingly suppressed during rapid pyrolysis. Another noticeable trend in Figure 6.4 is the higher proportions of ion-exchangeable Mg and Ca, especially for ion-exchangeable Mg which increases from ~18% to 43% as torrefaction temperature raised to 300 °C. This means that higher torrefaction temperature leads to more Mg/Ca bound to or retained in organic structures after pyrolysis, probably due to the more cross-linked structure formed during torrefaction. Ultimate analysis for chars finds less oxygen loss by rapid pyrolysis for torrefied biomass, which means that oxygen-containing groups retained in torrefied biomass have higher stability than those in raw biomass. Similar results have been observed by Meng et al..[173] They investigated the distribution of oxygen in pyrolytic products and found that higher torrefaction temperature can cause more oxygen to be left in biochar. The oxygen-containing cross-linked structure could be stronger and relatively difficult to be broken down and thus protect the associated Mg/Ca. Besides, for the cleaved structure due to the release of oxygen, Mg/Ca could take the place of the released oxygen to act as the new cross-linking point during rapid pyrolysis.[230] Therefore the higher torrefaction temperature facilitates the retention of ion-exchangeable Mg/Ca in chars. Moreover, the higher pyrolysis char yield for MC-

T300 means that more organic compounds with AAEM species associated with them are retained in the solid phase rather than being gasified or ejected, therefore increasing the ion-exchangeable proportions. The slightly higher proportions of water-soluble Ca than water-soluble Mg could be attributed to the formation of CaO (product of $CaCO_3$ and CaC_2O_4 decomposition). The noticeable drop in the proportion of the acid-insoluble Mg may be the consequence of the lower concentration of silicon in MC-T300 which is less than half of it in MC and MC-T220, as listed in Table 6.2.

6.5 The shape of torrefied biomass and their chars

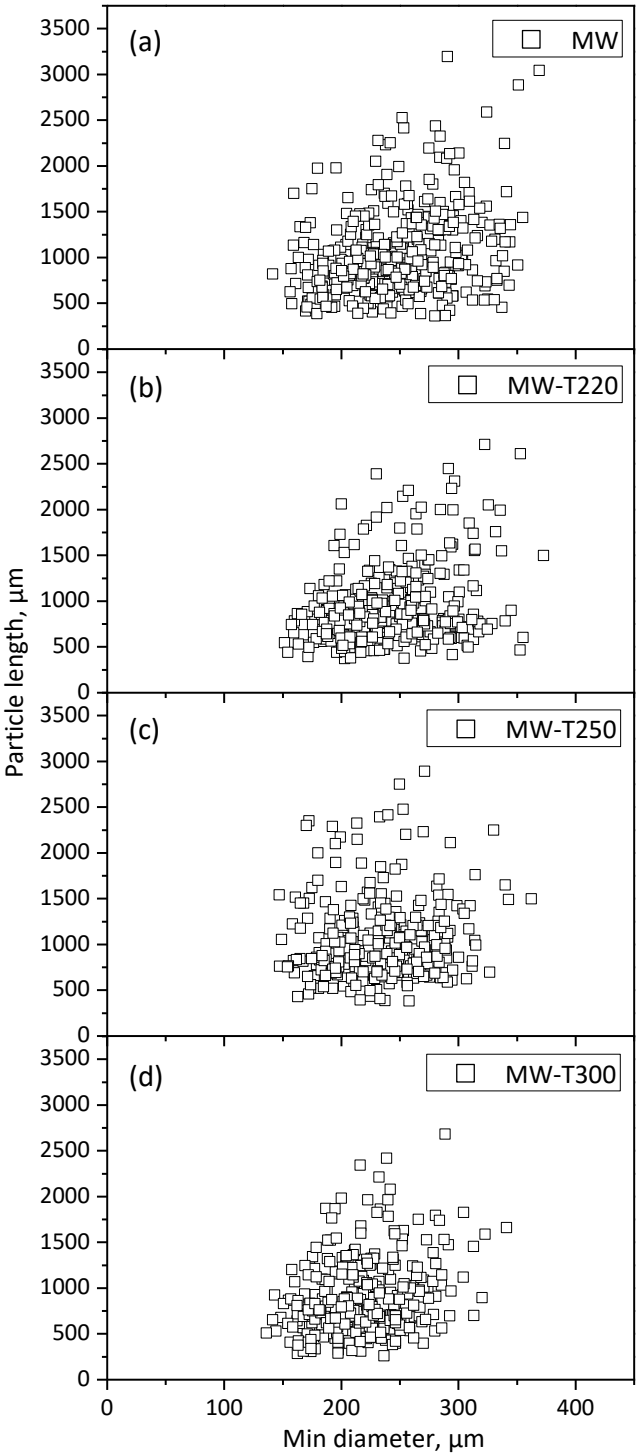

Figure 6.6 Correlation of particle length and minimum diameter for raw and torrefied biomass, (a) MW, (b) MW-T220, (c) MW-T250, and (d) MW-T300

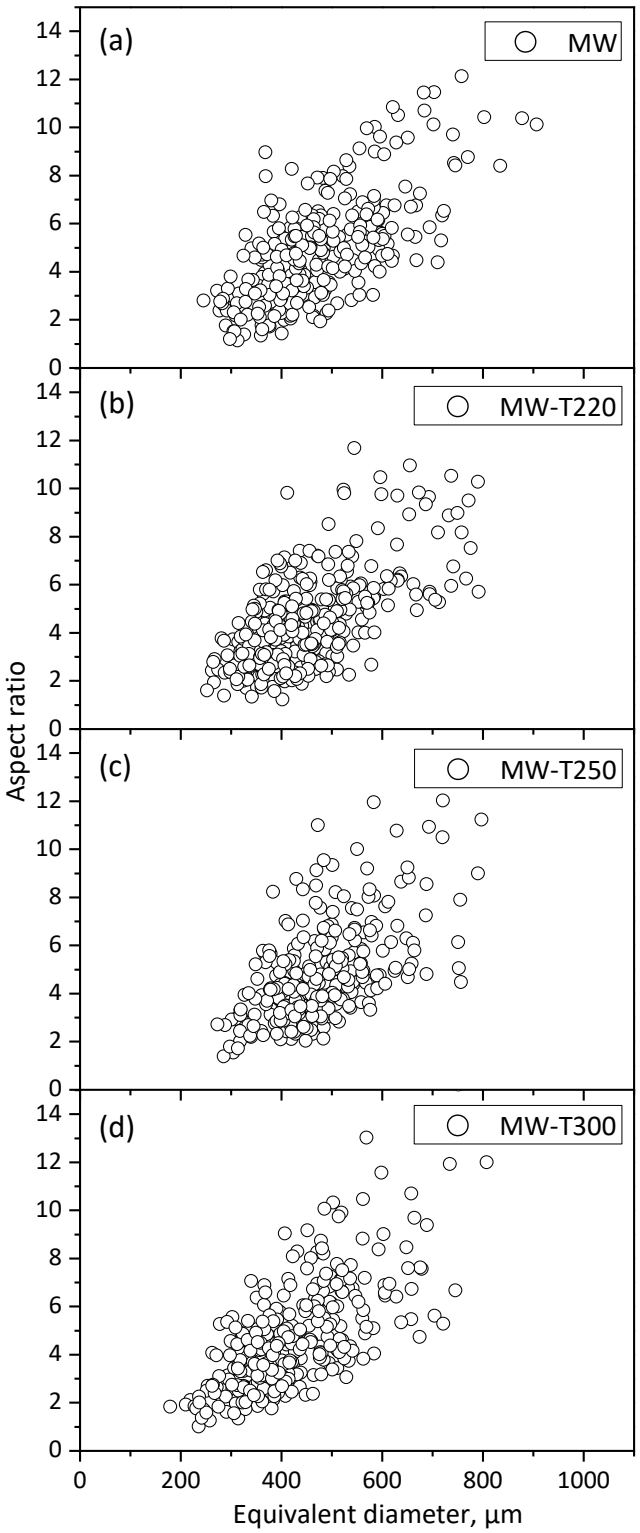

Figure 6.7 Correlation of aspect ratio and equivalent diameter for raw and torrefied biomass, (a) MW, (b) MW-T220, (c) MW-T250, and (d) MW-T300

Figure 6.6 and Figure 6.7 demonstrate the correlation of particle length vs. minimum (min) diameter and aspect ratio vs. equivalent diameter for raw and torrefied biomass. It can be seen that the particle length and min diameter for both raw and torrefied

biomass (MW-T220 and MW-T250) are in the range of 300-2500 µm and 150-350 µm while their aspect ratios and equivalent diameter are within 1.5-12 and 250-800 µm, respectively. Despite some dehydration and degradation of biomass constituents, the torrefaction process at <300 °C has negligible effects on particle size and shape. However, for MW-T300, its particle length and diameter are more concentrated between 250-2500 µm and 140-320 µm, probably due to severe dehydration, cross-linking, and charring reactions, and maybe the loss of some light particles during the collection of samples. Consequently, the equivalent diameter for MW-T300 shifts to 200-650 µm but the aspect ratio almost remains the same with other samples, which suggests the torrefaction has minimal effect on biomass particle shape.

The same shape parameters for pyrolyzed chars using raw and torrefied biomass are presented in Figure 6.8 and Figure 6.9. The particle length for chars is in the range of 100-700 µm, which is much lower than their parent samples, indicating significant biomass particle shrinkage occurred during rapid pyrolysis. However, the lower range of particle length for MC-T300 is 150 µm, being slightly larger than others. The min diameters for MC, MC-T220, and MC-T250 are within 75-225 µm, while for MC-T300, it moves to 100-275 µm. The equivalent diameter is a more straight-forward parameter to compare the particle size for chars. It can be found in Figure 6.9 that the equivalent diameter for char particles reduced more than half compared to their original biomass particles, which can be ascribed to the extensive devolatilization during rapid pyrolysis. Specifically, the equivalent diameter for MC, MC-T220, and MC-T250 are in the same range (100-300 µm), whereas for MC-T300, it is around 150-370 µm. The higher pyrolysis char yield for MC-T300 suggests that reactions such as polymerization and cross-linking are favored during pyrolysis after severe torrefaction treatment. It seems like these reactions also make the char structure more compact, causing a lower degree of shrinkage and therefore the larger particle size for MC-T300. The particle shape for char particles is represented by their aspect ratio and is shown in Figure 6.9. Unlike biomass particles, the aspect ratio range for char particles is much smaller, being 1-5 for MC, MC-T220, and MC-T250 and 1-4.5 for MC-T300, and most char particles have an aspect ratio <3. The slightly smaller value of aspect ratio for MC-T300 should be the consequence of its narrower particle length range and larger min diameter.

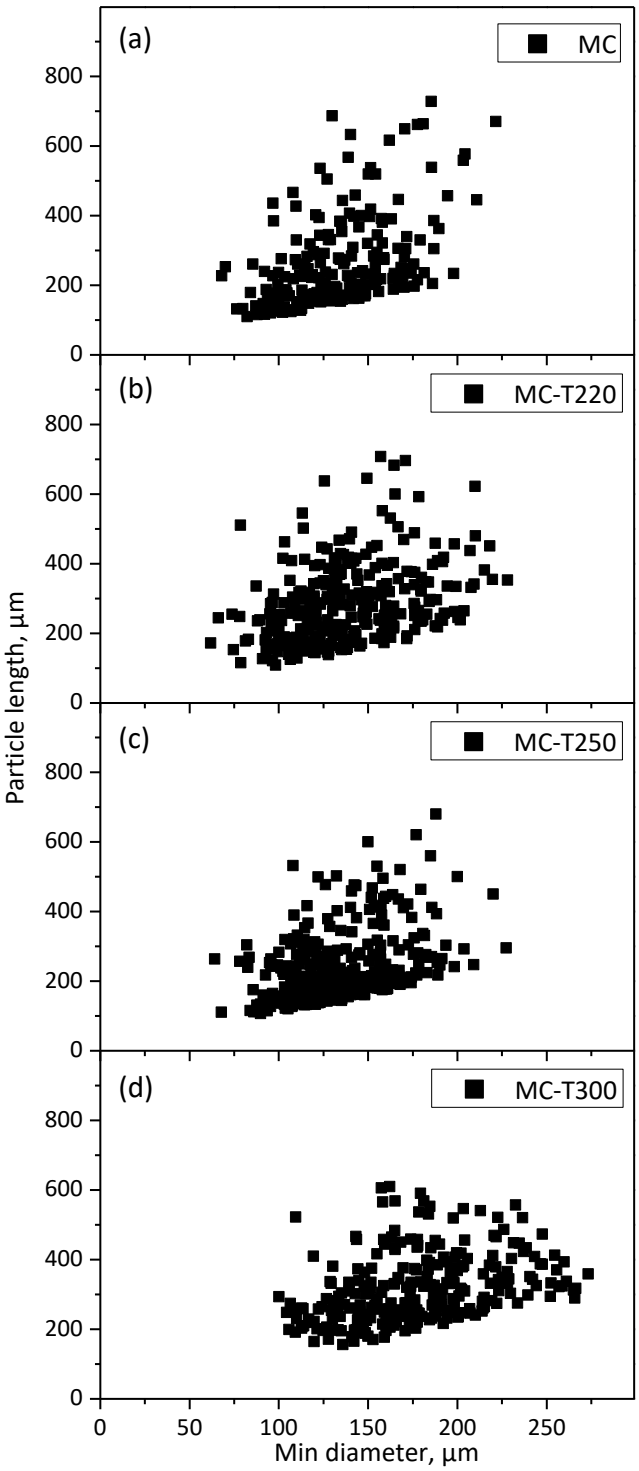

Figure 6.8 Correlation of particle length and minimum diameter for chars, (a) MC, (b) MC-T220, (c) MC-T250, and (d) MC-T300

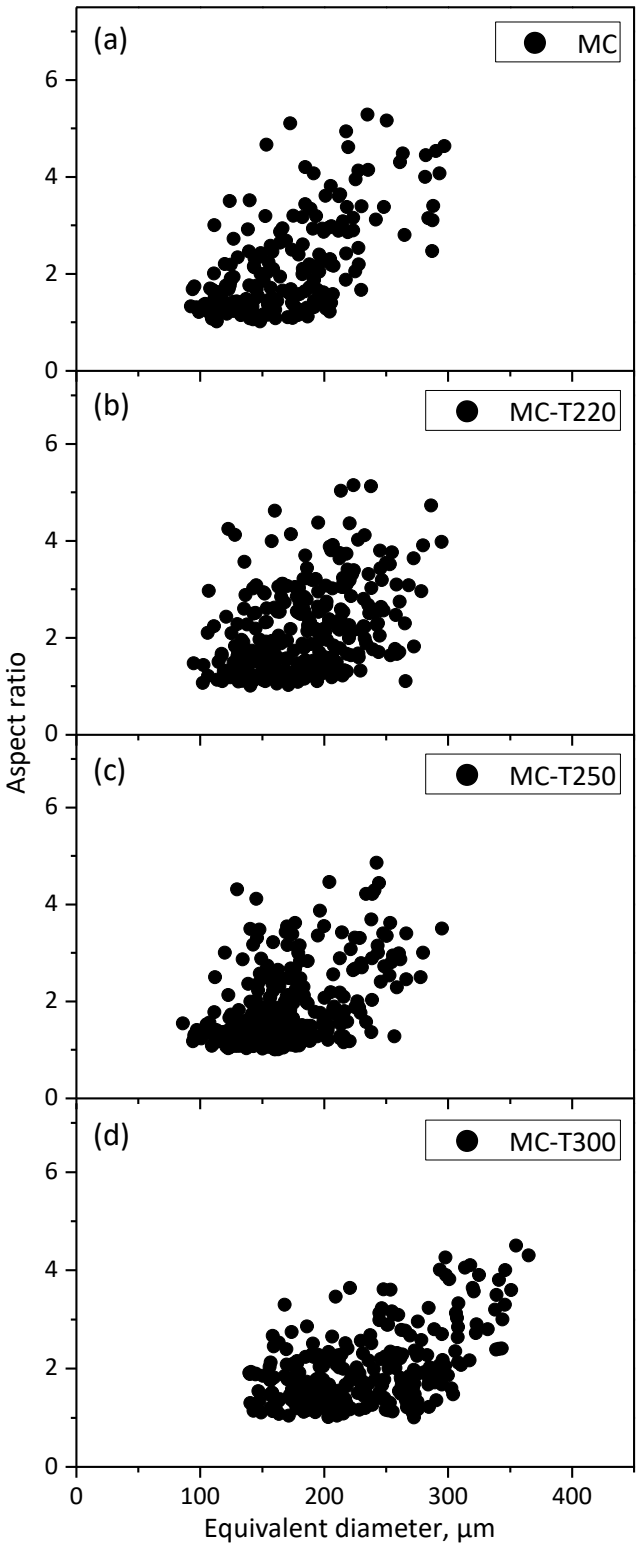

Figure 6.9 Correlation of aspect ratio and equivalent diameter for chars, (a) MC, (b) MC-T220, (c) MC-T250, and (d) MC-T300

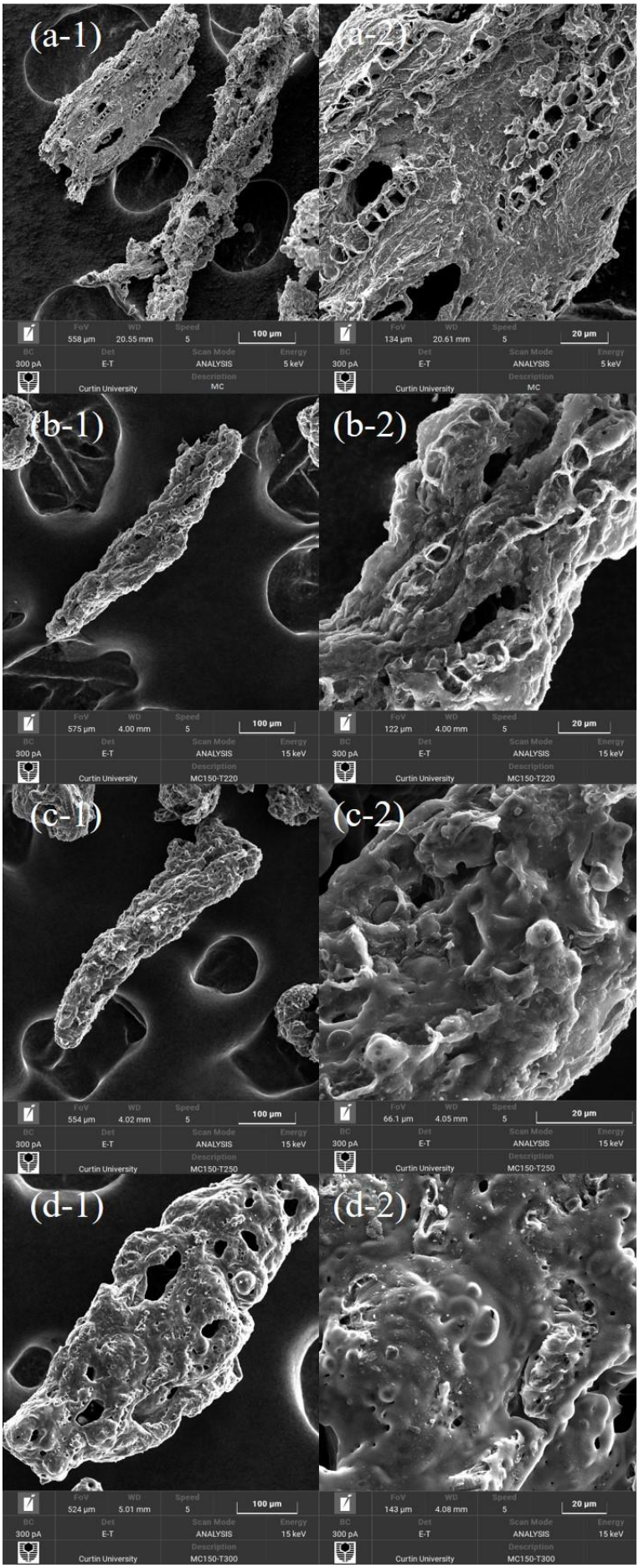
(a-1)
(a-2)
(b-1)
(b-2)
(c-1)
(c-2)
(d-1)
(d-2)

Figure 6.10 SEM images of chars produced from the rapid pyrolysis of torrefied biomass: (a-1) and (a-2) MC; (b-1) and (b-2) MC-T220; (c-1) and (c-2) MC-T250; (d-1) and (d-2) MC-T300

The SEM pictures for chars in Figure 6.10 show that both MC and MC-T220 have traces of fibrous structures on their rough surface. Those cavities and connected openings with clear edges resemble the remnant of the cell wall of xylem tissue, after the violent release of volatiles.[267] However, as shown in Table 6.3, the decomposition of hemicellulose (especially for xylan which is one of the three major secondary cell wall components for xylem) is significant after torrefaction at 300 °C. This could explain the lack of fibrous structures on the surface of MC-T300. The magnified SEM images show that the surface of MC-T300 is much smoother than the MC and MC-T220, indicating that MC-T300 has experienced severe plasticization during pyrolysis, which contributes to the lower aspect ratio for MC-T300. Similar phenomena have been observed previously.[83, 268-269] Tolvanen et al. pointed out that this phenomenon may be due to some liquid intermediates formed during torrefaction.[268] As the degree of plasticization of biomass is attributed to the formation of metaplast during the thermal conversion, it is possible that the liquid intermediates can facilitate the formation of metaplast and thus cause the severer plastic deformation of biomass structure. The experimental results by Pelaez-Samaniego et al. showed that the yield of lignin liquid intermediates reached the maximum at the torrefaction temperature of ~300°C,[270] which suggests that the effect of liquid intermediates on metaplast formation could be pronounced for MW-T300. The melting of surface structure is not significant for MC and MC-T220 probably because the pyrolysis at a high heating rate in DTF (~10^4 °C/s) makes the formation of metaplast as quick as the resolidification reactions,[271] and consequently the outline of the structure can be retained. However, with the abundant liquid intermediates in MW-T300 to promote the formation of metaplast and the lack of strong vascular structure like xylem, the surface of MC-T300 is easily softened and molten, becoming smoother after resolidification.

6.6 Conclusions

Rapid pyrolysis of raw and torrefied mallee wood (150-250 μm) was conducted at 1300 °C to study the effect of torrefaction temperature (220°C, 250°C, and 300°C) on the properties of chars. The direct determination of pyrolysis char yield by a novel

DTF system realizes the first investigation on the retention of AAEM species for torrefies biomass during pyrolysis with PF conditions. It is found that increasing torrefaction temperature can cause higher pyrolysis char yield, especially for biomass with high torrefaction temperature. This is ascribed to some reactions that happened during torrefaction (i.e., cross-linking and charring) alter the composition of the structural carbohydrate in torrefied biomass. The release of AAEM species is negligible during torrefaction but pronounced during rapid pyrolysis. Torrefied biomass has higher retention for AAEM species after rapid pyrolysis, compared to raw biomass, and raising torrefaction temperature from 220 °C to 300 °C can increase the retention of AAEM species from ~6% for Na, ~45% for K, ~70% for Mg, and 71% for Ca to ~9% for Na, ~63% for K, ~74% for Mg, and 75% for Ca. The reasons could be their more stable chemical forms and the various changes in organic structure during torrefaction. The chemical forms of AAEM species in chars show that the relative proportions of water-soluble Na and K decreased but ion-exchangeable and acid-soluble K increase with torrefaction temperature, indicating the stable existing status of Na and K in chars. The higher proportions of ion-exchangeable Mg and Ca indicate that more Mg and Ca are bonded to organic structures, which can be attributed to the higher stability of oxygen-containing groups in torrefied biomass. The significant reduction in acid-insoluble Mg and Ca in chars as torrefaction temperature rising may be mainly because of the lower concentration of silicon and more Mg and Ca bound to organic structures. Studies of the char morphology reveal that the torrefaction process has a negligible effect on the particle size and shape of biomass, whereas severe torrefaction can make the char particle size larger and aspect ratio smaller after pyrolysis, and the surface of those char particles seems to be smoother.

CHAPTER 7 A STUDY OF PARTICLE SIZE, SHAPE, AND RETENTIONS OF INORGANIC SPECIES DURING RAPID PYROLYSIS BASED ON INDUSTRIAL UTILIZATION OF TORREFIED WOOD CHIPS

7.1 Introduction

Woody biomass is often cut into large wood chips with dimensions of 5-50 mm.[272] Further pulverization of wood chips is needed to achieve a wider utility of biomass, such as palletization and co-combustion with coal in industrial power plants.[273] But the pulverization of biomass wood chips is extremely energy-consuming because of the poor grindability of biomass. Torrefaction is considered an effective method to improve the fuel characteristics of biomass as this pretreatment can reduce the moisture content, increase the energy density and grindability of biomass.[274] The detailed effect of torrefaction on the grindability of wood chips has been extensively studied.[46, 155, 275-276] However, no information about the shape of torrefied and ground particles was provided by these previous works despite the fact that the shape of biomass particles is critical to the thermoconversion processes by affecting the heat and mass transfer.[79, 142] Therefore, more data on the effect of torrefaction on the particle shape for ground wood chips are necessary.

There are even fewer studies mentioned the particle shape of torrefied biomass before fast pyrolysis. Although torrefied biomass powder which is regarded as a promising substituent to traditional coals,[273] there is still a lack of understanding for the rapid pyrolysis torrefied biomass at high temperature (>1100 °C) which relates to the conditions of industrial biomass co-firing with coal.[177, 254] The influence of particle size on the rapid pyrolysis of torrefied biomass powder has not been reported yet.

To address the above-mentioned knowledge gap, wood chips were torrefied at different temperatures than ground. Three torrefaction temperatures were used in this study: 220 °C, 250 °C, and 300 °C, representing mild, moderate, and severe torrefaction conditions. After pulverization, two size ranges (250-355 μm and 90-106 μm) were selected to carry out the rapid pyrolysis in a novel drop-tube furnace that

enables the direct determination of char yield at high heating rate and temperature (1300 °C). The prefix T220, T250, or T300 was added before MW300, MW100, PW300, and PW100 when referring to biomass samples torrefied at different temperatures. For example, T250-MW300 refers to the mallee wood chips torrefied at 250 °C and later sieved to 250-355 μm. Their char samples are represented by replacing W (wood) with C (char) as used in previous chapters. The focuses are the effect of torrefaction temperature on the properties of char particles they form after rapid pyrolysis, including char yield and the retention of inorganic species (mainly AAEM species), and the changes in particle shape and size. The properties of raw and torrefied biomass samples with different particle size fractions are summarized in Table 7.1-7.2.

Table 7.1 Proximate and ultimate analysis for raw and torrefied biomass

Samples		Moisture (wt%, ad[a])	Proximate analysis (wt%, db[b])			Ultimate analysis (wt%, daf[e])				Molar ratio	
			ash	VM[c]	FC[d]	C	H	N	O[f]	H/C	O/C
Raw	MW300	4.24	0.58	90.07	9.35	47.33	6.47	0.10	46.09	1.64	0.73
	MW100	4.35	0.61	91.67	7.72	46.51	6.49	0.13	46.87	1.68	0.76
T220	MW300	4.10	0.62	88.19	11.19	47.56	5.89	0.15	46.40	1.49	0.73
	MW100	4.38	0.66	90.49	8.85	47.14	6.15	0.12	46.59	1.57	0.74
T250	MW300	3.33	0.88	80.21	18.91	52.17	5.60	0.16	42.08	1.29	0.60
	MW100	3.65	0.92	81.83	17.25	51.16	5.64	0.14	43.06	1.32	0.63
T300	MW300	3.05	1.10	66.25	32.65	59.41	4.95	0.23	35.42	1.00	0.45
	MW100	3.36	1.25	68.74	30.01	59.25	5.51	0.19	35.05	1.12	0.44
Raw	PW300	4.15	0.24	93.25	6.51	45.39	6.33	0.07	48.21	1.67	0.80
	PW100	4.47	0.28	94.47	5.25	44.48	6.41	0.06	49.05	1.73	0.83
T220	PW300	3.46	0.27	90.59	9.14	48.85	5.37	0.06	45.72	1.32	0.70
	PW100	3.62	0.29	92.41	7.30	47.64	5.41	0.05	46.90	1.36	0.74
T250	PW300	2.90	0.30	82.68	17.02	50.51	4.98	0.07	44.44	1.18	0.66
	PW100	3.08	0.32	90.66	9.02	49.83	5.24	0.06	44.88	1.26	0.68
T300	PW300	2.18	0.45	70.61	28.94	59.11	4.71	0.06	36.12	0.96	0.46
	PW100	2.55	0.49	78.73	20.78	58.37	5.07	0.09	36.47	1.04	0.47

[a] air-dried; [b] dry-basis; [c] volatile Matter; [d] fixed carbon; [e] dry and ash-free basis; [f] by difference.

Table 7.2 Proximate and ultimate analysis for chars produced by pyrolysis of raw and torrefied biomass at 1300 °C

Samples		Moisture (wt%, ad[a])	Proximate analysis (wt%, db[b])			Ultimate analysis (wt%, daf[e])				Molar ratio	
			ash	VM[c]	FC[d]	C	H	N	O[f]	H/C	O/C
Raw	MC300	2.52	11.24	33.52	55.24	84.51	0.95	0.38	14.16	0.13	0.13
	MC100	3.03	12.32	30.94	56.74	90.45	1.24	0.42	7.89	0.16	0.07
T220	MC300	1.63	10.82	36.81	52.37	80.00	0.97	0.33	18.70	0.15	0.18
	MC100	2.14	17.12	41.64	41.24	91.66	1.17	0.36	6.82	0.15	0.06
T250	MC300	1.31	6.33	37.36	56.31	63.06	0.88	0.38	35.69	0.17	0.42
	MC100	1.68	8.06	42.41	49.53	72.74	0.97	0.33	25.96	0.16	0.27
T300	MC300	1.19	3.60	29.24	67.16	69.24	1.27	0.32	29.18	0.22	0.32
	MC100	1.21	4.29	37.25	58.46	79.39	1.39	0.50	18.73	0.21	0.18
Raw	PC300	1.84	6.43	20.77	72.80	82.52	1.02	0.19	16.27	0.15	0.15
	PC100	2.03	7.41	19.45	73.14	85.74	1.46	0.18	12.62	0.20	0.11
T220	PC300	1.64	5.86	28.73	65.41	77.18	0.65	0.21	21.97	0.10	0.21
	PC100	1.87	6.71	35.84	57.45	82.62	1.34	0.20	15.84	0.19	0.14
T250	PC300	1.59	4.46	40.65	54.89	64.52	0.61	0.15	34.72	0.11	0.40
	PC100	1.64	6.56	46.76	46.68	71.43	0.98	0.19	27.40	0.16	0.29
T300	PC300	1.16	1.97	32.12	65.91	74.60	0.77	0.22	24.41	0.12	0.25
	PC100	1.35	2.45	33.20	64.35	83.01	1.10	0.18	15.71	0.16	0.14

[a] air-dried; [b] dry-basis; [c] volatile Matter; [d] fixed carbon; [e] dry and ash-free basis; [f] by difference.

7.2 Characterization of raw and torrefied biomass samples

The properties of raw and torrefied biomass samples with different particle size fractions are summarized in Table 7.1. Bridgeman et al. reported that size reduction of biomass by milling can introduce variations of fuel properties for biomass in different size fractions, which was ascribed to the uneven distribution of large and tenacious organic materials between different size fractions.[277] However, data in Table 7.1 show that the pulverization process seems to have negligible effects on the properties of torrefied biomass with different particle sizes, most likely because the brittle structure after torrefaction makes the torrefied biomass powder have uniform constituents. It can be seen that torrefaction temperature has a key role in the properties of resultant torrefied biomass. The increased torrefaction temperature leads to lower contents of moisture and volatile matter, but higher contents of fixed carbon for both biomass species, while the ultimate analysis shows that it improves fuel properties of torrefied biomass by exhibiting higher content of carbon. Besides, the higher contents of ash for torrefied biomass indicate the accumulation of inorganic species in solid phase during torrefaction. These are the results of the degradation of the biomass components at high temperature, releasing small gaseous molecules such as CO, CO_2, CH_4, and H_2, as well as some moisture during torrefaction.[278] There is no noteworthy variance in the concentrations of AAEM species between samples with different particle sizes in Table 7.3, which further evidence the uniformity of torrefied biomass powder.

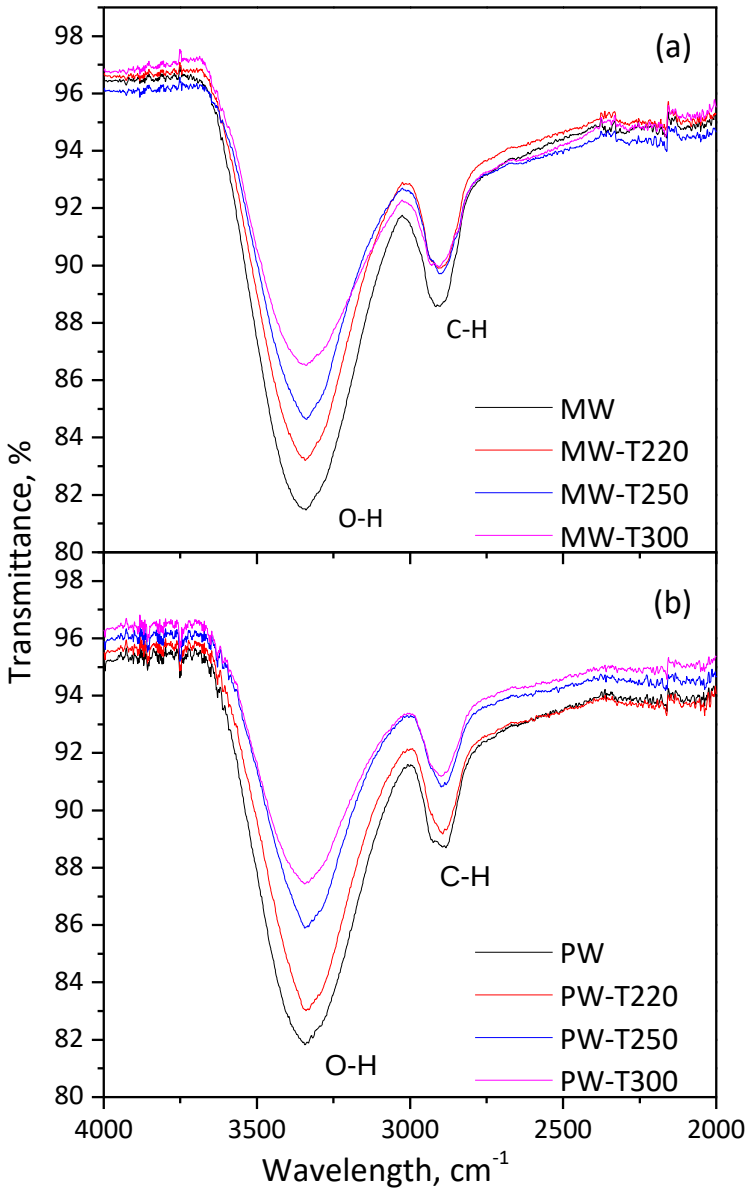

Figure 7.1 FTIR spectra for raw and torrefied mallee and pine wood powder after pulverization

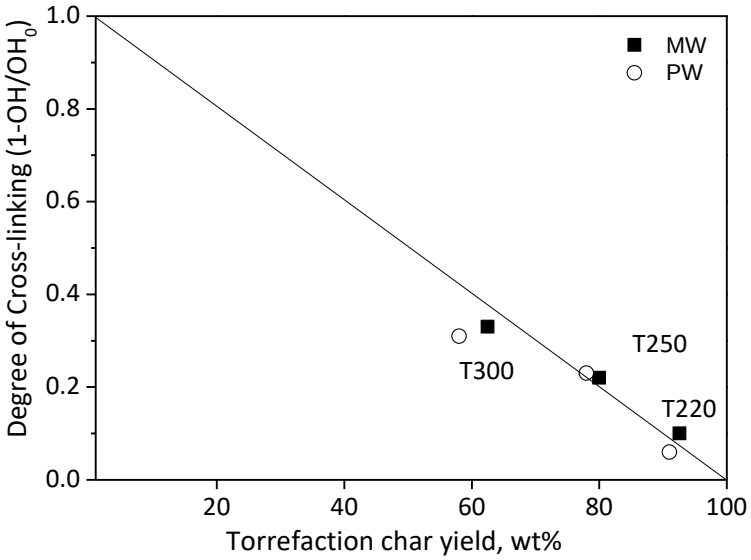

Figure 7.2 Torrefaction char yield of MW and PW at 220 °C, 250 °C, and 250 °C, and their degree of cross-linking at each torrefaction temperature

The molar ratios of O/C and H/C for mallee and pine wood are presented in Table 7.1. Generally speaking, as torrefaction temperature increases, the decrease of O/C vs. H/C has a linear relationship with the slope being approximately 0.5 regardless of their particle size, which suggests that the loss of oxygen and hydrogen is largely caused by dehydration during torrefaction. Many previous FTIR analyses mentioned that torrefied biomass exhibits higher intensity of certain structures, such as C-O-C and C=O, but lower –OH intensity, mainly owing to the cross-linking reactions and intramolecular dehydration reactions that have cross-linking behavior.[174, 260, 279-282] Chaiwat et al.[283] proposed a method to evaluate the degree of cross-linking based on the reasonable assumptions that the degree of cross-linking is proportional to the loss of hydroxyl group (OH) as they confirmed that the primary reaction for cross-linking during pyrolysis of cellulose is to produce H_2O at a low heating rate and low temperature. They defined the loss of hydroxyl group (OH) as $(OH_0\text{-}OH)/OH_0$, where OH_0 and OH were the initial and final amount of OH groups detected by FTIR, respectively. Using the same method, the degree of cross-linking for torrefied biomass in this study was determined via the changes of the OH spectra in solid samples obtained by FTIR (see Figure 7.1). Note that the possible tar generated during torrefaction is not considered due to the fact that the cross-linking contributed by tar is negligible at <300 °C for slow pyrolysis of cellulose.[283] The intensity of OH groups (peak at 3000-3600 cm^{-1}) is found to reduce with torrefaction temperature. The loss of

OH groups (degree of cross-linking) at different torrefaction temperature was then quantified and plotted in Figure 7.2 against the torrefaction char yields. The torrefaction char yields are 92.6%, 85.3%, and 55.1% for mallee wood and 89.7 %, 83.6%, and 51.2% for pine wood, at 220°C, 250°C, and 300°C, respectively. It shows that the degree of cross-linking has an inverse correlation with the torrefaction yield, in other words, cross-linking reactions are favored at high torrefaction temperature. The degree of cross-linking for MW and PW torrefied at 300 °C could be even higher if counting the increased tar yield in.[283] More cross-linked structure in torrefied biomass partly explains the changes in their properties, such as the higher contents of fixed carbon and the changes in H/C and O/C, and thus different pyrolysis behaviour is expected for torrefied biomass.

7.3 Shape of pulverized raw and torrefied wood chips for mallee and pine

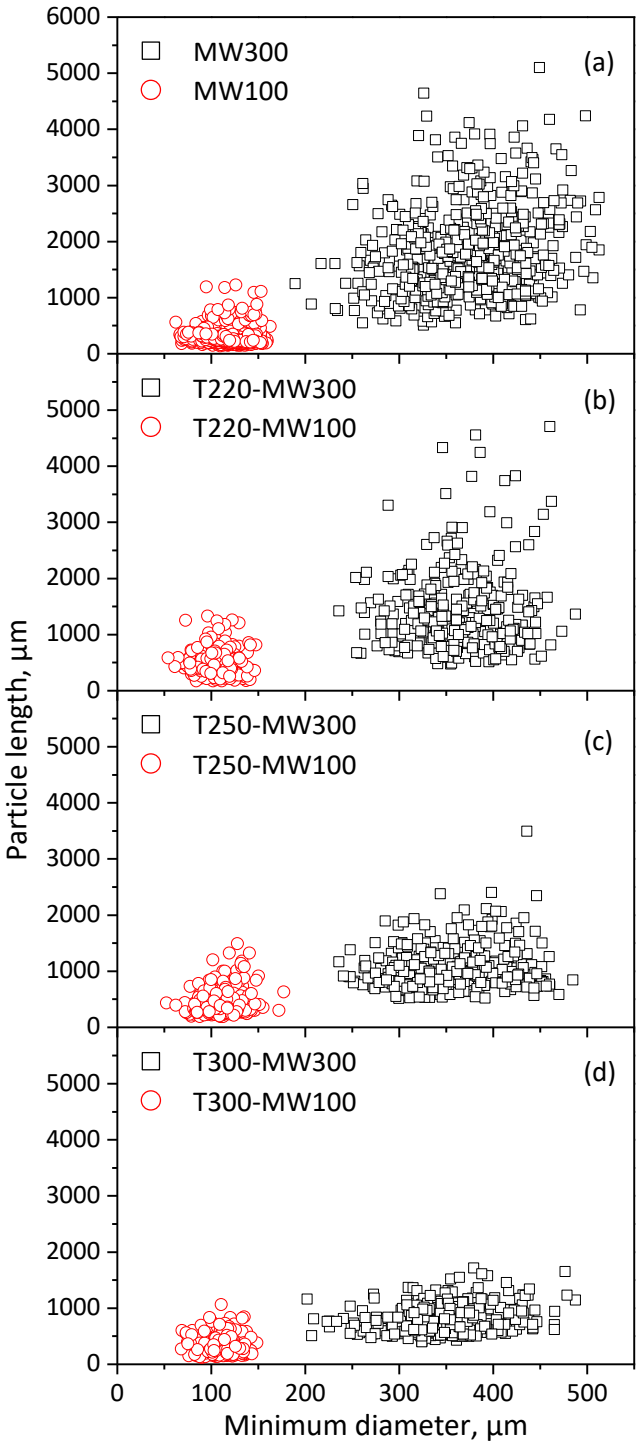

Figure 7.3 Correlation between the particle length and minimum diameter of pulverized and sieved (a) raw MW and (b-d) torrefied MW. T220, T250, and T300 in the legend refer to the torrefaction temperature at (b) 220 °C, (c) 250 °C, and (d) 300 °C, while MW300 and MW100 in the legend refer to the size fractions of 90-106 µm and 250-355 µm after sieving, respectively

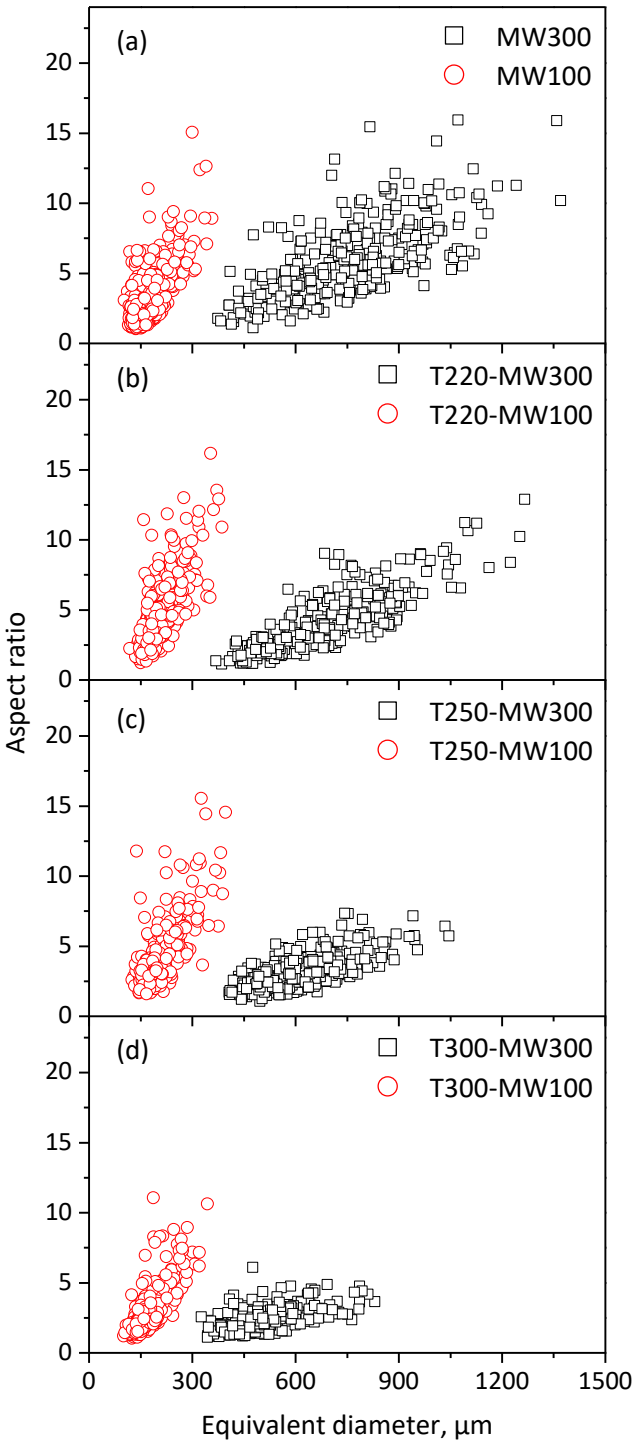

Figure 7.4 Correlation between the aspect ratio and equivalent diameter of pulverized and sieved (a) raw MW (b-d) torrefied MW. T220, T250, and T300 in the legend refer to the torrefaction temperature at (b) 220 °C, (c) 250 °C, and (d) 300 °C, while MW300 and MW100 in the legend refer to the size fractions of 90-106 µm and 250-355 µm after sieving, respectively

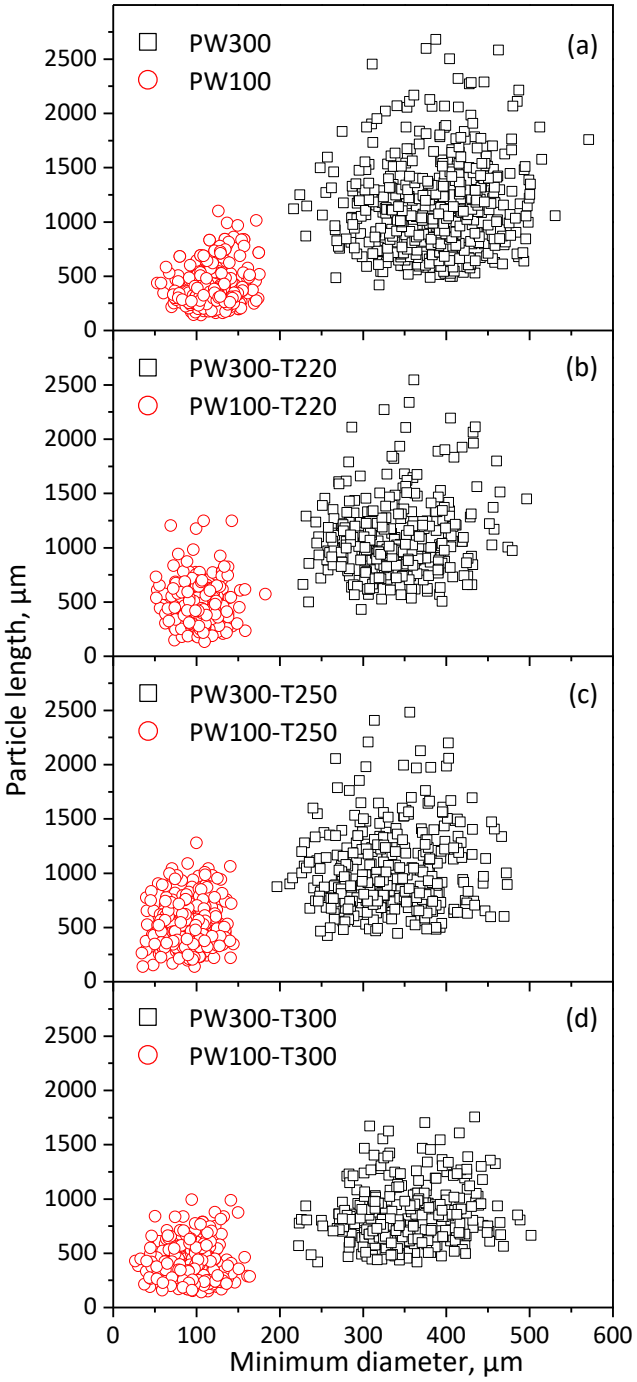

Figure 7.5 Correlation between the particle length and minimum diameter of pulverized and sieved (a) raw PW and (b-d) torrefied PW. T220, T250, and T300 in the legend refer to the torrefaction temperature at (b) 220 °C, (c) 250 °C, and (d) 300 °C, while PW300 and and PW100 in the legend refer to the size fractions of 90-106 µm and 250-355 µm after sieving, respectively

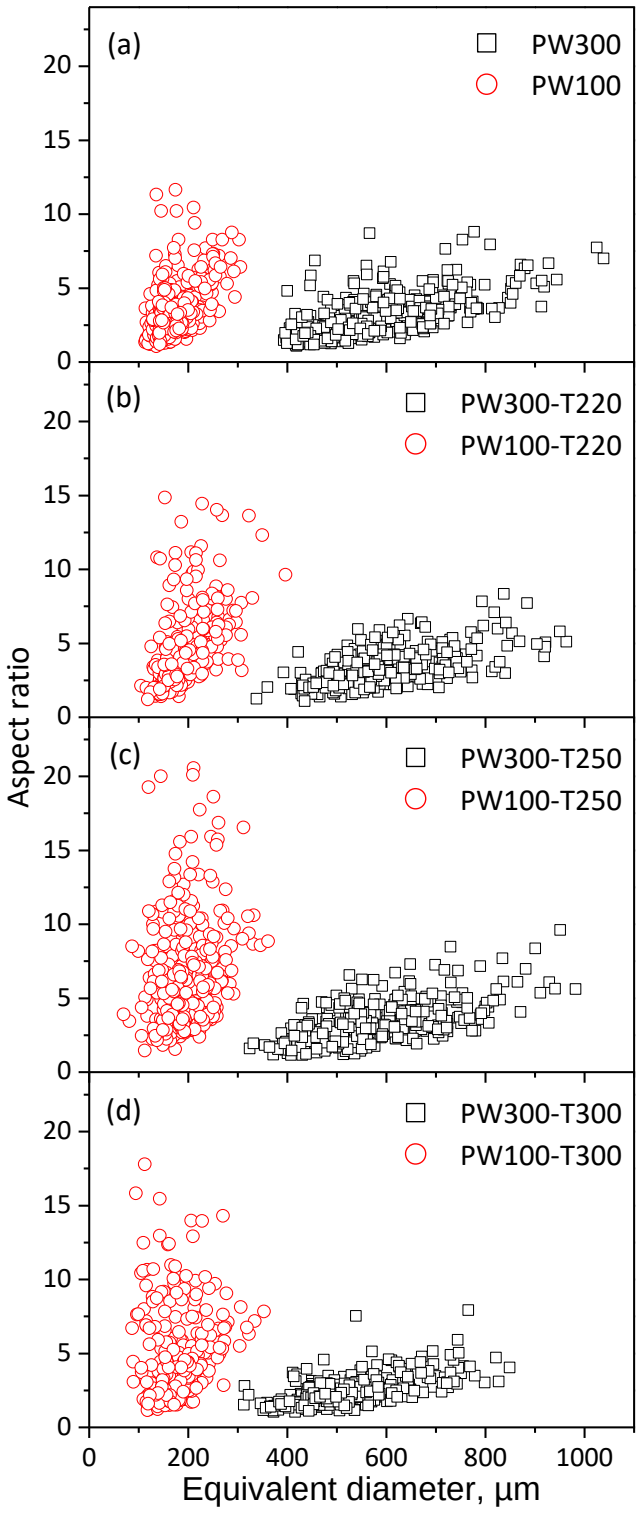

Figure 7.6 Correlation between the aspect ratio and equivalent diameter of pulverized and sieved (a) raw PW (b-d) torrefied PW. T220, T250, and T300 in the legend refer to the torrefaction temperature at (b) 220 °C, (c) 250 °C, and (d) 300 °C, while PW300 and PW100 in the legend refer to the size fractions of 90-106 µm and 250-355 µm after sieving, respectively

Size and shape parameters for pulverized mallee and pine wood particles are shown in Figure 7.3-7.6. Figure 7.3 and 7.5 present the correlation of particle length and minimum diameter for mallee and pine particles, while Figure 7.4 and 7.6 give the aspect ratio and equivalent diameter for them. It can be seen that the sieve size (250-355 µm and 90-106 µm) only roughly corresponds to the minimum diameter of particles while their particle length could be much larger, especially for raw biomass particles. The particle length distributions of MW300 and PW300 in Figure 7.3 (a) and Figure 7.5, (a) are extremely scattered, ranging in 500-4000 and 500-2500, respectively. Smaller particles (MW100 and PW100) have the same situation that their particle length reaches up to 1000 µm whereas their particle minimum diameter is only 60-170 µm. Long particle length but small diameter reflects their needle-like shape, which can be further quantified by their aspect ratio. As shown in Figure 7.4, (a), the aspect ratio for MW300 and MW100 are both up to 15 and have a positive correlation with the equivalent diameter. The distribution of equivalent diameter is very wide, ranging between ~350 µm to ~1200 µm for MW300, and ~100 µm to ~350 µm for MW100. Likewise, PW300 and PW100 exhibit high aspect ratio (~10) and broad equivalent diameter ranges. The elongated shape for raw biomass particles is the result of their anisotropic structure, which makes it much easier to break up along the longitudinal direction.

Panels b-d in Figure 7.3-7.6 illustrate the multiple effects of torrefaction on the shape of particles after pulverization. Most importantly, torrefaction can remarkably reduce the particle length, especially for large particles. After torrefaction at 220 °C, 250 °C, and 300 °C, the majority of T220-MW300, T250-MW300, and T300-MW300 particles have their particle length reduced to < 3000 µm, < 2000 µm, and < 1500 µm. Consequently, the upper range of aspect ratio decreased dramatically, from ~10 for T220-MW300, to ~7 for T250-MW300 and ~5 for T300-MW300. Moreover, the slightly smaller minimum diameter and remarkably shorter particle length of T300-MW300 make the range of its equivalent diameter shrinks to 300-900 µm, which is only half of the equivalent diameter range of MW300, approximately. Similarly, increasing torrefaction temperature reduce the upper range of particle length for large pine wood particles from 2500 µm to 1500 µm, therefore lowering the aspect ratio to 1-5 and the equivalent diameter to 300-800 µm.

However, such effects are not observed for particles in the size range of 90-106 μm. The particle length and minimum diameter for raw and torrefied MW100 and PW100 have no obvious difference, except a slight reduction on the upper limit of particle length for T300-MW100, which causes a small drop in its aspect ratio value from ~11 to ~8. Torrefied small pine particles (T250-PW100 and T300-PW100) even exhibit a less concentrated distribution of aspect ratio in panel c and d of Figure 7.6. Previous studies simply ascribed the better grindability of torrefied biomass to the embrittled lignocellulose structure and conclude that torrefaction could increase the sphericity of particles after pulverization.[44, 284] This study reveals that the particle size has to be considered when studying the particle shape because only the relatively large particles have a more spherical shape after torrefaction while the shape for smaller particles is basically not affected by torrefaction.

7.4 Effect of torrefaction on the properties of char with different size ranges after rapid pyrolysis

7.4.1 Characterization of char yield and properties

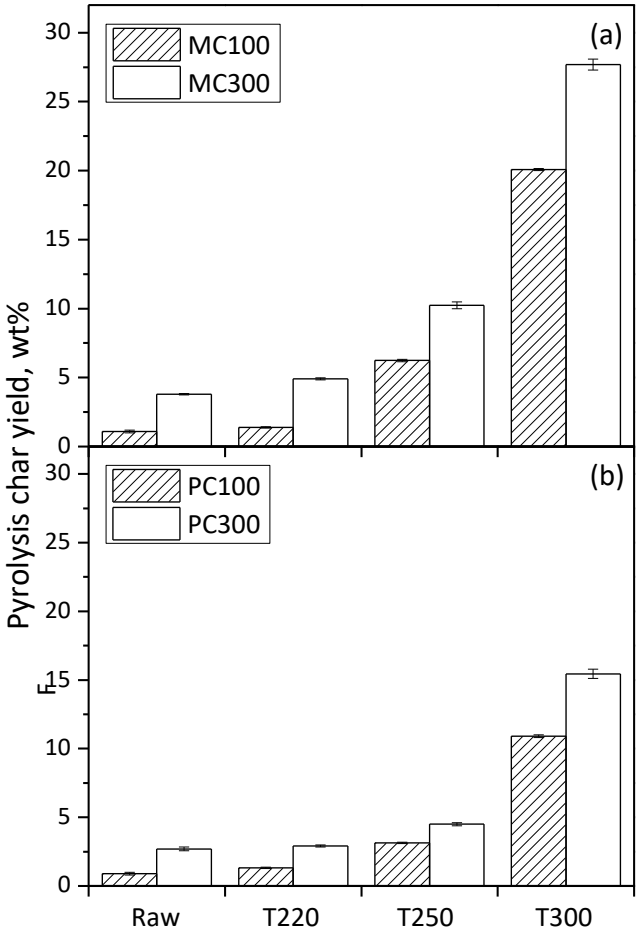

Figure 7.7 Pyrolysis char yields during the pyrolysis of pulverized raw and torrefied mallee wood in (a) and pine wood in (b). 100 and 300 in the legend refer to the size fractions of 90-106 µm and 250-355 µm, respectively

The pyrolysis char yields of raw and torrefied biomass particles are presented in Figure 7.7. Specifically, MW300 and MW100 have only 3.8% and 1.1% of char yields due to the high pyrolysis temperature (1300 °C) causing severe devolatilization.[87] The pyrolysis char yield rises slightly when mallee wood is pretreated at 220 °C, while torrefaction temperature at 250 °C further raises the yields to 10.24% and 6.24% for T250-MW300 and T250-MW100, respectively. Higher torrefaction temperature at 300 °C significantly increases the yields to 27.7% for T300-MW300 and to 20.1% for

T300-MW100. For pine wood, pyrolysis char yields for PW300, T220-PW300, T250-PW300, and T300-PW300 are 2.7%, 2.9%, 4.5%, and 15.5% while for PW100, T220-PW100, T250-PW100, and T300-PW100, the values are 0.9%, 1.3%, 3.1%, and 10.9%, respectively. The trend is obvious that higher torrefaction temperature facilitates the formation of char. It can be partly explained by the impacts of torrefaction on biomass components, namely the decomposition of cellulose and hemicellulose but the increase of the lignin content,[174, 273] which contributes more to the char formation than cellulose and hemicellulose during rapid pyrolysis.[102, 177, 285] Besides, the degree of cross-linking increases with torrefaction temperature as discussed above, and such cross-linking reactions could produce a more stable carbon matrix to survive the rapid pyrolysis.[177]

Table 7.3 Concentration of AAEM species in raw and torrefied biomass, wt%

Samples		Concentration of AAEM species in samples, wt%			
		Na	K	Mg	Ca
Raw	MW300	0.010±0.001	0.071±0.006	0.029±0.001	0.166±0.005
	MW100	0.011±0.001	0.069±0.002	0.026±0.002	0.157±0.008
T220	MW300	0.008±0.001	0.076±0.001	0.028±0.001	0.177±0.016
	MW100	0.008±0.001	0.074±0.004	0.024±0.002	0.165±0.003
T250	MW300	0.011±0.001	0.092±0.002	0.033±0.005	0.268±0.007
	MW100	0.010±0.001	0.089±0.001	0.035±0.001	0.238±0.009
T300	MW300	0.014±0.001	0.121±0.002	0.048±0.001	0.310±0.010
	MW100	0.014±0.001	0.128±0.004	0.049±0.001	0.338±0.009
Raw	MC300	0.067±0.001	1.167±0.003	0.601±0.007	3.224±0.021
	MC100	0.033±0.002	0.682±0.007	0.964±0.008	5.342±0.020
T220	MC300	0.061±0.001	1.210±0.001	0.371±0.004	3.185±0.012
	MC100	0.023±0.002	0.632±0.014	0.824±0.007	5.164±0.005
T250	MC300	0.037±0.002	0.726±0.001	0.228±0.001	1.922±0.034
	MC100	0.029±0.002	0.514±0.004	0.368±0.010	2.647±0.050
T300	MC300	0.028±0.001	0.402±0.002	0.159±0.001	0.990±0.006
	MC100	0.022±0.003	0.386±0.003	0.173±0.007	1.077±0.056

The concentrations of AAEM species in mallee chars are presented in Table 7.3. Overall, the concentrations of AAEM species in chars decrease with torrefaction temperature, mainly due to the less devolatilisation of organic materials "diluting" the concentrations. The impacts of particle size are in accordance with previous investigation on raw biomass done by the authors,[87] which is large particles having higher contents of Na and K but lower contents of Mg and Ca. This is because the higher retention of Mg and Ca leads to their accumulation in chars, especially in small

particles whose organic materials loss is significant. While the vaporization of Na and K is so strong in small particles, that it outweighs the loss of the organic materials, decreasing their contents in chars. It is interesting to notice that the difference in the contents of AAEM species between T250-MC300 and T250-MC100 is narrowed, and T300-MC300 and T300-MC100 have almost the same contents of AAEM species. It means that the impacts of particle size on the release of AAEM species are mitigated by increasingly stronger torrefaction, leaving a more uniform composition of inorganic species in char.

7.4.2 Effect of torrefaction temperature and particle size on the retentions of AAEM species

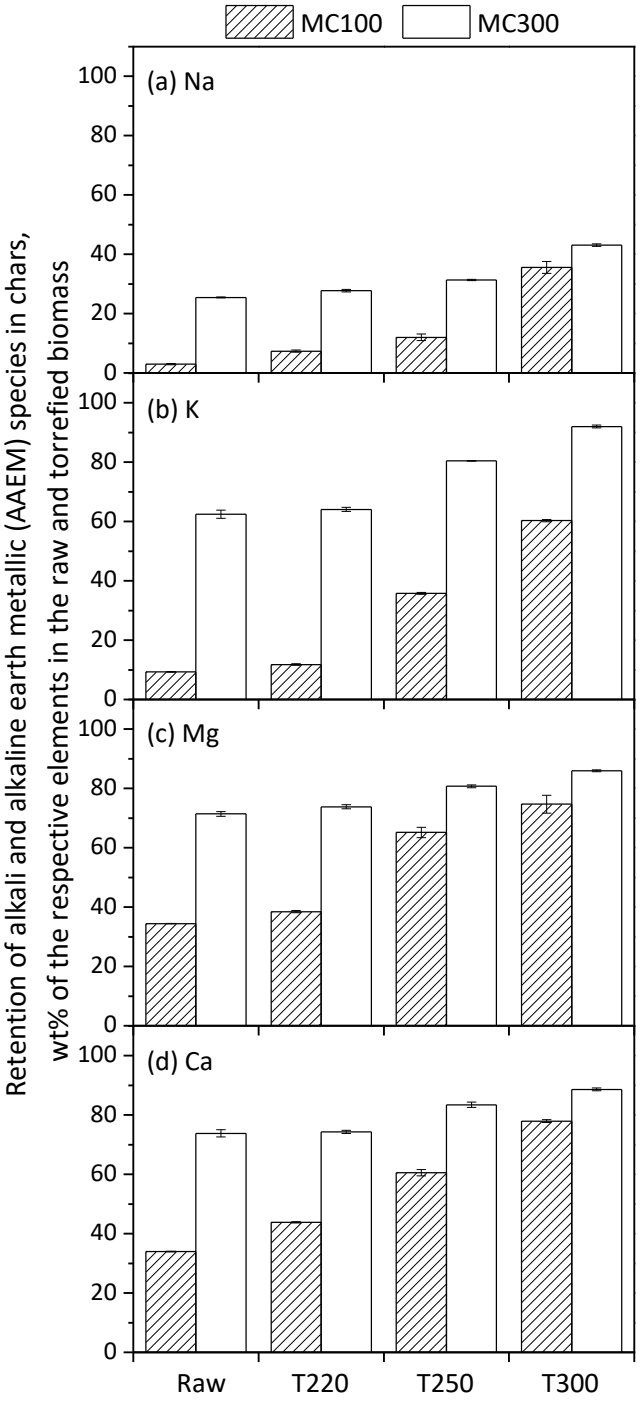

Figure 7.8 Overall retentions of AAEM species in chars produced from the pyrolysis of raw or torrefied biomass at 1300 °C, (a). Retention of Na; (b). Retention of K; (c). Retention of Mg; (d). Retention of Ca

To investigate the effects of particle size and torrefaction temperature on the release of AAEM species, the pyrolysis char yields and contents of AAEM species in mallee chars are used to calculate the retention of AAEM species after rapid pyrolysis. The results are presented in Figure 7.8. Only 25.5% of Na is retained in MC300 after rapid pyrolysis, while T220-MC300, T250-MC300, and T300-MC300 have their retention of Na increased to 27.8%, 31.3%, and 43.1%. The retention of K also increased from 64.1% for T220-MC300, to 80.5% for T250-MC300, eventually reaching 92.1% for T300-MC300, which is much higher compared to 62.5% of it in MC300. The increase in the retentions of Mg and Ca are not as significant as Na and K, for the retentions of Mg and Ca already reach ~70% for MC300. Increasing the torrefaction temperature to 300 °C gradually raised their retention to ~87% for T300-MC300. A previous study done by the authors has revealed that the chemical occurrence of AAEM species is more stable after torrefaction and the less intensive devolatilization reactions of torrefied biomass is also responsible for more AAEM species bound to char matrix after rapid pyrolysis. Therefore, the retention of AAEM species continuously increases as torrefaction temperature getting higher.

Attention is paid to the effect of particle size on the retention of AAEM species for torrefied biomass. The retention of AAEM species is generally higher for large biomass particles, which can be ascribed to several reasons including the lower heating rate, less thermal ejection, and longer inner-particle diffusion path for large particles.[87] The retentions of Na and K in MC100 are 3.0% and 9.3%, which are relative ~88% and ~85% less than the retention of Na and K in MC300, respectively. However, for T300-MC100, the retentions of Na and K increase to 35.6% and 60.3%, which are only ~17% and ~34% less than the retention of Na and K in T300-MC300 relatively. Likewise, as the percentages of Mg and Ca retained in MC100 are ~50% lower than in MC300, increasing torrefaction temperature to 300 °C makes the retention of Mg and Ca in T300-MC100 increase to ~75%, relatively lower by only ~14% compared to T300-MC300. Therefore, the effect of particle size on the retention of AAEM species during rapid pyrolysis is less important if pretreated by torrefaction and this phenomenon is increasingly obvious at higher torrefaction temperature. One possible reason could be the change in the actual particle size for torrefied biomass. Firstly, the discrepancy in particle size can bring about variation in heating rate, which eventually influences the pyrolysis reactions and the release of AAEM species.[62, 130, 286] Besides,

particle size has a direct influence on the length of diffusion path for AAEM species that are volatilized or transported by aerosols inside the particle. Moreover, the trapped elements have more possibilities to re-combine with the char matrix while they diffuse towards the surface. As shown by Figure 7.10, the equivalent diameter for MC100 and T300-MC100 are in the same range (90-350 μm) while the equivalent diameter for MC300 (350-1200 μm) is much larger than it for T300-MC300 (350-850 μm), which suggests that the difference in the actual particle size between T300-MW300 and T300-MW100 is smaller. The other reason could be the chemical properties of torrefied biomass that have multiple impacts on the release of AAEM species. Firstly, lower volatile matter content in torrefied biomass could make the pressure built up inside the particle slower and less intensive, in contrast to the rapid generation of volatile from raw biomass. In fact, the devolatilization of small raw biomass particles is so rapid that the high internal pressure turns the liquified char structure into hollow spheres and creates large openings on the surface.[87] Therefore, the vaporized AAEM species could be released directly without any mass transfer or diffusion process. However, the higher char yield of small torrefied biomass and the cross-sectional images of char particles (see section 7.5) suggests that there could be a compact internal structure that hinders the escape of AAEM species and facilitates the re-bonding of AAEM species with reactive char matrix. Besides, the internal pressure could enhance the thermal ejection of aerosols which might carry non-volatile AAEM species. Furthermore, the relatively stable chemical occurrence of AAEM species in torrefied biomass may prevent the quick release of them regardless of the particle size, and the higher O/C molar ratio of char produced by torrefied biomass indicates more possible sites on char matrix for AAEM species to bond through oxygen-containing functional groups. Those above-mentioned factors explain the significant increase in the retention of AAEM species for small and torrefied particles, which reduces the difference in the retention of AAEM species caused by particle size.

7.5 The effect of torrefaction on the shape of char particles with different size

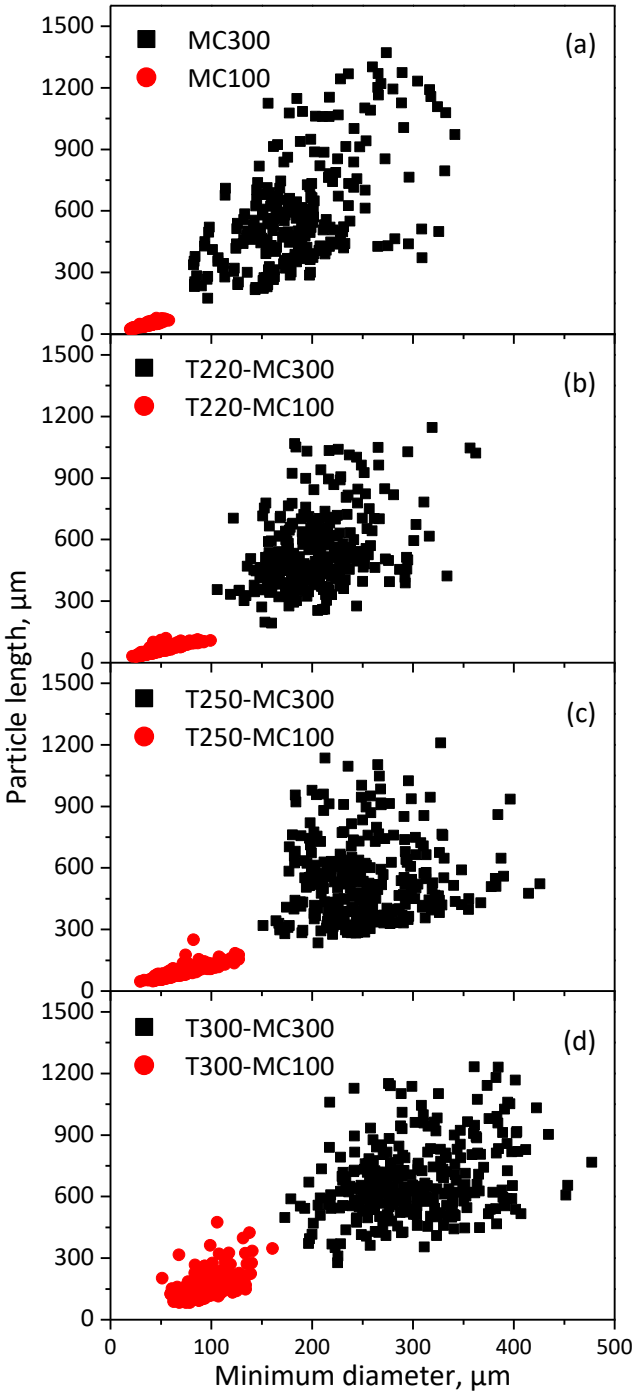

Figure 7.9 Correlation between the particle length and minimum diameter of chars produced by the rapid pyrolysis of (a) raw MW and (b-d) torrefied MW. T220, T250, and T300 in the legend refer to the torrefaction temperature at (b) 220 °C, (c) 250 °C, and (d) 300 °, while MC300 and MC100 refer to the size fractions of 90-106 µm and 250-355 µm, respectively

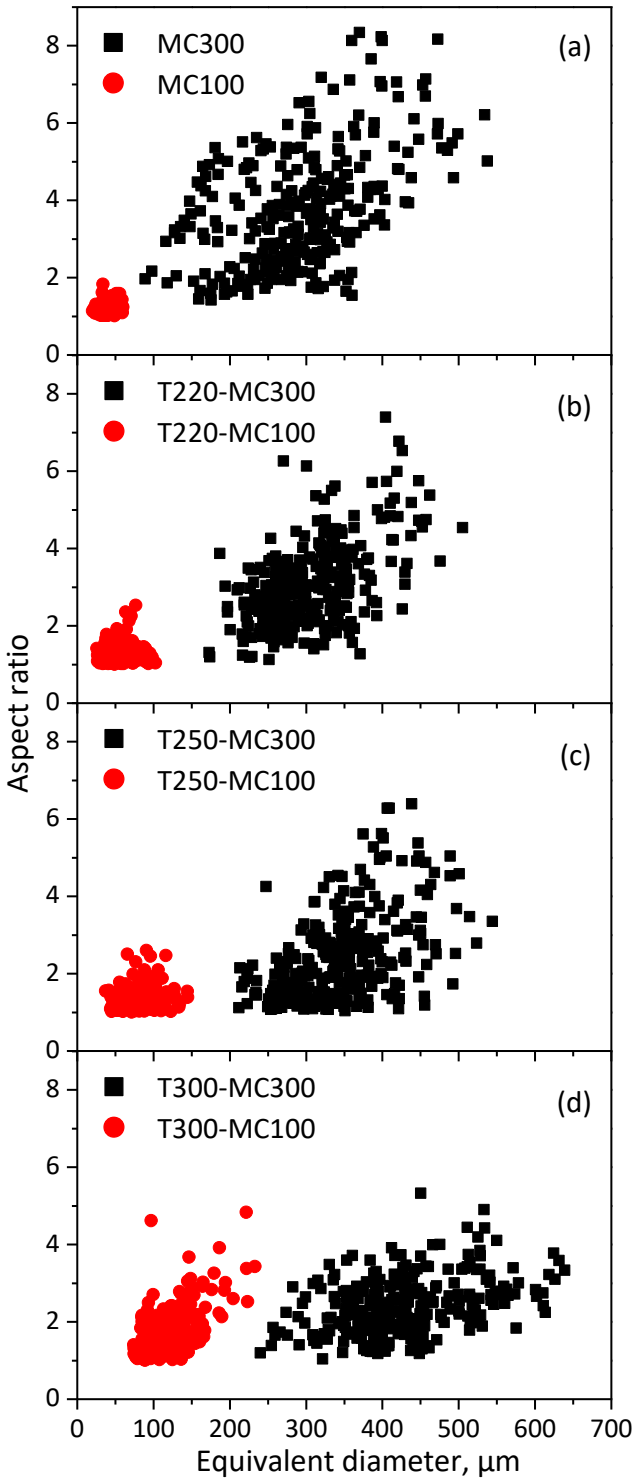

Figure 7.10 Correlation between the aspect ratio and equivalent diameter of chars produced by the rapid pyrolysis of (a) raw MW and (b-d) torrefied MW. T220, T250, and T300 in the legend refer to the torrefaction temperature at (b) 220 °C, (c) 250 °C, and (d) 300 °, while MC300 and MC100 refer to the size fractions of 90-106 µm and 250-355 µm, respectively

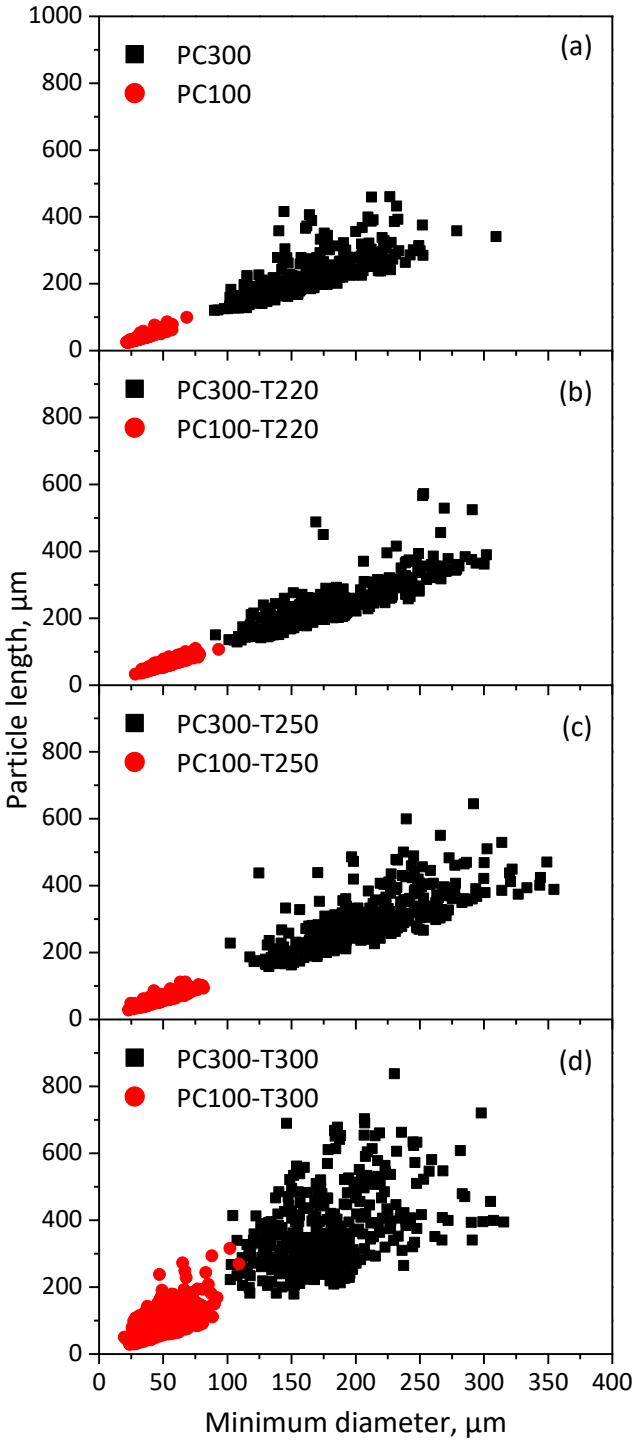

Figure 7.11 Correlation between the particle length and minimum diameter of chars produced by the rapid pyrolysis of (a) raw PW and (b-d) torrefied PW. T220, T250, and T300 in the legend refer to the torrefaction temperature at (b) 220 °C, (c) 250 °C, and (d) 300 °, while PC300 and PC100 refer to the size fractions of 90-106 µm and 250-355 µm, respectively

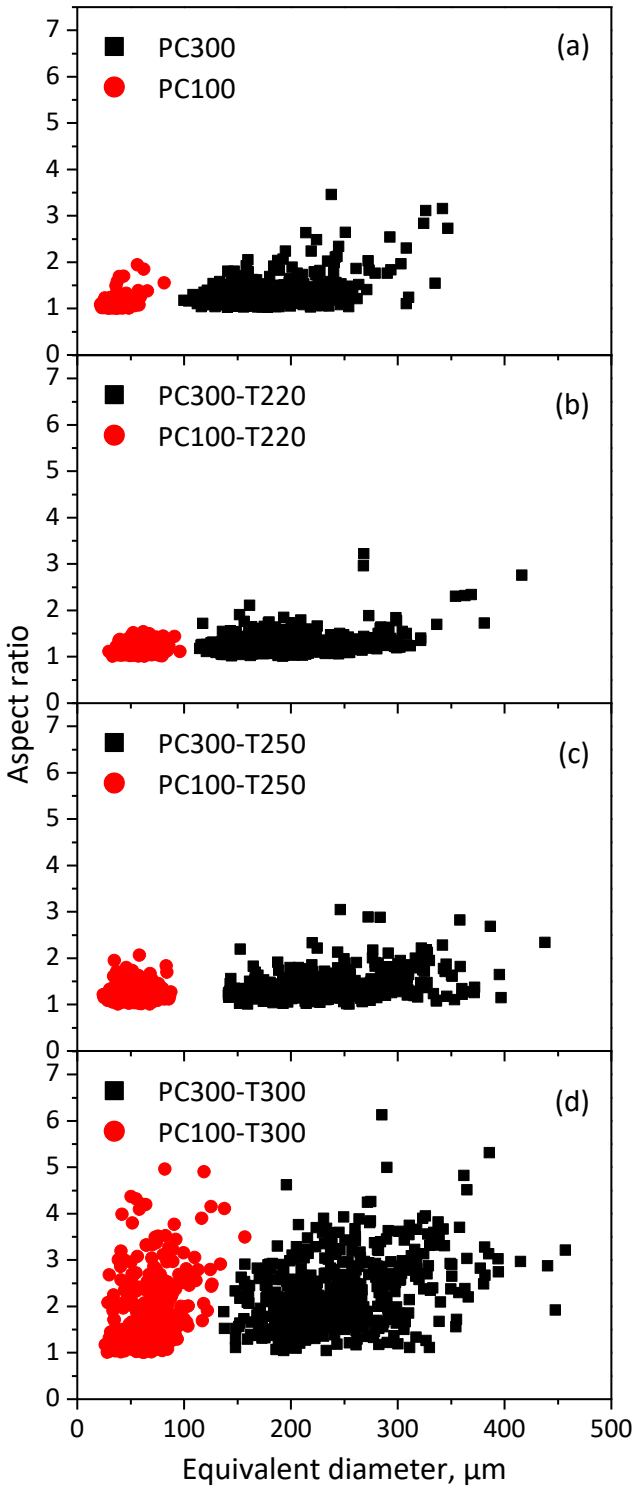

Figure 7.12 Correlation between the aspect ratio and equivalent diameter of chars produced by the rapid pyrolysis of (a) raw PW and (b-d) torrefied PW. T220, T250, and T300 in the legend refer to the torrefaction temperature at (b) 220 °C, (c) 250 °C, and (d) 300 °, while PC300 and PC100 refer to the size fractions of 90-106 µm and 250-355 µm, respectively

Figure 7.9 and Figure 7.11 present the particle length (PL) and minimum diameter (MD) for mallee and pine char particles. The correlations of aspect ratio and equivalent diameter for all char samples are shown in Figure 7.10 and Figure 7.12. The red and black colors in Figure 7.9-7.12 represent two initial size fractions of biomass in 90-106 μm and 250-355 μm, respectively.

The particle length and minimum diameter for MC300 vary between 150-1350 μm and 80-330 μm, which is much smaller than the original particles because of the severe devolatilezation and shrinking process. As the torrefaction temperature increases, the minimum diameter of large mallee char particles gradually increases to 100-350 μm for T220-MC300, 150-400 μm for T250-MC300, and 170-450 μm for T300-MC300. In the meantime, the scattered distribution of particle length narrows down to 300-1200 μm for T300-MC300. The changes of equivalent diameter for large char particles (250-355 μm) with different torrefaction temperatures also show that the shrinkage of particle dimensions for biomass torrefied at high temperature is minor because T300-MC300 nearly maintains the same equivalent diameter range of T300-MW300 which is between 300-800 μm, and the length and diameter for T300-MC300 are very close to the range of T300-MW300. Due to the similar particle dimensions including length and minimum diameter, the aspect ratio range for T300-MC300 (1-4) is thus very close to it for T300-MW300 (1-5). On the contrary, MC300 and T220-MC300 have a noticeable decrease in the aspect ratio range compared to their original particles, as the result of melting structure and shrunken particle dimensions. Likewise, the particle length for PC300 and T220-PC300 decreases a lot, therefore the aspect ratio for all of these particles is below 2, and the vast majority of them has the aspect ratio <1.5, suggesting the severe deformation of char particles.[8, 87] The increase in the aspect ratio starts to be noticeable when pine wood was torrefied at 250 °C. Similar to mallee wood, torrefaction at 300 °C keeps the aspect ratio for T300-PC300 as high as 1-4, which is also very close to the aspect ratio for T300-PW300 ranging in 1-5. The above observations indicate that pretreatment for biomass with torrefaction can prevent the shrinkage of particle dimensions and this effect is increasingly pronounced with higher torrefaction temperature. A possible reason for this is that the cell structure after torrefaction is strengthened by various reactions such as cross-linking and possible charring reactions for certain biomass components at high torrefaction temperature (300 °C). Besides, the higher pyrolysis char yield for torrefied biomass implies that

more organic materials are reserved after rapid pyrolysis, which acts as the inner support for the entire particle to assure its integrity. Additionally, the less intensive release of volatile matter generates fewer impacts towards the molten and delicate char structure at high temperature, which would help to keep the particle shape.

However, such effects of torrefaction on the size and shape of small mallee particles are less significant. Generally, small biomass particles exhibit a higher level of melting because of the higher heating rate they experienced.[87] Data points for MC100 and T220-MC100 in Figure 7.9 and 7.10 show that they are all near-spherical particles after rapid pyrolysis. Increasing torrefaction temperature slightly enlarges the particle dimensions for chars but only a small part of T250-MC100 particles have their aspect ratio reach >2, while the majority of them still have a dramatic decrease in aspect ratio compared to large mallee particles whose aspect ratio range between 1 to ~10. The melting for small pine wood particles is even more remarkable because most particles of PC100, T220-PC100, and T250-PC100 have their aspect ratio <1.5. Surprisingly, severe torrefaction at 300 °C can make the aspect ratio for both T300-MC100 and T300-PC100 in the same range as T300-MC300 and T300-PC300. This further stresses the significance of torrefaction at high temperature on the particle shape, which even outweighs the impacts of particle size.

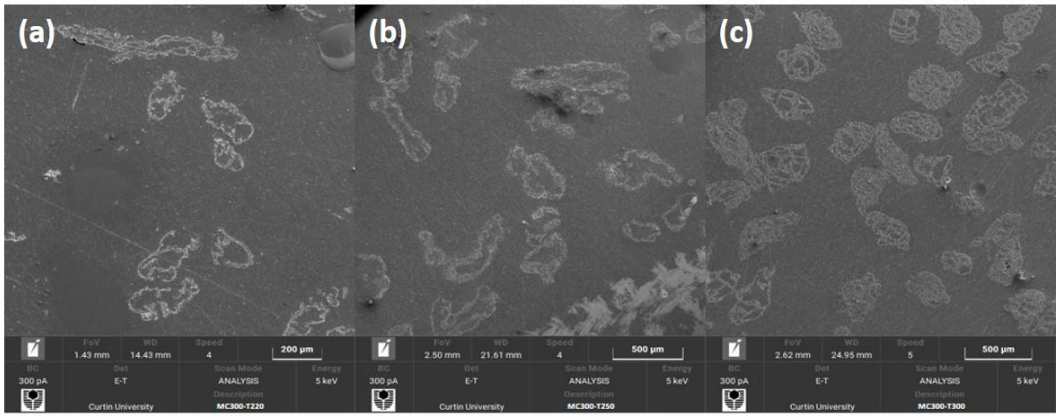

Figure 7.13 Cross-sectional images for (a): MC300-T220, (b): MC300-T250, and (c): MC300-T300

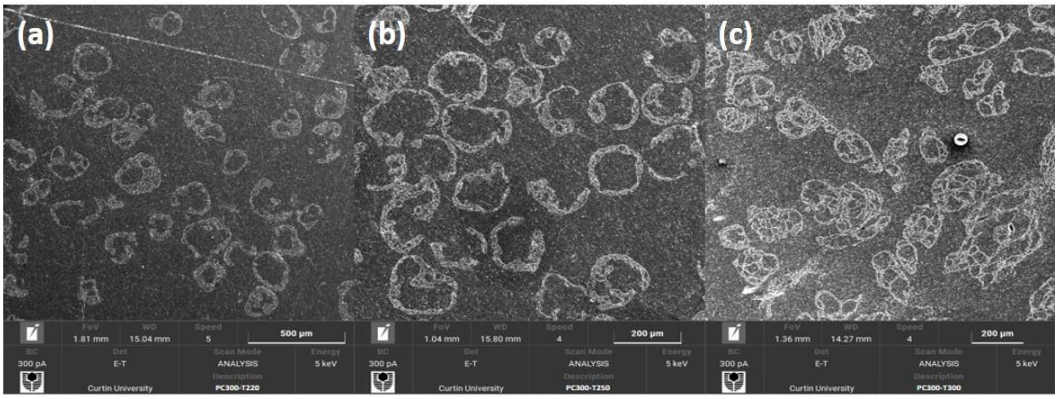

Figure 7.14 Cross-sectional images for (a): PC300-T220, (b): PC300-T250, and (c): PC300-T300

To further understand the morphology of char samples, cross-sectional characterization was carried out for large char particles (250-355 µm) and the representative images for each sample are presented in Figure 7.13 and Figure 7.14. The cross-sectional morphology for T220-MC300, T250-MC300 shows that most particles have a thin outer shell and large voids inside the particle, while particles of T220-PC300, T250-PC300 have a cenosphere shape. The main reason for this porous structure is expected to be the severe devolatilization that happened during rapid pyrolysis as char yield data show that >95% of organic matter is vaporized for raw and torrefied biomass (at torrefaction temperature of 220 °C and 250 °C). The volatiles generated are trapped inside the particle, then expand and create large voids due to cumulated internal pressure and the softened char matrix at high temperature and high heating rate.[8, 75] It is important to note that char particles with prior torrefaction at 300 °C have distinct cross-sectional structure. The images for T300-MC300 and T300-PC300 show that these char particles have a relatively solid char matrix with low porosity. Small pores distribute throughout the entire cross-section area of the particle, rather than one large void, which proves that more structures are retained in T300-MC300 and T300-PC300. This dense structure could provide more resistance to melting and swelling which are typical phenomena of biomass during rapid pyrolysis,[75] which explains the nearly unchanged particle dimensions and aspect ratio for T300-MC300 and T300-PC300 particles.

7.6 Conclusions

In this study, torrefaction for mallee and pine wood chips was conducted at 220 °C, 250 °C, and 300 °C, followed by pulverization and sieving. By analyzing the particle size and shape of two specific size factions (90-106 μm and 250-355 μm), it is found that higher torrefaction temperature significantly reduces the maximum particle length of large particles after pulverization from 4000 μm to 1500 μm for mallee wood and from 2500 μm to 1500 μm for pine wood as torrefaction temperature increased to 300 °C, which causes much lower aspect ratios for these particles. However, such effects were not observed for small particles, suggesting that the impact of a combined biomass pretreatment process (torrefaction and pulverization) on the particle shape varies with particle size. The increase in char yield after rapid pyrolysis of torrefied biomass samples with two particle size fractions at 1300 °C can be explained by their improved fuel properties after torrefaction. Analysis of the inorganic species in char samples shows that the retention of AAEM species increased with the rising torrefaction temperature, especially for Na and K. Retentions of AAEM species for raw mallee wood is strongly affected by particle size as retention of AAEM species is more than half lower in smaller particles than that in large particles. However, such difference in retention is gradually reduced when torrefaction is applied. When mallee wood samples are torrefied at 300 °C, the retentions of Na and K in small particles are relative ~17%, and ~34% lower, and retentions of Mg and Ca are relative ~14% lower, compared to large particles. Size and shape characterization of char samples via image analysis shows that a high torrefaction temperature causes a solid and dense internal structure in pyrolyzed char particles with large size, and this may be the reason for their low extent of shrinkage in particle dimensions. The melting for small particles is still quite obvious after mild or moderate torrefaction, yet with higher torrefaction temperatures, such as 300 °C, the aspect ratio of small char particles can reach up to 4, indicating stronger resistance to melting for small torrefied biomass.

CHAPTER 8 EFFECTS OF BIOMASS LEACHING ON THE PROPERTIES OF CHAR AFTER RAPID PYROLYSIS

8.1 Introduction

As reviewed previously, leaching of biomass prior to thermoconversions has been regarded as an effective and low-cost way to mitigate the problems caused by inorganic species in biomass. In addition to the reduction in inorganic element contents after leaching, investigations on the properties of leached biomass and the leachates show that there are physical and chemical changes in biomass structure and thermal behaviour.[185, 287] The thermal decomposition of leached biomass carried out in TGA shows some difference compared to raw biomass in the decomposition rate and temperature,[198] indicating that it is of great importance to investigate the detailed performance of leached biomass in different thermal conversions. There has been scattered studies focusing the ash behaviour,[181] the combustion and gasification of leached biomass in fluidized bed reactor,[184, 186] whereas the investigation carried under conditions of pulverized fuel combustion is rare for leached biomass, especially the rapid pyrolysis of leached biomass at high heating rate and high temperature (>1100 °C) which is the first step for biomass after being injected into the boiler.

Therefore, the objective of this chapter is to systematically investigate the impacts of water and acid leaching process on the shape and chemical properties of biomass, by conducting rapid pyrolysis of leached biomass at 1300 °C to compare the char yield, the release of inorganic species, and shape of char particles derived from the raw and leached biomass samples. Mallee wood (MW) powder is pulverized and sieved to the size range of 250-355 μm. Water-leached mallee wood by semi-continuous leaching method and acid-leached mallee wood by batch-leaching method are denoted as MW-H_2O, and MW-HCl respectively. Their char products are hereafter referred to as MC, MC-H_2O, and MC-HCl.

8.2 Properties of raw and leached biomass samples

Table 8.1 Proximate and ultimate analysis of the raw and leached biomass and their chars

Samples	Moisture (wt%, ad[a])	Proximate analysis (wt%, db[b])			Ultimate analysis (wt%, daf[e])				Molar ratio	
		ash	VM[c]	FC[d]	C	H	N	O[f]	O/C	H/C
Biomass										
MW	7.8	0.62	87.94	11.44	48.51	6.94	0.12	44.42	0.69	1.72
MW-H_2O	6.6	0.33	90.40	9.27	50.11	6.60	0.09	43.19	0.65	1.58
MW-HCl	7.5	0.02	87.64	12.34	50.63	6.83	0.08	42.46	0.63	1.62
Chars										
MC	3.5	11.70	36.77	51.53	86.14	1.66	0.38	11.82	0.10	0.23
MC-H_2O	2.5	9.46	63.84	58.70	81.62	1.86	0.46	16.06	0.15	0.27
MC-HCl	3.8	1.56	51.16	79.28	81.19	1.50	0.53	16.78	0.15	0.22

[a] air-dried; [b] dry-basis; [c] volatile matter; [d] fixed carbon; [e] dry and ash-free basis; [f] By difference.

Table 8.2 Concentrations of inorganic species in raw and leached biomass and their char

Samples	Concentration of AAEM species in samples, wt%				
	Na	K	Mg	Ca	Cl
Biomass					
MW	0.010	0.069	0.028	0.169	0.018
MW-H_2O	0.002	0.003	0.020	0.144	0.001
MW-HCl	<0.001	<0.001	<0.001	0.003	0.001
Char					
MC	0.054	0.913	0.501	3.049	-
MC-H_2O	0.019	0.071	0.548	4.091	-
MC-HCl	0.004	0.023	0.042	0.218	-

Table 8.3 Amount of organic matter leached from raw mallee wood by water and hydrochloric acid[a]

	TOC (% of total carbon)[b]	IC (% of total carbon)[c]
H_2O leachate	2.36 ± 0.03	0.006 ± 0.002
HCl leachate	2.40 ± 0.05	0.011 ± 0.001

[a]normalized to the total carbon contents in raw mallee wood; [b]total organic carbon; [c]inorganic carbon.

The properties of raw and leached biomass are listed in Table 8.1 and 8.2. It is obvious that leaching is and effective way to reduce the ash content in mallee wood. Water-leached MW-H_2O has only 0.33 % of ash compared to the original 0.62% of ash in MW.

This indicates that a large part of inorganic species in mallee wood is water-soluble, which could be sulfates, chlorides, and other compounds. After acid-leaching, the ash content in MW-HCl decreased to 0.02%, which means >95% of inorganic species in mallee wood can be leached out by 0.1M HCl.

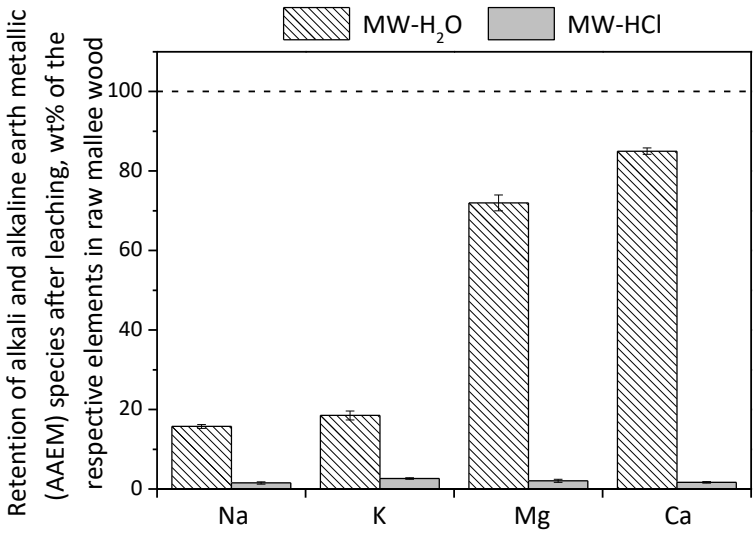

Figure 8.1 Retentions of AAEM species in biomass after leaching via H_2O and HCl

To investigate the leaching efficiency in detail, the contents of AAEM species in the water and acid leachates are analyzed. The results are normalized to the wt% of the original amount in MW and expressed as the retention of AAEM species after leaching (see Figure 8.1). It can be found that after water-leaching, 84.3% of Na and 81.5% of K in MW were removed while the leaching efficiency of Mg and Ca is much lesser, being only 28.3% and 15.5%, respectively. This is in agree with the previous analysis of the chemical occurrence of AAEM species done by the authors.[263] The work has shown that >80% of alkali metals in mallee wood are water soluble elements, such as alkali metal chlorides and sulfates, which is partly verified by the chorine contents for mallee wood samples in Table 8.2 that chlorine was almost eliminated after water-leaching. However, the water-soluble Mg and Ca only take up ~30 wt% and ~10 wt% of the respective elements in mallee wood, but the removal efficiencies for all AAEM species by 0.1M HCl solution reach up to >98%, corresponding to the <1% of acid-insoluble AAEM species in mallee wood.[263] The results of ultimate analysis show a small decrease in the contents of nitrogen and oxygen, thus the relatively higher content of carbon in mallee wood after leaching. This can be ascribed to the loss of some organic matters, such as extractives, and hydrolysis of the polysaccharides

happened during leaching process.[198, 288-289] However, the loss of carbon is insignificant compared to the reduction in the ash content, as Table 8.3 shows that only 2.36% and 2.40% of total carbon in MW is leached out by water and 0.1M HCl, respectively. This suggests that leaching can be an effective way to address the problems related to ash during biomass combustion/gasification, without causing a large loss of the organic matters.

8.3 Char yields and retentions of AAEM species

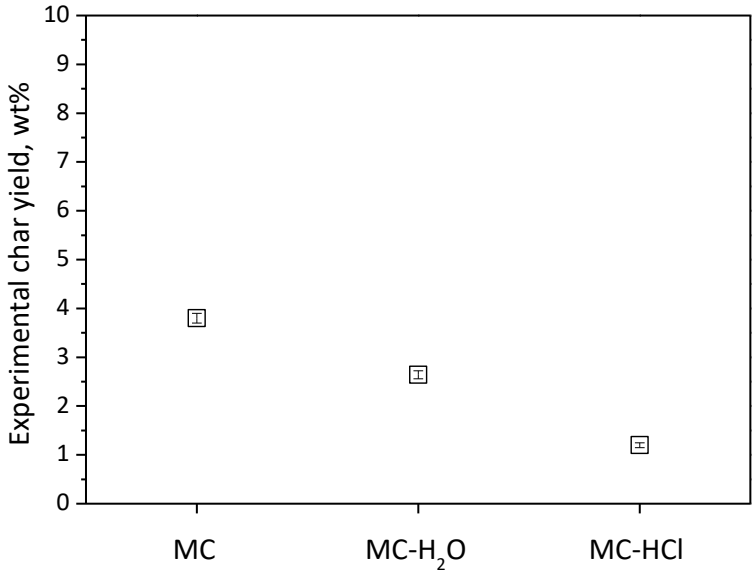

Figure 8.2 Char yields during the rapid pyrolysis of raw and leached biomass at 1300 °C

Raw, water-leached, and acid-leached mallee wood, (MW, MW-H_2O, MW-HCl) were subjected to rapid pyrolysis in a novel DTF at 1300 °C. The experimental char yields are plotted in Figure 8.2. Compared to the 3.8% char yield of MW, char yield of MW-H_2O decreased to 2.6% and acid-leached sample MW-HCl had the lowest char yield, being only 1.2%. Apart from the significant decrease in the ash content, the variance in other analyzed properties of biomass introduced by leaching is negligible. Therefore, it is believed that the presence of <1 wt% of inorganic matters in mallee wood can significantly contribute to the char formation, indicating their dominant role in the thermochemical conversion of biomass. The result is consistent with other studies that conducted pyrolysis for leached biomass at lower temperature and lower heating rate.[92, 288, 290-292] Studies focusing on the impacts of inorganic species on the yields of

pyrolysis products have revealed that AAEM species, especially K and Ca, can increase the char yield by inhibiting the decomposition of hydrocarbon and promoting the cross-linking reactions.[78, 174] Jiang et al. used different acids to wash rice straw and studied the decomposition of acid-leached samples with different concentrations of AAEM species via Thermogravimetric Fourier transforms infrared analysis (TG–FTIR).[293] Their results showed that alkali metals (Na and K) are related to the decomposition of hemicellulose while the concentration of Ca in samples determines the decomposition temperature of cellulose. Such effects of Ca was also reported by Jakab et al.,[294] Jensen et al.,[64] and Nowakowski et al.[103] Considering that AAEM species are the major inorganic elements in mallee wood and Ca has the highest content, the effects of leaching by removing the inorganic species can remarkably alter the reaction pathways during the rapid pyrolysis, and eventually decrease the char yield.[295]

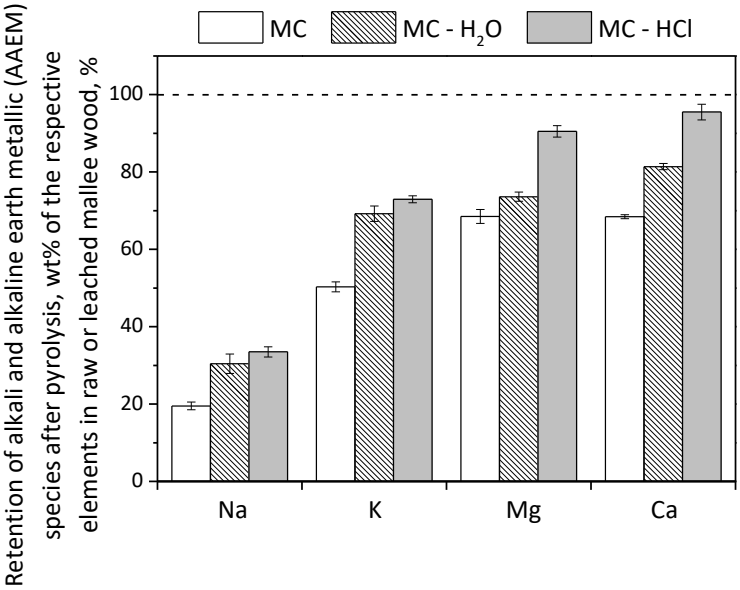

Figure 8.3 Retentions of AAEM species in char after rapid pyrolysis of raw and leached biomass

Emphasis was also placed on the retention of AAEM species during the rapid pyrolysis for leached mallee wood. As shown in Figure 8.1 that most alkali elements and a small part of alkaline earth elements were removed by water leaching, while almost all the AAEM species were lost after acid leaching. Based on the concentrations of AAEM species in char samples, raw or leached mallee wood samples (Table 8.2), and experimental char yields (Figure 8.2), the retention of AAEM species during rapid pyrolysis were determined and presented in Figure 8.3. In general, the retention of

AAEM species is lowest in MW and highest in MW-HCl, with MW-H_2O in the middle. Retentions of Na in MC, MC-H_2O, MC-HCl are 19.5%, 30.4%, and 33.5%, while retentions of K are 50.3%, 69.2%, and 72.9% in MC, MC-H_2O, MC-HCl, respectively. Mg and Ca have higher retentions, being 68.5% and 68.4% in MC, 73.6% and 81.4% in MC-H_2O, 90.5% and 95.5% in MC-HCl. It can be seen that the retentions of AAEM species increase with the increasingly aggressive leaching solutions. The very low retention of AAEM species in MC is the result of rapid devolatilization process of biomass at high temperature (1300 °C) causing element evaporation, thermal ejection, and the plastic deformation of char particles.[87] Besides, chlorides or sulphates are very likely to be the main form of the water-soluble elements which take up a large proportion of Na and K. Considering the melting temperature of alkali chlorides and sulphates being <900 °C, many Na/K chlorides and sulphates are decomposed and vaporized at 1300 °C, leading to their low retentions. After water-leaching, these chlorides and sulphates, along with other water-soluble salts are removed, and thus, the proportions of less reactive (acid-soluble and acid-insoluble) AAEM species become larger. The AAEM species left in leached mallee wood could bond with the organic structure, or have stable chemical forms with high melting points.[57] Therefore, during rapid pyrolysis, these elements tend to be incorporated into char matrix or form magnesium or calcium aluminosilicate compounds with high thermal stability. Moreover, chlorine, which is known to facilitate the release of alkali metals, is almost totally leached out by water.[125, 128] Consequently, the retentions of AAEM species are higher in MW-H_2O. After acid-leaching, the individual concentration of AAEM species is very low as the percentage of acid-insoluble AAEM species retained in MW-HCl is <1%. However, these elements are in the least reactive form and therefore, they have highest retentions after rapid pyrolysis.

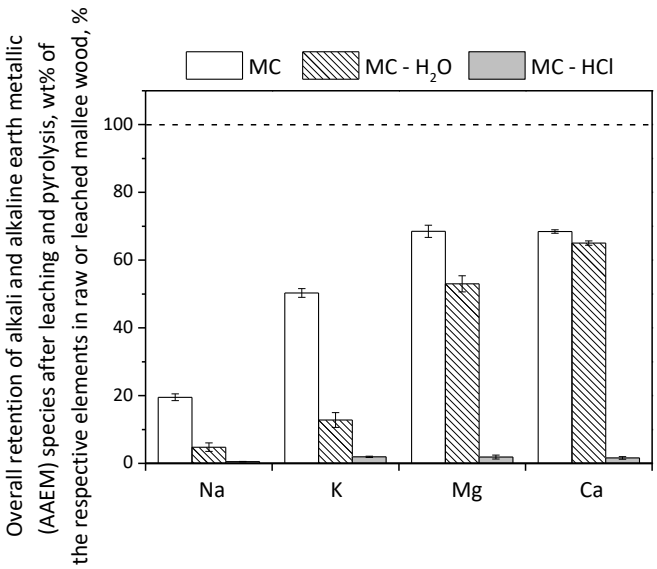

Figure 8.4 Overall retentions of AAEM species after leaching and rapid pyrolysis

Overall retentions of AAEM species combines the loss of elements during leaching process and the rapid pyrolysis and is shown in Figure 8.4. Due to the high leaching efficiency of Na and K by water, the overall retentions of Na and K in MC-H_2O are 4.8% and 12.8%, which are much less than the retentions in MC. The difference in the overall retentions of Mg and Ca in MC and MC-H_2O are smaller as only a small part of Mg and Ca are removed by water leaching. Less than 2% of AAEM species are retained in MC-HCl after leaching and pyrolysis despite the retentions of AAEM species are the highest for MC-HCl during rapid pyrolysis. Therefore, the leaching process has a major effect on the overall retentions of AAEM species as the leaching of AAEM species via water or acid is highly efficient.

8.4 Effects of leaching on particle shape and size

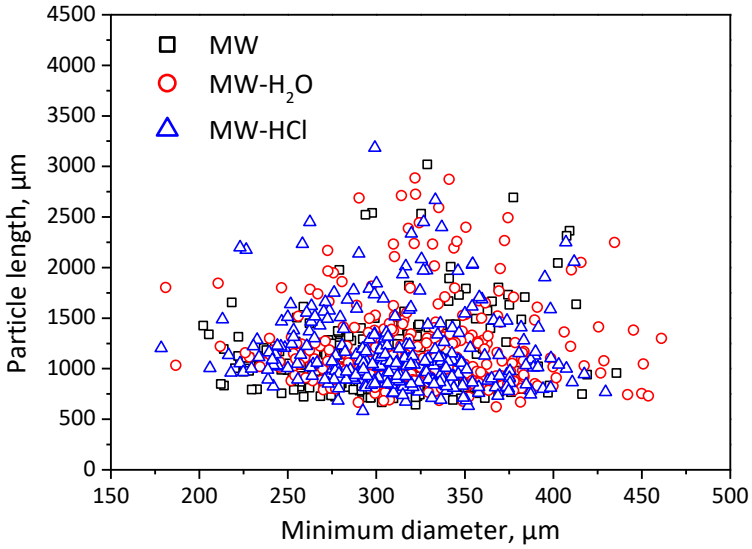

Figure 8.5 Correlation of particle length and minimum diameter for raw and leached biomass

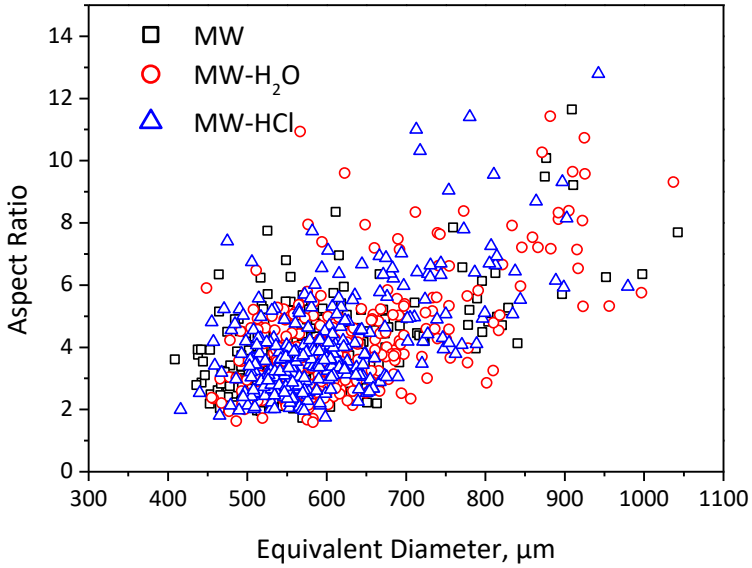

Figure 8.6 Correlation of aspect ratio and equivalent diameter for raw and leached biomass

Image analysis for MW and leached mallee wood particles were carried out. The size parameters (particle length and minimum diameter) are depicted in Figure 8.5 and the derived equivalent diameter and particle shape (indicated by aspect ratio) are shown in Figure 8.6. When mallee wood particles before and after leaching are presented

together, it is obvious that the leaching process does not introduce variation in particle size and shape because they have the same size and aspect ratio ranges.

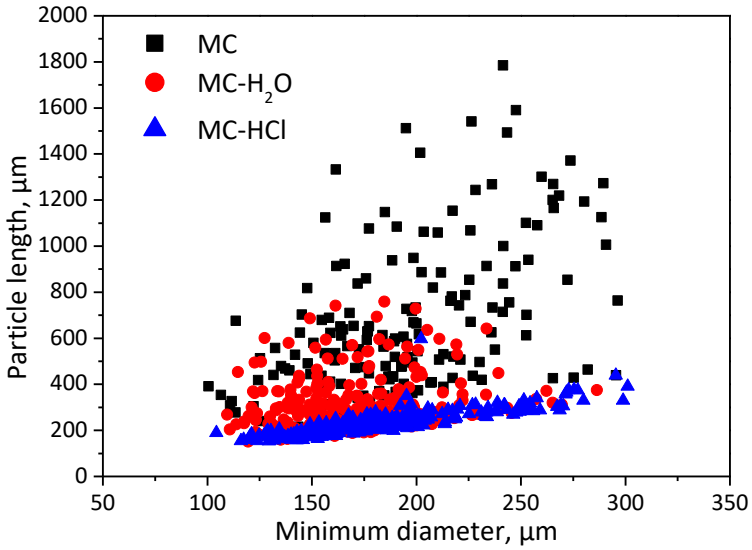

Figure 8.7 Correlation of particle length and minimum diameter for char particles produced by rapid pyrolysis of raw and leached biomass

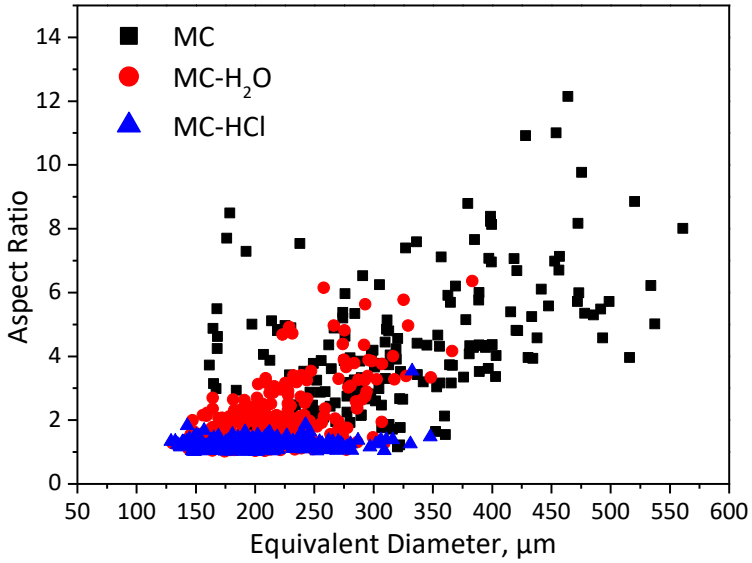

Figure 8.8 Correlation of aspect ratio and equivalent diameter for char particles produced by rapid pyrolysis of raw and leached biomass

However, size and shape parameters for char particles are very different after different leaching processes. The distribution of MC particles is very scattered (see Figure 8.7), with their particle length ranging from ~200 µm to up to 1800 µm and minimum diameter ranging from ~100 µm to ~300 µm. The much larger particle length is

responsible for the high aspect ratio of MC (up to 12) as shown in Figure 8.8. However, the range of particle length of MC-H_2O reduces to ~200 to ~800 and as a result, the aspect ratio of MC-H_2O decreases to <7, with many particles having their aspect ratio <2. This means that the deformation of MC-H_2O during rapid pyrolysis is more severe and many particles are unable to maintain their original elongated shape. MC-HCl particles experienced the most significant deformation here, which can be deduced from their almost equal particle length and minimum diameter, and low aspect ratio (<2). Considering the small variance in other properties apart from the ash content of MW-H_2O and MW-HCl, the distinct shape of their char particles is likely to be the result of the removal of inorganic species. A similar conclusion was drawn by Oudenhoven et al, by comparing the melting behavior of raw and acid-leached pine wood when pyrolyzed in a fluidized-bed reactor.[295] They believe that the more extensive melting phenomena is by large extend attributed to the removal of AAEM species and they also observed less melting if leached pine wood was back impregnated with AAEM species.

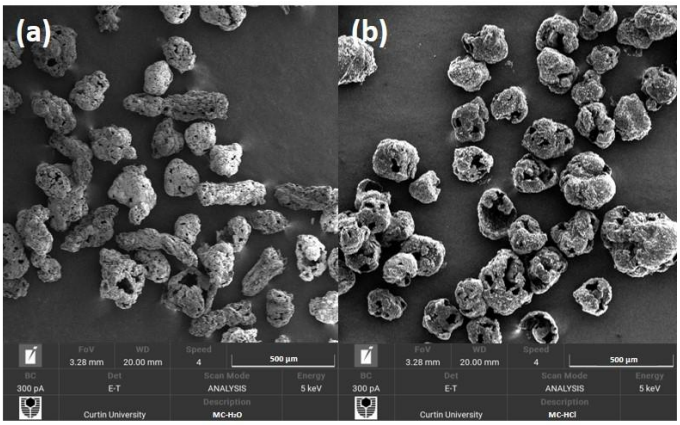

Figure 8.9 SEM pictures for MC-H_2O and MC-HCl particles, (a): MC-H_2O, (b): MC-HCl

In this study, SEM images for char samples (see Figure 8.9) show that MC-H_2O particles have a rough surface texture, large openings, an empty interior, and many being relatively round. However, the magnified surface morphology of MC-H_2O particles clearly shows signs of re-solidification, as the result of softening and melting.[82] Those spherical MC-HCl particles with scabrous surfaces indicate severe melting happened for mallee wood during rapid pyrolysis without AAEM species. A possible explanation for this is that AAEM species in mallee wood have the ability to

enhance the cross-linking reactions by acting as the joint point,[296] or catalyzing the conversion of bridges into interlinked structures.[43] Such effects can not only increase the char yield but also make the structure less fluid but more stable, with higher resistance to the high temperature.[43, 290]

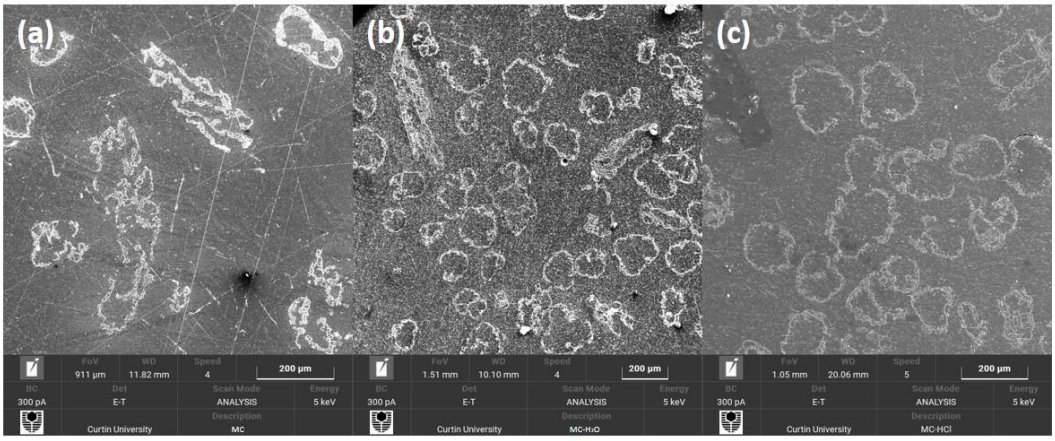

Figure 8.10 Cross-sectional images for char produced by the rapid pyrolysis of raw and leached biomass, (a): MC, (b): MC-H_2O, (c): MC-HCl

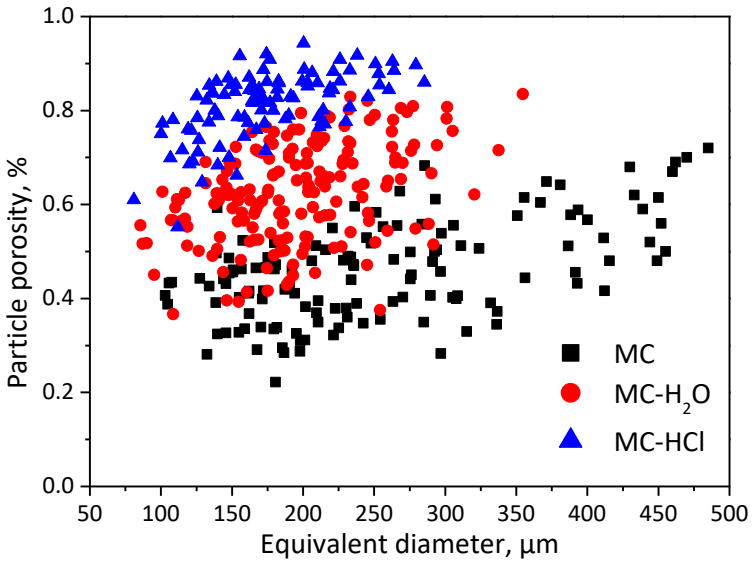

Figure 8.11 Cross-sectional porosity for char particles produced from the rapid pyrolysis of raw and leached biomass

The cross-section images for char particles were taken and presented in Figure 8.10. The difference in the internal structure for three char samples is obvious. The internal voids in MC particles have highly irregular shape and are separated by char matrix, while the MC-HCl particles are cenospheres with thin shell. The internal structure of

MC-H_2O char particles is a combination of MC and MC-HCl, which suggests that the degree of porosity is related to the extent of leaching. The quantitative analysis of porosity is summarized in Figure 8.11. It can be found that the average porosity for different char samples is in the order of MC < MC-H_2O < MC-HCl, which corresponds to the gradually higher char yield in the same order. Apart from the lower degree of cross-linked molecular structure due to the removal of AAEM species, another reason for the higher porosity in MC-H_2O and MC-HCl could be the swelling behavior of these char particles whose fluidity is stronger. Another finding is the higher porosity for larger particles. This can be explained because larger particle size (equivalent diameter) means longer diffusion time for pyrolysis gases produced inside the particle, consequently higher possibility for them to be trapped inside. These trapped gases can create internal voids which would be further enlarged as more gases produced and gas expand at high temperatures.

8.5 Conclusions

Mallee wood particles (250-355 μm) were leached by ultrapure water (semi-continuously) and 0.1 M hydrochloric acid to investigate the effects of leaching on the properties of biomass and their subsequent rapid pyrolysis behaviour. It is found that the reduction of ash content is the major change in biomass properties caused by leaching. Quantification of the AAEM species in raw mallee wood and leachates shows that water-leaching can remove ~80% of Na and K, ~30% of Mg and ~15% of Ca, while removal efficiency of acid-leaching can reach up to ~98% for all AAEM species. This indicates that the existence of Mg and Ca is more stable than Na and K in mallee wood. Rapid pyrolysis of raw and leached mallee wood shows the lower char yields for leached mallee wood, with the experimental char yields for raw mallee wood char, water-leached char and acid-leached char being 3.8%, 2.6% and 1.2%, respectively. Retentions of AAEM species were also analyzed. The results show that the retained AAEM species after increasingly aggressive leaching agents have higher retention after pyrolysis. Water-leaching and acid-leaching leads to an increase of ~5-20% and ~10-25% in retentions of AAEM species, respectively, as compared to the retention of in raw mallee wood. This is likely because the higher stability of retained AAEM species after leaching and the removal of chlorine which facilitate the vaporization of AAEM species. However, the overall retention of AAEM species

(include the loss of AAEM species during leaching and rapid pyrolysis) is dominated by the leaching efficiency. Therefore, despite the higher retentions during rapid pyrolysis, water-leaching and acid-leaching can effectively decrease the content of AAEM species in char. The image analysis of leached mallee wood and their char particles reveals that leaching has negligible impacts on the particle size and shape of biomass, whereas the morphology of their char particles is distinct. Char particles pyrolyzed from leached mallee wood have more spherical shape and stronger melting tendency. Acid leaching produces char with highest cross-sectional porosity, followed by water leaching. Particles with larger equivalent diameter exhibits higher porosity, probably due to more pyrolysis gases trapped inside the particle.

CHAPTER 9 CONCLUSIONS AND RECOMMENDATIONS

9.1 Introduction

This chapter summarizes the key findings from this Ph.D. study. The results provide a better understanding of the thermochemical conversions of biomass under conditions pertinent to pulverized fuel combustion and can instruct the utilization of biomass in co-firing power plants.

Overall, this thesis has systematically answered the long-standing question about the true char yield of biomass after rapid pyrolysis at high temperature, the release of inorganic species, and the transformation of particle shape and size under various conditions. Firstly, the effects of particle size on the rapid pyrolysis of mallee and pine wood were investigated, focusing on the properties of resultant char samples. Secondly, the evolution of physical and chemical properties during the rapid pyrolysis for wood particles was studied by varying their residence time inside the furnace. Thirdly, considering the potential of torrefaction as a pretreatment method for biomass, fundamental research about the properties of char after the rapid pyrolysis of torrefied wood powder was carried out to evaluate the effects of torrefaction temperature. Fourthly, this research simulated the industrial utilization of wood chips by torrefying and then pulverizing the wood chips, to further study the impacts of torrefaction on particle shape and size. Finally, water-leaching and acid-leaching, which are effective methods to mitigate the ash-related problems for biomass, were applied to mallee wood and their char after rapid pyrolysis were characterized.

In addition, based on the current study, this chapter provides some recommendations for further work.

9.2 Conclusions

9.2.1 Rapid pyrolysis of pulverized biomass at high temperature: effect of particle size on char yield, retentions of alkali and alkaline earth metallic species and char particle shape

- An increase in particle size favors the formation of char even at a high temperature as 1300 °C. It is likely due to the substantially lower heating rate experienced by large particles (250-355 μm), as the estimation of heating rate suggests that small particles (90-106 μm) are heated ~5.4 times faster than large particles. Lower heating rate for large particles indicates less extensive gasification of char matrix by CO_2 and H_2O and less profound thermal annealing of char, which favor the formation of char.
- The ash-tracer method significantly overestimates the char yield for biomass by 50-400%, especially for small particles.
- Retentions of AAEM species show that only < 20% of Na, < 50% of K, and 40-70% of Mg and Ca are retained in char after rapid pyrolysis for mallee and pine at 1300 °C, suggesting the extensive release of inorganic species.
- A decrease in particle size enhances the release of AAEM species, owing to the higher heating rate for small particles and less re-combination of released AAEM species with active char matrix.
- The particle size can also affect the shape of the resultant char. The lower overall heating rate experienced by large particles resulted in partial melting and retained fibrous structure, while the high heating rate for small particles promotes the melting and swelling of the cell structure, leaving the more spherical and smooth morphology.

9.2.2 The evolution of char properties during rapid pyrolysis of woody biomass at high temperature

- Rapid pyrolysis of mallee and pine wood is mostly completed at the particle residence time of 0.51s and 0.41s, obtaining char yields of 3.8% and 2.8%,

respectively. The low particle density and thin long flake shape of pine particles could be the reasons for its more rapid decrease in char yields.

- The retentions of AAEM species decrease with particle residence time but by a different extent for each AAEM species. About 70% of Mg and Ca, ~50% of K, and ~20% of Na are retained in mallee char at the particle residence time of ~0.5 s. However, for pine char, only ~50% of Mg and Ca, ~35% of K, and ~10% of Na are retained at the particle residence time of 0.68 s. The lower AAEM species retentions in pine char can be attributed to the higher fraction of water-soluble AAEM species in pine wood.
- The retentions of AAEM species in pine chars keep decreasing after 0.41s when pyrolysis is mostly completed, which can be attributed to the continuous reduction in O/C and H/C molar ratios for pine chars. This indicates that the nascent pine chars will undergo extensive annealing/thermal cracking, leading to the loss of oxygen-containing groups when exposed to high temperatures. However, for mallee chars, such a phenomenon is not observed, probably due to its higher and unchanged O/C molar ratios after 0.51s.
- Chemical fractionation of a partially pyrolyzed mallee char and a completely pyrolyzed mallee char shows that there is a decrease in water-soluble Na and K (from ~85% to ~40%) but an increase in ion-exchangeable Na and K (from ~10% to ~20-30%) during the early stage of pyrolysis. This suggests that the decomposed water-soluble Na and K can combine with oxygen-containing groups in char matrix during the thermochemical conversion.
- More than 50% of Mg and Ca transform from water-soluble and ion-exchangeable form to acid-soluble and acid-insoluble form as Mg and Ca become increasingly incorporated into the char matrix.
- Further pyrolysis leads to a reduction in ion-exchangeable AAEM species due to the loss of oxygen-containing groups.
- The melting of char structure begins at both ends of char particles as pyrolysis continues and severe deformation is observed at the later stage of pyrolysis, leading to significantly reduced particle length, diameter, and aspect ratio. Mallee char particles exhibit a progressive and steady decrease in dimensions, with the fibrous structure of the parent mallee wood still retained during the early stage of pyrolysis. However, pine wood has less resistance to particle

deformation during pyrolysis and more extensive deformation makes the pine char particles completely melt to spheres.

9.2.3 Rapid pyrolysis of pulverized biomass at high temperature: effects of torrefaction temperature on char yield, retention of alkali and alkaline earth metallic species and char particle shape

- Biomass structure is altered after torrefaction. At high torrefaction temperature (300 °C), the decomposition of hemicellulose (especially xylan) is significant and the content of acid-insoluble residue is doubled. Besides, torrefaction makes the chemical occurrence of AAEM species more stable in mallee wood, as the percentages of acid-soluble and acid-insoluble species increase but the percentages of water-soluble and ion-exchangeable species decrease.
- Increasing torrefaction temperature can cause higher char yield during rapid pyrolysis, and biomass being torrefied at 300 °C can yield three times more char after rapid pyrolysis compared to using raw biomass directly.
- The release of AAEM species is negligible during torrefaction but pronounced during rapid pyrolysis. Compared to the retentions of AAEM species for raw mallee, torrefied mallee wood has higher retention for AAEM species after rapid pyrolysis. Raising torrefaction temperature from 220 °C to 300 °C can increase the retentions of AAEM species a lot.
- The relative proportions of water-soluble Na and K decreased but ion-exchangeable and acid-soluble K increase in chars with higher torrefaction temperature, indicating the stable existing status of Na and K in char pretreated by torrefaction. But there is a significant reduction in the proportions of acid-insoluble Mg and Ca in chars as torrefaction temperature rising,
- Studies of the char morphology reveal that the torrefaction process has a negligible effect on the particle size and shape of biomass, whereas severe torrefaction can make the char particle size larger and aspect ratio smaller after pyrolysis, and the surface of those char particles seems to be smoother.

9.2.4 A study of particle size, shape, and retentions of inorganic species during rapid pyrolysis based on industrial utilization of torrefied wood chips

- The degree of cross-linking for torrefied biomass is quantified and found to have an inverse relation to the torrefaction yield.
- For torrefied wood chips, it is found that after pulverization and sieving, the particle length for large particles (250-355 μm) is significantly reduced with higher torrefaction temperature, which caused much lower aspect ratios for these particles. However, such effect of torrefaction was not observed for small particles (90-106 μm), suggesting that the impact of a combined biomass pretreatment process (torrefaction and pulverization) on the particle shape depends on the final particle size.
- The retentions of AAEM species in large and small particles increase with the rising torrefaction temperature, especially for Na and K. Such rise is more significant for small particles. Therefore, the difference in retention caused by particle size is gradually reduced with higher torrefaction temperature.
- A high torrefaction temperature causes less shrinkage and a solid/dense internal structure in pyrolyzed char particles with large size. The melting for small particles is still quite obvious after rapid pyrolysis, yet with higher torrefaction temperatures, such as at 300 °C, the aspect ratio of small char particles can reach up to 4, indicating stronger resistance to melting for small torrefied biomass.

9.2.5 Effects of biomass leaching on the properties of char after rapid pyrolysis

- Water-leaching can remove ~80% of Na and K, ~30% of Mg, and ~15% of Ca, while removal efficiency of acid-leaching can reach up to ~98% for all AAEM species for mallee wood.
- The lack of inorganic species, especially K and Ca, after leaching leads to a noticeable decrease in char yield after rapid pyrolysis at 1300 °C.
- Leaching with increasingly aggressive agents can cause more AAEM species to be retained in char after pyrolysis. Water-leaching and acid-leaching lead to an increase of ~5-20% and ~10-25% in retentions of AAEM species, respectively, as compared to the retentions using raw mallee wood.

- The overall retentions of AAEM species (include the loss of AAEM species during leaching and rapid pyrolysis) are dominated by the leaching efficiency. Despite the higher retentions during rapid pyrolysis, water-leaching and acid-leaching can effectively decrease the content of AAEM species in char.
- Negligible impact on the particle size and shape of biomass is found after leaching, whereas the morphology of char particles is distinct using leached biomass for rapid pyrolysis. Char particles pyrolyzed from leached mallee wood have a more spherical shape and a stronger melting tendency. Acid-leached mallee wood produces char with the highest cross-sectional porosity, followed by water-leached derived char and then raw mallee wood char.

9.3 Recommendations

Based on the outcome of this Ph.D. project, some future research is recommended to further fulfill the research gaps for an applicable and economical utilization of biomass:

1. For the first time in the field, this study reports accurate char yields from rapid pyrolysis of biomass with different particle sizes at high temperatures. In addition, the evolution of char yield was also accurately determined. Therefore, it is recommended that a systematic study should be carried out to evaluate or validate previous kinetic models developed for thermochemical conversion of biomass at high temperatures. Besides, it is suggested to establish a new model dedicated to the rapid pyrolysis of mallee wood to guide the utilization and research in Western Australia.
2. It is observed in this research that a significant amount of inorganic species are released during the thermochemical conversion of biomass. However, the exact releasing mechanism and the distribution of evaporated AAEM species should be further investigated.
3. The results from this research show that AAEM species have a significant impact on char morphology, but the effect of individual AAEM species on char morphology is still unclear. Thus, a systematic study should be carried out to study the effect of each major inorganic element on char morphology.
4. The transformation of biomass particle shape and size during the rapid pyrolysis at high temperature is quantitatively evaluated in this Ph.D. project, considering the wide particle shape, the pretreatment methods (torrefaction and

leaching) for raw biomass. However, another unique characteristic of biomass particles is their diverse particle shape after pulverization, which can introduce variations in heat and mass transfer even after being heated when the particle has the same mass. Therefore, more works are required to investigate the impacts of different particle shapes on the conversion process and the products.

5. This Ph.D. project focuses on the first stage of biomass thermochemical conversion in the pulverized-fuel furnaces. Future research should study the evolution of particle shape, the retentions of AAEM species, etc., during the subsequent stages of biomass combustion.
6. The results reported in this Ph.D. study are mostly experimental-based. It is suggested to further strengthen the interpretation of the results by modelling the pyrolysis process under conditions used in this study, which will generate valuable insight into the field.

REFERENCES

1. *Renewables 2018 Analysis and forecasts to 2023*; International Energy Agency: 2018.
2. Wang, X.; Kersten, S. R. A.; Prins, W.; van Swaaij, W. P. M., Biomass Pyrolysis in a Fluidized Bed Reactor. Part 2: Experimental Validation of Model Results. *Industrial & Engineering Chemistry Research* **2005,** *44* (23), 8786-8795.
3. Medic, D.; Darr, M.; Shah, A.; Potter, B.; Zimmerman, J., Effects of torrefaction process parameters on biomass feedstock upgrading. *Fuel* **2012,** *91* (1), 147-154.
4. Bartle, J. R.; Abadi, A., Toward Sustainable Production of Second Generation Bioenergy Feedstocks. *Energy & Fuels* **2010,** *24* (1), 2-9.
5. Wu, H.; Fu, Q.; Giles, R.; Bartle, J., Production of Mallee Biomass in Western Australia: Energy Balance Analysis. *Energy & Fuels* **2008,** *22* (1), 190-198.
6. Yu, Y.; Bartle, J.; Li, C. Z.; Wu, H., Mallee biomass as a key bioenergy source in western australia: Importance of biomass supply chain. *Energy & Fuels* **2009,** *23*, 3290-3299.
7. Panahi, A.; Levendis, Y. A.; Vorobiev, N.; Schiemann, M., Direct observations on the combustion characteristics of Miscanthus and Beechwood biomass including fusion and spherodization. *Fuel Processing Technology* **2017,** *166*, 41-49.
8. Cetin, E.; Gupta, R.; Moghtaderi, B., Effect of pyrolysis pressure and heating rate on radiata pine char structure and apparent gasification reactivity. *Fuel* **2005,** *84* (10), 1328-1334.
9. Goyal, H. B.; Seal, D.; Saxena, R. C., Bio-fuels from thermochemical conversion of renewable resources: A review. *Renewable and Sustainable Energy Reviews* **2008,** *12* (2), 504-517.
10. Czernik, S.; Bridgwater, A. V., Overview of Applications of Biomass Fast Pyrolysis Oil. *Energy & Fuels* **2004,** *18* (2), 590-598.
11. Jahirul, M. I.; Rasul, M. G.; Chowdhury, A. A.; Ashwath, N., Biofuels production through biomass pyrolysis- A technological review. *Energies* **2012,** *5*, 4952-5001.
12. Niemelä, N. P.; Nowak Delgado, R.; de Riese, T.; Tolvanen, H.; Fendt, S.; Spliethoff, H.; Joronen, T., Fuel-specific devolatilization parameters for detailed comparison of pulverized biomass fuels. *Fuel* **2021,** *286*, 119309.
13. Kannan, G. K.; Gupta, M.; Chandra Kapoor, J., Estimation of gaseous products and particulate matter emission from garden biomass combustion in a simulation fire test chamber. *Atmospheric Environment* **2005,** *39* (3), 563-573.
14. Yani, S.; Gao, X.; Wu, H., Emission of Inorganic PM10 from the Combustion of Torrefied Biomass under Pulverized-Fuel Conditions. *Energy & Fuels* **2015,** *29* (2), 800-807.
15. Fuller, A.; Maier, J.; Karampinis, E.; Kalivodova, J.; Grammelis, P.; Kakaras, E.; Scheffknecht, G., Fly Ash Formation and Characteristics from (co-)Combustion of an Herbaceous Biomass and a Greek Lignite (Low-Rank Coal) in a Pulverized Fuel Pilot-Scale Test Facility. *Energies* **2018,** *11* (6).
16. Zhang, Y.; Kajitani, S.; Ashizawa, M.; Miura, K., Peculiarities of Rapid Pyrolysis of Biomass Covering Medium- and High-Temperature Ranges. *Energy & Fuels* **2006,** *20* (6), 2705-2712.
17. Zanzi, R.; Sjöström, K.; Björnbom, E., Rapid pyrolysis of agricultural residues at high temperature. *Biomass and Bioenergy* **2002,** *23* (5), 357-366.

18. Bitowft, B.; Andersson, L. A.; Bjerle, I., Fast pyrolysis of sawdust in an entrained flow reactor. *Fuel* **1989,** *68* (5), 561-566.
19. Septien, S.; Valin, S.; Dupont, C.; Peyrot, M.; Salvador, S., Effect of particle size and temperature on woody biomass fast pyrolysis at high temperature (1000–1400 °C). *Fuel* **2012,** *97*, 202-210.
20. Dupont, C.; Commandré, J.-M.; Gauthier, P.; Boissonnet, G.; Salvador, S.; Schweich, D., Biomass pyrolysis experiments in an analytical entrained flow reactor between 1073K and 1273K. *Fuel* **2008,** *87* (7), 1155-1164.
21. Surup, G. R.; Foppe, M.; Schubert, D.; Deike, R.; Heidelmann, M.; Timko, M. T.; Trubetskaya, A., The effect of feedstock origin and temperature on the structure and reactivity of char from pyrolysis at 1300–2800 °C. *Fuel* **2019,** *235*, 306-316.
22. Smith, I. W., The combustion rates of coal chars: a review. *Symposium (International) on combustion* **1982,** *19*, 1045-1065.
23. Liaw, S. B.; Wu, H., A New Method for Direct Determination of Char Yield during Solid Fuel Pyrolysis in Drop-Tube Furnace at High Temperature and Its Comparison with Ash Tracer Method. *Energy & Fuels* **2019,** *33* (2), 1509-1517.
24. Manouchehrinejad, M.; van Giesen, I.; Mani, S., Grindability of torrefied wood chips and wood pellets. *Fuel Processing Technology* **2018,** *182*, 45-55.
25. Batidzirai, B.; Mignot, A. P. R.; Schakel, W. B.; Junginger, H. M.; Faaij, A. P. C., Biomass torrefaction technology: Techno-economic status and future prospects. *Energy* **2013,** *62*, 196-214.
26. Cahyanti, M. N.; Doddapaneni, T. R. K. C.; Kikas, T., Biomass torrefaction: An overview on process parameters, economic and environmental aspects and recent advancements. *Bioresource Technology* **2020,** *301*, 122737.
27. Schiemann, M.; Haarmann, S.; Vorobiev, N., Char burning kinetics from imaging pyrometry: Particle shape effects. *Fuel* **2014,** *134*, 53-62.
28. Edenhofer, O.; Pichs-Madruga, R.; Sokona, Y.; Farahani, E.; Kadner, S.; Seyboth, K.; Adler, A.; Baum, I.; Brunner, S.; Eickemeier, P.; Kriemann, B.; Savolainen, J.; Schlömer, S.; Stechow, C. v.; (eds.), T. Z. a. J. C. M., *IPCC(2014). Climate Change 2014: Mitigation of Climate Change. Contribution of Working Group III to the Fifth Assessment Report of the Intergovernmental Panel on Climate Change*. Cambridge University Press, Cambridge, United Kingdom and New York, NY, USA.: 2014.
29. Agency, T. E. P. Inventory of U.S. Greenhouse Gas Emissions and Sinks: 1990-2019.
30. Gyamfi, B. A.; Sarpong, S. Y.; Bein, M. A., The contribution of the anthropogenic impact of biomass utilization on ecological degradation: revisiting the G7 economies. *Environmental Science and Pollution Research* **2021,** *28* (9), 11016-11029.
31. Western Australian Climate Policy A plan to position Western Australia for a prosperous and resilient low-carbon future. Department of Water and Environmental Regulation, 2020.
32. Vassilev, S. V.; Baxter, D.; Andersen, L. K.; Vassileva, C. G., An overview of the chemical composition of biomass. *Fuel* **2010,** *89* (5), 913-933.
33. Bridgewater, A., Thermal conversion of biomass and waste: the status. *Birmingham (UK): Bio-Energy Research Group, Aston University* **2001**.
34. Zhang, L.; Xu, C.; Champagne, P., Overview of recent advances in thermo-chemical conversion of biomass. *Energ Convers Manage* **2010,** *51* (5), 969-982.

35. Stucley, C.; Schuck, S.; Sims, R.; Bland, J.; Marino, B.; Borowitzka, M.; Abadi, A.; Bartle, J.; Giles, R.; Thomas, Q., *Bioenergy In Australia: Status and Opportunities*. Bioenergy Australia: St Leonards NSW 2065: 2012.
36. Cooper, D.; Olsen, G.; Bartle, J., Capture of agricultural surplus water determines the productivity and scale of new low-rainfall woody crop industries. *Australian Journal of Experimental Agriculture* **2005,** *45* (11), 1369-1388.
37. Olsen, G.; Cooper, D.; Huxtable, D.; Carslake, J.; Bartle, J. *Developing multiple purpose species for large scale revegetation, Search Project Final Report (NHT Project 973849)*; 2004.
38. Shepherd M., B. J., Lee D. J, Brawner J., Bush D.,; Turnbull P., M. P., R Brown T., Simmons B., Henry R, Eucalypts as a biofuel feedstock. *Biofuels* **2011,** *2:6*, 639-657.
39. Brooksbank, K.; Lever, M.; Peterson, H.; Weybury, M., Biomass scoping study: opportunities for agriculture in Western Australia. Department of Agriculture and Food, W. A., Perth. Bulletin 4862., Ed. 2014.
40. Spliethoff, H.; Hein, K. R. G., Effect of co-combustion of biomass on emissions in pulverized fuel furnaces. *Fuel Processing Technology* **1998,** *54* (1), 189-205.
41. Aboyade, A. O.; Carrier, M.; Meyer, E. L.; Knoetze, H.; Görgens, J. F., Slow and pressurized co-pyrolysis of coal and agricultural residues. *Energ Convers Manage* **2013,** *65*, 198-207.
42. Demirbaş, A., Sustainable cofiring of biomass with coal. *Energ Convers Manage* **2003,** *44* (9), 1465-1479.
43. Trubetskaya, A.; Jensen, P. A.; Jensen, A. D.; Garcia Llamas, A. D.; Umeki, K.; Glarborg, P., Effect of fast pyrolysis conditions on biomass solid residues at high temperatures. *Fuel Processing Technology* **2016,** *143*, 118-129.
44. Karinkanta, P.; Ämmälä, A.; Illikainen, M.; Niinimäki, J., Fine grinding of wood – Overview from wood breakage to applications. *Biomass and Bioenergy* **2018,** *113*, 31-44.
45. Umeki, K.; Kirtania, K.; Chen, L.; Bhattacharya, S., Fuel Particle Conversion of Pulverized Biomass during Pyrolysis in an Entrained Flow Reactor. *Industrial & Engineering Chemistry Research* **2012,** *51* (43), 13973-13979.
46. Phanphanich, M.; Mani, S., Impact of torrefaction on the grindability and fuel characteristics of forest biomass. *Bioresource Technology* **2011,** *102* (2), 1246-1253.
47. Saastamoinen, J.; Aho, M.; Moilanen, A.; Sørensen, L. H.; Clausen, S.; Berg, M., Burnout of pulverized biomass particles in large scale boiler–single particle model approach. *Biomass and Bioenergy* **2010,** *34* (5), 728-736.
48. Gera, D.; Mathur, M. P.; Freeman, M. C.; Robinson, A., Effect of Large Aspect Ratio of Biomass Particles on Carbon Burnout in a Utility Boiler. *Energy & Fuels* **2002,** *16* (6), 1523-1532.
49. Mock, C.; Lee, H.; Choi, S.; Manovic, V., Combustion Behavior of Relatively Large Pulverized Biomass Particles at Rapid Heating Rates. *Energy & Fuels* **2016,** *30*, 10809-10822.
50. Maciejewska, A. K.; Veringa, H.; Sanders, J. P. M.; Peteves, S. D. *Co-firing of biomass with coal: constraints and role of biomass pretreatment*; Environmental Economics and Natural Resources, Biobased Chemistry and Technology, MGS: European Commission, Netherlands, 2006.
51. Nunes, L. J. R.; Matias, J. C. O.; Catalão, J. P. S., A review on torrefied biomass pellets as a sustainable alternative to coal in power generation. *Renewable and Sustainable Energy Reviews* **2014,** *40*, 153-160.

52. Williams, A.; Pourkashanian, M.; Jones, J. M., Combustion of pulverised coal and biomass. *Progress in Energy and Combustion Science* **2001,** *27* (6), 587-610.
53. Wang, G.; Zhang, J.; Shao, J.; Ren, S., Characterisation and model fitting kinetic analysis of coal/biomass co-combustion. *Thermochimica Acta* **2014,** *591*, 68-74.
54. Dai, J.; Sokhansanj, S.; Grace, J. R.; Bi, X.; Lim, C. J.; Melin, S., Overview and some issues related to co-firing biomass and coal. *The Canadian Journal of Chemical Engineering* **2008,** *86* (3), 367-386.
55. Heinzel, T.; Siegle, V.; Spliethoff, H.; Hein, K. R. G., Investigation of slagging in pulverized fuel co-combustion of biomass and coal at a pilot-scale test facility. *Fuel Processing Technology* **1998,** *54* (1), 109-125.
56. Misra, M. K.; Ragland, K. W.; Baker, A. J., Wood ash composition as a function of furnace temperature. *Biomass and Bioenergy* **1993,** *4* (2), 103-116.
57. Frandsen, F. J.; van Lith, S. C.; Korbee, R.; Yrjas, P.; Backman, R.; Obernberger, I.; Brunner, T.; Jöller, M., Quantification of the release of inorganic elements from biofuels. *Fuel Processing Technology* **2007,** *88* (11), 1118-1128.
58. Thy, P.; Barfod, G. H.; Cole, A. M.; Brown, E. L.; Jenkins, B. M.; Lesher, C. E., Trace metal release during wood pyrolysis. *Fuel* **2017,** *203*, 548-556.
59. Long, J.; Song, H.; Jun, X.; Sheng, S.; Lun-shi, S.; Kai, X.; Yao, Y., Release characteristics of alkali and alkaline earth metallic species during biomass pyrolysis and steam gasification process. *Bioresource Technology* **2012,** *116*, 278-284.
60. Okuno, T.; Sonoyama, N.; Hayashi, J.-i.; Li, C.-Z.; Sathe, C.; Chiba, T., Primary Release of Alkali and Alkaline Earth Metallic Species during the Pyrolysis of Pulverized Biomass. *Energy & Fuels* **2005,** *19* (5), 2164-2171.
61. Liaw, S. B.; Rahim, M. U.; Wu, H., Trace Elements Release and Particulate Matter Emission during the Combustion of Char and Volatiles from in Situ Biosolid Fast Pyrolysis. *Energy & Fuels* **2016,** *30*, 5766-5771.
62. Knudsen, J. N.; Jensen, P. A.; Dam-Johansen, K., Transformation and Release to the Gas Phase of Cl, K, and S during Combustion of Annual Biomass. *Energy & Fuels* **2004,** *18* (5), 1385-1399.
63. Chen, W.-H.; Du, S.-W.; Yang, T.-H., Volatile release and particle formation characteristics of injected pulverized coal in blast furnaces. *Energ Convers Manage* **2007,** *48* (7), 2025-2033.
64. Jensen, P. A.; Frandsen, F. J.; Dam-Johansen, K.; Sander, B., Experimental Investigation of the Transformation and Release to Gas Phase of Potassium and Chlorine during Straw Pyrolysis. *Energy & Fuels* **2000,** *14* (6), 1280-1285.
65. Zellagui, S.; Schönnenbeck, C.; Zouaoui-Mahzoul, N.; Leyssens, G.; Authier, O.; Thunin, E.; Porcheron, L.; Brilhac, J. F., Pyrolysis of coal and woody biomass under N2 and CO2 atmospheres using a drop tube furnace - experimental study and kinetic modeling. *Fuel Processing Technology* **2016,** *148*, 99-109.
66. Demirbas, A.; Arin, G., An Overview of Biomass Pyrolysis. *Energy Sources* **2002,** *24* (5), 471-482.
67. Wang, Q.; Zhao, W.; Liu, H.; Jia, C.; Xu, H., Reactivity and Kinetic Analysis of Biomass during Combustion. *Energy Procedia* **2012,** *17*, 869-875.
68. Biagini, E.; Narducci, P.; Tognotti, L., Size and structural characterization of lignin-cellulosic fuels after the rapid devolatilization. *Fuel* **2008,** *87* (2), 177-186.
69. Solomon, P. R.; Fletcher, T. H.; Pugmire, R. J., Progress in coal pyrolysis. *Fuel* **1993,** *72* (5), 587-597.

70. Steer, J. M.; Marsh, R.; Greenslade, M.; Robinson, A., Opportunities to improve the utilisation of granulated coals for blast furnace injection. *Fuel* **2015,** *151*, 40-49.
71. Kalkreuth, W.; Borrego, A. G.; Alvarez, D.; Menendez, R.; Osório, E.; Ribas, M.; Vilela, A.; Cardozo Alves, T., Exploring the possibilities of using Brazilian subbituminous coals for blast furnace pulverized fuel injection. *Fuel* **2005,** *84* (6), 763-772.
72. Hu, S.; Xiang, J.; Sun, L.; Xu, M.; Qiu, J.; Fu, P., Characterization of char from rapid pyrolysis of rice husk. *Fuel Processing Technology* **2008,** *89* (11), 1096-1105.
73. Johansen, J. M.; Jensen, P. A.; Glarborg, P.; De Martini, N.; Ek, P.; Mitchell, R. E., High Heating Rate Devolatilization Kinetics of Pulverized Biomass Fuels. *Energy & Fuels* **2018,** *32* (12), 12955-12961.
74. Johansen, J. M.; Gadsbøll, R.; Thomsen, J.; Jensen, P. A.; Glarborg, P.; Ek, P.; De Martini, N.; Mancini, M.; Weber, R.; Mitchell, R. E., Devolatilization kinetics of woody biomass at short residence times and high heating rates and peak temperatures. *Applied Energy* **2016,** *162*, 245-256.
75. Biagini, E.; Simone, M.; Tognotti, L., Characterization of high heating rate chars of biomass fuels. *Proceedings of the Combustion Institute* **2009,** *32* (2), 2043-2050.
76. Dall'Ora, M.; Jensen, P. A.; Jensen, A. D., Suspension Combustion of Wood: Influence of Pyrolysis Conditions on Char Yield, Morphology, and Reactivity. *Energy & Fuels* **2008,** *22* (5), 2955-2962.
77. Trubetskaya, A.; Jensen, P. A.; Jensen, A. D.; Steibel, M.; Spliethoff, H.; Glarborg, P.; Larsen, F. H., Comparison of high temperature chars of wheat straw and rice husk with respect to chemistry, morphology and reactivity. *Biomass and Bioenergy* **2016,** *86*, 76-87.
78. Trubetskaya, A.; Jensen, P. A.; Jensen, A. D.; Steibel, M.; Spliethoff, H.; Glarborg, P., Influence of fast pyrolysis conditions on yield and structural transformation of biomass chars. *Fuel Processing Technology* **2015,** *140*, 205-214.
79. Lu, H.; Ip, E.; Scott, J.; Foster, P.; Vickers, M.; Baxter, L. L., Effects of particle shape and size on devolatilization of biomass particle. *Fuel* **2010,** *89*, 1156-1168.
80. Septien, S.; Valin, S.; Peyrot, M.; Dupont, C.; Salvador, S., Characterization of char and soot from millimetric wood particles pyrolysis in a drop tube reactor between 800°C and 1400°C. *Fuel* **2014,** *121*, 216-224.
81. Shim, H.-S.; Hurt, R. H., Thermal Annealing of Chars from Diverse Organic Precursors under Combustion-like Conditions. *Energy & Fuels* **2000,** *14* (2), 340-348.
82. Cetin, E.; Moghtaderi, B.; Gupta, R.; Wall, T. F., Influence of pyrolysis conditions on the structure and gasification reactivity of biomass chars. *Fuel* **2004,** *83*, 2139-2150.
83. McNamee, P.; Darvell, L. I.; Jones, J. M.; Williams, A., The combustion characteristics of high-heating-rate chars from untreated and torrefied biomass fuels. *Biomass and Bioenergy* **2015,** *82*, 63-72.
84. Gil, M. V.; Riaza, J.; Álvarez, L.; Pevida, C.; Rubiera, F., Biomass devolatilization at high temperature under N2 and CO2: Char morphology and reactivity. *Energy* **2015,** *91*, 655-662.
85. Biagini, E.; Lippi, F.; Tognotti, L., Characterization of a lab-scale platinum filament pyrolyzer for studying the fast devolatilization of solid fuels. *Fuel* **2006,** *85* (17), 2408-2418.

86. Ballantyne, T. R.; Ashman, P. J.; Mullinger, P. J., A new method for determining the conversion of low-ash coals using synthetic ash as a tracer. *Fuel* **2005,** *84* (14), 1980-1985.
87. Shen, Q.; Liaw, S. B.; Costa, M.; Wu, H., Rapid Pyrolysis of Pulverized Biomass at a High Temperature: The Effect of Particle Size on Char Yield, Retentions of Alkali and Alkaline Earth Metallic Species, and Char Particle Shape. *Energy & Fuels* **2020,** *34* (6), 7140-7148.
88. Leth-Espensen, A.; Glarborg, P.; Jensen, P. A., Predicting Biomass Char Yield from High Heating Rate Devolatilization Using Chemometrics. *Energy & Fuels* **2018,** *32* (9), 9572-9580.
89. Davidsson, K. O.; Korsgren, J. G.; Pettersson, J. B. C.; Jäglid, U., The effects of fuel washing techniques on alkali release from biomass. *Fuel* **2002,** *81* (2), 137-142.
90. Dayton, D. C.; Jenkins, B. M.; Turn, S. Q.; Bakker, R. R.; Williams, R. B.; Belle-Oudry, D.; Hill, L. M., Release of Inorganic Constituents from Leached Biomass during Thermal Conversion. *Energy & Fuels* **1999,** *13* (4), 860-870.
91. Eom, I.-Y.; Kim, K.-H.; Kim, J.-Y.; Lee, S.-M.; Yeo, H.-M.; Choi, I.-G.; Choi, J.-W., Characterization of primary thermal degradation features of lignocellulosic biomass after removal of inorganic metals by diverse solvents. *Bioresource Technology* **2011,** *102* (3), 3437-3444.
92. Fahmi, R.; Bridgwater, A. V.; Darvell, L. I.; Jones, J. M.; Yates, N.; Thain, S.; Donnison, I. S., The effect of alkali metals on combustion and pyrolysis of Lolium and Festuca grasses, switchgrass and willow. *Fuel* **2007,** *86* (10), 1560-1569.
93. Abdullah, H.; Mediaswanti, K. A.; Wu, H., Biochar as a fuel: 2. Significant differences in fuel quality and ash properties of biochars from various biomass components of mallee trees. *Energy & Fuels* **2010,** *24*, 1972-1979.
94. Bryers, R. W., Fireside slagging, fouling, and high-temperature corrosion of heat-transfer surface due to impurities in steam-raising fuels. *Progress in Energy and Combustion Science* **1996,** *22* (1), 29-120.
95. Werkelin, J.; Skrifvars, B.-J.; Zevenhoven, M.; Holmbom, B.; Hupa, M., Chemical forms of ash-forming elements in woody biomass fuels. *Fuel* **2010,** *89* (2), 481-493.
96. Khazraie Shoulaifar, T.; DeMartini, N.; Zevenhoven, M.; Verhoeff, F.; Kiel, J.; Hupa, M., Ash-Forming Matter in Torrefied Birch Wood: Changes in Chemical Association. *Energy & Fuels* **2013,** *27* (10), 5684-5690.
97. Zhao, H.-b.; Song, Q.; Wu, X.-y.; Yao, Q., Study on the Transformation of Inherent Potassium during the Fast-Pyrolysis Process of Rice Straw. *Energy & Fuels* **2015,** *29* (10), 6404-6411.
98. van Lith, S. C.; Jensen, P. A.; Frandsen, F. J.; Glarborg, P., Release to the Gas Phase of Inorganic Elements during Wood Combustion. Part 2: Influence of Fuel Composition. *Energy & Fuels* **2008,** *22* (3), 1598-1609.
99. DeGroot, W. F.; Shafizadeh, F., The influence of exchangeable cations on the carbonization of biomass. *Journal of Analytical and Applied Pyrolysis* **1984,** *6* (3), 217-232.
100. Benson, S. A.; Holm, P. L., Comparison of Inorganic Constituents in Three Low-Rank Coals. *Industrial & engineering chemistry product research and development* **1985,** *24* (1), 145-149.
101. Baxter, L. L.; Miles, T. R.; Miles Jr, T.; Jenkins, B.; Dayton, D.; Milne, T.; Bryers, R.; Oden, L., Alkali deposits found in biomass boilers: The behavior of inorganic material in biomass-fired power boilers--Field and laboratory experiences. Volume 2. **1996**.

102. Raveendran, K.; Ganesh, A.; Khilar, K. C., Influence of mineral matter on biomass pyrolysis characteristics. *Fuel* **1995,** *74* (12), 1812-1822.
103. Nowakowski, D. J.; Jones, J. M.; Brydson, R. M.; Ross, A. B., Potassium catalysis in the pyrolysis behaviour of short rotation willow coppice. *Fuel* **2007,** *86* (15), 2389-2402.
104. Teng, H.; Wei, Y.-C., Thermogravimetric Studies on the Kinetics of Rice Hull Pyrolysis and the Influence of Water Treatment. *Industrial & Engineering Chemistry Research* **1998,** *37* (10), 3806-3811.
105. Bradbury, A. G. W.; Sakai, Y.; Shafizadeh, F., A kinetic model for pyrolysis of cellulose. *Journal of Applied Polymer Science* **1979,** *23* (11), 3271-3280.
106. Aho, A.; DeMartini, N.; Pranovich, A.; Krogell, J.; Kumar, N.; Eränen, K.; Holmbom, B.; Salmi, T.; Hupa, M.; Murzin, D. Y., Pyrolysis of pine and gasification of pine chars – Influence of organically bound metals. *Bioresource Technology* **2013,** *128*, 22-29.
107. Stephanidis, S.; Nitsos, C.; Kalogiannis, K.; Iliopoulou, E. F.; Lappas, A. A.; Triantafyllidis, K. S., Catalytic upgrading of lignocellulosic biomass pyrolysis vapours: Effect of hydrothermal pre-treatment of biomass. *Catalysis Today* **2011,** *167* (1), 37-45.
108. Liden, A.; Berruti, F.; Scott, D., A kinetic model for the production of liquids from the flash pyrolysis of biomass. *Chemical engineering communications* **1988,** *65* (1), 207-221.
109. Nik-Azar, M.; Hajaligol, M. R.; Sohrabi, M.; Dabir, B., Mineral matter effects in rapid pyrolysis of beech wood. *Fuel Processing Technology* **1997,** *51* (1), 7-17.
110. Jensen, A.; Dam-Johansen, K.; Wójtowicz, M. A.; Serio, M. A., TG-FTIR Study of the Influence of Potassium Chloride on Wheat Straw Pyrolysis. *Energy & Fuels* **1998,** *12* (5), 929-938.
111. Jones, J. M.; Darvell, L. I.; Bridgeman, T. G.; Pourkashanian, M.; Williams, A., An investigation of the thermal and catalytic behaviour of potassium in biomass combustion. *Proceedings of the Combustion Institute* **2007,** *31* (2), 1955-1963.
112. Halim, N.; Tajima, A.; Asano, S.; Kudo, S.; Hayashi, J.-i., Change in Catalytic Activity of Potassium during CO2 Gasification of Char. *Energy & Fuels* **2020,** *34* (1), 225-234.
113. Wu, H.; Hayashi, J.-i.; Chiba, T.; Takarada, T.; Li, C.-Z., Volatilisation and catalytic effects of alkali and alkaline earth metallic species during the pyrolysis and gasification of Victorian brown coal. Part V. Combined effects of Na concentration and char structure on char reactivity. *Fuel* **2004,** *83* (1), 23-30.
114. Hu, J.; Liu, L.; Cui, M.; Wang, J., Calcium-promoted catalytic activity of potassium carbonate for gasification of coal char: The synergistic effect unrelated to mineral matter in coal. *Fuel* **2013,** *111*, 628-635.
115. Jiang, M.-Q.; Zhou, R.; Hu, J.; Wang, F.-C.; Wang, J., Calcium-promoted catalytic activity of potassium carbonate for steam gasification of coal char: Influences of calcium species. *Fuel* **2012,** *99*, 64-71.
116. Perander, M.; DeMartini, N.; Brink, A.; Kramb, J.; Karlström, O.; Hemming, J.; Moilanen, A.; Konttinen, J.; Hupa, M., Catalytic effect of Ca and K on CO2 gasification of spruce wood char. *Fuel* **2015,** *150*, 464-472.
117. Zolin, A.; Jensen, A.; Jensen, P. A.; Frandsen, F.; Dam-Johansen, K., The Influence of Inorganic Materials on the Thermal Deactivation of Fuel Chars. *Energy & Fuels* **2001,** *15* (5), 1110-1122.

118. Kajita, M.; Kimura, T.; Norinaga, K.; Li, C.-Z.; Hayashi, J.-i., Catalytic and Noncatalytic Mechanisms in Steam Gasification of Char from the Pyrolysis of Biomass. *Energy & Fuels* **2010,** *24* (1), 108-116.
119. Yuan, X.; Fan, S.; Choi, S. W.; Kim, H.-T.; Lee, K. B., Potassium catalyst recovery process and performance evaluation of the recovered catalyst in the K2CO3-catalyzed steam gasification system. *Applied Energy* **2017,** *195*, 850-860.
120. Kramb, J.; Gómez-Barea, A.; DeMartini, N.; Romar, H.; Doddapaneni, T. R. K. C.; Konttinen, J., The effects of calcium and potassium on CO2 gasification of birch wood in a fluidized bed. *Fuel* **2017,** *196*, 398-407.
121. Khazraie Shoulaifar, T.; DeMartini, N.; Karlström, O.; Hupa, M., Impact of organically bonded potassium on torrefaction: Part 1. Experimental. *Fuel* **2016,** *165*, 544-552.
122. Saddawi, A.; Jones, J. M.; Williams, A.; Le Coeur, C., Commodity Fuels from Biomass through Pretreatment and Torrefaction: Effects of Mineral Content on Torrefied Fuel Characteristics and Quality. *Energy & Fuels* **2012,** *26* (11), 6466-6474.
123. Skrifvars, B.-J.; Backman, R.; Hupa, M., Characterization of the sintering tendency of ten biomass ashes in FBC conditions by a laboratory test and by phase equilibrium calculations. *Fuel Processing Technology* **1998,** *56* (1), 55-67.
124. Raveendran, K.; Ganesh, A., Adsorption characteristics and pore-development of biomass-pyrolysis char. *Fuel* **1998,** *77* (7), 769-781.
125. Johansen, J. M.; Jakobsen, J. G.; Frandsen, F. J.; Glarborg, P., Release of K, Cl, and S during Pyrolysis and Combustion of High-Chlorine Biomass. *Energy & Fuels* **2011,** *25* (11), 4961-4971.
126. Zhang, Z.-H.; Song, Q.; Yao, Q.; Yang, R.-M., Influence of the Atmosphere on the Transformation of Alkali and Alkaline Earth Metallic Species during Rice Straw Thermal Conversion. *Energy & Fuels* **2012,** *26* (3), 1892-1899.
127. Zhao, H.; Song, Q.; Yao, Q., Release and transformation of K and Cl during the pyrolysis of KCl-loaded cellulose. *Fuel* **2018,** *226*, 583-590.
128. Björkman, E.; Strömberg, B., Release of Chlorine from Biomass at Pyrolysis and Gasification Conditions1. *Energy & Fuels* **1997,** *11* (5), 1026-1032.
129. Chen, H.; Chen, X.; Qiao, Z.; Liu, H., Release and transformation characteristics of K and Cl during straw torrefaction and mild pyrolysis. *Fuel* **2016,** *167*, 31-39.
130. Keown, D. M.; Favas, G.; Hayashi, J.-i.; Li, C.-Z., Volatilisation of alkali and alkaline earth metallic species during the pyrolysis of biomass: differences between sugar cane bagasse and cane trash. *Bioresource Technology* **2005,** *96* (14), 1570-1577.
131. Quyn, D. M.; Wu, H.; Bhattacharya, S. P.; Li, C.-z., Volatilisation and catalytic effects of alkali and alkaline earth metallic species during the pyrolysis and gasification of Victorian brown coal . Part II . Effects of chemical form and valence. **2002,** *81*, 151-158.
132. Davidsson, K. O.; Stojkova, B. J.; Pettersson, J. B. C., Alkali Emission from Birchwood Particles during Rapid Pyrolysis. *Energy & Fuels* **2002,** *16* (5), 1033-1039.
133. Baxter, L. L.; Miles, T. R.; Miles, T. R.; Jenkins, B. M.; Milne, T.; Dayton, D.; Bryers, R. W.; Oden, L. L., The behavior of inorganic material in biomass-fired power boilers: field and laboratory experiences. *Fuel Processing Technology* **1998,** *54* (1), 47-78.
134. Podczeck, F.; Mia, Y., The influence of particle size and shape on the angle of internal friction and the flow factor of unlubricated and lubricated powders. *International Journal of Pharmaceutics* **1996,** *144*, 187-194.

135. Robinson, D. a.; Friedman, S. P., Observations of the effects of particle shape and particle size distribution on avalanching of granular media. *Physica A* **2002,** *311*, 97-110.
136. Cleary, P. W., The effect of particle shape on simple shear flows. *Powder Technology* **2008,** *179*, 144-163.
137. Rezaei, H.; Lim, C. J.; Lau, A.; Sokhansanj, S., Size, shape and flow characterization of ground wood chip and ground wood pellet particles. *Powder Technology* **2016,** *301*, 737-746.
138. Paulrud, S.; Mattsson, J. E.; Nilsson, C., Particle and handling characteristics of wood fuel powder: effects of different mills. *Fuel Processing Technology* **2002,** *76* (1), 23-39.
139. Svoboda, K.; Pohořelý, M.; Hartman, M.; Martinec, J., Pretreatment and feeding of biomass for pressurized entrained flow gasification. *Fuel Processing Technology* **2009,** *90* (5), 629-635.
140. Hughes, E. E.; Tillman, D. A., Biomass cofiring: status and prospects 1996. *Fuel Processing Technology* **1998,** *54* (1), 127-142.
141. Guo, Q.; Chen, X.; Liu, H., Experimental research on shape and size distribution of biomass particle. *Fuel* **2012,** *94*, 551-555.
142. Saastamoinen, J.; Aho, M.; Moilanen, A.; Sørensen, L. H.; Clausen, S.; Berg, M., Burnout of pulverized biomass particles in large scale boiler – Single particle model approach. *Biomass and Bioenergy* **2010,** *34*, 728-736.
143. Leth-Espensen, A.; Li, T.; Glarborg, P.; Løvås, T.; Jensen, P. A., The influence of size and morphology on devolatilization of biomass particles. *Fuel* **2020,** *264*, 116755.
144. Xiumin, J.; Chuguang, Z.; Che, Y.; Dechang, L.; Jianrong, Q.; Jubin, L., Physical structure and combustion properties of super fine pulverized coal particle. *Fuel* **2002,** *81* (6), 793-797.
145. Pattanotai, T.; Watanabe, H.; Okazaki, K., Effects of particle aspect ratio on pyrolysis and gasification of anisotropic wood cylinder. *Fuel* **2015,** *150*, 162-168.
146. Wadell, H., Volume, shape, and roundness of quartz particles. *The Journal of Geology* **1935,** *43* (3), 250-280.
147. Lédé, J.; Li, H. Z.; Villermaux, J.; Martin, H., Fusion-like behaviour of wood pyrolysis. *Journal of Analytical and Applied Pyrolysis* **1987,** *10* (4), 291-308.
148. Narayan, R.; Antal, M. J., Thermal Lag, Fusion, and the Compensation Effect during Biomass Pyrolysis. *Industrial & Engineering Chemistry Research* **1996,** *35* (5), 1711-1721.
149. Niksa, S.; Kerstein, A. R., On the role of macromolecular configuration in rapid coal devolatilization. *Fuel* **1987,** *66* (10), 1389-1399.
150. Ma, Z.; Merkus, H. G.; de Smet, J. G.; Heffels, C.; Scarlett, B., New developments in particle characterization by laser diffraction: size and shape. *Powder Technology* **2000,** *111* (1-2), 66-78.
151. Zygourakis, K., Effect of pyrolysis conditions on the macropore structure of coal-derived chars. *Energy & Fuels* **1993,** *7* (1), 33-41.
152. Guerrero, M.; Ruiz, M. P.; Alzueta, M. U.; Bilbao, R.; Millera, A., Pyrolysis of eucalyptus at different heating rates: studies of char characterization and oxidative reactivity. *Journal of Analytical and Applied Pyrolysis* **2005,** *74* (1), 307-314.
153. Singh, R. N., Equilibrium moisture content of biomass briquettes. *Biomass and Bioenergy* **2004,** *26* (3), 251-253.

154. Chen, W.-H.; Kuo, P.-C., Torrefaction and co-torrefaction characterization of hemicellulose, cellulose and lignin as well as torrefaction of some basic constituents in biomass. *Energy* **2011,** *36* (2), 803-811.
155. Arias, B.; Pevida, C.; Fermoso, J.; Plaza, M. G.; Rubiera, F.; Pis, J. J., Influence of torrefaction on the grindability and reactivity of woody biomass. *Fuel Processing Technology* **2008,** *89* (2), 169-175.
156. Fagernäs, L.; Brammer, J.; Wilén, C.; Lauer, M.; Verhoeff, F., Drying of biomass for second generation synfuel production. *Biomass and Bioenergy* **2010,** *34* (9), 1267-1277.
157. Pang, S.; Mujumdar, A. S., Drying of Woody Biomass for Bioenergy: Drying Technologies and Optimization for an Integrated Bioenergy Plant. *Drying Technology* **2010,** *28* (5), 690-701.
158. Wu, K.-T.; Tsai, C.-J.; Chen, C.-S.; Chen, H.-W., The characteristics of torrefied microalgae. *Applied Energy* **2012,** *100*, 52-57.
159. Felfli, F. F.; Luengo, C. A.; Suárez, J. A.; Beatón, P. A., Wood briquette torrefaction. *Energy for Sustainable Development* **2005,** *9* (3), 19-22.
160. Yan, W.; Acharjee, T. C.; Coronella, C. J.; Vásquez, V. R., Thermal pretreatment of lignocellulosic biomass. *Environmental Progress & Sustainable Energy* **2009,** *28* (3), 435-440.
161. Bergman, P. C.; Kiel, J. H. In *Torrefaction for biomass upgrading*, Proc. 14th European Biomass Conference, Paris, France, 2005; pp 17-21.
162. Gilbert, P.; Ryu, C.; Sharifi, V.; Swithenbank, J., Effect of process parameters on pelletisation of herbaceous crops. *Fuel* **2009,** *88* (8), 1491-1497.
163. Pahla, G.; Ntuli, F.; Muzenda, E., Torrefaction of landfill food waste for possible application in biomass co-firing. *Waste Management* **2018,** *71*, 512-520.
164. Chen, Z.; Wang, M.; Jiang, E.; Wang, D.; Zhang, K.; Ren, Y.; Jiang, Y., Pyrolysis of Torrefied Biomass. *Trends in Biotechnology* **2018,** *36* (12), 1287-1298.
165. Ren, S.; Lei, H.; Wang, L.; Bu, Q.; Chen, S.; Wu, J., Thermal behaviour and kinetic study for woody biomass torrefaction and torrefied biomass pyrolysis by TGA. *Biosystems Engineering* **2013,** *116* (4), 420-426.
166. Mi, B.; Liu, Z.; Hu, W.; Wei, P.; Jiang, Z.; Fei, B., Investigating pyrolysis and combustion characteristics of torrefied bamboo, torrefied wood and their blends. *Bioresource Technology* **2016,** *209*, 50-55.
167. Chen, D.; Li, Y.; Deng, M.; Wang, J.; Chen, M.; Yan, B.; Yuan, Q., Effect of torrefaction pretreatment and catalytic pyrolysis on the pyrolysis poly-generation of pine wood. *Bioresource Technology* **2016,** *214*, 615-622.
168. Ren, S.; Lei, H.; Wang, L.; Yadavalli, G.; Liu, Y.; Julson, J., The integrated process of microwave torrefaction and pyrolysis of corn stover for biofuel production. *Journal of Analytical and Applied Pyrolysis* **2014,** *108*, 248-253.
169. Zhang, S.; Hu, B.; Zhang, L.; Xiong, Y., Effects of torrefaction on yield and quality of pyrolysis char and its application on preparation of activated carbon. *Journal of Analytical and Applied Pyrolysis* **2016,** *119*, 217-223.
170. Wannapeera, J.; Fungtammasan, B.; Worasuwannarak, N., Effects of temperature and holding time during torrefaction on the pyrolysis behaviors of woody biomass. *Journal of Analytical and Applied Pyrolysis* **2011,** *92*, 99-105.
171. Chen, H.; Chen, X.; Qin, Y.; Wei, J.; Liu, H., Effect of torrefaction on the properties of rice straw high temperature pyrolysis char: Pore structure, aromaticity and gasification activity. *Bioresource Technology* **2017,** *228*, 241-249.

172. Gogoi, D.; Bordoloi, N.; Goswami, R.; Narzari, R.; Saikia, R.; Sut, D.; Gogoi, L.; Kataki, R., Effect of torrefaction on yield and quality of pyrolytic products of arecanut husk: An agro-processing wastes. *Bioresource Technology* **2017,** *242*, 36-44.
173. Meng, J.; Park, J.; Tilotta, D.; Park, S., The effect of torrefaction on the chemistry of fast-pyrolysis bio-oil. *Bioresource Technology* **2012,** *111*, 439-446.
174. Zheng, A.; Zhao, Z.; Chang, S.; Huang, Z.; Wang, X.; He, F.; Li, H., Effect of torrefaction on structure and fast pyrolysis behavior of corncobs. *Bioresource Technology* **2013,** *128*, 370-377.
175. Zhang, H.; Shao, S.; Jiang, Y.; Vitidsant, T.; Reubroycharoen, P.; Xiao, R., Improving hydrocarbon yield by two-step pyrolysis of pinewood in a fluidized-bed reactor. *Fuel Processing Technology* **2017,** *159*, 19-26.
176. Chen, D.; Zheng, Z.; Fu, K.; Zeng, Z.; Wang, J.; Lu, M., Torrefaction of biomass stalk and its effect on the yield and quality of pyrolysis products. *Fuel* **2015,** *159*, 27-32.
177. Pielsticker, S.; Möller, G.; Gövert, B.; Kreitzberg, T.; Hatzfeld, O.; Yönder, Ö.; Angenent, V.; Hättig, C.; Schmid, R.; Kneer, R., Influence of biomass torrefaction parameters on fast pyrolysis products under flame-equivalent conditions. *Biomass and Bioenergy* **2018,** *119*, 392-410.
178. Li, T.; Geier, M.; Wang, L.; Ku, X.; Güell, B. M.; Løvås, T.; Shaddix, C. R., Effect of Torrefaction on Physical Properties and Conversion Behavior of High Heating Rate Char of Forest Residue. *Energy & Fuels* **2015,** *29* (1), 177-184.
179. Mourant, D.; Wang, Z.; He, M.; Wang, X. S.; Garcia-Perez, M.; Ling, K.; Li, C.-Z., Mallee wood fast pyrolysis: Effects of alkali and alkaline earth metallic species on the yield and composition of bio-oil. *Fuel* **2011,** *90* (9), 2915-2922.
180. Wu, H.; Yip, K.; Kong, Z.; Li, C. Z.; Liu, D.; Yu, Y.; Gao, X., Removal and recycling of inherent inorganic nutrient species in mallee biomass and derived biochars by water leaching. *Industrial and Engineering Chemistry Research* **2011,** *50*, 12143-12151.
181. Arvelakis, S.; Gehrmann, H.; Beckmann, M.; Koukios, E., Effect of leaching on the ash behavior of olive residue during fluidized bed gasification. *Biomass and Bioenergy* **2002,** *22* (1), 55-69.
182. Jenkins, B. M.; Bakker, R. R.; Wei, J. B., On the properties of washed straw. *Biomass and Bioenergy* **1996,** *10* (4), 177-200.
183. Turn, S. Q.; Kinoshita, C. M.; Ishimura, D. M., Removal of inorganic constituents of biomass feedstocks by mechanical dewatering and leaching. *Biomass and Bioenergy* **1997,** *12* (4), 241-252.
184. Arvelakis, S.; Gehrmann, H.; Beckmann, M.; Koukios, E. G., Agglomeration problems during fluidized bed gasification of olive-oil residue: evaluation of fractionation and leaching as pre-treatments. *Fuel* **2003,** *82* (10), 1261-1270.
185. Skoulou, V.; Kantarelis, E.; Arvelakis, S.; Yang, W.; Zabaniotou, A., Effect of biomass leaching on H2 production, ash and tar behavior during high temperature steam gasification (HTSG) process. *International Journal of Hydrogen Energy* **2009,** *34* (14), 5666-5673.
186. Arvelakis, S.; Vourliotis, P.; Kakaras, E.; Koukios, E. G., Effect of leaching on the ash behavior of wheat straw and olive residue during fluidized bed combustion. *Biomass and Bioenergy* **2001,** *20* (6), 459-470.
187. Park, D.; Yun, Y.-S.; Park, J. M., Reduction of Hexavalent Chromium with the Brown Seaweed Ecklonia Biomass. *Environmental Science & Technology* **2004,** *38* (18), 4860-4864.

188. Figueira, M. M.; Volesky, B.; Ciminelli, V. S. T.; Roddick, F. A., Biosorption of metals in brown seaweed biomass. *Water Research* **2000,** *34* (1), 196-204.
189. Chen, J. P.; Yang, L., Chemical Modification of Sargassum sp. for Prevention of Organic Leaching and Enhancement of Uptake during Metal Biosorption. *Industrial & Engineering Chemistry Research* **2005,** *44* (26), 9931-9942.
190. Sciban, M.; Klasnja, M.; Skrbic, B., Modified hardwood sawdust as adsorbent of heavy metal ions from water. *Wood Science and Technology* **2006,** *40* (3), 217.
191. Arvelakis, S.; Koukios, E. G., Physicochemical upgrading of agroresidues as feedstocks for energy production via thermochemical conversion methods. *Biomass and Bioenergy* **2002,** *22* (5), 331-348.
192. Partanen, J.; Backman, P.; Hupa, M., The effect of HCl on the formation of calcium silicates in sand beds in fluidized bed boilers. *Combustion and Flame* **2002,** *130* (4), 376-380.
193. Ergudenler, A.; Ghaly, A. E., Agglomeration of silica sand in a fluidized bed gasifier operating on wheat straw. *Biomass and Bioenergy* **1993,** *4* (2), 135-147.
194. Tan, H.; Wang, S.-r., Experimental study of the effect of acid-washing pretreatment on biomass pyrolysis. *Journal of Fuel Chemistry and Technology* **2009,** *37* (6), 668-672.
195. Sadaka, S.; Negi, S., Improvements of biomass physical and thermochemical characteristics via torrefaction process. *Environmental Progress & Sustainable Energy* **2009,** *28* (3), 427-434.
196. Mayer, Z. A.; Apfelbacher, A.; Hornung, A., Effect of sample preparation on the thermal degradation of metal-added biomass. *Journal of Analytical and Applied Pyrolysis* **2012,** *94*, 170-176.
197. Fahmi, R.; Bridgwater, A. V.; Donnison, I.; Yates, N.; Jones, J. M., The effect of lignin and inorganic species in biomass on pyrolysis oil yields, quality and stability. *Fuel* **2008,** *87* (7), 1230-1240.
198. Banks, S.; Nowakowski, D.; Bridgwater, A., Fast pyrolysis processing of surfactant washed Miscanthus. *Fuel Processing Technology* **2014,** *128*, 94-103.
199. Gao, X.; Wu, H., Effect of sampling temperature on the properties of inorganic particulate matter collected from biomass combustion in a drop-tube furnace. *Energy & Fuels* **2010,** *24*, 4571-4580.
200. Deng, C.; Liaw, S. B.; Wu, H., Characterization of Size-Segregated Soot from Pine Wood Pyrolysis in a Drop Tube Furnace at 1300° C. *Energy & Fuels* **2019,** *33* (3), 2293-2300.
201. Liaw, S. B.; Wu, H., Leaching characteristics of organic and inorganic matter from biomass by water: Differences between batch and semi-continuous operations. *Industrial and Engineering Chemistry Research* **2013,** *52*, 4280-4289.
202. Hayashi, J.-I.; Iwatsuki, M.; Morishita, K.; Tsutsumi, A.; Li, C.-Z.; Chiba, T., Roles of inherent metallic species in secondary reactions of tar and char during rapid pyrolysis of brown coals in a drop-tube reactor. *Fuel* **2002,** *81* (15), 1977-1987.
203. Miles, P. D.; Smith, W. B., *Specific gravity and other properties of wood and bark for 156 tree species found in North America*. US Department of Agriculture, Forest Service, Northern Research Station: 2009; Vol. 38.
204. Lautenberger, C.; Fernandez-Pello, C., A model for the oxidative pyrolysis of wood. *Combustion and Flame* **2009,** *156* (8), 1503-1513.
205. Whitaker, S., Forced convection heat transfer correlations for flow in pipes, past flat plates, single cylinders, single spheres, and for flow in packed beds and tube bundles. *AIChE Journal* **1972,** *18* (2), 361-371.

206. Chen, S. H. P.; Saxena, S. C., Thermal conductivity of argon in the temperature range 350 to 2500 K. *Molecular Physics* **1975,** *29* (2), 455-466.
207. Zhang, M.; Gao, X.; Wu, H., A method for the quantification of alkali and alkaline earth metallic species in bioslurry fuels. *Energy & Fuels* **2013,** *27*, 6823-6830.
208. Rahim, M. U.; Gao, X.; Wu, H., Determination of chlorine in solid fuels using an improved Eschka method. *Fuel* **2014,** *129*, 314-317.
209. Sluiter, A.; Hames, B.; Ruiz, R.; Scarlata, C.; Sluiter, J.; Templeton, D.; Crocker, D. *Determination of structural carbohydrates and lignin in biomass*; 2008; pp 1-16.
210. Sluiter, A.; Ruiz, R.; Scarlata, C.; Sluiter, J.; Templeton, D. *Determination of Extractives in Biomass*; 2008.
211. Liaw, S. B.; Yu, Y.; Wu, H., Association of inorganic species release with sugar recovery during wood hydrothermal processing. *Fuel* **2016,** *166*, 581-584.
212. Rabaçal, M.; Pereira, S.; Costa, M., Review of Pulverized Combustion of Non-Woody Residues. *Energy & Fuels* **2018,** *32* (4), 4069-4095.
213. Zanzi, R.; Sjöström, K.; Björnbom, E., Rapid high-temperature pyrolysis of biomass in a free-fall reactor. *Fuel* **1996,** *75* (5), 545-550.
214. Heo, H. S.; Park, H. J.; Yim, J.-H.; Sohn, J. M.; Park, J.; Kim, S.-S.; Ryu, C.; Jeon, J.-K.; Park, Y.-K., Influence of operation variables on fast pyrolysis of Miscanthus sinensis var. purpurascens. *Bioresource Technology* **2010,** *101* (10), 3672-3677.
215. Wei, L.; Xu, S.; Zhang, L.; Zhang, H.; Liu, C.; Zhu, H.; Liu, S., Characteristics of fast pyrolysis of biomass in a free fall reactor. *Fuel Processing Technology* **2006,** *87* (10), 863-871.
216. Dupont, C.; Commandre, J.-M.; Gauthier, P.; Boissonnet, G.; Salvador, S.; Schweich, D., Biomass pyrolysis experiments in an analytical entrained flow reactor between 1073 K and 1273 K. *Fuel* **2008,** *87* (7), 1155-1164.
217. Strandberg, A.; Holmgren, P.; Wagner, D. R.; Molinder, R.; Wiinikka, H.; Umeki, K.; Broström, M., Effects of Pyrolysis Conditions and Ash Formation on Gasification Rates of Biomass Char. *Energy & Fuels* **2017,** *31* (6), 6507-6514.
218. Farrow, T. S.; Sun, C.; Snape, C. E., Impact of CO2 on biomass pyrolysis, nitrogen partitioning, and char combustion in a drop tube furnace. *Journal of Analytical and Applied Pyrolysis* **2015,** *113*, 323-331.
219. Sun, S.; Tian, H.; Zhao, Y.; Sun, R.; Zhou, H., Experimental and numerical study of biomass flash pyrolysis in an entrained flow reactor. *Bioresource Technology* **2010,** *101* (10), 3678-3684.
220. Moghtaderi, B.; Meesri, C.; Wall, T. F., Pyrolytic characteristics of blended coal and woody biomass. *Fuel* **2004,** *83* (6), 745-750.
221. Li, J.; Bonvicini, G.; Tognotti, L.; Yang, W.; Blasiak, W., High-temperature rapid devolatilization of biomasses with varying degrees of torrefaction. *Fuel* **2014,** *122*, 261-269.
222. Wang, G.; Silva, R. B.; Azevedo, J. L. T.; Martins-Dias, S.; Costa, M., Evaluation of the combustion behaviour and ash characteristics of biomass waste derived fuels, pine and coal in a drop tube furnace. *Fuel* **2014,** *117*, 809-824.
223. Palumbo, A. W.; Bartel, C. J.; Sorli, J. C.; Weimer, A. W., Characterization of products derived from the high temperature flash pyrolysis of microalgae and rice hulls. *Chemical Engineering Science* **2019,** *196*, 527-537.
224. Holmgren, P.; Wagner, D. R.; Strandberg, A.; Molinder, R.; Wiinikka, H.; Umeki, K.; Broström, M., Size, shape, and density changes of biomass particles during rapid devolatilization. *Fuel* **2017,** *206*, 342-351.

225. Mettler, M. S.; Vlachos, D. G.; Dauenhauer, P. J., Top ten fundamental challenges of biomass pyrolysis for biofuels. *Energy & Environmental Science* **2012,** *5*, 7797.
226. Zhang, Y.; Kajitani, S.; Ashizawa, M.; Miura, K., Peculiarities of rapid pyrolysis of biomass covering medium-and high-temperature ranges. *Energy & Fuels* **2006,** *20* (6), 2705-2712.
227. Zhou, S.; Garcia-Perez, M.; Pecha, B.; McDonald, A. G.; Westerhof, R. J. M., Effect of particle size on the composition of lignin derived oligomers obtained by fast pyrolysis of beech wood. *Fuel* **2014,** *125*, 15-19.
228. Teixeira, A. R.; Mooney, K. G.; Kruger, J. S.; Williams, C. L.; Suszynski, W. J.; Schmidt, L. D.; Schmidt, D. P.; Dauenhauer, P. J., Aerosol generation by reactive boiling ejection of molten cellulose. *Energy & Environmental Science* **2011,** *4* (10), 4306-4321.
229. Wu, H.; Quyn, D. M.; Li, C.-Z., Volatilisation and catalytic effects of alkali and alkaline earth metallic species during the pyrolysis and gasification of Victorian brown coal. Part III. The importance of the interactions between volatiles and char at high temperature. *Fuel* **2002,** *81* (8), 1033-1039.
230. Li, C.-Z.; Sathe, C.; Kershaw, J. R.; Pang, Y., Fates and roles of alkali and alkaline earth metals during the pyrolysis of a Victorian brown coal. *Fuel* **2000,** *79* (3-4), 427-438.
231. Guizani, C.; Jeguirim, M.; Valin, S.; Limousy, L.; Salvador, S., Biomass chars: The effects of pyrolysis conditions on their morphology, structure, chemical properties and reactivity. *Energies* **2017,** *10* (6), 796.
232. Zhao, Y.; Feng, D.; Zhang, Y.; Huang, Y.; Sun, S., Effect of pyrolysis temperature on char structure and chemical speciation of alkali and alkaline earth metallic species in biochar. *Fuel Processing Technology* **2016,** *141*, 54-60.
233. Gao, X.; Chen, Y.; Sheng, C.; Wu, H., Interaction between sodium vapor and reactor wall during biomass combustion and its influence on measurement of particulate matter emission. *Fuel* **2016,** *165*, 260-263.
234. Liaw, S. B.; Deng, C.; Wu, H., A Novel Two-Stage Alumina Reactor System for Burning Volatiles Generated in Situ from Biosolid: Effect of Pyrolysis Temperature and Combustion Conditions on PM1 Emission. *Energy & Fuels* **2018,** *32* (9), 9438-9447.
235. Chen, X.; Liaw, S. B.; Wu, H., Effect of water vapour on particulate matter emission during oxyfuel combustion of char and in situ volatiles generated from rapid pyrolysis of chromated-copper-arsenate-treated wood. *Proceedings of the Combustion Institute* **2019,** *37* (4), 4319-4327.
236. Biagini, E.; Tognotti, L. In *Characterisation of biomass chars*, Clean Air 2003, Seventh International Conference on Energy for a Clean Environment, Instituto Superior Tecnico: 2003.
237. Trubetskaya, A.; Surup, G.; Shapiro, A.; Bates, R. B., Modeling the influence of potassium content and heating rate on biomass pyrolysis. *Applied Energy* **2017,** *194*, 199-211.
238. Szemmelveisz, K.; Szűcs, I.; Palotás, Á. B.; Winkler, L.; Eddings, E. G., Examination of the combustion conditions of herbaceous biomass. *Fuel Processing Technology* **2009,** *90* (6), 839-847.
239. French, R. J.; Milne, T. A., Vapor phase release of alkali species in the combustion of biomass pyrolysis oils. *Biomass and Bioenergy* **1994,** *7* (1-6), 315-325.

240. Richards, G. N.; Zheng, G., Influence of metal ions and of salts on products from pyrolysis of wood: Applications to thermochemical processing of newsprint and biomass. *Journal of Analytical and Applied Pyrolysis* **1991,** *21* (1-2), 133-146.
241. Liu, W.-J.; Li, W.-W.; Jiang, H.; Yu, H.-Q., Fates of Chemical Elements in Biomass during Its Pyrolysis. *Chemical Reviews* **2017,** *117* (9), 6367-6398.
242. Rahim, M. U.; Gao, X.; Wu, H., Release of chlorine from the slow pyrolysis of NaCl-loaded cellulose at low temperatures. *Proceedings of the Combustion Institute* **2015,** *35* (3), 2891-2896.
243. Motzfeldt, K., The Thermal Decomposition.of Sodium Carbonate by the Effusion Method. *The Journal of Physical Chemistry* **1955,** *59* (2), 139-147.
244. Wei, X.; Huang, J.; Liu, T.; Fang, Y.; Wang, Y., Transformation of Alkali Metals during Pyrolysis and Gasification of a Lignite. *Energy & Fuels* **2008,** *22* (3), 1840-1844.
245. Dollimore, D., The thermal decomposition of oxalates. A review. *Thermochimica Acta* **1987,** *117*, 331-363.
246. McKee, D. W.; Spiro, C. L.; Kosky, P. G.; Lamby, E. J., Catalysis of coal char gasification by alkali metal salts. *Fuel* **1983,** *62* (2), 217-220.
247. Sreekanth, M.; Kolar, A. K.; Leckner, B., Transient thermal behaviour of a cylindrical wood particle during devolatilization in a bubbling fluidized bed. *Fuel Processing Technology* **2008,** *89* (9), 838-850.
248. Fu, P.; Hu, S.; Xiang, J.; Sun, L.; Su, S.; Wang, J., Evaluation of the porous structure development of chars from pyrolysis of rice straw: Effects of pyrolysis temperature and heating rate. *Journal of Analytical and Applied Pyrolysis* **2012,** *98*, 177-183.
249. Hu, Q.; Yang, H.; Xu, H.; Wu, Z.; Lim, C. J.; Bi, X. T.; Chen, H., Thermal behavior and reaction kinetics analysis of pyrolysis and subsequent in-situ gasification of torrefied biomass pellets. *Energ Convers Manage* **2018,** *161*, 205-214.
250. Chen, W.-H.; Kuo, P.-C., A study on torrefaction of various biomass materials and its impact on lignocellulosic structure simulated by a thermogravimetry. *Energy* **2010,** *35* (6), 2580-2586.
251. Zhang, S.; Su, Y.; Xu, D.; Zhu, S.; Zhang, H.; Liu, X., Effects of torrefaction and organic-acid leaching pretreatment on the pyrolysis behavior of rice husk. *Energy* **2018,** *149*, 804-813.
252. Li, L.; Huang, Y.; Zhang, D.; Zheng, A.; Zhao, Z.; Xia, M.; Li, H., Uncovering Structure–Reactivity Relationships in pyrolysis and gasification of biomass with varying severity of torrefaction. *ACS Sustainable Chemistry & Engineering* **2018,** *6* (5), 6008-6017.
253. Cai, W.; Fivga, A.; Kaario, O.; Liu, R., Effects of Torrefaction on the Physicochemical Characteristics of Sawdust and Rice Husk and Their Pyrolysis Behavior by Thermogravimetric Analysis and Pyrolysis–Gas Chromatography/Mass Spectrometry. *Energy & Fuels* **2017,** *31* (2), 1544-1554.
254. Barontini, F.; Biagini, E.; Tognotti, L., Characterization of the devolatilization products of selected second generation biofuels. In *18th IFRF Members' Conference - Flexible and clean fuel conversion in industry*, International Flame Research Foundation: Freising, Germany, 2015; Vol. 28, pp 1-12.
255. Khazraie Shoulaifar, T.; DeMartini, N.; Willför, S.; Pranovich, A.; Smeds, A. I.; Virtanen, T. A. P.; Maunu, S.-L.; Verhoeff, F.; Kiel, J. H. A.; Hupa, M., Impact of Torrefaction on the Chemical Structure of Birch Wood. *Energy & Fuels* **2014,** *28* (6), 3863-3872.

256. Vorobiev, N.; Becker, A.; Kruggel-Emden, H.; Panahi, A.; Levendis, Y. A.; Schiemann, M., Particle shape and Stefan flow effects on the burning rate of torrefied biomass. *Fuel* **2017,** *210*, 107-120.
257. Niu, Y.; Lv, Y.; Lei, Y.; Liu, S.; Liang, Y.; Wang, D.; Hui, S. e., Biomass torrefaction: properties, applications, challenges, and economy. *Renewable and Sustainable Energy Reviews* **2019,** *115*, 109395.
258. Barta-Rajnai, E.; Babinszki, B.; Sebestyén, Z.; Czirok, S. I.; May, Z.; Jakab, E.; Czégény, Z., On the significance of potassium and chlorine content of lignocellulose during torrefaction. *Journal of Analytical and Applied Pyrolysis* **2018,** *135*, 32-43.
259. Zheng, A.; Zhao, Z.; Chang, S.; Huang, Z.; Zhao, K.; Wei, G.; He, F.; Li, H., Comparison of the effect of wet and dry torrefaction on chemical structure and pyrolysis behavior of corncobs. *Bioresource Technology* **2015,** *176*, 15-22.
260. Chang, S.; Zhao, Z.; Zheng, A.; He, F.; Huang, Z.; Li, H., Characterization of Products from Torrefaction of Sprucewood and Bagasse in an Auger Reactor. *Energy & Fuels* **2012,** *26* (11), 7009-7017.
261. Shen, Q.; Liaw, S. B.; Costa, M.; Wu, H., Rapid pyrolysis of pulverised biomass at high temperature: Effect of particle size on char yield, retentions of alkali and alkaline earth metallic species and char particle shape. *Energy & Fuels* **2020**.
262. Wornat, M. J.; Hurt, R. H.; Yang, N. Y.; Headley, T. J., Structural and compositional transformations of biomass chars during combustion. *Combustion and Flame* **1995,** *100* (1-2), 131-143.
263. Shen, Q.; Liaw, S. B.; Wu, H., Evolution of Char Properties during Rapid Pyrolysis of Woody Biomass Particles under Pulverized Fuel Conditions. *Energy & Fuels* **2021,** *35* (19), 15778-15789.
264. Andrea Jordan, C.; Akay, G., Speciation and distribution of alkali, alkali earth metals and major ash forming elements during gasification of fuel cane bagasse. *Fuel* **2012,** *91* (1), 253-263.
265. Mlonka-Mędrala, A.; Magdziarz, A.; Gajek, M.; Nowińska, K.; Nowak, W., Alkali metals association in biomass and their impact on ash melting behaviour. *Fuel* **2020,** *261*, 116421.
266. Khazraie Shoulaifar, T.; DeMartini, N.; Ivaska, A.; Fardim, P.; Hupa, M., Measuring the concentration of carboxylic acid groups in torrefied spruce wood. *Bioresource Technology* **2012,** *123*, 338-343.
267. Bock, J. H.; Norris, D. O., *Forensic Plant Science*. 1st ed.; Academic Press: 2016.
268. Tolvanen, H.; Kokko, L.; Raiko, R., Fast pyrolysis of coal, peat, and torrefied wood: Mass loss study with a drop-tube reactor, particle geometry analysis, and kinetics modeling. *Fuel* **2013,** *111*, 148-156.
269. Fisher, E. M.; Dupont, C.; Darvell, L. I.; Commandré, J. M.; Saddawi, A.; Jones, J. M.; Grateau, M.; Nocquet, T.; Salvador, S., Combustion and gasification characteristics of chars from raw and torrefied biomass. *Bioresource Technology* **2012,** *119*, 157-165.
270. Pelaez-Samaniego, M. R.; Yadama, V.; Garcia-Perez, M.; Lowell, E.; McDonald, A. G., Effect of temperature during wood torrefaction on the formation of lignin liquid intermediates. *Journal of Analytical and Applied Pyrolysis* **2014,** *109*, 222-233.
271. Gale, T. K.; Bartholomew, C. H.; Fletcher, T. H., Decreases in the swelling and porosity of bituminous coals during devolatilization at high heating rates. *Combustion and Flame* **1995,** *100* (1), 94-100.

272. Strehler, A., Technologies of wood combustion. *Ecological Engineering* **2000,** *16*, 25-40.
273. Du, S.-W.; Chen, W.-H.; Lucas, J. A., Pretreatment of biomass by torrefaction and carbonization for coal blend used in pulverized coal injection. *Bioresource Technology* **2014,** *161*, 333-339.
274. Barskov, S.; Zappi, M.; Buchireddy, P.; Dufreche, S.; Guillory, J.; Gang, D.; Hernandez, R.; Bajpai, R.; Baudier, J.; Cooper, R.; Sharp, R., Torrefaction of biomass: A review of production methods for biocoal from cultured and waste lignocellulosic feedstocks. *Renewable Energy* **2019,** *142*, 624-642.
275. Bridgeman, T. G.; Jones, J. M.; Williams, A.; Waldron, D. J., An investigation of the grindability of two torrefied energy crops. *Fuel* **2010,** *89* (12), 3911-3918.
276. Repellin, V.; Govin, A.; Rolland, M.; Guyonnet, R., Energy requirement for fine grinding of torrefied wood. *Biomass and Bioenergy* **2010,** *34* (7), 923-930.
277. Bridgeman, T. G.; Darvell, L. I.; Jones, J. M.; Williams, P. T.; Fahmi, R.; Bridgwater, A. V.; Barraclough, T.; Shield, I.; Yates, N.; Thain, S. C.; Donnison, I. S., Influence of particle size on the analytical and chemical properties of two energy crops. *Fuel* **2007,** *86* (1), 60-72.
278. Chen, D.; Gao, A.; Cen, K.; Zhang, J.; Cao, X.; Ma, Z., Investigation of biomass torrefaction based on three major components: Hemicellulose, cellulose, and lignin. *Energ Convers Manage* **2018,** *169*, 228-237.
279. Zheng, A.; Zhao, Z.; Huang, Z.; Zhao, K.; Wei, G.; Wang, X.; He, F.; Li, H., Catalytic Fast Pyrolysis of Biomass Pretreated by Torrefaction with Varying Severity. *Energy & Fuels* **2014,** *28* (9), 5804-5811.
280. Ibrahim, R. H. H.; Darvell, L. I.; Jones, J. M.; Williams, A., Physicochemical characterisation of torrefied biomass. *Journal of Analytical and Applied Pyrolysis* **2013,** *103*, 21-30.
281. Wang, S.; Dai, G.; Ru, B.; Zhao, Y.; Wang, X.; Zhou, J.; Luo, Z.; Cen, K., Effects of torrefaction on hemicellulose structural characteristics and pyrolysis behaviors. *Bioresource Technology* **2016,** *218*, 1106-1114.
282. Chaiwat, W.; Hasegawa, I.; Kori, J.; Mae, K., Examination of Degree of Cross-Linking for Cellulose Precursors Pretreated with Acid/Hot Water at Low Temperature. *Industrial & Engineering Chemistry Research* **2008,** *47* (16), 5948-5956.
283. Chaiwat, W.; Hasegawa, I.; Tani, T.; Sunagawa, K.; Mae, K., Analysis of Cross-Linking Behavior during Pyrolysis of Cellulose for Elucidating Reaction Pathway. *Energy & Fuels* **2009,** *23* (12), 5765-5772.
284. Acharya, B.; Sule, I.; Dutta, A., A review on advances of torrefaction technologies for biomass processing. *Biomass Conversion and Biorefinery* **2012,** *2* (4), 349-369.
285. Zheng, A.; Jiang, L.; Zhao, Z.; Huang, Z.; Zhao, K.; Wei, G.; Wang, X.; He, F.; Li, H., Impact of Torrefaction on the Chemical Structure and Catalytic Fast Pyrolysis Behavior of Hemicellulose, Lignin, and Cellulose. *Energy & Fuels* **2015,** *29* (12), 8027-8034.
286. Shen, J.; Wang, X.-S.; Garcia-Perez, M.; Mourant, D.; Rhodes, M. J.; Li, C.-Z., Effects of particle size on the fast pyrolysis of oil mallee woody biomass. *Fuel* **2009,** *88* (10), 1810-1817.
287. Yu, C.; Thy, P.; Wang, L.; Anderson, S. N.; VanderGheynst, J. S.; Upadhyaya, S. K.; Jenkins, B. M., Influence of leaching pretreatment on fuel properties of biomass. *Fuel Processing Technology* **2014,** *128*, 43-53.

288. Xu, M.; Sheng, C., Influences of the Heat-Treatment Temperature and Inorganic Matter on Combustion Characteristics of Cornstalk Biochars. *Energy & Fuels* **2012,** *26* (1), 209-218.
289. Liu, X.; Bi, X. T., Removal of inorganic constituents from pine barks and switchgrass. *Fuel Processing Technology* **2011,** *92* (7), 1273-1279.
290. Stefanidis, S. D.; Heracleous, E.; Patiaka, D. T.; Kalogiannis, K. G.; Michailof, C. M.; Lappas, A. A., Optimization of bio-oil yields by demineralization of low quality biomass. *Biomass and Bioenergy* **2015,** *83*, 105-115.
291. Deng, L.; Zhang, T.; Che, D., Effect of water washing on fuel properties, pyrolysis and combustion characteristics, and ash fusibility of biomass. *Fuel Processing Technology* **2013,** *106*, 712-720.
292. Vamvuka, D.; Sfakiotakis, S., Effects of heating rate and water leaching of perennial energy crops on pyrolysis characteristics and kinetics. *Renewable Energy* **2011,** *36* (9), 2433-2439.
293. Jiang, L.; Hu, S.; Sun, L.-s.; Su, S.; Xu, K.; He, L.-m.; Xiang, J., Influence of different demineralization treatments on physicochemical structure and thermal degradation of biomass. *Bioresource Technology* **2013,** *146*, 254-260.
294. Jakab, E.; Mészáros, E.; Borsa, J., Effect of slight chemical modification on the pyrolysis behavior of cellulose fibers. *Journal of Analytical and Applied Pyrolysis* **2010,** *87* (1), 117-123.
295. Oudenhoven, S. R. G.; Lievens, C.; Westerhof, R. J. M.; Kersten, S. R. A., Effect of temperature on the fast pyrolysis of organic-acid leached pinewood; the potential of low temperature pyrolysis. *Biomass and Bioenergy* **2016,** *89*, 78-90.
296. Iraola-Arregui, I.; Van Der Gryp, P.; Görgens, J. F., A review on the demineralisation of pre- and post-pyrolysis biomass and tyre wastes. *Waste Management* **2018,** *79*, 667-688.

Every reasonable effort has been made to acknowledge the owners of copyright material. I would be pleased to hear from any copyright owner who has been omitted or incorrectly acknowledged.

APPENDIX I: COPYRIGHT PERMISSION STATEMENTS

Chapter 2, Reprinted (adapted) with permission from (Liaw, S. B.; Wu, H., A New Method for Direct Determination of Char Yield during Solid Fuel Pyrolysis in Drop-Tube Furnace at High Temperature and Its Comparison with Ash Tracer Method. Energy & Fuels 2019, 33 (2), 1509-1517.). Copyright (2019) American Chemical Society.

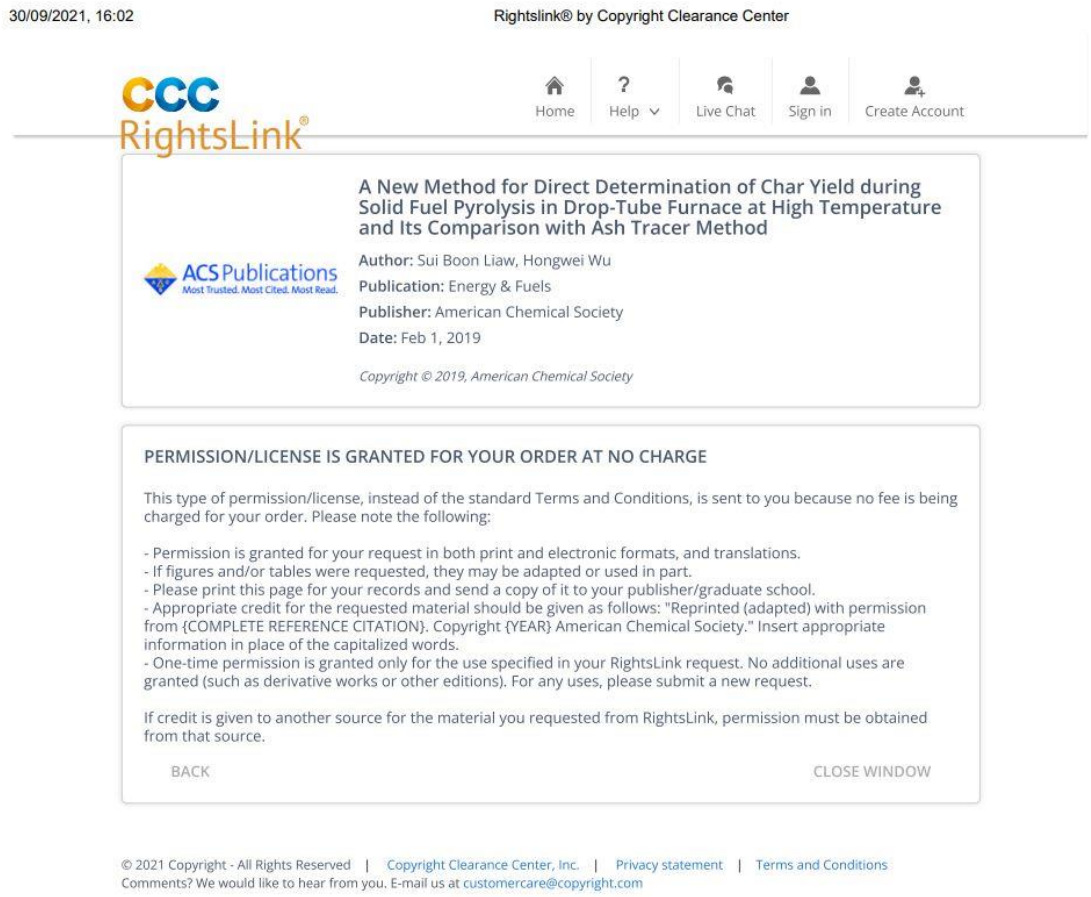

30/09/2021, 16:02 Rightslink® by Copyright Clearance Center

CCC RightsLink®

Home | Help | Live Chat | Sign in | Create Account

ACS Publications
Most Trusted. Most Cited. Most Read.

A New Method for Direct Determination of Char Yield during Solid Fuel Pyrolysis in Drop-Tube Furnace at High Temperature and Its Comparison with Ash Tracer Method

Author: Sui Boon Liaw, Hongwei Wu
Publication: Energy & Fuels
Publisher: American Chemical Society
Date: Feb 1, 2019

Copyright © 2019, American Chemical Society

PERMISSION/LICENSE IS GRANTED FOR YOUR ORDER AT NO CHARGE

This type of permission/license, instead of the standard Terms and Conditions, is sent to you because no fee is being charged for your order. Please note the following:

- Permission is granted for your request in both print and electronic formats, and translations.
- If figures and/or tables were requested, they may be adapted or used in part.
- Please print this page for your records and send a copy of it to your publisher/graduate school.
- Appropriate credit for the requested material should be given as follows: "Reprinted (adapted) with permission from {COMPLETE REFERENCE CITATION}. Copyright {YEAR} American Chemical Society." Insert appropriate information in place of the capitalized words.
- One-time permission is granted only for the use specified in your RightsLink request. No additional uses are granted (such as derivative works or other editions). For any uses, please submit a new request.

If credit is given to another source for the material you requested from RightsLink, permission must be obtained from that source.

BACK CLOSE WINDOW

© 2021 Copyright - All Rights Reserved | Copyright Clearance Center, Inc. | Privacy statement | Terms and Conditions
Comments? We would like to hear from you. E-mail us at customercare@copyright.com

Chapter 4, Reprinted (adapted) with permission from (Shen, Q.; Liaw, S. B.; Costa, M.; Wu, H., Rapid Pyrolysis of Pulverized Biomass at a High Temperature: The Effect of Particle Size on Char Yield, Retentions of Alkali and Alkaline Earth Metallic Species, and Char Particle Shape. Energy & Fuels 2020, 34 (6), 7140-7148.). Copyright (2020) American Chemical Society.

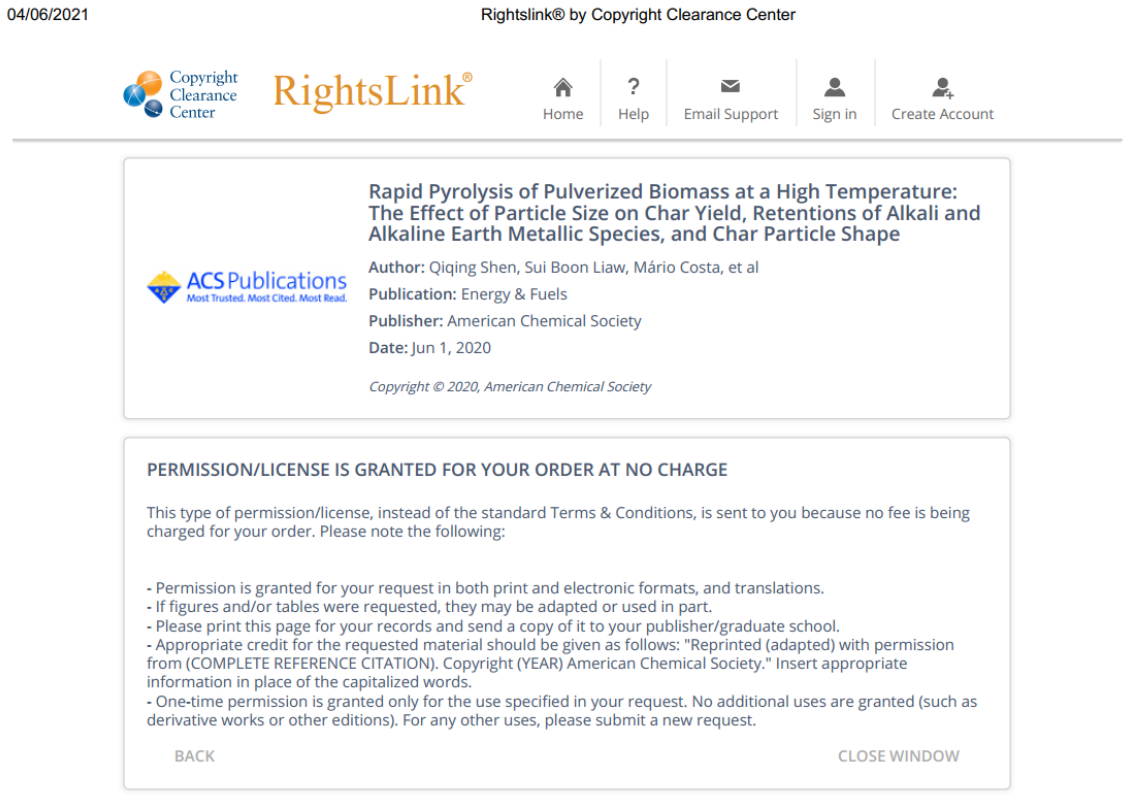

04/06/2021 Rightslink® by Copyright Clearance Center

Copyright Clearance Center RightsLink® Home Help Email Support Sign in Create Account

ACS Publications Most Trusted. Most Cited. Most Read.

Rapid Pyrolysis of Pulverized Biomass at a High Temperature: The Effect of Particle Size on Char Yield, Retentions of Alkali and Alkaline Earth Metallic Species, and Char Particle Shape

Author: Qiqing Shen, Sui Boon Liaw, Mário Costa, et al
Publication: Energy & Fuels
Publisher: American Chemical Society
Date: Jun 1, 2020

Copyright © 2020, American Chemical Society

PERMISSION/LICENSE IS GRANTED FOR YOUR ORDER AT NO CHARGE

This type of permission/license, instead of the standard Terms & Conditions, is sent to you because no fee is being charged for your order. Please note the following:

- Permission is granted for your request in both print and electronic formats, and translations.
- If figures and/or tables were requested, they may be adapted or used in part.
- Please print this page for your records and send a copy of it to your publisher/graduate school.
- Appropriate credit for the requested material should be given as follows: "Reprinted (adapted) with permission from (COMPLETE REFERENCE CITATION). Copyright (YEAR) American Chemical Society." Insert appropriate information in place of the capitalized words.
- One-time permission is granted only for the use specified in your request. No additional uses are granted (such as derivative works or other editions). For any other uses, please submit a new request.

BACK CLOSE WINDOW

Chapter 4, Reprinted (adapted) with permission from (Shen, Q.; Liaw, S. B.; Costa, M.; Wu, H., Evolution of Char Properties during Rapid Pyrolysis of Woody Biomass Particles under Pulverized Fuel Conditions. Energy & Fuels 2021, 35, (19), 15778-15789.) Copyright (2021) American Chemical Society.

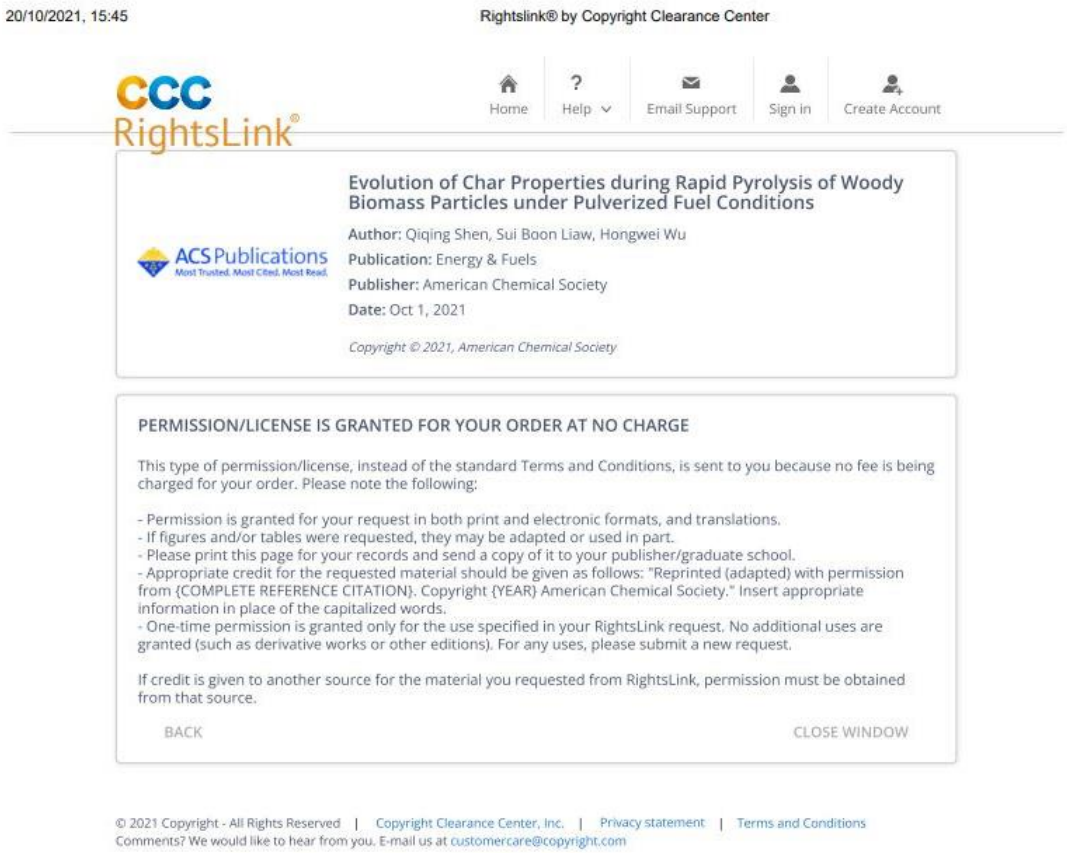

APPENDIX II: ATTRIBUTION TABLES

[1] **Shen, Q.**; Liaw, S. B.; Costa, M.; Wu, H., Rapid Pyrolysis of Pulverized Biomass at a High Temperature: The Effect of Particle Size on Char Yield, Retentions of Alkali and Alkaline Earth Metallic Species, and Char Particle Shape. Energy & Fuels 2020, 34 (6), 7140-7148.

Authors and full affiliations:

	Conception and design	**Experiments conduction & data acquisition**	**Data processing & analysis**	**Interpretation & discussion**	**Manuscript writing, revision and finalization**	**Final Approval**
Qiqing Shen	×	×	×	×	×	×
I acknowledge that these represent my contribution to the above research output. Sign:						
Sui Boon Liaw				×	×	×
I acknowledge that these represent my contribution to the above research output. Sign:						
Mário Costa	×			×	×	×
Author deceased						
Hongwei Wu	×		×	×	×	×
I acknowledge that these represent my contribution to the above research output. Sign:						

[2] **Shen, Q.**; Liaw, S. B.; Wu, H., Evolution of Char Properties during Rapid Pyrolysis of Woody Biomass Particles under Pulverized Fuel Conditions. Energy & Fuels 2021, 35, (19), 15778-15789.

Authors and full affiliations:

	Conception and design	**Experiments conduction & data acquisition**	**Data processing & analysis**	**Interpretation & discussion**	**Manuscript writing, revision and finalization**	**Final Approval**
Qiqing Shen	×	×	×	×	×	×
I acknowledge that these represent my contribution to the above research output. Sign:						
Sui Boon Liaw				×	×	×
I acknowledge that these represent my contribution to the above research output. Sign:						
Hongwei Wu	×		×	×	×	×
I acknowledge that these represent my contribution to the above research output. Sign:						